Development of Versatile Luminescent Sensors

JENNINGS, LAURA

Durham University

Department of Chemistry

Development of Versatile Luminescent Sensors

Laura Jennings

A thesis submitted for the degree of Doctor of Philosophy

2018

Declaration

The work described herein was undertaken at the Department of Chemistry, Durham University between October 2015 and September 2018. All of the work is my own, except where specifically stated otherwise. No part has previously been submitted for a degree at this or any other university

Statement of Copyright

Abstract

Lanthanide based probes and sensors have been widely utilised over the past few decades, particularly in the study of biological processes. The favourable photoluminescent properties of the lanthanide ions and the use of functionalised macrocyclic ligands that permit tuneable excitation means there is now a plethora of examples, across the scientific literature.

An azaxanthone-based chromophore has been incorporated into a cyclen ligand, and the ability of this complex to bind to proteins has been studied further, examining the possibility of personalised medicine. The complex competes with selectively chosen pharmaceutical compound in binding to the acute phase serum protein α_1-AGP. This complex is one of the first examples which uses CPL to monitor a binding event.

The same chromophore, as well as the azathioxanthone analogue, have been utilised further in cyclen based complexes, with the aim of binding the controversial herbicide, glyphosate. Selectivity for glyphosate against other potential competitors has been studied, testing the ability of a series of structurally related complexes to operate in a variety of media.

The final chapter looks at a new family of compounds, which bear an extended chromophore and a tripicolylamine based arm. Again, these were tested for their ability to bind glyphosate selectively, in a range of media. Time-gated methodology was used to allow any unwanted organic auto-fluorescence to be removed, particularly in samples which may contain a lot of biological compounds. Following these studies, one complex was selected, testing whether the complex can be used to calculate the concentration of glyphosate in extract from spiked wheat and oat grains. This complex was able to be used over the range 0.5 to 60 micromolar of glyphosate with a limit of around 4 micromolar.

Acknowledgements

Firstly, I would like to thank Professor David Parker FRS, for the opportunity to work on such an interesting and relevant project, and for the support and aid throughout.

Secondly, to Dr. Robert Pal, for all his help, for fixing both my problems, and all the machines when they inevitably break and answering all of my 'stupid' questions.

I would also like to thank the DP/RP group members throughout my time here, particularly Alice, who has gone through this with me and helped keep me sane. The GS group have also been incredibly supportive and dealt with my many rants.

Thanks must also go to the NMR spectroscopy staff, the mass spectrometry service staff, Dr Aileen Congreve and the HPLC service in the separation of the enantiomers, and to Dr. Mark Fox for his DFT calculations.

To Prof. Robert Edwards and Dr. Lami Nnamonu, for their support in the glyphosate part of my project, for their knowledge about the herbicide and biochemistry and sourcing the wheat grains.

Thank you to my family for their support in getting me here in the first place, and pretending to be interested in my work despite having no idea what I am actually doing.

Finally, thanks to Josh, you've been okay.

Abbreviations

α_1-AGP	alpha-1 acid glycoprotein
α_1-ATT	alpha-1 antitrypsin
9-N_3	1,4,7-triazacyclononane
12-N_4	1,4,7,10-tetraazacyclododecane
AC	Alternating current
ADP	Adenosine diphosphate
AMI	Acute myocardial infarction
AMPA	Aminomethylphosphonic acid
aq	Aqueous
ATP	Adenosine triphosphate
br	Broad
BSA	Bovine serum albumin
Conc.	Concentrated
CD	Circular dichroism/carbon dots
CML	Chronic myelogenous leukaemia
CPL	Circularly polarised luminescence
CRA	Chiral resolving agent
CV	Cyclic voltammetry
cyclen	1,4,7,10-Tetraazacyclododecane
d	Doublet
DC	Direct current
DCM	Dichloromethane
DFT	Density Functional Theory
DMF	*N*,*N*-dimethylformamide
DMSO	Dimethylsulfoxide
DOTA	1,4,7,10-Tetraazacyclododecane-1,4,7,10-tetraacetic acid
ECG	Electrocardiogram
ECHA	European Chemical Agency
ECL	Electrochemical luminescence
EFSA	European Food Safety Authority
ELISA	Enzyme-linked immunosorbent assay
EPA	Environmental Protection Agency
EPSP	5-Enolpyruvylshikimate-3-phosphate

ER	Endoplasmic reticulum
ESI	Electrospray ionisation
ESMS	Electrospray mass spectrometry
EU	European Union
FA	Formic acid
FD	Fluorescence detection
Fmoc-Cl	9-Fluorenylmethyl chloroformate
FRET	Förster resonance energy transfer
Glu	Glutamate
GMC	Glyphosate metal complex
hERG	Human ether à-go-go-related gene
hfbc	Heptafluorobutylyrylcamphorato
HPLC	High performance liquid chromatography
HRMS	High resolution mass spectrometry
HSA	Human serum albumin
IARC	International Agency for Research on Cancer
ICT	Internal charge transfer
ISC	Intersystem crossing
LC	Liquid chromatography
LDA	Linear discrimination analysis
LED	Light emitting diode
LOQ	Limit of quantification
LOD	Limit of detection
m	Multiplet
m.p.	Melting point
MES	2-(*N*-morpholino)ethanesulfonic acid
MOR	μ-opioid receptor
MRL	Minimal residual levels
MS	Mass spectrometry
MWCNT	Multi-walled carbon nanotube
NBS	*N*-bromosuccinimide
NIR	Near infrared
NMR	Nuclear magnetic resonance
NP	Nanoparticles

PCA	Principle component analysis
PEM	Photoelastic modulator
PMT	Photomultiplier tube
PPA	Polyphosphoric acid
q	Quartet
QTOF	Quadrupole time-of-flight
s	Singlet
SAM	Self-assembled monolayer
SAP	Square anti-prismatic
Ser	Serine
SOM	Small organic molecule
SPE	Solid phase extraction
t	Triplet
TFA	Trifluoroacetic acid
THF	Tetrahydrofuran
Thr	Threonine
TLC	Thin layer chromatography
TQD	Tandem quadrupole detector
Tyr	Tyrosine
UV	Ultraviolet
WHO	World Health Organisation

Table of Contents

1. Introduction

1.1 Overview

Luminescence in its various forms has been known for centuries through chemiluminescence, bioluminescence and photoluminescence, defined by their mode of excitation. Bioluminescence is the oldest known form, with references made by Pliny the elder, and described by Aristotle after his observations of 'cold light' in animals and fungi.[1] An early mention of chemiluminescence was made by Vincenzo Cascariolo, in the early 17th century, who observed a purple-blue light from impure barium sulfide.[2] However, the work in this thesis will focus on photoluminescence; the spontaneous emission of light following the absorption of photons.

Lanthanide photoluminescence has been used in a plethora of scientific and technological fields, including the authentication of documents and bank notes, to cell imaging and assays. [3–6] In this work, the use of lanthanide complexes as a probe for different analytes is discussed and developed, exploiting their unusual properties.

One of the key advantages is the long-lived luminescent lifetime of terbium and europium complexes in particular. The lifetime of these being in the millisecond domain, compared to nanoseconds for most organic and transition metal complexes, which permit time-gated emission spectra to be acquired. This allows the unwanted organic luminescence to be eliminated. This is particularly useful if investigating biological media, where auto-fluorescence can interfere with results. For example, lanthanide complexes have been used to probe biologically relevant anionic species, such as phosphates or bicarbonate as these species are involved in a diverse range of metabolic pathways.[7–10] Upon binding the analyte there is a dramatic change in spectral form and emission intensity. The sharp and unique emission lines from lanthanide spectra allow small changes in the spectral form to be discerned, as well as having the potential to probe the structure of the complex and the competitive binding of analytes.

All of these properties have been well researched and discussed particularly over the past two decades.[11,12] The more recent development of circularly polarised luminescence (CPL) is also starting to gain traction in the lanthanide community.[13,14] The potential to gain more information about the chiral structure of a complex, as well the binding mode or coordination environment, is being investigated, partially driven by the ubiquitous nature of chirality within biology.

This thesis will explore the use of lanthanide complexes in both CPL and time-gated experiments to study the use of these compounds in 'real-life' situations. Reversible binding will be monitored through changes in emission, as well as addressing any sampling problems which arise in the process.

1.2 Luminescent Lanthanide Complexes

1.2.1 Photoluminescence

The term photoluminescence is inclusive of both fluorescence and phosphorescence, the radiative decay from a spin allowed and spin forbidden transition respectively. The 'allowed' or 'forbidden' aspect of the transition stems from the Laporte rule which states that a transition must include a change in parity.[15] This obviously assumes perfect quantum numbers which is rarely the case, so even with a forbidden transition, emission is often observed, albeit with a much weaker intensity coupled with a longer lifetime than those seen with an allowed transition. The relaxation of the Laporte rule comes through the coupling of vibrational and electronic states, which distorts the symmetry around the metal ion sufficiently to allow the transition.

1.2.2 Lanthanide Luminescence

The unusual luminescent properties of lanthanide complexes mostly stem from the forbidden nature of the *f-f* transition. As it is disallowed, once the lanthanide is in an excited state, it takes time for relaxation to occur via radiative decay, hence the long lifetime. However, this is often seen as a positive and is a well utilised property, with the negative aspect being that it is often paired with a small extinction coefficient and therefore, a low quantum yield. These features create a potential problem when designing a complex, as the emission must be sufficiently intense to be observable quickly.

Furthermore, owing to the lanthanide contraction, there is little overlap of orbitals between the lanthanide and any ligand, so the ligand has less influence on the form of the emission spectrum, in comparison to transition metal coordination complexes. Hence, lanthanide complexes tend to have distinct emission with sharp bands. However, the nature of the ligand has a measureable effect on lanthanide spectra. Indeed, variation in the ligand field determines the crystal field parameter, B_0^2, which can be calculated from the change in the $\Delta J = 1$ band in europium emission, for example.[16]

The distinct emission bands from the lowest energy excited states, range in energy through the lanthanide series. Each lanthanide emits in its own distinct region. For example, europium and terbium emit in the visible region, giving rise to red and green light respectively. Others emit in the near IR (NIR), such as neodymium, ytterbium and erbium. Figure 1.1 shows the relevant energy levels of the lanthanides.

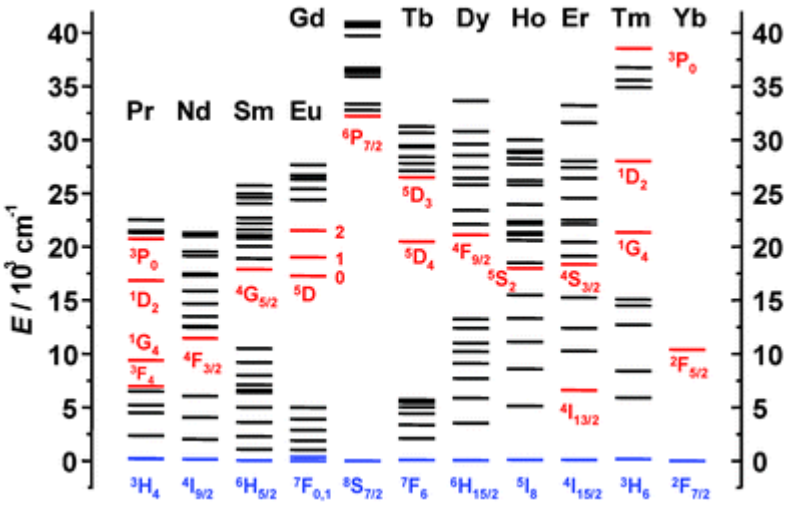

Figure 1.1- Energy level diagram for lanthanides with the ground state (blue) and the excited states from which radiative decay can be observed (red)[17]

The energy gap between the first excited state and the ground state should be considered in terms of what the lanthanide complex will be used for. For example, if the energy gap is too small, the number of viable non-radiative pathways increase and hence lanthanide emission intensity decreases. Europium, terbium and gadolinium all have large energy gaps, with gadolinium in the UV region. This is important to note, as gadolinium complexes are not appropriate for use in biological media, due to the potential of UV damage. Consequently, it is predominantly europium and terbium which have been investigated. Furthermore, uses in displays for example, are normally limited to europium and terbium.

Europium is more commonly used in emission studies, compared to terbium, partially due to the lowest level excited state, $^5D_0$ being non-degenerate. The effect of this on the spectra is that fine structure in each band arises due to the degeneracy of the ground states, ^7F_n (n=0-7). Hence, europium spectra are not only the simplest to interpret, but are also those from which information is most easily extracted.

Additionally, the long-lived luminescent lifetimes of the lanthanide metals allows for time-gated experiments to be achieved. Particularly in biological media, there is a level

of short-lived organic fluorescence, which could mask or interfere with the lanthanide emission. Up to a 10 microsecond delay after excitation could be used, for example, before emission is collected, to remove any competing fluorescence.

1.2.3 Sensitising Ligands

Due to the forbidden nature of the *f-f* transition, not only is the emission lifetime long, but it is also difficult to excite the lanthanide directly with their low (5 dm^3 mol^{-1} cm^{-1}) molar extinction coefficient. Although possible using certain lasers, it is inefficient, so most researchers utilise sensitising ligands. These are often conjugated organic chromophores which when excited, transfer energy to the lanthanide excited state, from which it can relax. The first report was published in the 1940s by Weissman, focussing mainly on europium but stating it was also observed for terbium and samarium.[18] In the paper, he also discussed the effect of solvent and temperature in the process, which later was referred to as the 'antenna effect'.

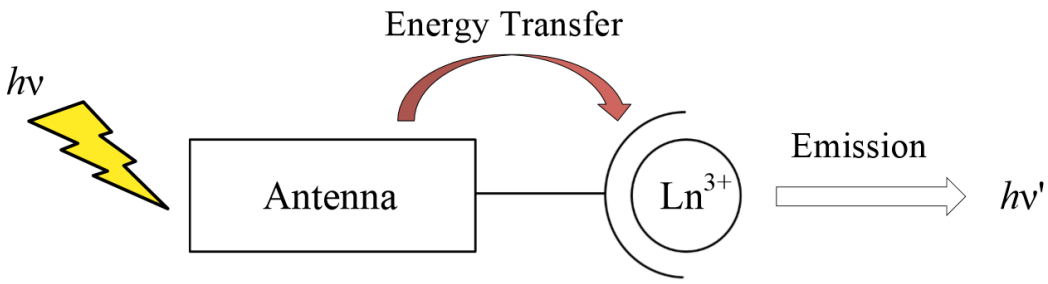

Figure 1.2 - A simplified sketch to illustrate the antenna effect

The chromophore can be designed specifically for the lanthanide and for the final use of the complex. For example, solubility, charge, and sample uptake in biological systems can be varied through modification of the chromophore. There are a number of probes which are designed to investigate a biological process that are not soluble in water, and therefore require the use of DMSO.[19–21] The chromophore, as well as the rest of the ligand, should be designed in such a way that it can be used directly, according to its original intended use. As such, a wide range of chromophores has been used to sensitise lanthanide emission.[22–26]

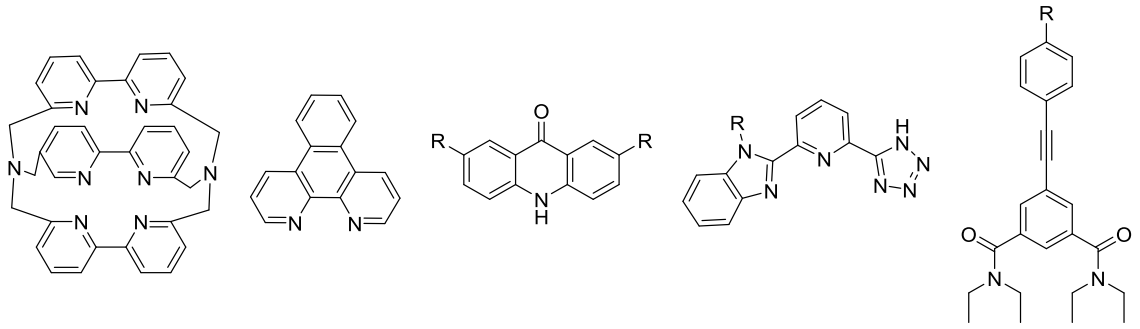

Figure 1.3 - The structures of a number of chromophore that have been used to excite lanthanides[22–26]

Excitation of the antenna preferably occurs at a wavelength close to the maximum absorbance of the chromophore. Ideally, this would also be at an excitation wavelength that aligns with laser or LED excitation sources, e.g. at 365 nm or 380 nm, which are commercially available LED wavelengths. Once the chromophore is excited, it relaxes very quickly via vibronic relaxation to the lowest lying S_1 state, as described by Kasha's rules.[27] This process occurs on the timescale of 10^{-13} to 10^{-11} seconds. From the S_1 state there are three main pathways the process can follow. The first is non-radiative decay back down to the S_0 state. The second is a radiative process down to S_0 giving fluorescence, which takes 10^{-9} to 10^{-7} seconds. The third option is to undergo intersystem crossing (ISC) to the excited T_1 state, which is the most common pathway in lanthanide luminescence.

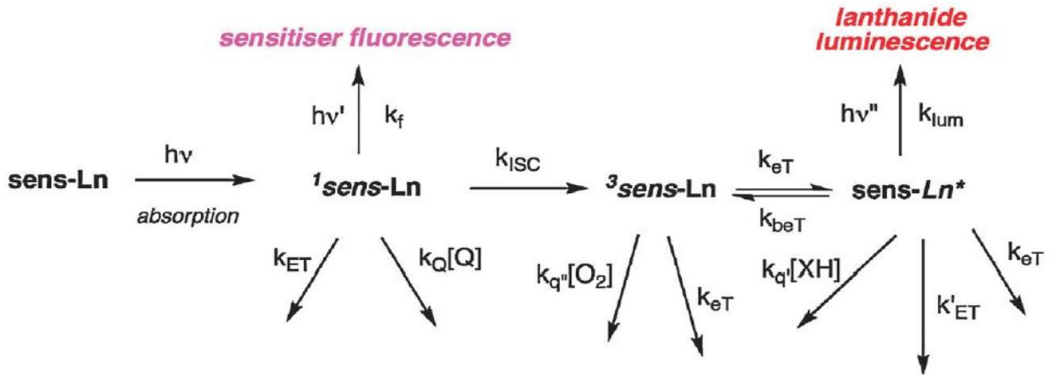

Figure 1.4 - Schematic showing some potential pathways of relaxation when utilising the antenna effect[28]

From the triplet state, there are a number of options. Again the option of a non-radiative pathway back to S_0 is a possibility, as well as a radiative option, phosphorescence. This can occur over a timescale of 10^{-4} seconds to hours, which is how 'glow-in-the-dark' objects work. The third option in lanthanide complexes is energy transfer from the chromophore's T_1 state to a lanthanide excited state. Similar pathways are available for the lanthanide excited states as the chromophore T_1, including back transfer to the

chromophore T_1 state. When the lanthanide excited state luminesces, it is typically on the micro- to millisecond timescale.

The transfer of energy between the chromophore and the lanthanide can go through two potential pathways, Förster or Dexter which are through space and bonds respectively. Due to the lanthanide contraction, the lanthanide 4*f* orbitals provide poor overlap with those of the ligand and as such, it is unlikely that this transfer occurs via a Dexter mechanism. It is therefore assumed in most cases to be a Förster mechanism, and this pathway displays an r^{-6} dependency. Therefore, when designing an antenna ligand, it must lie sufficiently close in space to the lanthanide to allow efficient energy transfer. The energy transfer actually takes place through a dipole-dipole interaction between the orbitals of the organic chromophore and the 4*f* orbitals of the lanthanide ion.

Although this is the most common pathway to achieve maximum lanthanide luminescence, there are various points in which non-radiative decay can occur. For example, the triplet excited state can be quenched by triplet oxygen. In the design of the chromophore, these and other pathways should be considered to maximise lanthanide luminescence.

An alternative method to lanthanide excitation is through an ICT (internal charge transfer) state on the chromophore.[29–31] These states exist where there is an electron withdrawing and electron donating group that are linked via π-conjugation.[32] The greater the charge difference between the groups, the larger the bathochromic shift. The same effect can also be induced by increasing the length of the conjugated chain, and these states often correspond to the visible region. The large Stokes shift which is often observed in this system is due to the reorganisation of the excited state which has a different dipole moment to the ground state. Therefore, the relaxation is highly dependent on the donor/acceptor pair as well as solvent polarity due to differential stabilisation of the excited state. The states are also thermally activated, resulting in a temperature dependence.

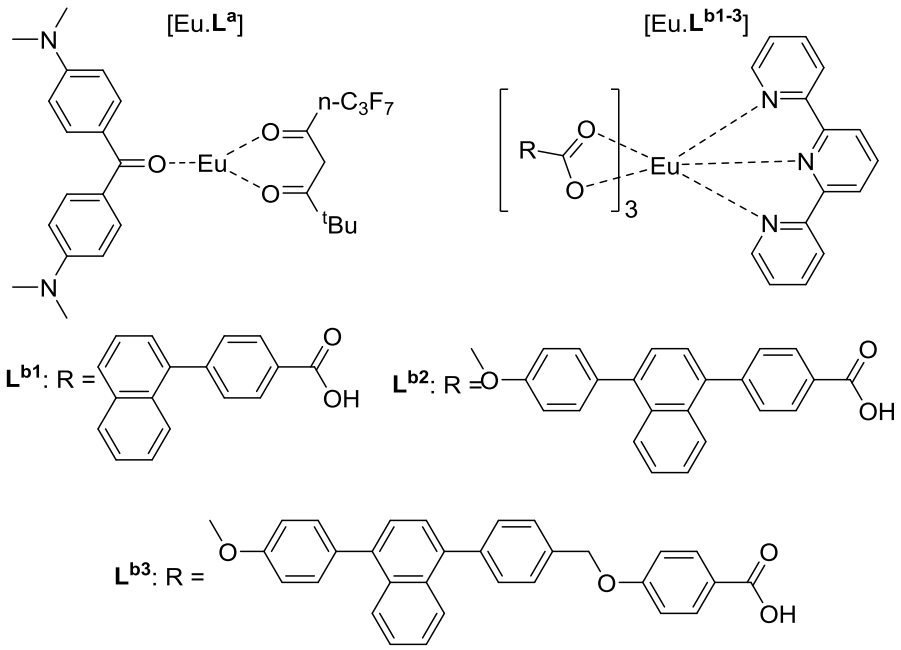

*Figure 1.5 – The structures of [Eu.**L**^{a}]*[29] *(left) and [Eu.**L**$^{b1-3}$]*[31] *(right), that are excited through ICT states*

Significantly fewer examples are seen of singlet excited state sensitisation. It was first proposed in 1969 by Kleinerman who proved it was a viable process.[33] However, transfer from the triplet state can still occur, if this energy transfer is faster than the singlet state. The first confirmed case wasn't reported until 2004 by Yang *et al*.[34]

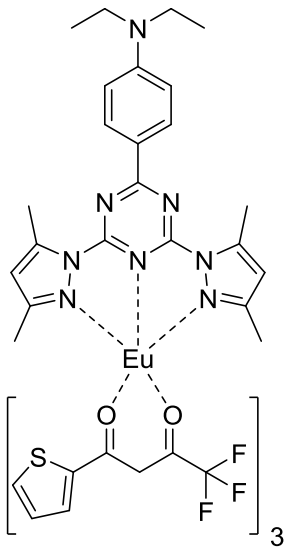

*Figure 1.6 – The structure of [Eu.**L**^{c}]*[34]

Using time-resolved experiments, they showed that the decay of the singlet excited state of [Eu.**L**^{c}] matched the rise time of the $^{5}D_{1}$ excited state of 1.8 ns; the triplet excited state was proven to have a lifetime of 3.9 s, through low temperature measurements.

However, examples of singlet sensitisation are still much rarer, with most examples using the triplet excited state. This can be depicted more simply on a Jablonski diagram.

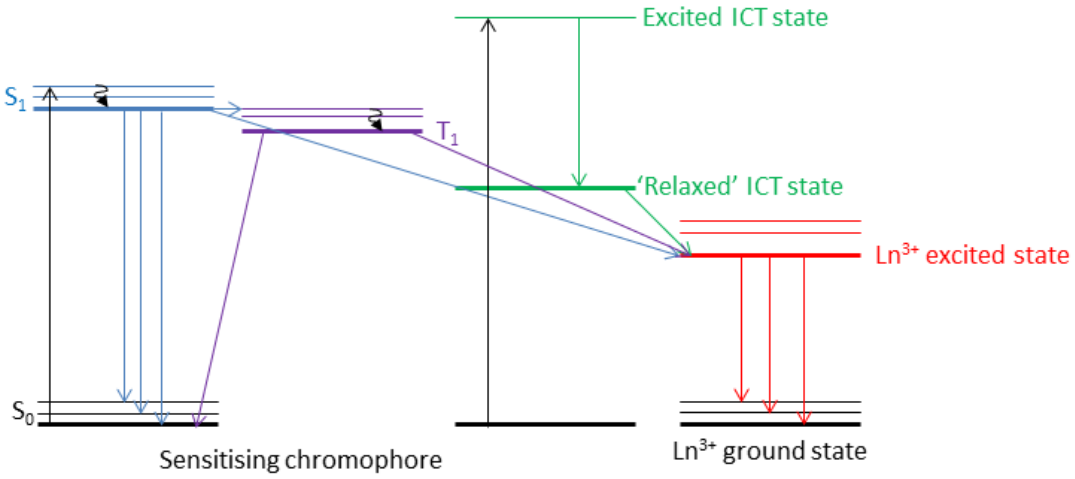

Figure 1.7 - A Jablonski diagram displaying possible ways to sensitise the lanthanide excited state using a sensitising chromophore

One of the main points to ensure efficient phosphorescence via the T_1 state of the chromophore is that it should be higher in energy than the excited state of the lanthanide, but be close enough in energy to allow efficient transfer. If the difference in energy is too great, the brightness (Equation 1.1) of the probe is compromised. However, the energy of the chromophore T_1 should be more than 19,000 cm^{-1} in europium or 22,000 cm^{-1} in terbium, to allow an energy gap greater than 1,700 cm^{-1}. This situation ensures back transfer from the lanthanide to the chromophore does not occur quickly. These points need to be balanced to optimise efficient lanthanide luminescence.

One comprehensive study saw 41 compounds synthesised which were used to compare the lanthanide luminescent quantum yield and the triplet excited state.[35] A clear correlation between the two was observed for both europium and terbium. They also found that quantum yields decreased due to back transfer to terbium when the ligand triplet state was below 22, 300 cm^{-1}. For europium, the precise numbers were more difficult due to multiple excited states, but again, it was found that the best sensitisation was close to the $^5D_0$ excited state, but when the gap was too close, a large decrease in luminescence was observed.

A high quantum yield is an essential feature of a good luminescent probe to ensure a good signal-to-noise ratio in both total luminescence and CPL. It can be related to many aspects of ligand design, including those discussed above. Essentially, the quantum

yield is the ratio of the number of photons emitted compared to the number absorbed. The quantum yield (ϕ) and the molar extinction coefficient (ε(λ)) of a ligand determines the brightness $B(\lambda)$ of a probe.

$$B(\lambda) = \varepsilon(\lambda)\phi_{em} \quad \textbf{(1.1)}$$

The molar extinction coefficient is a constant that is described by the Beer-Lambert Law;

$$A(\lambda) = \varepsilon(\lambda)cL \quad \textbf{(1.2)}$$

The molar extinction coefficient is proportional to concentration (c) and is constant for a compound in a given solvent and wavelength. It is therefore regularly used to calculate the concentration of compounds at the micro-molar level.

1.2.4 Ligands for Ln(III) Complexes

A plethora of chromophores and ligands exist that have been used to sensitise lanthanide ions. This section will focus on europium and terbium complexes as these are the main two metal ions which emit in the visible spectrum and therefore are most commonly used in luminescence studies.

Thus far, the focus has been on good chromophores which have high brightness, but the stability of the coordination complex is also imperative. Going back to uses in biological systems, lanthanide metals are toxic if not encapsulated in a kinetically and thermodynamically inert complex as they may replace Ca^{2+}. The similar sized radius and high charge means lanthanides can bind to the same binding sites as calcium, as well as being taken up into bone tissue, which can affect biological pathways, altering physiological processes.[36] For a stable complex, a high coordination number is necessary (preferably 8- or 9-) with hard donor ligands such as nitrogen and oxygen, which bind strongly to lanthanide ions.

1,4,7,10-Tetraazacyclododecane-1,4,7,10-tetraacetic acid (DOTA) and related ligands have been used widely as MRI contrast agents as they have good kinetic stability. Commercially known as Dotarem, $[Gd(DOTA)(H_2O)]^-$, was first used in vivo in 1986 as an alternative to $[Gd(DTPA)(H_2O)]^{2-}$ (Magnevist) (Figure 1.8).[37]

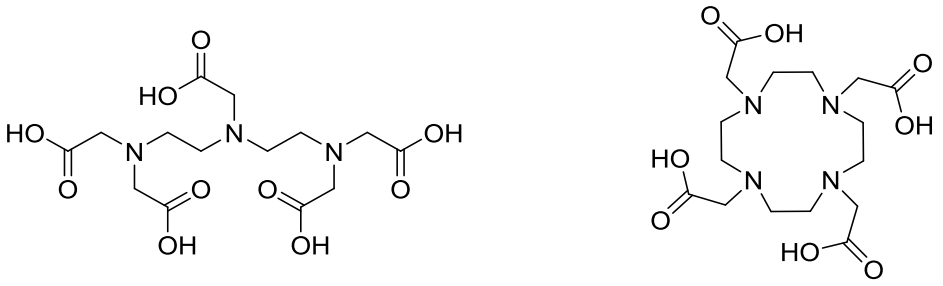

Figure 1.8 - DPTA (left) and DOTA (right)

$[Gd(DOTA)(H_2O)]^-$ possess more favourable relaxation properties compared to $[Gd(DTPA)(H_2O)]^{2-}$, and has the added benefit that the logK_{ML} values are higher, with 24.7 compared to 22.3 respectively for the gadolinium complexes.[38] The reason for the favourable binding constants in each case is due to the 'chelate effect', which reduces the entropic contribution of chelation of the lanthanide metal ion compared to complex formation with multiple mono-dentate ligands. The stability of the lanthanide DOTA complexes is greater than those of DPTA due to the 'macrocyclic effect'. It is similar in nature to the chelate effect, but as the macrocycle is already formed before complexation, it reduces the entropic penalty compared to the open chain analogue and gives rise to higher log*K* values.

The ligand cyclen and the octadentate derivative DOTA form the basis of a number of ligands which have been used as multimodal contrast agents as well as for luminescence studies.[39,40] Modifications to both the cyclen ring itself or the *N*-substituents can alter the ligand properties, allowing the synthesis of a range of complexes for a variety of uses.

The hexadentate 9-N_3 equivalent is called NOTA, where similar modifications to the parent ring aids the creation of a library of NOTA derivatives. Groups such as pyridines with a carboxylate group in the 6-position allow for three additional coordination sites, taking the coordination number up to nine, and is therefore suitable for stable lanthanide complex formation.[41] The possibility of substituting the carboxylate group for a phosphinate group has also been explored, (Figure 1.9).[42]

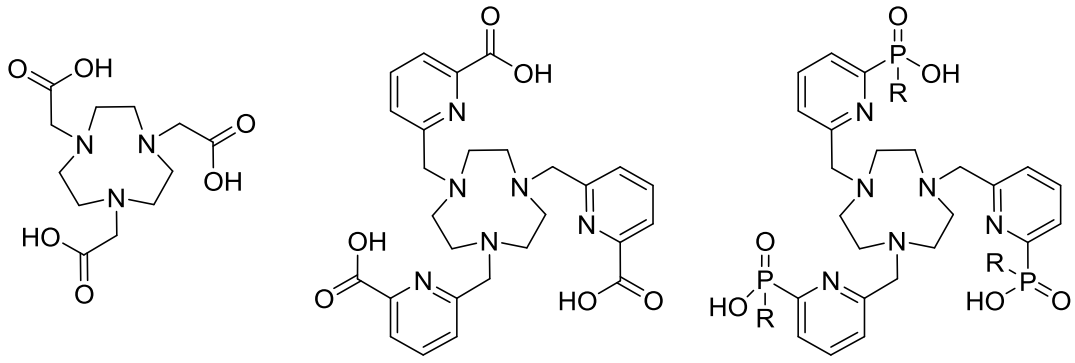

Figure 1.9 - Structure of NOTA (left), H_3tpatcn (centre), and the phosphinate analogue (right)[42]

The use of the pyridine group serves two purposes, as it can act as a sensitiser for the lanthanide ion, in addition to coordinating to the metal centre. However, simple pyridines with either phosphate or carboxylate groups absorb at or close to 280 nm which is not an appropriate wavelength for use in biological media for example. [43,44]

To rectify this, an extended chromophore can be utilised. With the addition of an electron rich aryl group connected through an alkyne linker, a charge separation along the axis of the chromophore is created. This creates an internal charge transfer (ICT) absorption band, which has a much higher molar extinction coefficient, compared to a pyridine group alone. It's first use as a lanthanide chromophore was in the 1990s as a label in immunohistochemistry.[45] It has since been engineered in 9-N_3 complexes and used with EDTA complexes with improved quantum yields. Use of [EuEDTA-$\mathbf{L}^{\mathbf{d\text{-}i}}$] (Figure 1.10) gave quantum yields of over 20% with one being three times higher than previously reported ligands in this class.[46]

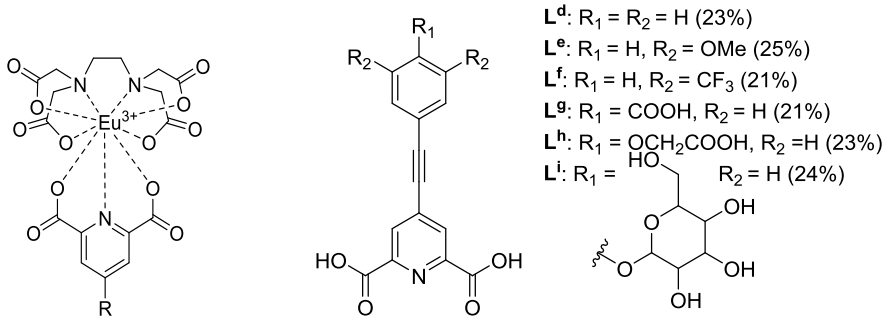

Figure 1.10 - (Left) Structure of [EuEDTA-$\mathbf{L}^{\mathbf{d\text{-}i}}$], (right) structure of $\mathbf{L}^{\mathbf{d\text{-}i}}$, with quantum yields ($H_2O$, 295 K) in brackets[46]

A series of 9-N_3 based complexes exist in which the use of these ligands to sensitise europium has been reported.[47,48] Many, but not all, use all three arms to ensure a nine coordinate environment. The pyridine is generally adorned with a carboxylate or

phosphinate group, with a variety of substituents on the aryl ring, most commonly substituted in the para position.

Work in 2008 looked at the possibility of sensitising a number of lanthanide ions, including near-infrared emitters such as neodymium and ytterbium.[30] The most efficient behaviour was found with europium complexes; quantum yields of about 40% in DCM were measured in this study and the authors predicted that further development of these brighter complexes would be very efficient for bio-probes. Following on from this work, both quantum yields and water solubility was improved. One complex in water gave a quantum yield of 32%, one of the highest reported in this solvent.[49]

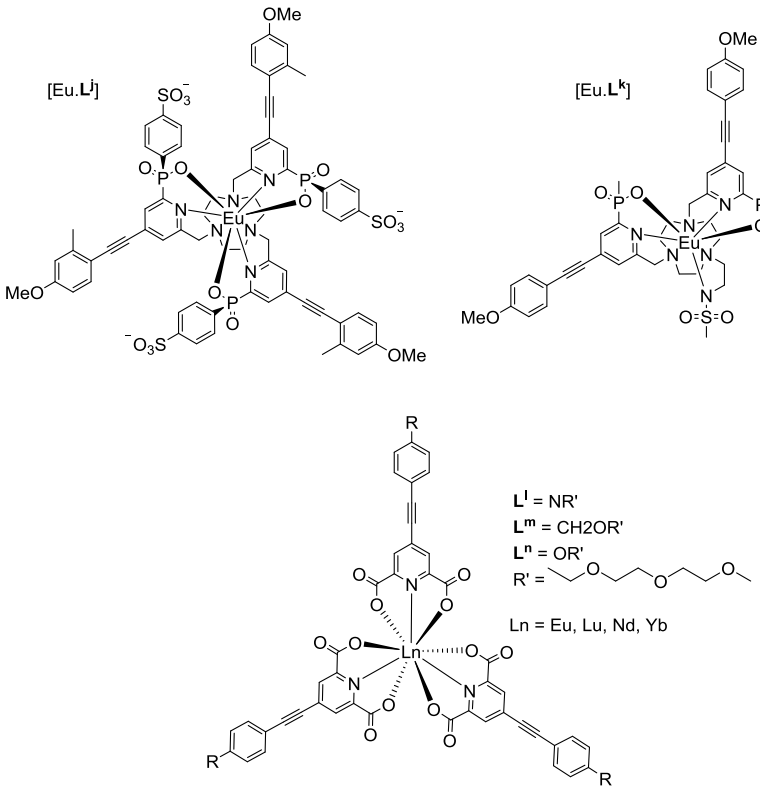

Figure 1.11 - The structure of europium complexes which utilise the extended chromophore[32,49,50]

More practical uses for these complexes have developed over time. For example, [Eu.**L**^{k}] (Figure 1.11) was used to monitor the pH in the endoplasmic reticulum (ER) of living cells.[50] The complex localised selectively in the ER. On protonation, the nitrogen in the sulphonamide arm detached from the europium, and was replaced with an inner sphere water. This process led to a decrease in emission intensity, as well as a change in the spectral form, allowing for ratiometric measurements. The change in pH could also be tracked using the change in lifetime. This emission behaviour is associated with the quenching effect of the bound water, at lower pH, and the reduction in intensity is not

ideal. The broad absorption maximum of the ICT transition in the complex is at 322 nm, and excitation at 355 and 365 nm is possible, so it can be safely used in cells without killing them. The use of time-gated acquisition allowed removal of organic auto-fluorescence, which could have otherwise obscured the europium emission.

Azaxanthones and azathioxanthones (Figure 1.12) have also been investigated as potential ligands for europium in biological media. The triplet state energy level was measured to lie at 24, 800 cm^{-1}, which is sufficiently high in energy to ensure minimal back donation from terbium, successfully sensitising both terbium and europium.[51] There are relatively few examples of its use in the literature thus far.

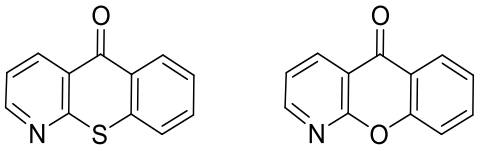

Figure 1.12 - Structure of axathiozanthone (left) and axazanthone (right)

An example of a europium cyclen based complex, [EuDAPA2], was found to successfully allow measurement of citrate and lactate in various biological media.[52] The 380 nm excitation for the azathioxanthone, and 336 nm for azaxanthone means that variety of excitation sources can be used.[53] Usefully, the aforementioned long fluorescence lifetimes of europium and terbium complexes allow the use of time-gated experiments to remove organic fluorescence interference.

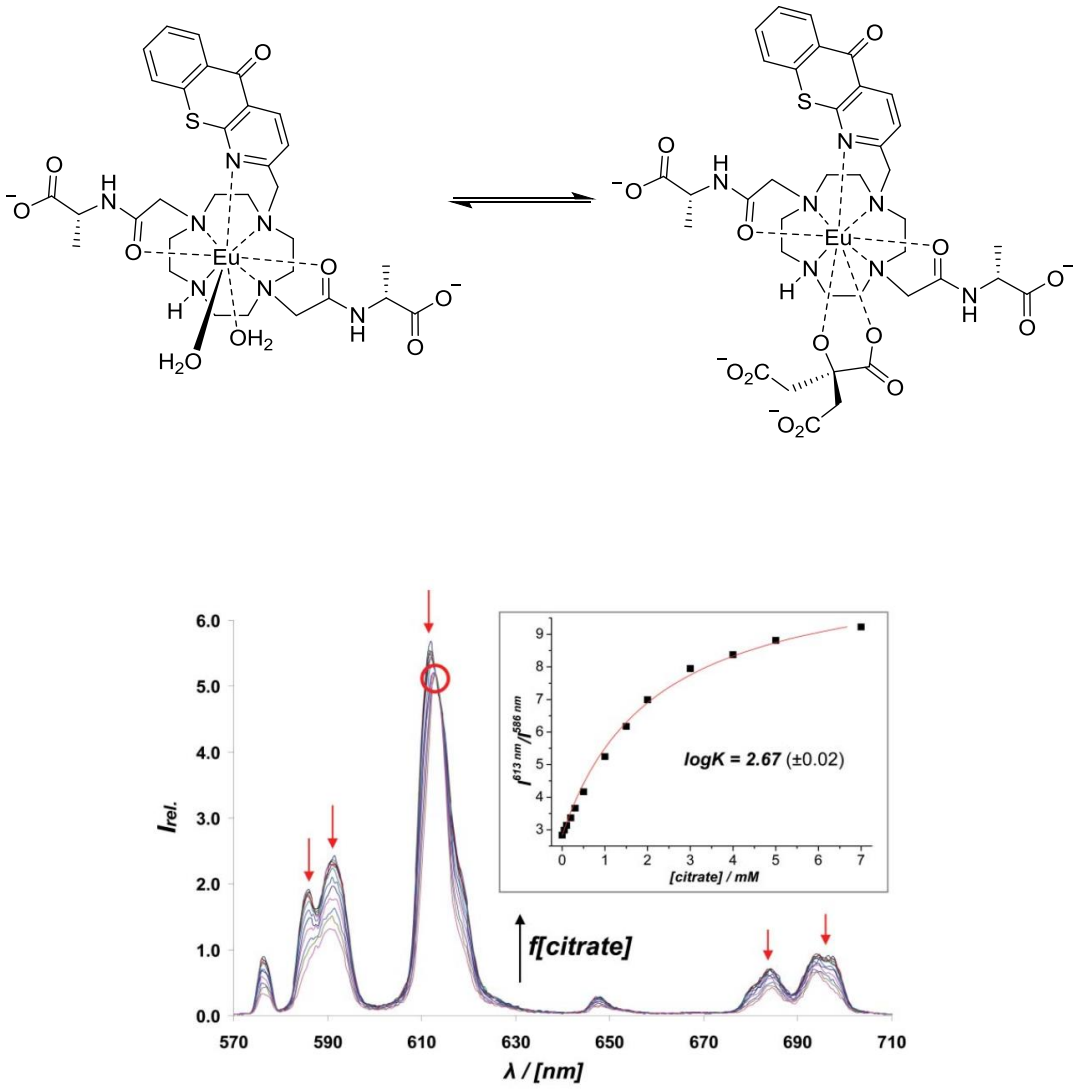

Figure 1.13 - Mechanism of how citrate binds to [EuDAPA2][52] (top) and the change in the emission spectrum upon addition of citrate (bottom) with the calculated binding curve (inset)

Citrate binds reversibly to the complex in a bidentate fashion, through the hydroxyl and the α-carboxylate groups, replacing two inner sphere waters. This binding event results in an increase in emission intensity, a change in spectral form and the lengthening of the luminescence lifetime. The 'switch-on' effect is another advantage for this complex. The importance of this probe's development is due to the fact that irregularities in low level of citrate can be indicative of prostate cancer.[54] Lactate can also bind to the complex in an analogous manner, but with a smaller binding constant. Therefore, a known excess of lactate was used to make up part of the assay to saturate lactate binding, and thereby ensure any change in emission spectral form was purely due to citrate.

The related azaxanthone chromophore, has been used in conjunction with terbium (Figure 1.14) to detect potassium.[55] K^+ is commonly found in biological systems, where

it influences a number of physiological processes. Selective binding over sodium, another common ion used in biological systems, is highly sought after due to the similarity of the two ions and their differing relative concentrations, making discrimination difficult. However, the toxicity of the complex was highlighted in the cell studies so further use of the compound in biological systems would not be advised.

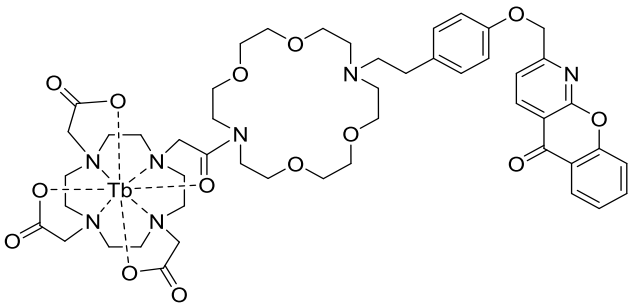

*Figure 1.14 - Structure of the [Tb.**L**^{o}]*[55]

This complex is designed slightly differently with the chromophore being separated from terbium by a diaza-18-crown-6 moiety. In the absence of the potassium ion, little terbium emission is observed. Upon binding of the ion in the crown, there is a preference for π-bonding between the crown and the aryl ether and hence the chromophore is brought significantly closer to the terbium ion, leading to enhanced emission.

A further example of an azaxanthone chromophore being used in the detection of biologically relevant compounds involved a dynamically racemic complex that binds alpha-1-acid glycoprotein (α_1-AGP) and alpha-1-antitrypsin (α_1-ATT).[56] These are both proteins found in the blood whose concentration changes dramatically in response to inflammation. Both were found to have an increase in emission intensity upon binding to the complex. Again, it is likely due to the replacement of a bound water with a glutamate side chain carboxylate. Binding was signalled by induced CPL, the concept of which will be discussed in the following section.

1.3 Circularly Polarised Luminescence

Circularly polarised luminescence (CPL) has been known since the 1940s but the method for the detection of this type of luminescence was developed decades later.[57] CPL is now a relatively well known technique, often used in conjunction with CD (circular dichroism). CPL is the emissive analogue of CD and gives information about the excited state of a compound based on the differential emission of left and right

circularly polarised light. It is inherently more sensitive than CD and is less affected by background luminescence.

1.3.1 Background and Theory

Light is classically known to be made of two main components, the magnetic and electric field vectors. CPL occurs because two components of the electric field vector are out of sync by a quarter of a wavelength. Depending on which of the two components are first, you can get left- or right- handed CP light (Figure 1.15).

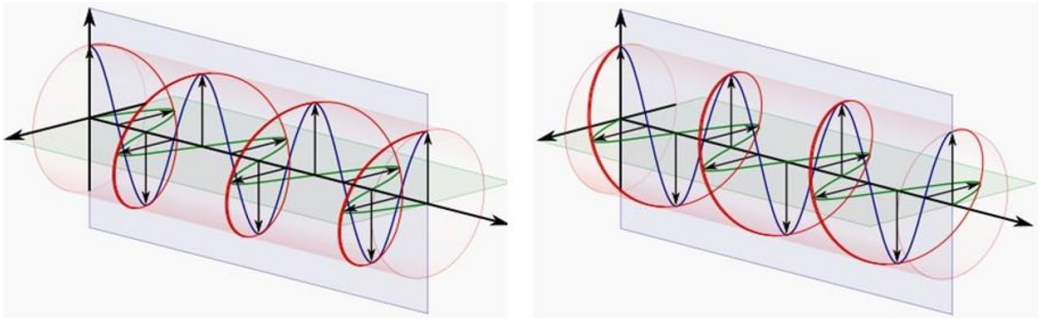

Figure 1.15 - Left and right circularly polarised light. The two perpendicular components of the electric field vector are depicted in blue and green

In CPL a measurement is made of the left versus right circularly polarised spontaneous emission, ΔI.

$$\Delta I = I_L(\lambda) - I_R(\lambda) \quad \textbf{(1.3)}$$

However, measuring absolute emission values can be difficult. CPL is most commonly reported as the dissymmetry value (g_{em}), defined in Equation **1.4**.

$$g_{em} = \frac{2(I_L(\lambda) - I_R(\lambda))}{(I_L(\lambda) + I_R(\lambda))} \quad \textbf{(1.4)}$$

Here, $I_L(\lambda)$ and $I_R(\lambda)$ are the intensities of left and right polarised emission respectively. It follows that the maximum values of g_{em} are ±2 and the absence of any circularly polarised luminescence gives a value of zero.

Alternatively, you can link the dissymmetry factor to the rotatory and dipole strength of the relevant transitions. A study by Emeis and Oosterhoff showed that these transitions can be linked to the electric dipole moment and the magnetic dipole moment.[58] Simplified, you can write the dissymmetry factor as:

$$g_{em} = \frac{4R_{ab}}{D_{ab}} \quad \textbf{(1.5)}$$

R_{ab} is the rotatory strength of the transition. It influences the sign and magnitude of the CPL signal. It can also be written as Equation **1.6**:

$$R_{ab} = |\mu||m|cos\tau \quad \textbf{(1.6)}$$

Where μ is the electric and m is the magnetic transition dipole, and τ is the angle between the two transition dipole moments. The dipole strength (D_{ab}) of the transition also plays an important role in the dissymmetry factor, contributing to the total emission.

$$D_{ab} = |\mu|^2 + |m|^2 \quad \textbf{(1.7)}$$

Substituting these two parameters into the equation for g_{em} gives:

$$g_{em} = \frac{4|\mu||m|cos\tau}{|\mu|^2 + |m|^2} \quad \textbf{(1.8)}$$

As the magnitude of the electric transition dipole moment is typically much greater than the magnetic transition dipole moment, we can assume the contribution of m^2 is negligible, and this can be simplified to give the equation:

$$g_{em} = \frac{4|\boldsymbol{m}|}{|\boldsymbol{\mu}|} cos\tau \quad \textbf{(1.9)}$$

The difference in electronic and magnetic dipole moments can be important in CPL detection. For example, in europium emission, the $\Delta J = 1$ transition is magnetic dipole allowed and electric dipole forbidden. Hence the $\Delta J = 1$ band typically gives large g_{em} values.

However, any chiroptical transition requires a non-vanishing rotational strength and for *f-f* transitions, such as those observed in lanthanide complexes, a vanishing rotational strength is expected. There are two mechanism that allow this for lanthanide species, static and dynamic coupling.[14] In static coupling, mixing of 4*f* and 5*d* orbitals may provide the odd parity necessary for the non-vanishing rotational strength. However, this can only happen if the coordination sphere is chiral so covalent contribution to the bonds between the lanthanide and the donor atoms must invoke such hybrids. However, lanthanide interactions with donor atoms are not known to be strongly covalent, and

therefore only weakly effect the metal ion. This mechanism varies with the twist angle of the ligand, and a maximum is reached when $\phi = 22.5^0$. For complex with much larger twist angles, static coupling is low and therefore, a second mechanism comes into play. It is possible to observe dynamic coupling between lanthanide and nearby ligand transitions, which have non-zero electric dipole allowed character. If the lanthanide is excited, its associated electric quadrupole induces an electric dipole moment on the ligand, which provides the necessary dissymmetry for a transition to be observed. For this mechanism to work, the metal centre and the ligand must be spatially close.

1.3.2 Instrumentation

Only in recent years has a commercially available spectrometer been marketed, the JASCO CPL-200.[59] A consequence of this is that there remain a number of 'in-house' spectrometers that were custom built in different departments which are fairly sensitive to CPL detection.[60] As there are a number of differences between each instrument, standardisation of measurements can be problematic. However, the essential components of the spectrometer set up are comparable.

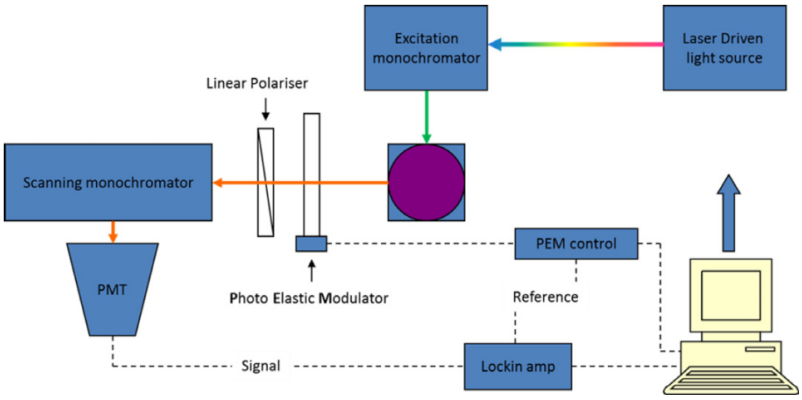

Figure 1.16 - A typical set up of a CPL spectrometer[61]

The incident light used to excite the sample, usually a laser driven light source, is typically linearly polarised or unpolarised. The high intensity increases the likelihood of photochemical degradation, but gives rise to a brighter CPL signal. The light is detected and modulated at 90° to the direction of this light (to stop saturation of the detector) by the photoelastic modulator (PEM). This is usually some form of isotropically clear optical material that becomes anisotropic on application of a stress period. The PEM is driven by AC light at a frequency of approximately 50 kHz and therefore acts as an oscillating quarter-wave plate. The consequence of which is the deceleration of light, which transforms left and right polarised light into linearly

polarised light. The light passes through a linear polariser, tilted to 45˚ and directed to the monochromator. It then goes through a photomultiplier tube (PMT) before detection. Early instrument designs, such as the one set up in Figure 1.16, used a lock in amplifiers to detect the difference in AC and DC current which is converted into the CPL and total luminescence signals respectively. Photon counting detectors are more commonly used now, which are both more reliable and easier to calibrate.

1.3.3 CPL Probes

The first set of chiral probes studied were small organic molecules (SOMs) which were examined during the discovery of CPL. Emeis and Oosterhof used bicyclic chiral ketones and studied the n→π* transition.[58] These compounds generally had weak fluorescence, and π conjugation was extended in an attempted to improve their oscillator and rotatory strengths. Other organic molecules which have been investigated include helicenes, and various twisted polycyclics.[62,63]

1.3.3.1 CPL of Small Organic Molecules

High dissymmetry is achieved when you have a transition that is magnetic dipole allowed and electric dipole disallowed, as highlighted in Equation **1.9**. Unlike lanthanide complexes, organic compounds do not usually have such a transition leading to difficulties when attempting to increase g_{em}. Despite the poor dissymmetry factor, a lot of research has sought to develop organic molecules that exhibit CPL activity, and seek a wide range of applications including sensors, displays and dyes.[64–66]

Due to the poor g_{em} values, the use of organic compounds as CPL emissive biological probes has not been deeply investigated. Dipyrrolyldiketone boron complexes are linear motifs and their luminescence properties arise following binding with anions, such as halides or amino acids.[67] A dimer of two of these complexes with a phenylene bridge can bind to halide ions resulting in an induced CPL response due to ion pairing between the chiral cations and the anion.[65] To bind bigger anions, a longer spacer group is necessary to form a large enough cavity. With a terphenyl linker, which can either be meta-meta-meta or para-ortho-para, it is possible to bind amino acids to these π-conjugated moieties and induce a CPL signal which is dependent on the chirality of the anion binding.[68]

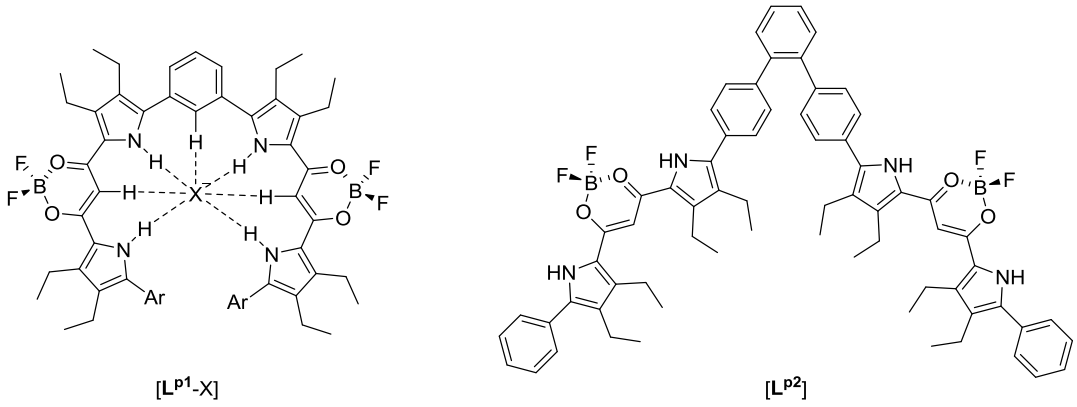

*Figure 1.17 - (Left) A dimer binding a small anion [**L**^{p1}-X] (X = halide). (Right) A terphenyl bridged complex capable of binding L-amino acids [**L**^{p2}]*[68]

However, the complex only gives rise to small induced g_{em} values, with a maximum of $7x10^{-4}$ at 553 nm.[68] The experiments were repeated at -50 ˚C as it was hypothesised this would more tightly curl the helices around the anion and change the ratios of the two diastereoisomers. Even at these temperatures, the g_{em} values were in the region of 10^{-3}; although this is an improvement by a factor of 10, the values themselves are still very small.

More recently a CPL-SOMs based on bis(haloBODIPY) have been studied.[69] One such example adopted a helical conformation in chloroform which gave rise to g_{em} values of ±0.001.[70] It was also found that with a small structural change in the compounds, opposite CPL signals were observed. Thus, upon replacing the nitrogen in *RR*-**L**^{q1} for oxygen (*RR*-**L**^{q2}), the CPL signal goes preferentially from left-handed light to right. Such a small modification in the compound leading to opposite chirality is an exciting piece of research.

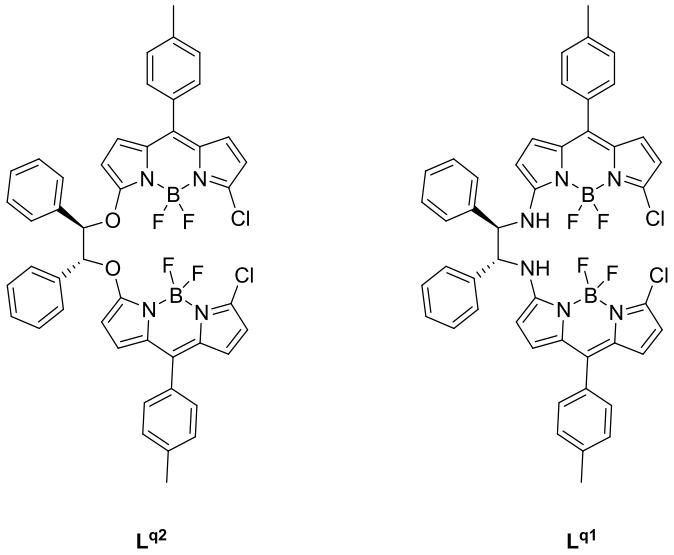

Figure 1.18 - RR- enantiomer of two chiral CPL-SOMs based on haloBODIPY moieties[70]

All SOM probes investigated so far have very small g_{em} values, in the region of 10^{-4}. However, whilst these values are still too low to be of use as CPL emissive biological probes, this research is good ground work for their longer term use, such as in 3D displays, security and informational storage.

1.3.3.2 CPL in Transition Metal Complexes

The use of heavy metals can offer an advantage in helicene chemistry in particular. For example, it can act as a template, as is well known through coordination chemistry of transition metals. Furthermore, as it is possible to vary the metal centre or the coordination sphere geometry, it offers a method to tune the chiroptical and electronic properties of the complexes. A number of metal complexes have been investigated, including those of platinum and rhenium.[71] There are fewer examples of rhenium complexes owing to the poorer overlap of rhenium *d* orbitals with the conjugated system. Hence, the g_{em} values for rhenium are smaller (g_{em}~10^{-3}) than have been found with platinum (g_{em}~10^{-2}).[72] Iridium complexes have also been investigated, but show smaller g_{em} values than with platinum, for similar reasons (g_{em}~10^{-3}).[73]

An example of the use of an organometallic helicene has been reported as a pH probe.[74] The study looked at the comparison of an organic and organometallic system. The change of pH in the organic helicene resulted in no change in the g_{em} values. However, in the organometallic system upon protonation, the g_{em} value doubled.

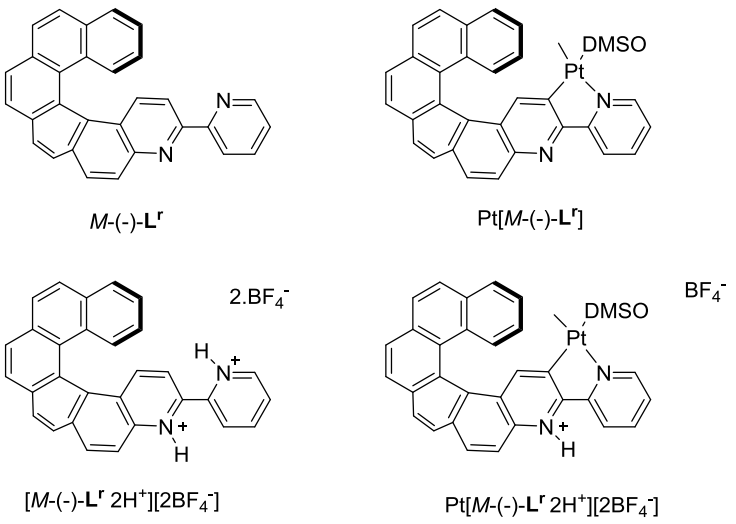

*Figure 1.19 - Organic and organometallic helicenes M-(–)-**L**^{s} with potential as a CPL probe*[74]

Both enantiomers of this helical structure *P*-(+)- and *M*-(–)- were made, confirmed by their mirror image CPL spectra, with the pronated ligand giving g_{em} values of +3.2 x 10^{-3} and -2.5 x 10^{-3} at 590 nm respectively. For Pt[*P*-(-)-L^{r}] and Pt[*M*-(-)-L^{r}], g_{em} values of +1 x 10^{-3} and -1.1 x 10^{-3} were found. Upon protonation of the platinum complexes, the CPL activity is approximately doubled giving g_{em} values of +1.8 x 10^{-3} and -2.2 x 10^{-3} for *P* and *M* isomers respectively, where λ_{max} = 590 nm. By comparing the response of the organic and organometallic helicenes, using various techniques, the compounds can be considered as multi-modal probes. However, these values are still an order of magnitude lower than those previously found in platinum complexes and there are other ways in which the probe works in a more effective manner (CD and UV/vis) which means it is unlikely to be used purely as a CPL probe.

The highest known g_{em} value for a platinum helicene was publish in 2014, where enantiopure complexes were obtained following column chromatography and recrystallization (Figure 1.20).[72] All complexes gave g_{em} values in the expected region of transition metals of $10^{-3/-4}$, with the exception of **L**^{s6}. This gave a value of 10^{-2}, which is the highest value obtained for a molecular helicene. Of note in this paper, is that upon the addition of the metal ion, the g_{em} value increases the CPL signal by approximately 100-fold.

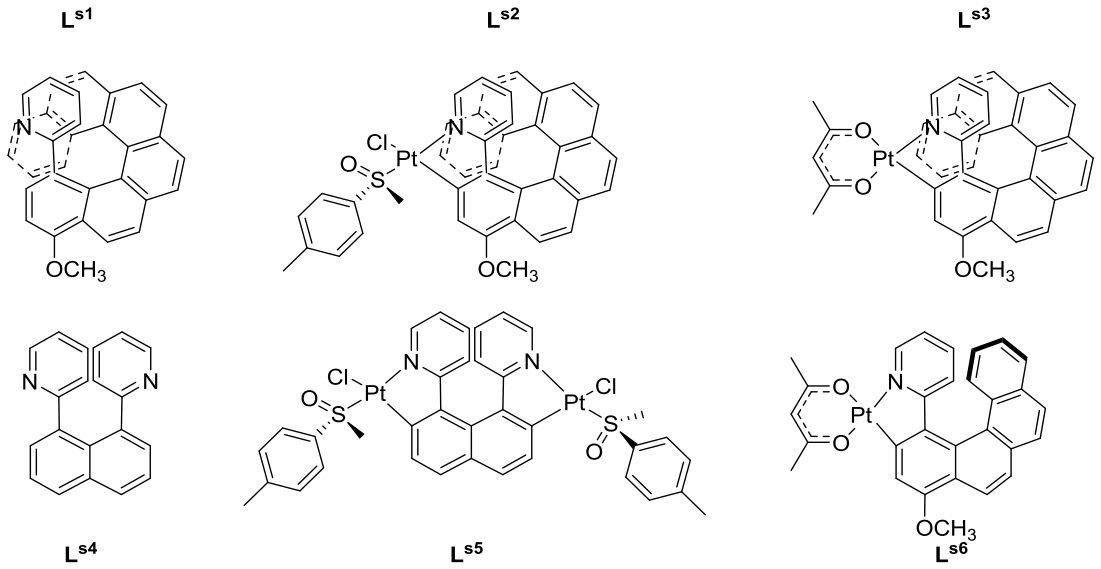

Figure 1.20 - Structure of ***L****$^{s1-6}$*

Another point to note is that previously reported helicenes have all been fluorescent systems. The spin-orbit coupling of the platinum(II) valence orbitals promotes rapid ISC to the T_1 state, which diminishes the fluorescence intensity and is accompanied by phosphorescence.

Even though transition metal complexes do give g_{em} values which are an order or two higher than SOMs, these values are still very small and liable to error. Further improvement in the size of the CPL signal is needed before these complexes can be considered for biological systems in particular.

1.3.3.3 CPL Studies of Lanthanide Complexes

Lanthanides, particularly europium and terbium are useful optical probes, and are used in a number of other luminescent studies due to their attractive photophysical properties including their narrow emission bands and long luminescence lifetimes. With CPL, they have a further advantage of large emission dissymmetry factors.[75] They act as pure spherical emitters, which negates the problem of anisotropy.

There is a wide range of europium complexes that are CPL active, with an intense $\Delta J = 1$ band. This transition has purely magnetic dipole character which is a requirement for large dissymmetry factors. Although terbium's transitions are not as favourable, it generally has higher luminescence intensity which can be useful in obtaining a signal. There are relatively few other examples of reported CPL active lanthanide complexes. However, Richardson's classification, which identified which transitions have expected high dissymmetry factors, suggests that samarium's $^4G_{5/2}$ to $^6H_{5/2}$ transition should be as

favourable as terbium's main transition.[76] Unfortunately, due to multiphoton quenching, samarium complexes are often weakly luminescent, and there are very few reported CPL active complexes.[77,78] However, one example, Cs[Sm((+)hfbc)$_4$], gives a g_{em} value of -1.15 and +1.15.[79]

The highest ever recorded g_{em} value is a europium complex with a value of +1.38. The complex studied was a tetrakis((+)-3-heptafluorobutylyrylcamphorato) (hfbc) lanthanide(III) complex with a caesium counterion.[80] The nature of the alkali metal counterion was important with a 9-fold increase in g_{em} between Na and Cs, and a significantly smaller g_{em} value in the absence of an alkali metal cation.

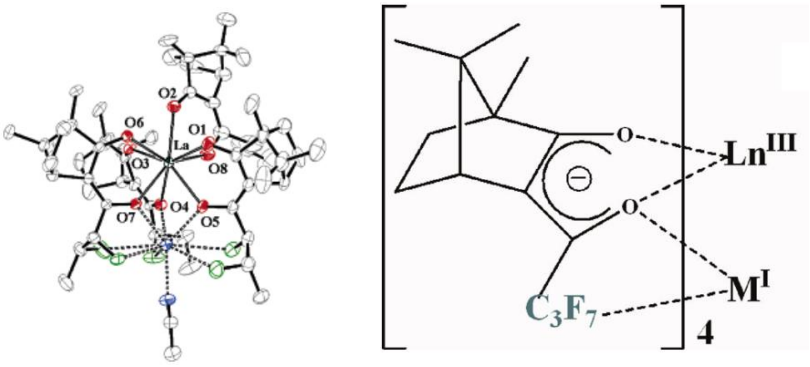

Figure 1.21 - (Left) A crystal structure of Na[Eu((+)-hfbc$_4$].CH$_3$CN.[81] *(Right) The structure of one ligand and how it is predicted to interact with both the lanthanide ion and alkali metal*

Further studies changing the alkali metal ion were conducted.[79] An increase in CPL intensity with increasing ionic radius of the metallic ion was observed in chloroform. In acetonitrile, the effect was not observed to the same extent, with much less variation in the g_{em} value. Therefore, the authors declared that solvent does play a significant role in the intensity of the emission. However, they did not consider a possible role of aggregation in rationalising this behaviour, nor any shift in the orientation of the main component of the magnetic susceptibility tensor with solvent or cation variation in the ion-pair.

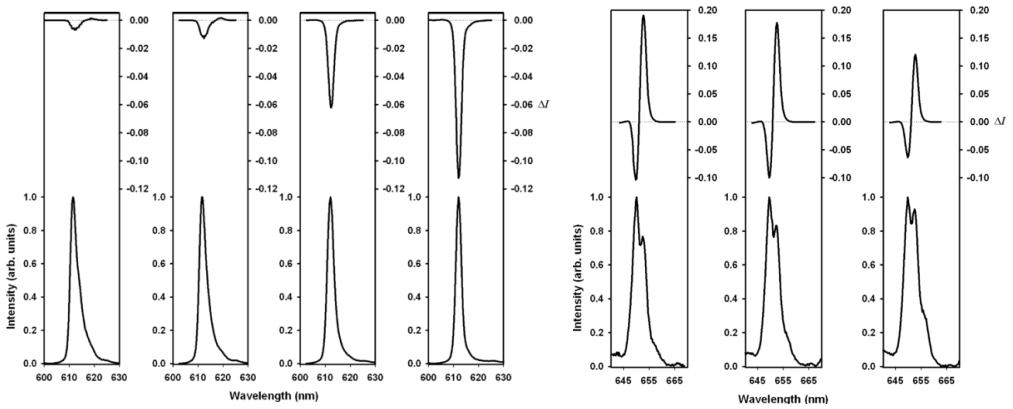

Figure 1.22 - The CPL (top) and total emission (bottom) signals of the (left) ΔJ = 2 transition from (left to right) Na-Eu, K-Eu, Rb-Eu and Cs-Eu, and (right) the ΔJ = 3 transition in (left to right) EtOH, CH_3CN and $CHCl_3$[79]

Due to the high g_{em} value, further work has examined potential uses. After mixing the europium complex with polyvinylcarbazole (PVK) and 1,3-bis[2-(4-tert-butylphenyl)-1,3,4-oxadiazo-5-yl]benzene (OXD7) a doped thin film was formed for use as a circularly polarised LED. A g_{em} value of +0.75 in the film was measured, which although is far below the complex in solution, it is the highest ever measured for a CP LED.[82]

One of the few examples of stable and enantiomerically pure *f*-helicates that display europium centred CPL was reported by the Gunnlaugsson group.[83] A dimetallic europium structure with three identical helicate ligands was investigated. Excitation of the naphthalene antenna at 340 nm gave rise to relatively large dissymmetry factors of -0.23 for the 593 nm transition ($\Delta J = 1$). However, all of these examples were examined in acetonitrile and methanol and are not applicable to more competitive media.

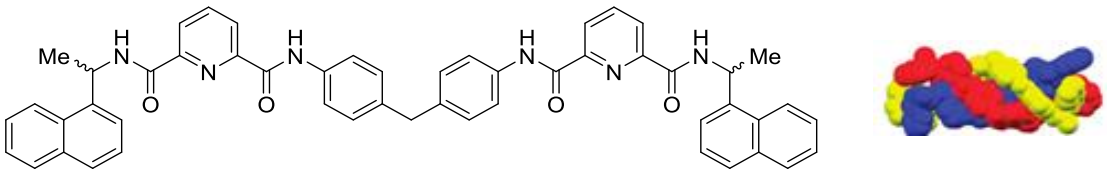

Figure 1.23 - (Left) Structure of $\boldsymbol{L^u}$ *used in complex. (Right) 3-D structure of the europium complex*[83]

In other work, changes in the CPL fingerprint upon binding to different proteins has been investigated. It was found that the CPL of one enantiomer of a lanthanide complex changed upon binding to human and bovine serum albumin.[84]

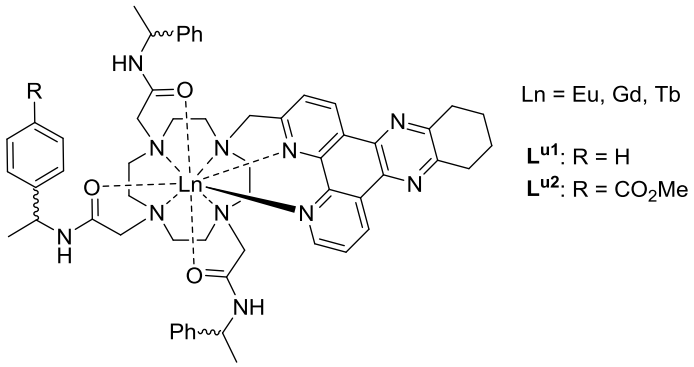

*Figure 1.24 - The racemic structure of [Ln.**L**^{u1,2}]*

The complex, [Ln.**L**^{u1}], for example, was found to bind to 'drug site II' reversibly, inverting the CPL signal, suggesting that there is a radical change in complex helicity upon binding. The effect was only seen with the (*SSS*)-Δ complex, and only with serum albumin. The only change in the CPL spectrum for the (*RRR*)-Λ complex upon binding was a decreased signal. The lack of change in only one enantiomer makes the complex a unique chiroptical probe, specific to reversible albumin binding.

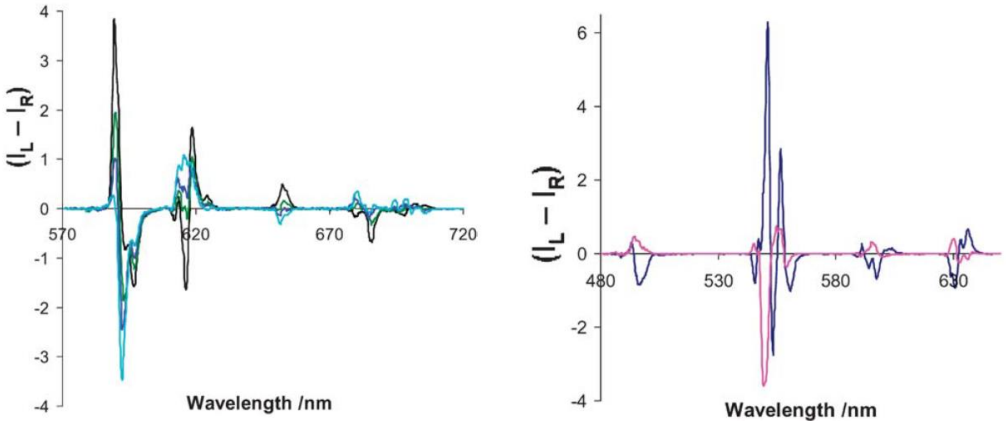

*Figure 1.25 - The CPL spectra of (*SSS*)-Δ –[Eu.**L**^{u1}]$^{3+}$ (left, black) with BSA (blue/green) and (*SSS*)-Δ-[Tb.**L**^{u2}]$^{3+}$ (right, black) and in the presence of BSA (pink)*[84]

Other responsive probes include those that induce a CPL signal upon anion binding. One such example is a set of dynamically racemic europium complexes (Figure 1.26) with which induced CPL spectra are observed upon binding to certain phosphorylated amino acids, e.g. O-phosphono-Ser and Thr.[85] Chemoselective binding of the phosphate oxygen to the lanthanide centre occurs in this case.

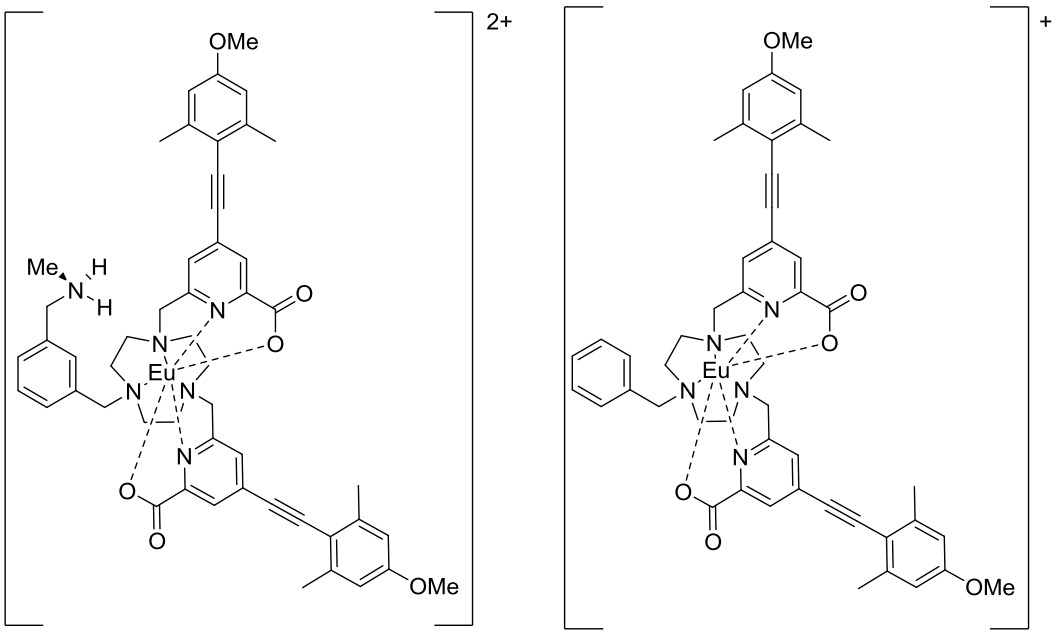

*Figure 1.26 - Structures of [Eu.**L**^{v1}] and [Eu.**L**^{v2}]*[85]

In a control experiment, it was shown that the CPL response did not occur for the non-phosphorylated peptide. It is also interesting to note that there is no CPL response when O-P-Tyr itself was added. The O-P-Tyr residue must be part of the peptide chain for a CPL response to be induced. Upon binding to a phosphorylated peptide chain, a g_{em} value of +0.10 were observed, one of the highest induced CPL values observed with a dynamically racemic europium complex in purely aqueous media.

It was also possible to see a change in sign of the CPL signal when different peptides were used; suggesting the chiral response of the bound species is associated with the particular peptide rather than just the presence of one amino acid. The solubility of these complexes was their downfall, with 50% MeOH being necessary. The issue needs to be addressed, perhaps with analogues bearing peripheral sulfonate groups to allow more extensive studies.

The complexes, [Eu.**L**$^{v1-2}$] are not the only examples of dynamically racemic complexes exhibiting chiral properties upon binding to biologically important proteins. Other europium and terbium complexes have also been explored, examining their use in binding lactate and malate.[61]

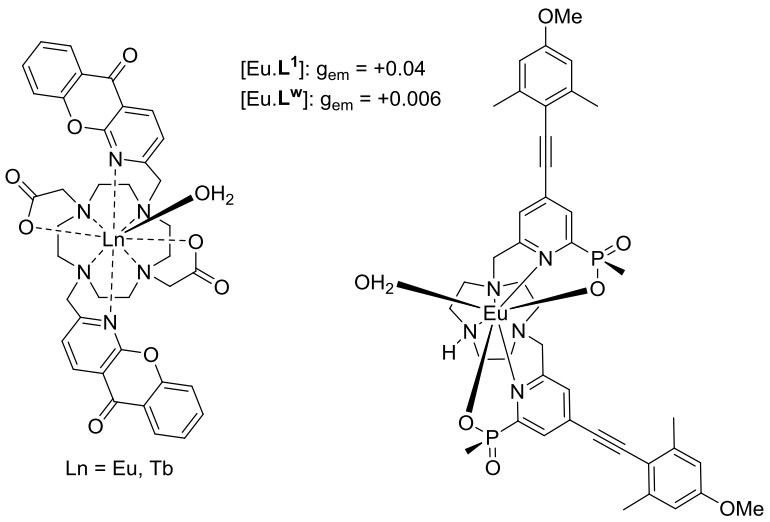

*Figure 1.27 - Two complexes, [Ln.**L**^{1}]$^{+}$ (Ln = Eu, Tb) (left) and [Eu.**L**^{w}] (right,) which were found to bind bioactive anions to give a chiroptical response*[61]

For each of these complexes, binding of lactate was associated with an induced CPL signal. It was found in the $\Delta J = 2$ manifold, that [Eu.**L**^{1}]$^{+}$ had a g_{em} value (+0.04) almost an order of magnitude greater than that of [Eu.**L**^{w}] (+0.006). It is thought the difference in g_{em} values stem from the different ways that lactate binds. For [Eu.**L**^{1}]$^{+}$, dissociation of one azaxanthone nitrogen is followed by formation of a five-membered chelate involving the hydroxyl and acid groups of the lactate. However, when [Eu.**L**^{w}] binds to lactate, it does so in a bidentate fashion through the carboxylate group alone.[86] The helicity of the complex was determined by the nature of the enantiomer bound, with the g_{em} values being equal and opposite for addition of *R*- and *S*- enantiomers. Furthermore, the binding constants for the two enantiomers to [Eu.**L**^{w}] were identical (log$K$ = 2.41 (±0.05)). The strong binding behaviour coupled with the strong CPL signal means these complexes offer a good basis for further development, allowing CPL to be used to track changes in helicity of such lanthanide ternary complexes.

Although CPL has been known to exist for nearly 40 years, taking information directly from experimental spectra is still difficult. For example, it is not usually possible to assign absolute configuration by inspection of the CPL spectrum. Work has been carried out into related structures to see if empirical rules can be determined, and it is thought that a stable range of helical complexes, including [Ln.**L**^{x1}] and [Ln.**L**^{x2}] could be used to achieve this.[87]

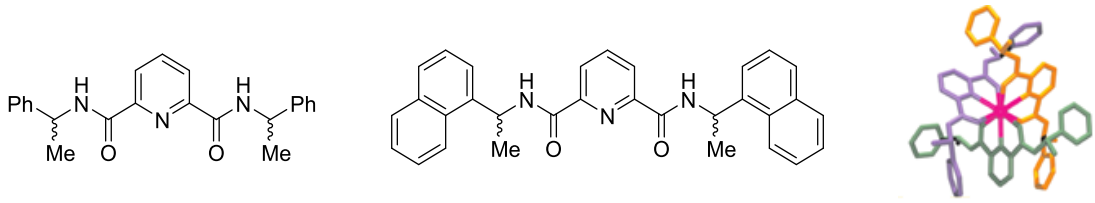

Figure 1.28 - Two ligands $\boldsymbol{L^{x1}}$ *(left) and* $\boldsymbol{L^{x2}}$ *(centre) that could potentially be used to work out empirical rules for CPL and (right) crystal structure of* Λ*-[Eu.((R,R)-*$\boldsymbol{L^{x1}}$*)*$_3$*]*$^{3+}$[87]

One such example of this approach involved the series of tetrakis((+)-3-hfbc) lanthanide(III) complexes which have a high symmetry, as previously mentioned [Page 24].[79] It was found that a positive CPL value in the $\Delta J = 1$ band was consistent with a Δ configuration of the ligand.

Although this is true for these symmetric complexes, more general rules should be considered to help calculate the local configuration from the CPL data. To attempt this, studies have looked at the development of a series of cyclen based structures.[88] One study concluded that there are three major factors that determine the CPL data; firstly the nature of the ligand, as the axial donor plays a large role in the hypersensitive transitions as well as magnetic dipole allowed transitions where it contributes to *J*-mixing; the second is the helical twist of the complex which can be written as $\sin 2\theta \cos 2\theta$ for SAP (square anti-prismatic) complexes; thirdly, the angle between the electric and magnetic dipole moment transition vectors which determines the rotatory strength.[89]

Work has also been carried out on several series of triazacyclonane compounds.[42] It is easier to study structurally similar compounds and in one study, they all bore two aralkynyl pyridyl moieties allowing space for chiral carboxylates, which induced a CPL signal upon binding.[90] It was found in all cases, that an *R*- chiral carboxylate gave rise to emission typical of a Δ complex.

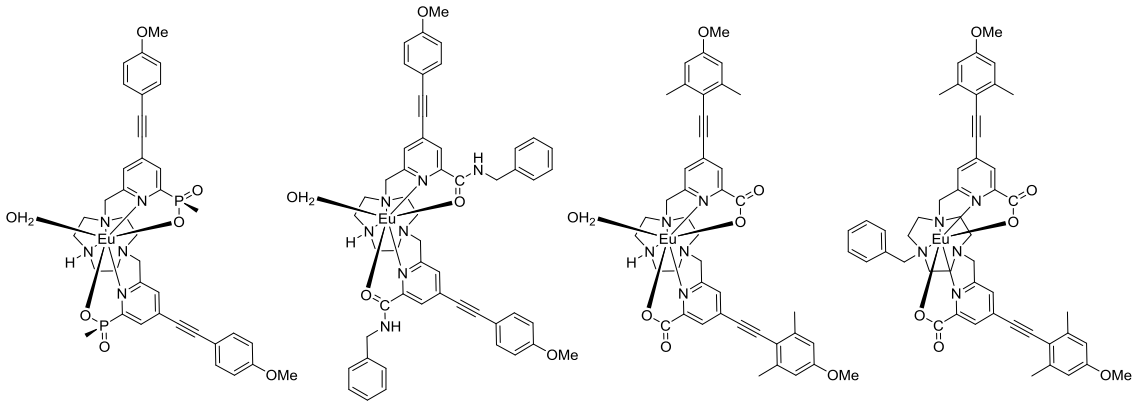

Figure 1.29 - The structures of four triazacyclonane with arylkynyl pyridyl moieties used in a structural study[90]

Advancement in this field continues, and the configuration can be calculated for some complexes, particularly if it is structurally similar to complexes already studied. For a completely new complex however, this method may not be reliable.

1.4 Alpha-1-acid Glycoprotein as a Chiral Protein

A vast number of proteins exist within the blood stream for a variety of reasons, from transport such as haemoglobin, to immune response such as the immunoglobulins. Many also interact with drugs and can have an important effect on their bioavailability. Serum albumin, exists in high concentration, with levels of approximately 30-50 g/L (0.4-0.7 mM) as quoted by Weaving.[91] However, this protein does not seem to have such an effect on changes in drug bioavailability as other proteins such as alpha-1-glypcoprotein (α_1-AGP). This is due to the fact that levels of HSA remain relatively constant in all conditions, whereas α_1-AGP concentration can change dramatically in an inflammatory response.

α_1-AGP is a 183 chain amino acid, a 41-43 kDa glycoprotein, with a pI of 2.8-3.8.[92] Its normal concentration is in the range 0.6-1.2 mg/mL (15-29 μM), which means it only contributes to 1-3% of the total plasma protein. It is also a positive acute phrase protein, meaning that its concentration increases several fold in response to inflammation or stress.[93] The concentration of this protein is known to be affected by a wide range of situations. Men have slightly higher levels than women, and its levels have been reported to increase in females with age, but not males.[94] This behaviour is important as it has a wide range of applications, some of which are known while others are still being investigated. For example, it is thought to play a key role in immune function and to have anti-neutrophil and anti-complement activity.[95] It has also been found to bind to a

wide range of neutral and alkaloid drugs as well as steroids, having a serious consequence on their bioavailability.[96,97]

α_1-AGP has two main genetic polymorphs, A and F1*S.[98] The genetic differences in the polymorphs mean that they do not have identical drug binding abilities. The level of glycosylation can also vary as quoted by Hochepied, and many studies thus far, concentrate on a mixture of these variants. [92] There are five *N*-linked glycosylation sites, and the level of glycosylation changes with varying conditions.[99,100] It has been shown, that varying levels of glycosylation can have an effect on the biological properties of the protein. Furthermore, variation can occur within one person under a range of conditions. For example, if they get pregnant, or if they suffer from hepatitis.[101,102]

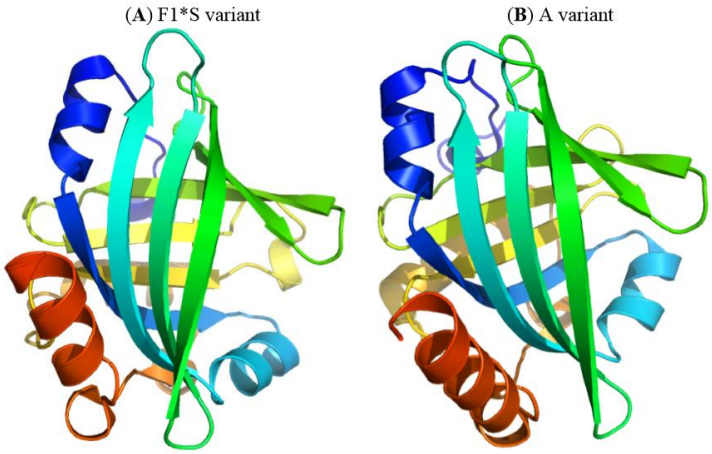

*Figure 1.30 - The protein structure the F1*S (left) and A (right) variant of α_1-AGP*[103]

HSA is well known to bind a wide range of acidic drugs, whereas α_1-AGP binds predominantly basic drugs, as well as some neutral drugs, both of endogenous and exogenous origin. Due to HSA's binding preference and predominance, it has generally been assumed that α_1-AGP does not affect the free concentration of acidic drugs. However, studies show that the association constants to α_1-AGP are sufficiently high, particularly when concentrations are elevated, that variations in protein concentration may affect the bioavailability of some acidic drugs.[104]

Up to seven sites on α_1-AGP at 4 °C have been described for estradiol, an endogenous steroid, whereas only a single site has been found to bind acidic drugs.[105,106] It is also believed that acidic drugs, which have an affinity for this site, also bind to site I on HSA, or the warfarin site. Drugs that contain a carboxylic acid group and bind to drug site II on HSA (diazepam site) generally have a poor affinity for α_1-AGP.[107]

The difference in drug binding between genetic variants, F1*S and A has been partially investigated.[108,109] In some cases, there is no selectivity between the two polymorphs, but in others there is total preference for one over the other.[110] However, as stated before, most of the research in binding to α_1-AGP has been undertaken using a mixture of polymorphs and there is not much reliable data detailing the differences between the two and why they bind so differently.

1.5 Pharmaceuticals; Methadone, Imatinib, Disopyramide

The pharmacological drugs being investigated within this thesis, in the context of competitive α_1-AGP binding, are all basic drugs that are used in a wide range of treatments. Methadone, disopyramide and imatinib all work on the body in various ways, and each has been shown to bind strongly to the protein α_1-AGP, with an affinity in the range of 10^5 to 10^6 M^{-1}. These drugs were also specifically chosen due to their λ_{max} being sufficiently low to avoid competitive absorption with the chromophore, with values of 270 nm, 254 nm, and 292 nm respectively.[111]

Two of the three (methadone and disopyramide) are chiral compounds, which is important to note because of the potential for the two enantiomers to have different pharmacological effects. It is also important to note that for these drugs, increased levels of α_1-AGP could limit the bioavailability of the drugs, which may have important ramifications on the physiological response.

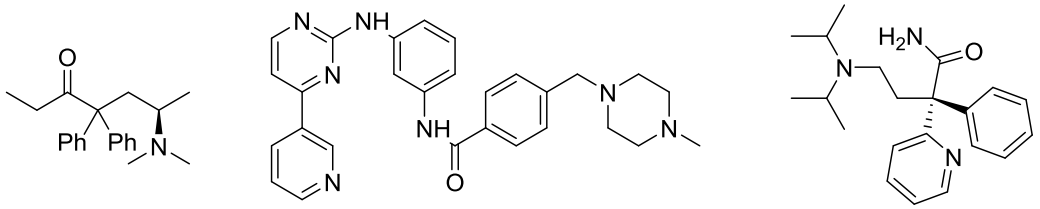

Figure 1.31 - Three drugs being investigated in this report, S-methadone (left), imatinib (middle) and S-disopyramide (right)

Methadone is used in pain medication, but is also used in maintenance therapy to treat morphine and heroin addiction. In the treatment of addiction, too low a dosage of methadone causes 'cold turkey' like symptoms which often leads to a relapse. However, too high a dose can lead to feelings of euphoria and overdose, so the concentration given to the patient is important. The binding of methadone to α_1-AGP was interpreted in terms of two types of binding sites with the stronger one giving a K_a value of $4x10^5$ M^{-1}.[112] It was also found that methadone could be displaced from these binding sites by

other drugs, such as chlorpromazine and imipramine. It has been hypothesised that the reason for the low percentage of complete abstinence from opioids from this particular treatment could be due to varying levels of α_1-AGP.[113]

The two enantiomers of methadone are known to elicit different clinical responses. Indeed, some maintenance treatment centres only prescribe (*R*)-methadone over the racemic due to fears of QT interval prolongation (Figure 1.32), which is linked to (*S*)-methadone, as well as being able to give a lower dose.[114] However, the single enantiomer is more expensive, and it is not currently widespread practice to prescribe solely (*R*)-methadone.

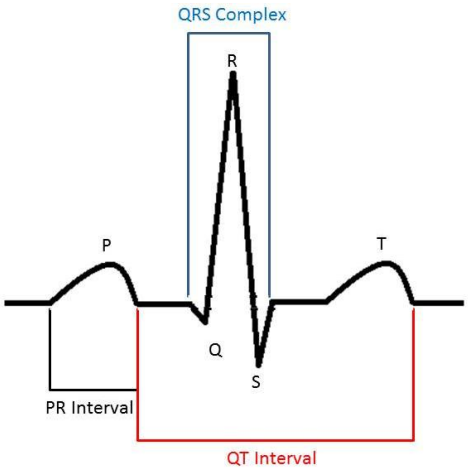

Figure 1.32 - An ECG diagram highlighting the PR interval, the QRS complex and the QT interval

Thus far, no experiments have been done specifically on the binding of the two enantiomers of methadone with α_1-AGP. However, due to the different properties, their efficacy and differences in how they act in the body have been studied. (*R*)-methadone is a μ-opioid receptor agonist (MOR), which mimics endogenous compounds such as endorphins and enkephalins. Hence, at high enough concentrations, a euphoric high is achieved. (*S*)-Methadone is a poor MOR agonist, but can block hERG (human Ether-à-go-go-Related Gene) channels which has been postulated to be the reason behind the problems with arrhythmia and sudden death that have been found in some patients taking methadone.[115,116]

Racemic disopyramide is used in the treatment of ventricular tachycardia. This illness is defined as a regular and fast heart rate, which can potentially lead to cardiac arrest if untreated.[117,118] It occurs due to improper electrical signals in the ventricles of the heart. Symptoms can go unnoticed if it occurs for only a small amount of time, or can cause dizziness and chest pain. It can be diagnosed through an electrocardiogram (ECG)

which shows a heartbeat faster than 120 beats per minute and at least three wide QRS complexes in a row.[119]

Disopyramide is a 'class 1a' antiarrhythmic agent meaning it works as a sodium channel blocker. It decreases the uptake of sodium during the initial stages of the heart beat that prolongs the PR interval, slowing down propagation of the action potential from the atria to the ventricles. It has been found that levels of α_1-AGP increase two-fold when acute myocardial infarction (AMI) occurs, which has implications for the efficacy of disopyramide.[120]

In one study, the two enantiomers of disopyramide were separated by chiral HPLC and the individual binding constants to α_1-AGP were calculated. The binding constants were found to be log$K$ = 3.20 and 3.47 (303 K).[121] Clearly, there is a small difference in binding between the two enantiomers but what the research did not report, is the configuration assignment of the enantiomers. It was shown that the enantiomer which eluted second had a higher binding constant compared to the first, for α_1-AGP. However, both of these values are two orders of magnitude smaller than with the A variant of α_1-AGP, suggesting that the genetic variation may play a hugely different role.

Imatinib, sold commercially as Gleevec, is used in the treatment of multiple cancers, including chronic myelogenous leukemia (CML).[122] CML is associated with the Philadelphia chromosome, which leads to the formation of BRC-ABL gene fusion.[123,124] It translates into an enzyme, BRC-Abl, a tyrosine kinase, which is stuck in the 'on' position. Therefore, the addition of phosphate groups to tyrosine becomes unregulated, activating a cascade of proteins leading to rapid cell division. Imatinib targets tyrosine kinase to slow the growth of this cancer. Up until the 1980s, this form of cancer was thought to be untreatable, but now there is complete or nearly complete cytogenetic remission in up to 80% of patients.[122] However, studies have shown that imatinib binds to α_1-AGP, but the level of available drug could increase in the presence of other drugs which bind to α_1-AGP, such as clindamycin.[125]

The three drugs discussed above have each been shown to bind with varying degrees of affinity to α_1-AGP. Although direct comparisons cannot be made between the drugs, the literature binding constants do give a good idea on their relative free energies of binding. The reason they cannot be compared directly is due to the fact that different

research groups have explored the area using a variety of experimental conditions, with different pH, temperature and solvent conditions. These can each lead to variations in the binding affinity to α_1-AGP. Furthermore, some studies examined particular variants of the protein, e.g. comparing A and F1*S, while others examine a mixture of these polymorphs.

Table 1.1 - Literature binding constants of the pharmaceuticals to α_1-AGP. (298 K, pH 7.4 in buffer unless stated otherwise, where not stated in the literature, these conditions are assumed.) (–) Values not documented in the literature

Drug	log*K* - unfractionated α_1-AGP (M^{-1})	log*K* - A variant	log*K* - F1*S variant	Absorption maximum (nm)
Imatinib	6.38 (±0.2)[126]	–	6.23 (±0.05)[126]	292
Methadone	5.60 (±0.08)[112a]	6.00 (±0.05)[127]	–	270
Disopyramide	3.20, 3.47[121b]	6.40 (±0.02)[127]	–	254

Methadone and disopyramide have been shown to bind to the A variant of α_1-AGP with log*K* values of 6.00 (±0.05) and 6.40 (±0.02) respectively.[127] These numbers suggest disopyramide binds more strongly than methadone, but it is possible that binding to the second variant of α_1-AGP could be very different. The value for methadone is similar to the value reported for unfractionated α_1-AGP, suggesting that the variants give similar values of binding.

There are a number of different binding studies reported on imatinib. Again, they were undertaken with different conditions and the method used to calculate the binding constant is different in each case. They do, however, all give values of the same order i.e. approximately 10^6. The binding of imatinib to F1*S was also investigated, and a binding constant of 1.7 (±0.2) x 10^6 was found at 37 °C. The A variant on the other hand was found not only to bind more weakly to α_1-AGP but also was less specific.[126]

1.6 Glyphosate as a Herbicide

Glyphosate (*N*-(phosphonomethyl)glycine) is a broad-spectrum, post-emergence, systemic herbicide which is popular due to the increasing demands of intensive farming. It was first discovered to have herbicidal properties by Monsanto in the early 1970s, was patented in 1974 as the active ingredient in Roundup and by 1980 was already one

[a] 37˚C
[b] pH 4.0

of the fastest selling herbicides.[128] Since the patent expired in 2000, it has become the most widely used herbicide by volume, being manufactured and sold by various companies around the globe.[129] The popularity of glyphosate was firmly established as Monsanto developed 'Roundup Ready' crops, such as cotton, corn and soybean which were resistant to the herbicide and are now widely grown.[130]

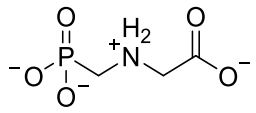

Figure 1.33 - Structure of glyphosate

However, over the past few years, increasing concern over the safety of the chemical led to thorough investigations into the possibility of its potential carcinogenic properties.[131] Thus far the IARC (International Agency for Research on Cancer) in 2015 is the only international organisation to label glyphosate as potentially carcinogenic to humans. In the same year the EFSA (European Food Safety Authority) found that it was 'unlikely to pose any carcinogenic hazard to humans'.[132] These opposing views led the EU to ask for an independent study to be completed by the European Chemicals Agency (ECHA). In June 2017, they declared that there was not sufficient scientific evidence to classify glyphosate as carcinogenic.[133] Nevertheless, wide-spread concerns with the herbicide has led to a shorter renewal period of five years rather than the standard 15 by the European Commission in December 2017. The use of glyphosate was banned in the state of California in July 2017, who proclaimed that the herbicide is carcinogenic.[134,135] The following year, a court case in the same state found that glyphosate was the cause of a former groundskeepers cancer.[136]

It was initially thought to be one of the safest herbicides in existence, as it works via disruption of the Shikimate biosynthetic pathway that does not exist in mammals.[137,138] Specifically, glyphosate is absorbed through the foliage and minimally through the roots, where it then migrates to the tips of the plant. Here, it inhibits the enzyme EPSP synthase, which is necessary for growth. EPSP synthase catalyses the reaction between shikimate-3-phosphate and phosphoenolpyruvate, to form 5-enolpyruvylshikimate-3-phosphate (EPSP) (Figure 1.34). The Shikimate pathway synthesises aromatic amino acids: phenylalanine, tryptophan and tyrosine.[139] Without these essential amino acids, the plant cannot survive.

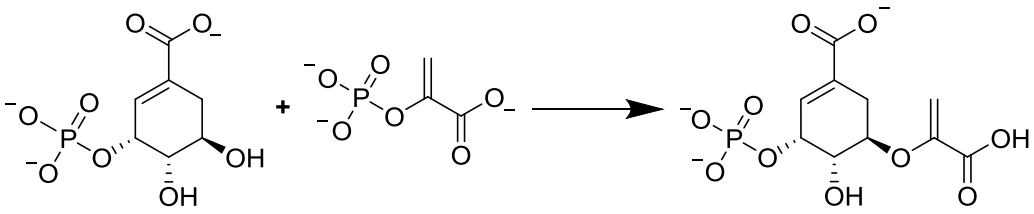

Figure 1.34 - The reaction between shikimate-3-phosphate and phosphoenolpyruvate to form EPSP

Owing to its controversial nature, limits on the presence of glyphosate in food and water have been set by a number of agencies around the world. It is generally considered that current levels in drinking water are well below dangerous concentrations and as such, neither the WHO, the EU, nor the UK regulatory authorities have set an MRL (minimal residual level). However, the US EPA has set a precautionary limit of 0.7 mg/L (4.1 μM) although levels this high have never been detected in drinking water.[140] Glyphosate has also been found to decompose relatively rapidly in chlorinated water, into phosphate, carbon dioxide, methanediol and nitrate, and so it is unlikely large concentrations will be found in tap water.[141]

It is generally accepted that the main source of glyphosate for the general populous is through diet, and therefore, limits have been set by a number of organisations across the world to ensure that food contains low levels of glyphosate.[142–145] Grain, fruit and vegetables have all been given MRLs to ensure the level of glyphosate consumed is well below 'dangerous levels'. For the EU, the MRL for oat is 20 mg/kg (0.1 mM) and for wheat grains is 10 mg/kg (59 μM).

There is a need to monitor glyphosate concentrations in food produce to ensure levels remain below the MRLs set by regulatory bodies. As most of these MRLs are in the millimolar or even micromolar range, there is a need to be able to detect glyphosate accurately at low concentrations. There are currently a wide range of techniques which that can be used, but most require either a professional skill set, or expensive equipment, which limit widespread usage. An ideal detection method should be simple and portable.

1.6.1 Current Methods of Detection

The initial analysis for glyphosate in the late 1970s involved HPLC.[146] However, since glyphosate has neither a chromophore nor fluorophore, it can be difficult to detect as it elutes from the column. A way round this is a derivatisation step e.g., with Fmoc-Cl which allows glyphosate to be more sensitively detected.[147]

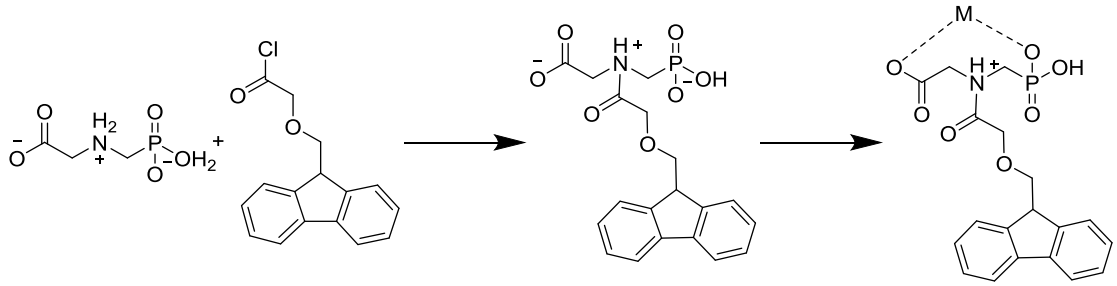

Figure 1.35 - The reaction of glyphosate with Fmoc-Cl to allow glyphosate to be detected by fluorescence, and the formation of a GMC

The need for this specialised step, as well as the need for expensive equipment, means this procedure is neither quick nor cheap. It does, however, give a good limit of detection (LOD) of 2.5 μg/mL (15 μM). Techniques have been derived for a range of samples, including palm oil, breast milk, and soil samples.[148–150] Some of these techniques have a limit for detection of less than 1 ng/mL (6.0 nM) and are very specific. Different columns and changes in techniques may be required depending on the sample, whether solid, liquid or contaminated with other analytes that may interfere with accurately measuring the concentrations of glyphosate.

Mass spectrometry can also be used to detect glyphosate[151] and is often used in tandem with other techniques. One such example examined the effect that salt matrices have on RP-LC-HESI-MS/MS (reverse phase liquid chromatography heated electrospray ionisation tandem mass spectrometry).[152] Such an approach is necessary for environmental samples such as seawater, in which a number of different metal ions are present that can be problematic due to the formation of glyphosate metal complexes (GMC). Fmoc-Cl was used for the derivatisation of the target, before the use of mass spectrometry.

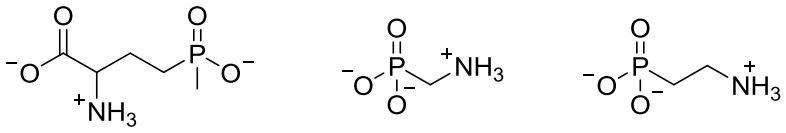

Figure 1.36 - The structures of glufosinate (left), AMPA (middle) and 2-AEP (right)

Glyphosate was tested along with glufosinate, its metabolite AMPA (aminomethylphosphonic acid), and 2-AEP (2-aminoethylphosphate). Glyphosate was the only compound to form the metal complex that led to a change in the retention time by approximately seven minutes. However, the presence of some cations, for example, Cu^{2+}, Co^{2+}, Zn^{2+} and Mn^{2+} prevented glyphosate detection whereas Ca^{2+}, Mg^{2+}, and Sr^{2+}

contributed to altering the retention time. Hence, the different retention times for glyphosate in numerous samples can be ascribed to the varying concentration of these metal ions and hence the formation of GMC. Such behaviour needs to be taken into account when developing techniques with water samples using mass spectrometry.

However, both of these techniques can be expensive and alternatives have been sought. In the last decade with the growing level of interest in glyphosate analysis, the number of techniques used to detect it has also increased. These techniques revolve around a few basic ideas. Better HPLC and MS techniques are constantly being developed, and colormetric, luminescence procedures or electrochemiluminescence (ECL) methods are also being studied.

1.6.2 Electrochemical Analysis Methods for Detecting Glyphosate

Electrochemical luminescence (ECL) may occur during an electrochemical reaction in solution. It is found when an electrochemically generated species undergoes electron-transfer reactions to an excited state that emits light. It was first discovered in the 1960s,[153] but the use of $[Ru(bpy)_3]^{2+}$ as a luminophore didn't occur until the 1970s, and is now the most commonly used.[154] In this example, glyphosate acts as the co-reactant, which produces strongly reducing intermediates, with which the luminophore reacts, to generate the excited states.[155] It is the secondary alkyl amine which gives it its co-reactant properties.

$$Ru(bpy)_3^{2+} \longrightarrow Ru(bpy)_3^{3+} + e^- \quad (1)$$

$$Ru(bpy)_3^{3+} + Gly \longrightarrow Ru(bpy)_3^{2+} + Gly^{\bullet+} \quad (2)$$

$$Gly^{\bullet+} \longrightarrow Gly(-H)^{\bullet} + H^+ \quad (3)$$

$$Ru(bpy)_3^{3+} + Gly(-H)^{\bullet} \longrightarrow [Ru(bpy)_3^{2+}]^* + products \quad (4)$$

$$[Ru(bpy)_3^{2+}]^* \longrightarrow [Ru(bpy)_3^{2+}] + h\nu \quad (5)$$

Figure 1.37 - The electronic process in which $[Ru(bpy)_3]^{2+}$ is used to detect glyphosate

The above equations show that glyphosate (Gly) can be detected via this technique. It has a detection limit of 1.7 ng/mL (0.01 μM) with a linear range of five orders of magnitude. It utilises $Ru(bpy)_3^{2+}$ deposited on gold electrodes modified with self-assembled monolayers (SAM) of alkanethiol derivatives. The use of SAM allows for careful design of the electrode surface, and hence its properties, through the choice of terminal functional groups. A bare gold surface, an ionisable terminal group (-COOH) and as a control, a non-ionisable terminal methyl group was tested, with the carboxylic acid group giving the lowest limit of quantification (LOQ) of 6.4 μM.

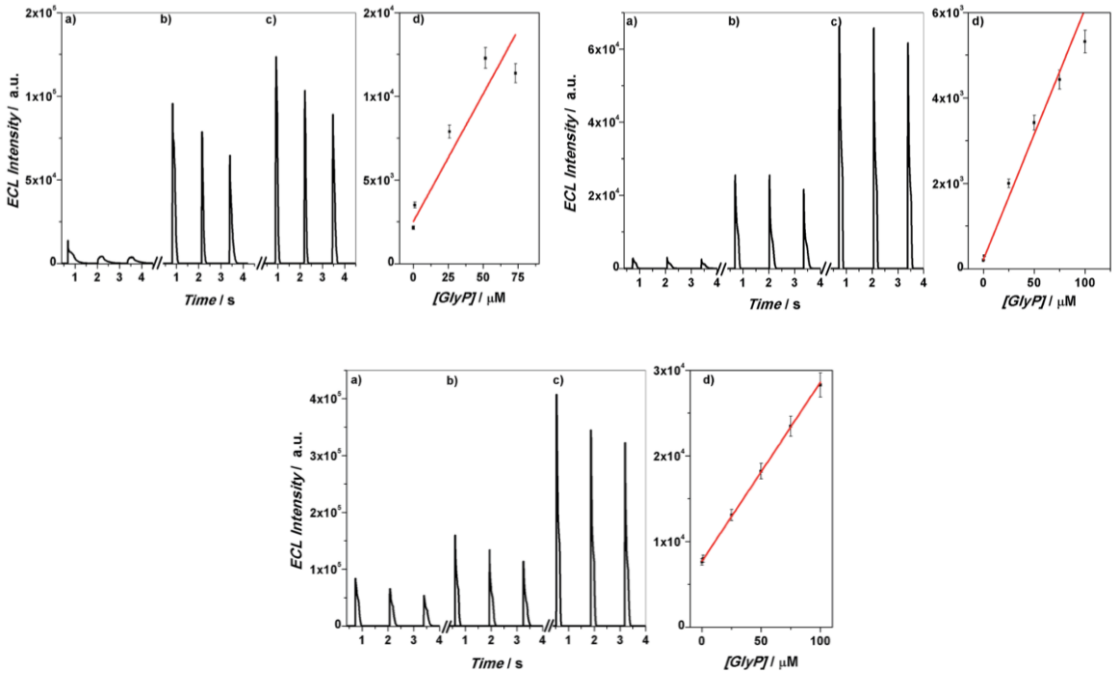

Figure 1.38 - ECL intensity vs. time for a potential jump between 0 vs 1.25 V to a bare Au electrode (left), to an Au/SAM-CH_3 electrode (right) and to an Au/SAM-COOH electrode (bottom). Electrolyte: 0.1 mM $Ru(bpy)_3^{2+}$ in a pH 8 phosphate buffer. (a) with no glyphosate, (b) 0.25 μM glyphosate, (c) 100 μM glyphosate, and (d) calibration curve for glyphosate[155]

Such a level is sufficiently low to detect glyphosate in water at the limit set by the EPA. However, other examples of herbicides with secondary alkyl-amines were not tested and the work was done only in pure water, under argon. The technique allows for detection of glyphosate without derivatisation of the target and may result in a cheaper alternative to either HPLC or MS. However, the lack of testing in real samples, and the sensitivity of these electrodes to outside influences would limit its use in the field.

Another group has used ECL in a similar $[Ru(bpy)_3]^{2+}$-based system using screen-printed electrodes with multi-walled carbon nanotubes (MWCNT) as well as testing the use of a gold surface.[156] It was found that MWCNT decorated with ZnO gave the best results, with a limit of detection of 1 μM for both glyphosate and its metabolite AMPA.

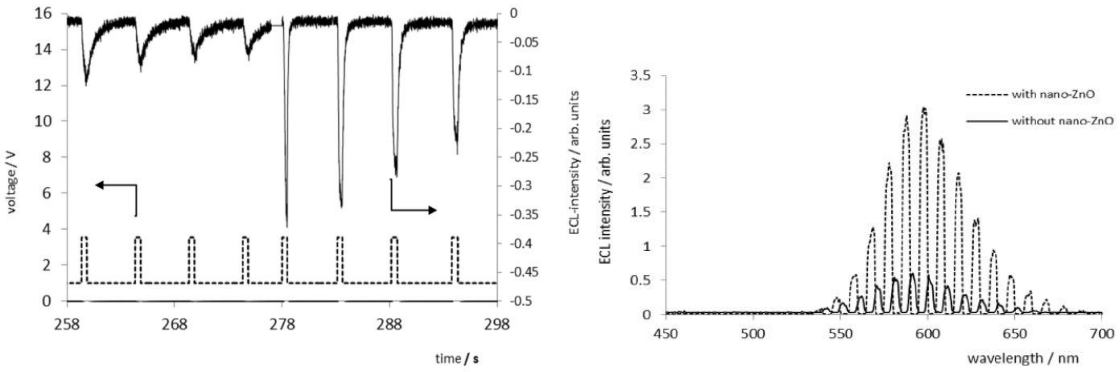

Figure 1.39- (Left) ECL signal of 1 μM/L glyphosate (solid line) as a function of electrical excitation pulse (pulse width 0.5 s; dotted line) with (right four signals) and without nano-ZnO (left four signals). (Right) Chemiluminescence spectrum of $[Ru(bpy)_3]^{2+}$ (100 μM/L) with glyphosate (10 μM/L) as coreactant, with (0.1 mg) and without nano-ZnO. The chemiluminescence spectrum was recorded as follows: wavelength scan 450–700 nm; scan speed 300 nm/min; electrical excitation pulse width 0.1 s; frequency 0.5 s−1; pulse height 1– 3.54 V[156]

Fast amperometry has also been investigated as a method of detecting glyphosate.[156] However, neither glyphosate nor AMPA are electroactive, and so must be complexed with copper, which yields similar detection limits as those found with ECL. Again, the lack of testing of multiple analytes, and the need to prepare an electrode for the fast amperometry method increases cost and decreases speed; the MWCNT electrode could not be cleaned and therefore a new electrode had to be used every time, which can result in slight variations in current. The LOD is also higher than the previous study and hence is not as useful.

An electrochemical sensor has been developed based on molecularly imprinted polypyrrole (MIPPy).[157] These sensors were fabricated on gold electrodes with pyrrole and glyphosate as a template. Cyclic voltammetry (CV) was used to monitor the irreversible oxidation of pyrrole at 1.0 V. Glyphosate was then removed from the electrode through an over-oxidation process, involving scanning between –1.3 V and +1.2 V for 20 cycles in 0.1 M NaOH solution.

To investigate the efficiency of these electrodes, varying levels of glyphosate were incubated under optimised conditions. A linear relationship was discovered between 5 and 800 ng/mL (30 nM - 4.7 μM), with a LOD of 0.27 ng/mL (1.6 nM). The selectivity was tested with AMPA, chlorpyrifos and aldicarbs which all show little change in current with a MIPPy electrode. The recovery of glyphosate in tap water and cucumber was found to be 73-99% between 10-50 ng/mL (60-300 nM) and gave approximately the same values as those derived from LC-MS/MS. This technique therefore showed good selectivity and sensitivity over a large linear range.

1.6.3 Colorimetry, Fluorescence and Absorbance Methods of Glyphosate Detection

Chang *et al.* investigated the use of CuO doped MWCNT to detect the concentration of glyphosate.[158] The MWCNT/CuO nanomaterial was seen to catalyse H_2O_2 to H_2O and the oxidation of Amplex Red to resorforin. However, this effect was diminished in the presence of glyphosate, which disrupts the catalytic activity of the nanotube. This results in decreased fluorescence intensity at 590 nm compared to that observed in the absence of glyphosate. This wavelength could be monitored to give a limit of detection 0.67 ng/mL (4 nM) and a linear range of 0.002-0.01 ng/mL (0.01-0.06 nM).

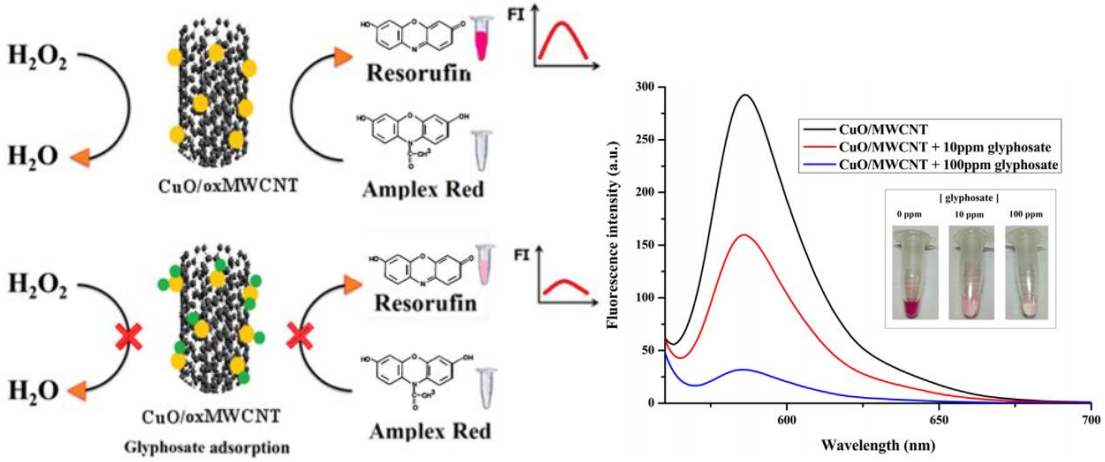

Figure 1.40 - A simplified diagram signalling how glyphosate inhibits the catalytic activity (left) and the change in colour and fluorescence intensity (right)[158]

A small number of other potentially interfering pesticides were also tested. No large change in emission intensity occurred, suggesting high selectivity. The method was also successfully tested with a number of 'real-life' samples, including lake water and tap water. However, this is a 'turn-off sensor', and ideally, a 'turn-on' sensor is preferred, as with the former, high concentrations of analyte can lead to poor signal-to-noise ratios and inaccurate readings.

This system is not the only example of glyphosate inhibiting the catalytic ability of a compound. It was found that Cu^{2+} could catalyse the reaction of 3,3,5,5 – tetramethylbenzidine (TMB) to oxTMB with hydrogen peroxide, which results in a colour change.[159] Glyphosate inhibits this process by binding to the copper and hence the absorbance change could be used to monitor the reaction. However, this approach was far less successful, as the limit of detection was only 0.17 g/mL (1 M).

An example of a sensor array has been described that is designed to detect a range of organophosphates through enhancement of fluorescence intensity. The array was

prepared through the macromolecular self-assembly of two sensing elements, (G5.F) and (G5.MUP$_m$),[160] where G5 is a generation 5 PAMAM dendrimer, F is fluorescein and MUP is 4-methylumbelliferyl phosphate. The latter two compounds were chosen as they are highly fluorescent dianions in aqueous solutions, whose emission is quenched upon binding to the dendrimer.

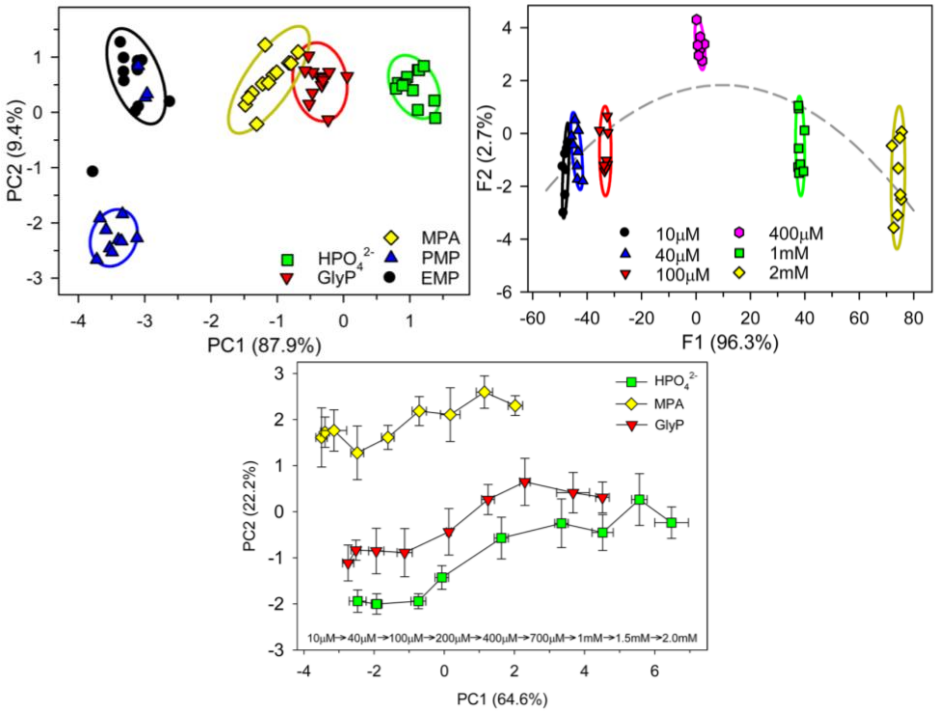

Figure 1.41 - The 2D PCA plot with 500μM of anaylte (right) the LDA score plot for the quantitative analysis of glyphosate (left) and the response of the sensor array to phosphoate, glyphosate and MPA from 10 μM to 2 mM (bottom)[160]

Following addition of a range of organophosphates, the fluorescence of F and MUP is restored as displacement occurs, and usefully each organophosphate displays different displacement behaviour. The absorbance, fluorescence intensity, and anisotropy at different wavelengths were studied in a multimodal microwell plate reader. The spectral data was evaluated using the statistical methods, principle component analysis (PCA) and linear discriminant analysis (LDA). The resulting 2-D PCA plot for five different phosphates at 0.1 mg/mL (0.8 mM), show clear clustering with definite discriminatory capacity. At lower concentrations 0.08 mg/mL (0.5 mM) discrimination is less clear, particularly between methylphosphonate (MPA) and glyphosate.

The LDA score plot, as well as the PCA data, were drawn up for glyphosate, with concentrations ranging from 1.7 μg/mL (10 μM) to 0.3 mg/mL (2 mM), and showed good qualitative analysis. The limit of detection of this method was 0.5 μg/mL (3.0 μM) which is sufficient for the US EPA MRL in drinking water. However, it is good enough

to be able to recognise different organophosphates at neutral pH and the starting materials are both cheap and commercially available.

Indicator displacement methods which use intramolecular interactions have also been explored. Such methods were hoped to overcome the low sensitivity of other dye displacement assays due to low dye-receptor affinity.[161] Typically the sensor exhibits a change in fluorescence when the chromophore is displaced by anions in the receptor. A number of compounds were synthesised, in particular, compound $\mathbf{L^{y1}}$ which features thiourea and amide groups as anion recognition moieties and a naphthyl carboxylate moiety as a chromophore. It was found upon addition of anions to $\mathbf{L^{y1}}$ that fluorescence quenching was seen, but with compound $\mathbf{L^{y2}}$ an increase in emission was observed. Compound $\mathbf{L^{y2}}$ is similar to $\mathbf{L^{y1}}$, and incorporates two naphthalimide moieties to generate fluorescence. $\mathbf{L^{y1}}$ is switch off as in the ground state, the naphthyl carboxylate is fixed in position from hydrogen bonding. However, displacement upon addition of a guest increases the degrees of freedom of the carboxylate and therefore deactivation through rotation and vibration is possible. The paper rationalises the increase in emission upon addition of a guest with $\mathbf{L^{y2}}$ due to the increased rigidity of the host, which limits rotation and vibration and therefore fewer paths for non-radiative decay.

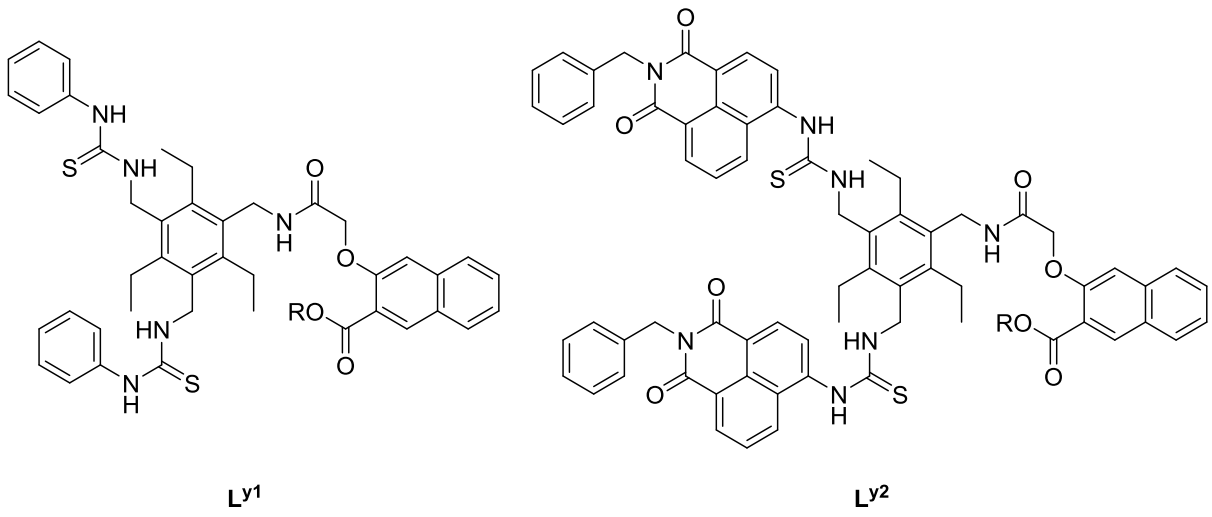

$\mathbf{L^{y1}}$ $\mathbf{L^{y2}}$

Figure 1.42 - Structure of $\boldsymbol{L^{y1}}$(left) and $\boldsymbol{L^{y2}}$ (right)[161]

These compounds were embedded into a hydrophilic polyurethane matrix which could be cast onto plates with a 200 nL volume containing different anions, including glyphosate. Using LDA, discrimination between different anions could be made. The quantification of glyphosate was also investigated, and a LOD of 0.2 mg/L (1.2 μM) was determined, again well below the US EPA limit for drinking water.

There are a number of other examples that use colorimetric methods of analysis to detect glyphosate. One example involved 2-mercapto-5-nitrobenzimidazole capped silver nanoparticles (MNBZ-Ag NPs) using Mg^{2+} as a trigger and tuner.[162] Various metal ions were tested with the nanoparticles and glyphosate as tuners, and it was found Mg^{2+} was superior.

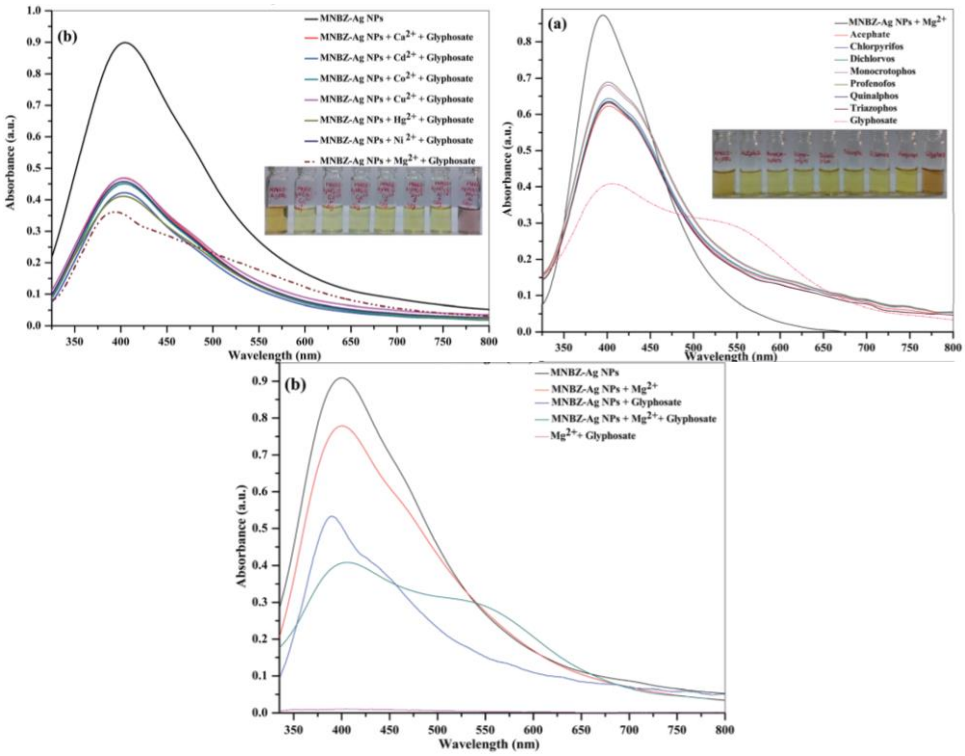

Figure 1.43 - (Left)UV-visible absorption spectra of MNBZ-Ag NPs in the presence of glyphosate (10 μM) with various metal ions (Ca^{2+},Cd^{2+},Co^{2+},Cu^{2+},Hg^{2+},Ni^{2+} and Mg^{2+},50 μM) as tuners. (Inset) Photographic images illustrating the corresponding colorimetric response. (Right) Absorption spectra of MNBZ-Ag NPs with Mg^{2+} ion in the presence of different organophosphorus pesticides (acephate, chlorpyriphos, dichlorvos, monocrotophos, profenophos, quinalphos, triazophos, 1.0 mM) and glyphosate (10 mM). (Inset) Photographic image illustrating the corresponding colorimetric response. (Bottom) The SPR band spectral changes of MNBZ-Ag NPs with and without glyphosate (10 mM) and Mg^{2+} ion, glyphosate (without MNBZ-Ag NPs) with Mg^{2+} ion (50 μM)[162]

Upon addition of glyphosate, complex formation of MNBZ-Ag NPs-Mg^{2+} occurred leading to a colour change from yellow to orange-red and a shift in the surface plasmon resonance (SPR) band from 399 to 517 nm was observed (Figure 1.43). The LOD was 2.8 ng/mL (17 nM) and it showed good selectivity over other pesticides present at 1 mM. Complex formation requires both the presence of glyphosate and the magnesium ion. Without Mg^{2+}, the limit of detection is 5.4 mg/mL (32 mM), i.e. not sufficiently sensitive to detect glyphosate at its MRLs dictated by the US EPA and the EU.

The use of a nanofiber based colorimetric sensor strip has also been developed. Derivatisation of glyphosate is required and must be reacted with carbon disulphide,

resulting in the formation of dithiocarboxy(phosphonomethyl) carbamic acid (Figure 1.44).[163]

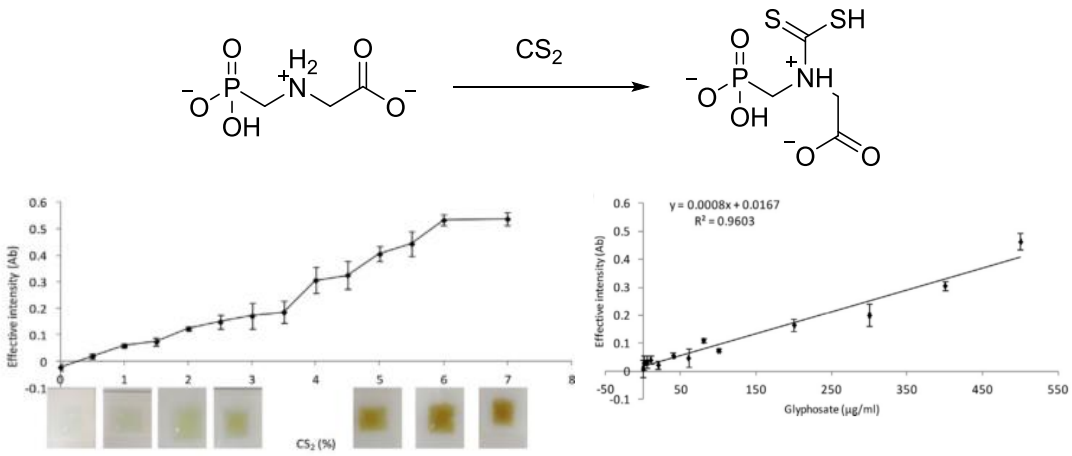

Figure 1.44 - (Top) Derivatisation of glyphosate with carbon disulphide. (Bottom left) The colour change upon increasing percentage of carbon disulphide (0-7%) with 1000 µg/mL of glyphosate in 30 µL. (Bottom right) The calibration curve for glyphosate (0.1-500 µg/m) in a 30 µL sample size

The dithiocarbamic acid interacts with copper on the poly(vinyl alcohol) (PVA) nanofibre sensor strip to give a colour change from blue to yellow. Although this system gives a fast response (1-3 s), has a low LOD 0.1 mg/L (0.6 µM) and was stable for up to 20 days at 23 ˚C, studies found the response was pH dependent. The colour change was only observed at pH 11 and 12 which the paper claimed was due to the deprotonation of the amine group on glyphosate. The deprotonation allowed the formation of the dithiocarbamic acid intermediate which subsequently allowed the formation of the metal complex, hence pH 12 was chosen as the optimum pH. Further experiments confirmed that this technique was also susceptible to interference from other analytes found in environmental water samples, particularly at low glyphosate concentration. It led to recovery of 128% at lower concentrations of glyphosate which meant pre-treatment of water samples were required before testing. The requirement for pre-treatment of the water sample means it is unlikely to be a cost-effective method. Furthermore, both carbon disulphide and the resulting glyphosate derivative are potentially toxic. Hence, the disposal of the assay kit could also be costly.

Other reported examples have explored the use of lanthanide doped nano-particles (NPs) and a TR-FRET-IDA (time resolved Förster resonance energy transfer indicator displacement assay) to detect glyphosate and similar herbicides.[164] The TR-FRET of the $LiYF_4$:Ce/Tb NPs was used to ensure any organic short-lived luminescence would not

affect the indicator. This is another example of a 'switch-off' sensor, where glyphosate displaced indicators from the nano-particle, causing emission to decrease.

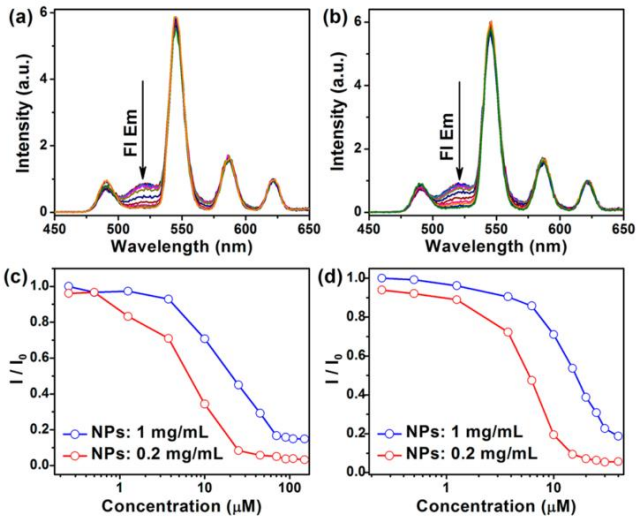

Figure 1.45 - (Top) Normalised at 622 nm time resolved titrations of NPs and fluorescein sodium (FI) with (left) glyphosate and (right) AMPA in Tris buffer (pH 7.0). (Bottom) Displacement curve of NPs and FI with (left) glyphosate and (right) AMPA[164]

Studies revealed that this technique could distinguish between 11 different anions, although this experiment was only carried out in aqueous buffer and not tested on any environmental samples. For glyphosate, a LOD of 0.13 μg/mL (0.78 μM) was found which is well below the EPA drinking water limit.

Another example of FRET based detection utilised thioglycolic acid capped CdTe quantum dots and cysteamine stabilised gold NPs. Together they form a FRET donor-acceptor system.[165] The NPs quench the quantum dot emission, but in the presence of glyphosate, aggregation of the NPs leads to recovery of the emission.

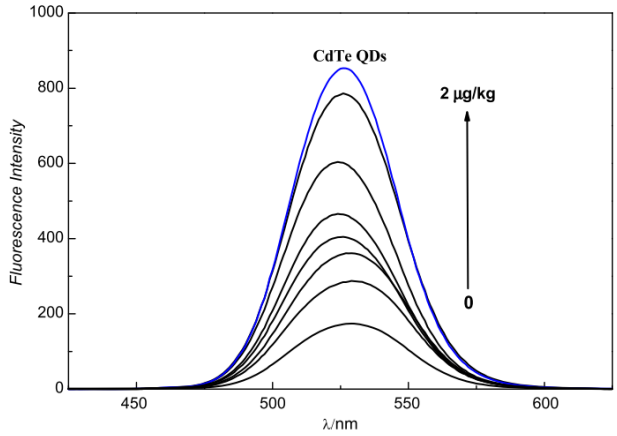

Figure 1.46 - Emission spectra of CdTe QDs-AuNPs with increasing concentrations of glyphosate in apple matrix[151]

Again, the system showed good sensitivity with a LOD of 9.8 ng/kg (0.06 nM) and a linear range of 0.02-2.0 μg/kg, which is well below the limit set by China where this study was conducted.[151] The method was successfully able to detect low levels of glyphosate in apples. However, no real competition studies were carried out allowing a comparison of glyphosate against other herbicides or biologically relevant compounds.

A more selective method using 'switch-on' luminescence uses carbon dots (CD) tagged to glyphosate antibodies and has been tested with other herbicides.[166] In solution, Fe_3O_4-glyposate was added to the luminescent CD-antibody where glyphosate bound to the antibody. Applying a magnet to the bottom of the cell pulled the fluorescence CDs down due to the magnetic iron, showing little fluorescence. However, in the presence of free glyphosate, the antibodies bind to this competitively with the iron compound. Therefore, upon application of the magnet, the fluorescent CDs are not attracted to the bottom of the cell and therefore are observed in the general solution. Selectivity came from the presence of the glyphosate specific antibodies.

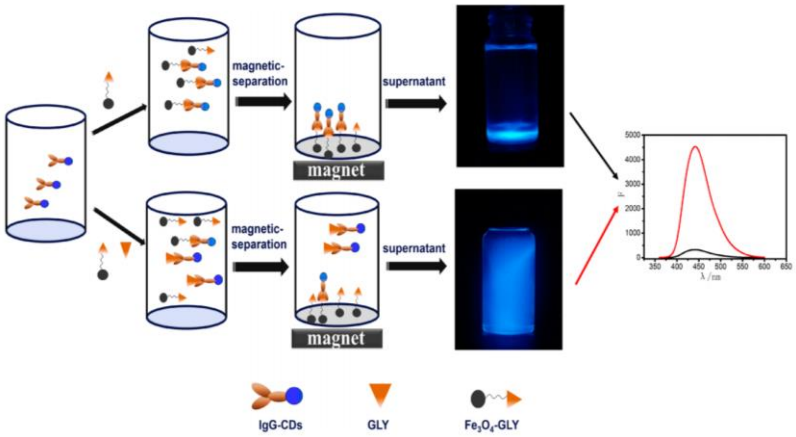

Figure 1.47 - The detection scheme of CD with glyphosate antibodies, which shows the increase in emission intensity upon glyphosate[166]

A detection limit of 0.8 ng/mL (4.7 nM) was found for glyphosate, with a linear response region for glyphosate concentrations between 0.01 and 80 μg/mL (59 nM – 0.5 mM). The system was tested in a number of different sample types including soil, tea and in cells where recovery ranged from 87-104%. It is a simple, selective and sensitive technique that operates over a range of concentrations.

Tripier *et al*. synthesised a glyphosate, and ATP (adenosine triphosphate) sensor, which could be used via NMR, absorbance, fluorescence, and potentiometric methods.[167] They studied two similar compounds, $\mathbf{L^{z1}}$ and $\mathbf{L^{z2}}$ **(**Figure 1.48). $\mathbf{L^{z1}}$ possesses an anthracenyl

fluorophore on the 4-position of the pyridine ring which allows the compound to be used as a fluorescence probe.

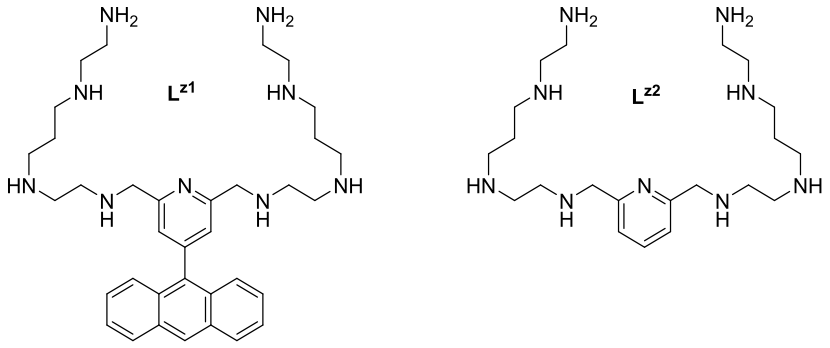

Figure 1.48 - The structure of $\mathbf{L^{z1}}$ *(left) and* $\mathbf{L^{z2}}$ *(right) as their free amines*[167]

The protonation behaviour and anion complexation studies were carried out with $\mathbf{L^{z1}}$ and $\mathbf{L^{z2}}$ and showed similar behaviour, in terms of protonation and the binding affinity for glyphosate and ATP. Both ligands at pH 7 predominately have a charge of +4, but upon addition of ATP or glyphosate becomes +6, and either analyte effects the emission in $\mathbf{L^{z1}}$.The binding constants for glyphosate and ATP for $\mathbf{L^{z1}}$ were measured using absorbance, fluorescence and potentiometric data with log*K* values of 4.7, 4.8 and 4.2 determined respectively. Although this is a promising result, the log*K* values for ATP were 5.2, 4.6 and 4.9 showing similar binding constants, raising concerns over any selectivity for phosphorus oxyanions. No other biologically relevant anions were tested and since the binding is electrostatic, it is likely there would be a number of other anions which would interfere with results in biologically relevant samples, for both glyphosate and ATP.

Another technique which has a low LOD is an enzyme-linked immunosorbent assay (ELISA) which was initially developed in the 1970s.[168] One such example developed by Hall *et. al.* has a detection limit of 7.6 μg/mL (45 μM) and a linear range of 10-1000 μg/mL (59 μM – 5.9 mM).[169] This method was tested in the presence of the metabolite AMPA, glufosinate and other structurally similar compounds. There appeared to be no cross-reactivity with the assay with the exception of glyphosine (Figure 1.49). The results from this paper were comparable with the results found from HPLC with reduced cost, sample preparation time and solvent use.

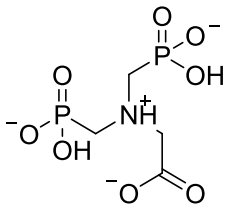

Figure 1.49 - The structure of glyphosine

However, a report in 2017 suggested that the commercially available ELISA test may not be as accurate as originally claimed. Ultra-high performance liquid chromatography in tandem with mass spectral (UHPLC-MS/MS) techniques stated that around the limit of detection 0.075 mg/mL (0.4 mM), ELISA's accuracy and precision are low.[170] However, at 0.30 mg/mL (1.8 mM) and around MRLs, ELISA performed much better. In general, the results from the commercial ELISA and UHPLC-MS/MS linearly correlated, but the differences ranged from 1% for oats to 40% in barley. It was suggested that this ELISA may not be as accurate as believed, but is a complementary technique to more accurate and precise techniques.

Whilst, both mass spectrometry and HPLC techniques are very accurate they have the disadvantage that they require derivatisation of glyphosate, e.g. with Fmoc-Cl, as well as being expensive and requiring the user to have specialist technical knowledge. However, the selectivity and sensitivity of these techniques mean they remain the chosen methods to measure the glyphosate concentration accurately. The US EPA for example uses 'Method 547' in which HPLC, post-column derivatisation and fluorescence are used to detect glyphosate in drinking water.[171] This classic method uses o-phthalaldehyde-2-mercaptoethanol as the fluorophore rather than Fmoc-Cl.

1.7 Project Aims

The aims of this project are two-fold, and involve predominately europium (III) complexes to determine the concentration of target species at low concentrations.

The first part will look at the competitive binding of pharmaceuticals to α_1-AGP, displacing the europium complex from the protein binding site. The binding constant of the complex to α_1-AGP has been used to select certain pharmaceuticals, which are known to have similar binding constants to ensure competitive binding. Predominately, changes in lanthanide luminescence have been followed monitoring total emission intensity. However, the development of CPL has allowed this technique to be used for the first time in such analysis.

Furthermore, as a number of drugs are chiral, with some being supplied as a single enantiomer, research into how each enantiomer may react differently with α_1-AGP has been examined. A secondary aspect of this study relates to using the information from these experiments to make detailed analysis, in keeping with the desire to develop personalised medicines.

The second part of this thesis looks at the selective binding of a number of europium complexes to glyphosate. Glyphosate is the most commonly used herbicide and current methods of detection, although accurate, can be slow and costly.

There are potentially many problems with the detection of glyphosate. Firstly, its selective detection as similar biological structures, either derived from glycine or inorganic phosphate, may also bind to the complexes. The metabolites of glyphosate and other herbicides with a similar structure, such as glufosinate, could also be potential competitors in detection. Secondly, glyphosate is not commonly found in tap water owing to the decomposition of glyphosate in the presence of chlorine, so the detection of glyphosate in more relevant media should be studied. The complexes are first to be tested in a buffer solution in water. However, more complicated media, such as river water and grain extracts are also tested. The challenge is to make a complex that does not bind to other common species found in river water, nor to any biological macromolecules. It must also work well in a range of environments to maximize its scope and utility.

The binding of glyphosate to the europium complex is to be examined using the intensity ratio of europium emission bands, to allow effective use of small, portable instruments that are already in existence.

2. α_1-AGP Binding Drugs

In previous studies, [Eu.$\mathbf{L^1}$]$^+$ was found to bind to α_1-AGP with a log*K* value of 5.73 (±0.06).[56] The binding event could be tracked through the induction of a CPL signal, which was coupled to an increase in total europium emission intensity. Upon binding to the protein, a nitrogen atom from one azaxanthone chromophore, dissociates from the metal, allowing α_1-AGP to bind through a carboxylate oxygen atom of the Glu-64 amino acid (Figure 2.1). It also loses an inner sphere bound water molecule in the process. The loss of this water is evident through the change in emission lifetime, and hence, the increase in emission intensity. Drugs with similar binding constants to α_1-AGP as [Eu.$\mathbf{L^1}$]$^+$ could induce competitive binding that could be tracked by monitoring changes in both total emission and CPL intensity.

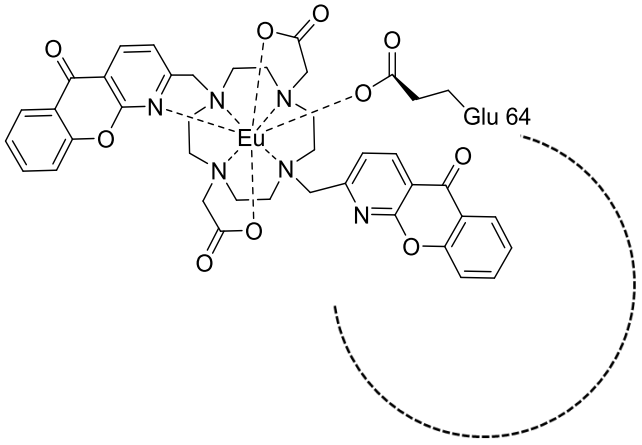

Figure 2.1 - A schematic of how [Eu.$\boldsymbol{L^1}$]$^+$ binds to α_1-AGP[56]

2.1 Synthesis and characterisation of ligands and complexes

The synthesis (Scheme 2.1) of the ligand, $\mathbf{L^1}$, began by reacting cyclen with benzyl chloroformate at pH 2.5 to facilitate *trans*-disubstution.[172] The product mixture was recrystallized from diethyl ether and DCM to remove any mono- or tri-substituted by-products. The desired *trans*-dicarbamate, **1**, was subsequently reacted with *tert*-butylbromoacetate to give the ester **2**, before deprotection by means of catalytic hydrogenation to afford the amine **3**.

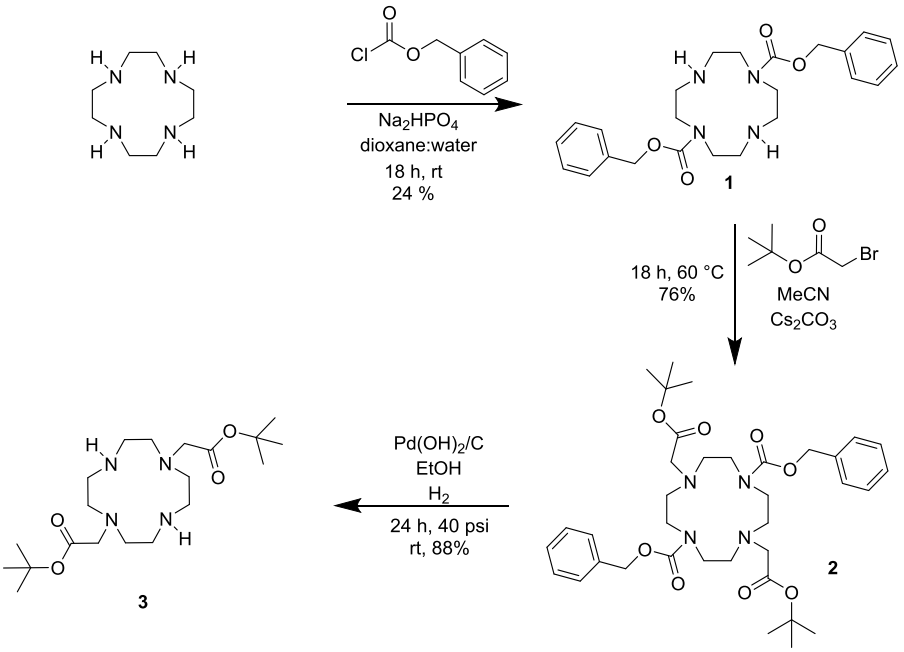

*Scheme 2.1 - Synthesis of **3***

The chromophore was synthesised in three steps following a previously published procedure (Scheme 2.2).[173] The initial step involved the reaction of sodium phenolate with 2-chloro-6-methylnicotinic acid. The product of this reaction, **4**, was stirred in polyphosphoric acid (PPA) for 24 h at 120 ˚C to yield **5** as a crystalline solid. In the final step of chromophore synthesis, radical bromination of 2-methyl-1-azaxanthone was achieved with *N*-bromosuccinimide (NBS), using benzoyl peroxide as the initiator. The desired mono-bromo derivative, **6**, was separated by column chromatography before being used in the alkylation of cyclen (Scheme 2.4).

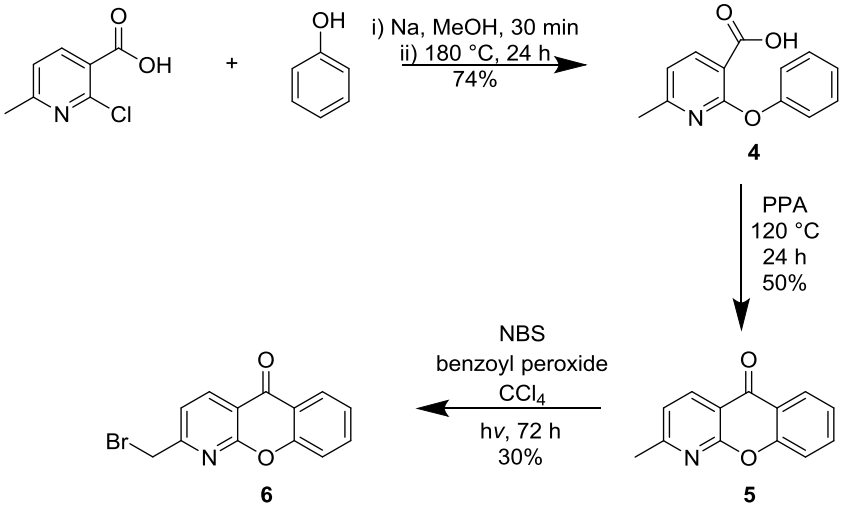

*Scheme 2.2 - Synthesis of the chromophore, **6***

The final bromination step gave a maximum yield of 30%, with two by-products of similar yield, the starting material and the di-brominated compound. However, both were still useful if collected through column chromatography. The starting material could be recycled into the same reaction once again. In the case of the di-brominated compound, selective removal of a single bromine is possible with diethylphosphite and diisopropylamine, reacting for 10 minutes at 0 ˚C before quenching the reaction in iced water (Scheme 2.3).

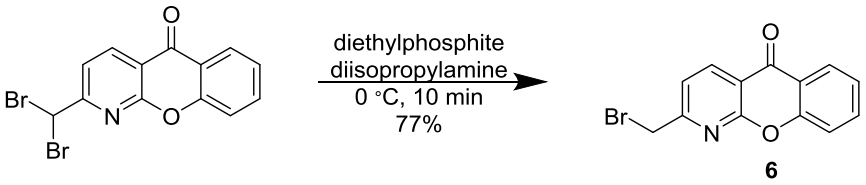

Scheme 2.3 - Debromination of 2,2-dibromomethyl-1-azaxanthone

The alkylation of the two chromophores onto **3**, gave **7** (Scheme 2.4). The *t*-butyl groups were removed under acidic conditions, before complexation with $Ln(OAc)_3$ (Ln = Eu, Tb) yielded the final complex which was purified by reverse phase HPLC.

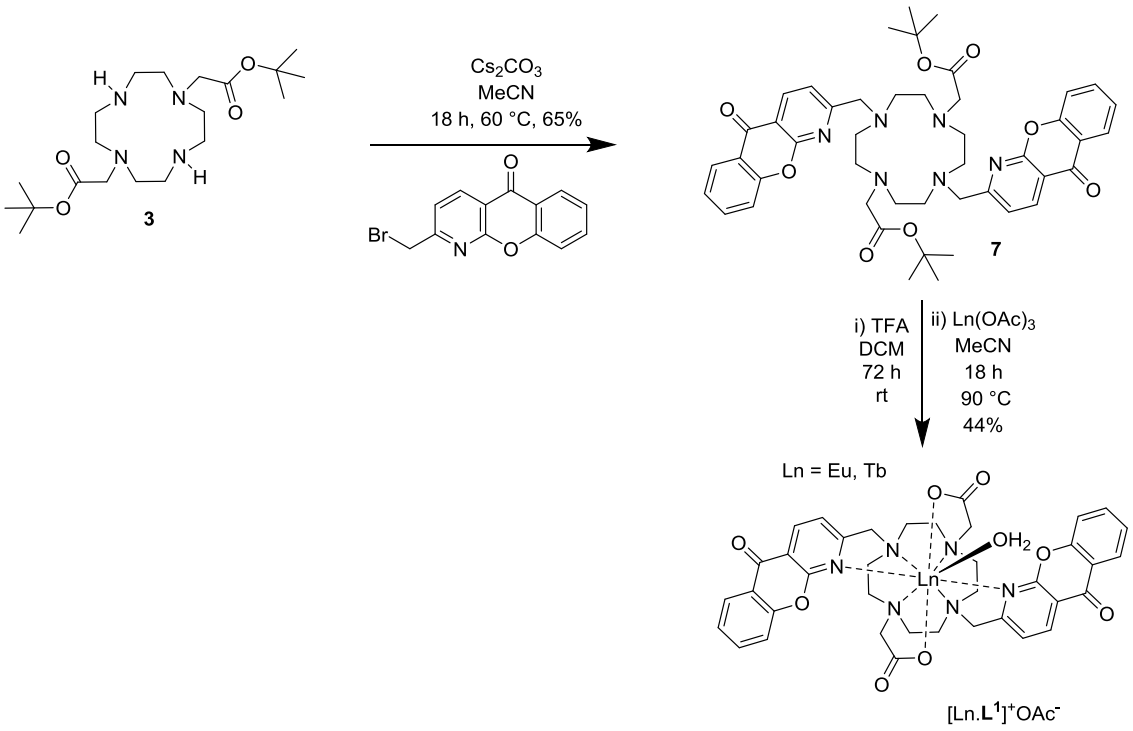

Scheme 2.4 - Synthesis of $[Ln.\boldsymbol{L^1}]^+$

The final reaction was monitored by emission spectroscopic analysis of the reaction mixture, by excitation at 336 nm. As the energy transfer from the two chromophores to the lanthanide ion is very efficient, with little back transfer, there should be no ligand

fluorescence in the final complex, in accordance with completion of the complexation reaction. The presence of any unreacted ligand can be seen through a broad organic fluorescence emission band around 400 nm. Only strong emission was found in the relevant regions for the lanthanide being probed.

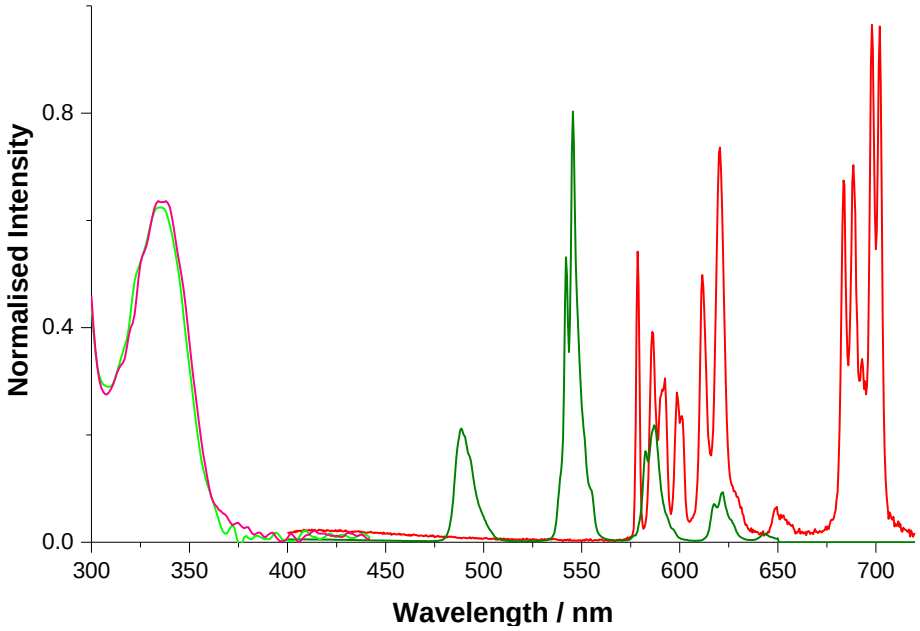

*Figure 2.2 - The excitation and emission of [Eu.**L**^{1}]$^{+}$(red) and [Tb.**L**^{1}]$^{+}$(green)*

2.2 Binding Studies of [Ln.L^{1}]$^{+}$ with Selected Pharmaceuticals

Initial binding studies were carried out with [Eu.**L**^{1}]$^{+}$ and [Tb.**L**^{1}]$^{+}$ in a similar manner to those conducted by Carr *et. al.* in 2012.[56] The complexes were dissolved in a 1 mL solution of 0.1 M NaCl, to ensure that the ionic strength remains constant throughout the titration. Physiological pH, 7.4, was maintained using $NaOH_{(aq)}$ and $HCl_{(aq)}$ to ensure that the human protein, α_1-AGP did not denature. However, errors could potentially come in at this point with the lack of buffer. Changes in bicarbonate in solution could change the pH and as such effect the results obtained. Furthermore, with such strong acid and bases, it is possible to overshoot and large swings in pH could have a detrimental effect on the protein.

α_1-AGP was added incrementally to the complex solution, and binding events were tracked using changes in emission intensity and spectral form, in both total emission and CPL. The lifetimes at the start and end of the titration were also recorded.

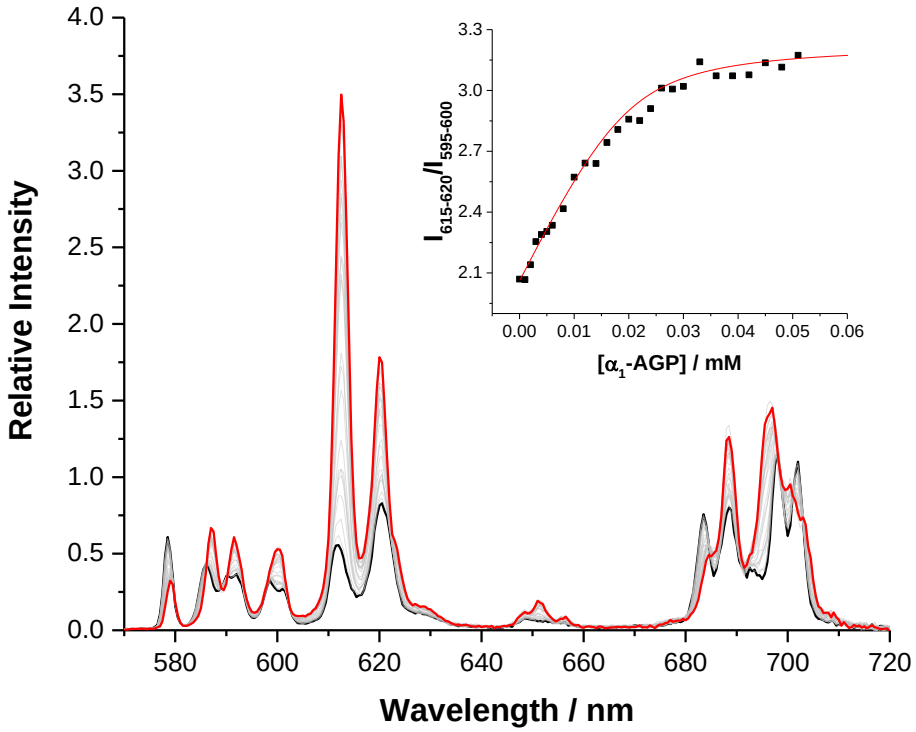

*Figure 2.3 - Changes in the emission spectrum of [Eu.**L**^{1}]$^{+}$ with increasing concentrations of α_1-AGP up to 50μM (30 μM complex, 0.1 M NaCl, pH = 7.4, 295 K). (Inset) The ratio of 615-620 nm / 595-600 nm as a function of increasing concentrations of α_1-AGP*

As expected, upon addition of α_1-AGP to [Eu.**L**^{1}]$^{+}$, an increase in total emission intensity was observed. There was also a change in spectral form, particularly in two of the bands in the ΔJ = 2 transition, whose intensity changed relative to one another. A more dramatic change also occurred in the ΔJ = 4 manifold. By plotting the ratio of ΔJ = 2 / ΔJ = 1 (615-620 nm / 595-600 nm) emission intensities as a function of α_1-AGP, a binding constant of log$K$ = 5.65 (±0.03) was calculated, which is within error of the previously stated literature value of 5.73 (±0.06).[56] The log$K$ value was calculated using Equation **5.2** and the errors in the parenthesis are due to statistical error in the fit of the line to the raw data. All log$K$ values throughout the thesis were calculated in this manner.

Other experimental errors which could come into play include the concentrations of all solutions, change in temperature and slight changes in pH. Repetitions of titrations were carried out to minimise the effect of any random errors. There could also be slight error in the ratio of the luminescent studies, but this is less likely with strong luminescence. Experiments were carried out in a temperature controlled room, with the pH being checked before and after each scan was carried out.

The initial observation of an increase in emission intensity was expected to be the result of the loss of an inner sphere water molecule. The O-H oscillators in water are well-known non-radiative quenchers of the europium excited state, so a loss of water would be expected to be coupled with greater emission intensity and a longer lifetime of the emission.

The lifetime of the complex was measured by analysis of europium emission decay profiles. Information from these profiles were recorded for the complex and the adduct in H_2O and D_2O. The inner sphere water number (*q)* can be obtained using Equation **2.1**.[174]

$$q = A\left(\frac{1}{\tau_{H_2O}} - \frac{1}{\tau_{D_2O}} - 0.25 - 0.075x\right) \qquad \textbf{(2.1)}$$

In this equation, *A* is a proportionality constant, which for europium is 1.2 ms, and *x* is the number of coordinated amide N-H bonds, which in this complex, is zero. It is also important to note that the error in *q* is ±0.3, which is significant, when the values are generally between 0-2. The lifetimes in H_2O and D_2O of the complex and the adduct formed with α_1-AGP are listed in Table 2.1. As expected, the complex has a *q* value of approximately one suggesting the presence of a single water molecule in the inner coordination sphere. Upon forming the adduct, the *q* value drops to approximately zero, consistent with the expulsion of water from the inner coordination sphere.

*Table 2.1 - Lifetimes and calculated q value of [Eu.**L**^{1}]$^{+}$ and the adduct formed with α_1-AGP*

Complex	Lifetime in H_2O (τ_1) (ms)	Lifetime in D_2O (τ_1) (ms)	*q* value
[Eu.**L**^{1}]$^{+}$	0.50	1.69	1.4
[Eu.**L**^{1}]:α_1-AGP	0.96	1.47	0.1

An analogous experiment, with the addition of α_1-AGP to [Tb.**L**^{1}]$^{+}$ was also carried out. Although very similar results would be expected, the overall emission intensity was significantly quenched. Owing to this decrease, the planned experiments designed for this complex with different pharmaceuticals were very difficult, as emission has significantly decreased. Furthermore, the binding curve of [Tb.**L**^{1}]$^{+}$ to α_1-AGP was not simple to analyse, implying that more than one binding event was taking place.

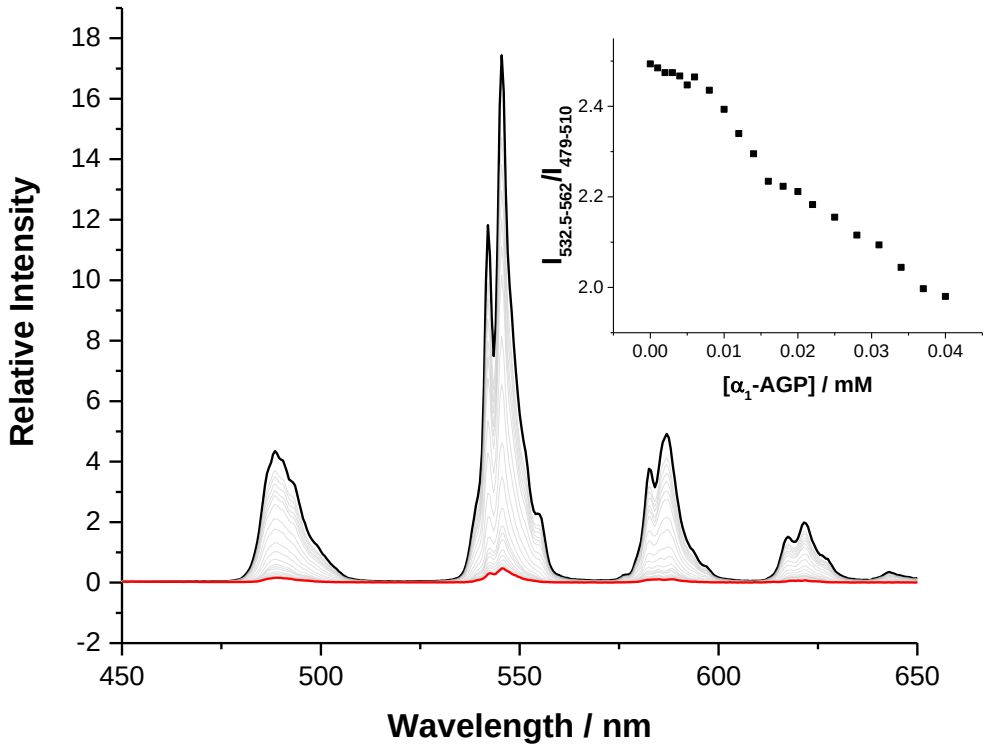

*Figure 2.4 - Changes in the emission spectrum of [Tb.**L**^{1}]$^{+}$ (black) with increasing concentration of α_1-AGP up to 40μM (red) (30 μM complex, 0.1 M NaCl, pH = 7.4, 295 K). (Inset) The intensity ratio of 532.5-562 nm / 498-510 nm as a function of increasing α_1-AGP concentration*

It is thought the reason for the marked decrease in emission is related to the sensitivity of certain Tb^{3+} complexes to undergo charge transfer quenching.[175] In α_1-AGP, there is an electron rich tyrosine-37 residue which may lie close to the opening of the binding site.[56] This amino acid could form an exciplex with the electron deficient Tb-coordinated azaxanthone which may explain the significant quenching that is observed upon the complex binding with α_1-AGP.

A trial titration of [Tb.**L**^{1}]$^{+}$:α_1-AGP (1:1) with increasing concentration of a drug was conducted to see if it would be possible to use this complex as a probe nonetheless. Incremental additions of imatinib (Figure 2.8) were tracked through total emission alone, and the same intensity ratio (532.5-562 nm / 497-510 nm) that was used in the titration of α_1-AGP was utilised again (Figure 2.5).

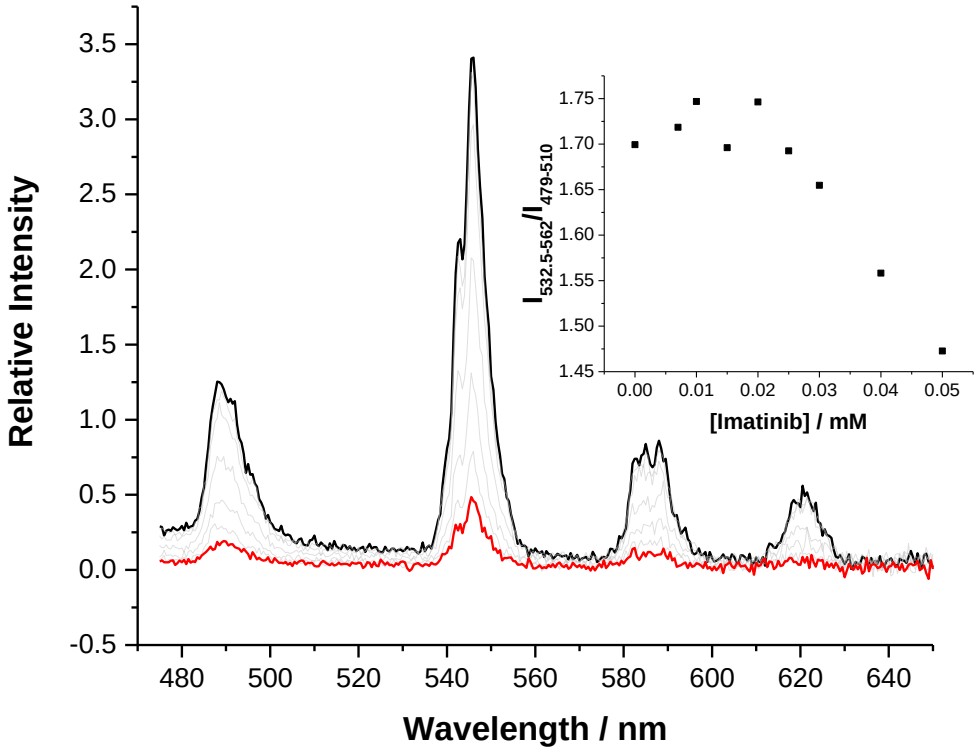

*Figure 2.5 - Changes in the emission spectrum of [Tb.**L**^{1}]$^{+}$:α_1-AGP (black) (30 μM, 1:1, 0.1 M NaCl, pH = 7.4, 295 K) with increasing imatinib concentration up to 50 μM (red). (Inset) The intensity ratio of 532.5-562 nm / 479-510 nm as a function of increasing imatinib concentration*

Upon increasing the concentration of imatinib, there was an overall decrease in emission intensity, and the signal-to-noise ratio continued to deteriorate. Furthermore, the ratio that could have potentially been used, did not divulge any useful information. Due to these initial poor results, it was decided that further tests were to be carried out using [Eu.**L**^{1}]$^{+}$alone.

For the titration of α_1-AGP into [Eu.**L**^{1}]$^{+}$, CPL spectra were also collected. In solution, there is a dynamic equilibrium between the enantiomers of the complex. Hence, there is a racemic mixture, and no observable CPL signal. To explain the modes of chirality possible in this complex, it is easiest to consider a C_4 symmetric complex such as [Ln.DOTA]$^{-}$. [Ln.DOTA]$^{-}$ can exist in four different isomers, with two pairs of enantiomers.

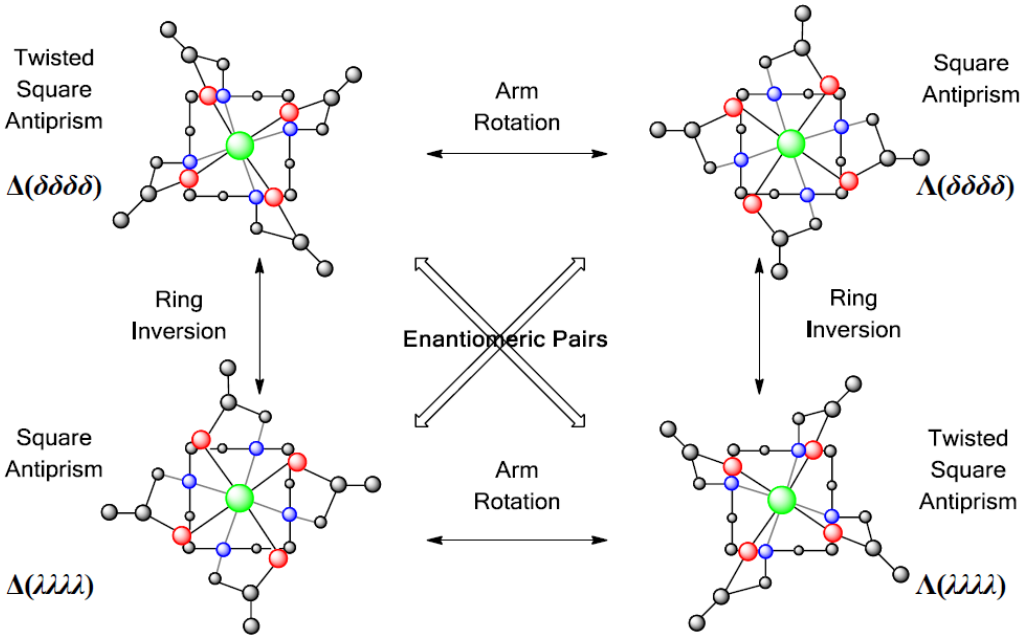

Figure 2.6 - The schematic representation of the four isomers of [Ln.DOTA] [176]

The δ and λ chirality element arises from the cyclen ring chelate. The N-C-C-N dihedral angle in each chelate ring can either be at an angle of +60° or -60° respectively, and the system can interconvert between the two states through cooperative ring inversion. The second type of chirality comes from the dihedral angle of the N-C-C-O chelate. These angles are the same sign in relation to each other, and give rise to either Δ or Λ. Again these can interconvert through cooperative arm rotation. In solution, all of these stereoisomers of DOTA can interconvert rapidly on the emission timescale at room temperature so if examined by CPL, no signal is observed. However, this is not the case in all complexes.

The complex, [Eu.$\mathbf{L^1}$]$^+$, is only C_2 symmetric, and therefore the isomers in solution are slightly different, but the same basic principles apply. In solution, the complex rapidly converts between the isomers, but upon binding to α_1-AGP, [Eu.$\mathbf{L^1}$]$^+$ preferentially forms one preferred chiral diasteroisomeric complex, and a CPL signal can now be observed.

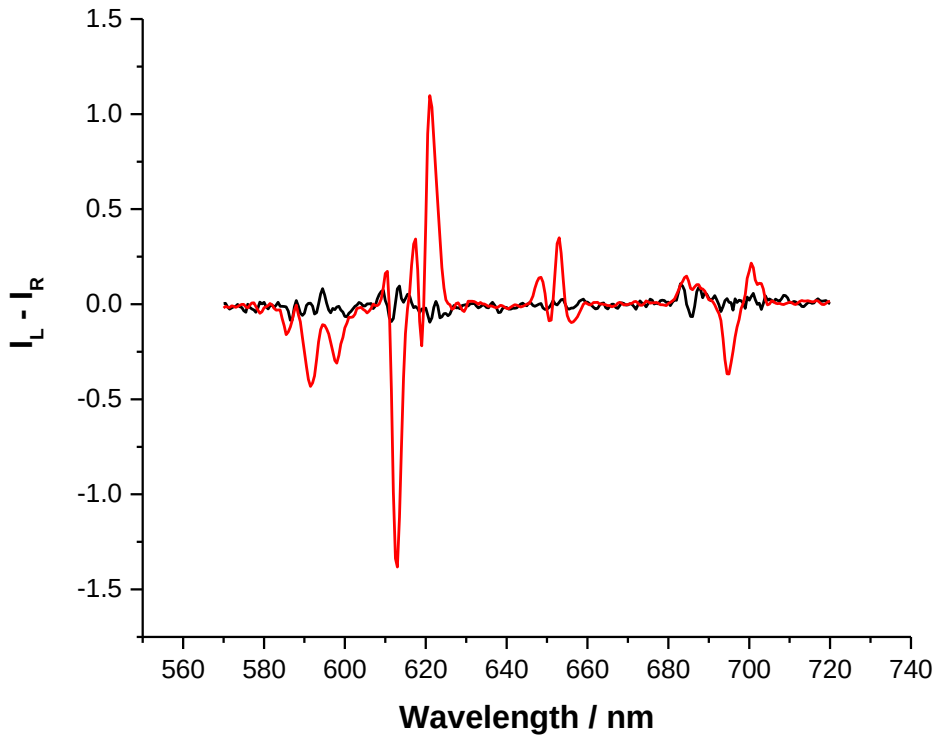

*Figure 2.7 - The CPL spectra of [Eu.**L**^{1}]$^{+}$ (black) and the 1:1 adduct of [Eu.**L**^{1}]$^{+}$ with α_1-AGP (red) (30 μM, 0.1 M NaCl, pH 7.4, 295 K)*

Two large signals of opposite helicity are observed within the $\Delta J = 2$ band, which have potential to be used to investigate the system without large errors originating from poor signal-to-noise ratios. As the selected pharmaceuticals bind to the same site on α_1-AGP as the complex, it is expected that upon addition of a drug, a decrease in the intensity of the CPL signal will be observed. This is due to the drug displacing the complex bound to the protein, so free [Eu.**L**^{1}]$^{+}$ will return to its dynamic equilibrium with no preference for a particular enantiomer.

Following initial investigations with α_1-AGP, binding studies with the three selected pharmaceuticals were undertaken. The three chosen are imatinib, disopyramide and methadone. Each was found in the literature to bind to α_1-AGP at the same site as the complex, with binding constants of similar magnitudes, as well as having absorbance maxima far from the 336 nm excitation wavelength of the complex.[56,110,112,177]

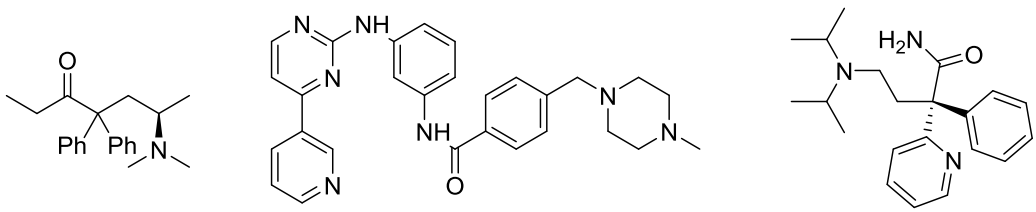

Figure 2.8 - The structures of S-methadone (left), imatinib (middle) and S-disopyramide (right)

In each titration, the conditions were identical. The complex and protein were in a 1:1 ratio (30 μM), in a 1 mL aqueous solution of 0.1 M NaCl at pH 7.4 and 295 K. Again, the pH was maintained with $NaOH_{(aq)}$ and $HCl_{(aq)}$ when appropriate. The concentration of the complex was calculated by measuring the absorbance at 336 nm and using the Beer-Lambert law. Incremental addition of the drugs was carried out, and the binding event was followed using total luminescence emission and CPL spectroscopy. In addition, emission lifetimes were recorded at the beginning and end of each titration.

2.2.1 Total Emission Spectroscopy Analysis

Total emission spectroscopy is widely used to follow binding events over a wide range of applications. In lanthanides in particular, the sharp emission bands, some of which are hypersensitive to coordination perturbation, can give a lot of information about a binding event. Information can be extracted from both the overall emission intensity and the change in shape of the spectral form. Although the drug is not thought to bind directly to the complex, it will change the coordination around it, as it replaces the complex in the binding site of α_1-AGP.

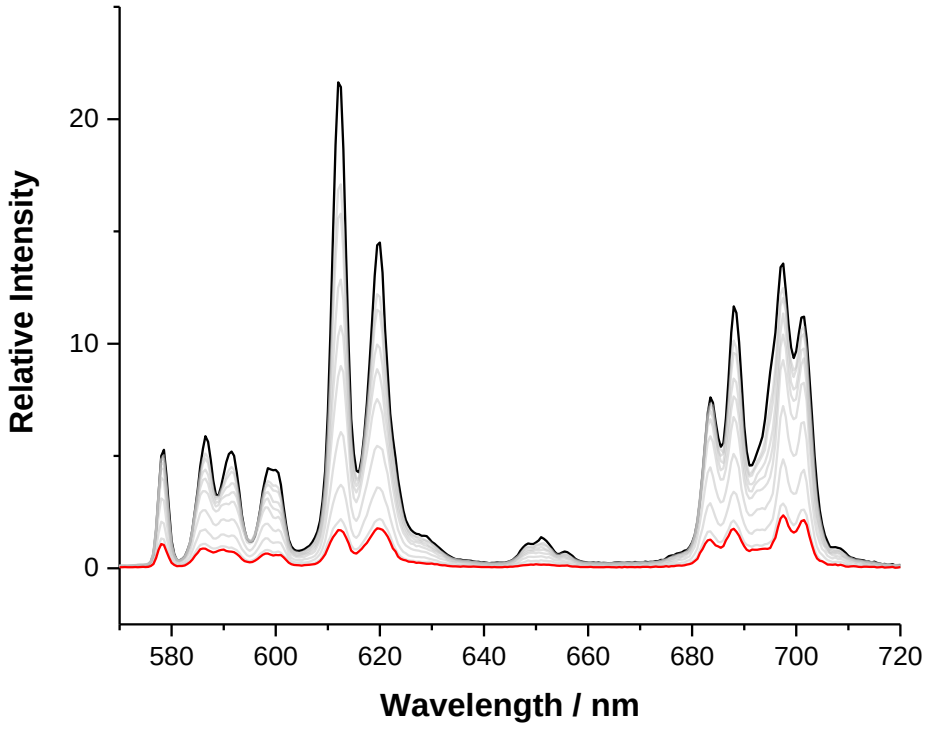

Figure 2.9 - Changes in the emission spectra of $[Eu.\mathbf{L^1}]^+$:α_1-AGP (black) (30 μM, 1:1, 0.1 M NaCl, pH 7.4, 295 K) with increasing concentrations of imatinib up to 12.5 μM (red)

As predicted, there was a clear and distinct decrease in emission intensity for each of the three drugs studied. Moreover, there is a change in the spectral form, particularly in the $\Delta J = 2$ manifold where the two major bands are of approximately the same intensity

after the addition of the pharmaceuticals. This change is compared to the fingerprint of the complex adduct with α_1-AGP, where the intensity at 610 nm is stronger than that of 620 nm. Similarly to the studies with α_1-AGP binding, it is possible to follow the competitive binding, by examining the intensity ratio of the 615-620 nm / 595-600 nm bands.

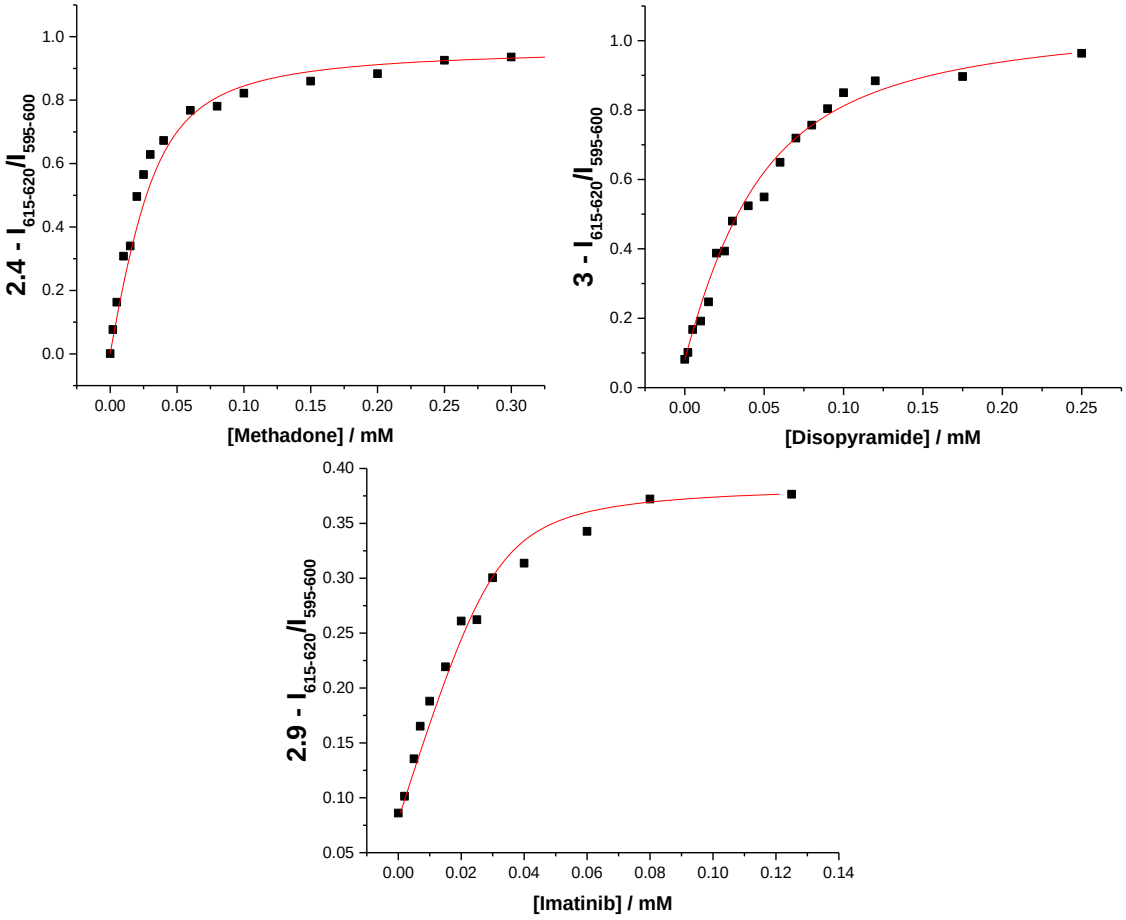

*Figure 2.10 - The binding curves of [Eu.**L**^{1}]$^+$: α_1-AGP (30 μM, 1:1, 0.1 M NaCl, pH = 7.4, 295 K) with increasing concentrations of methadone (left), disopyramide (right), and imatinib (bottom)*

Log*K* values were determined as for the complex with α_1-AGP. The ratio of intensity of sections of the ΔJ = 2 / ΔJ = 1 manifolds (615-620 nm / 595-600 nm) were plotted against increasing drug concentration. These bands in particular are regularly chosen, due to the large change observed in the co-ordinately hypersensitive ΔJ = 2 band compared to the absence of significant change in the electronic dipole forbidden ΔJ = 1 transition.

Table 2.2 - The experimental and literature logK values of the three drugs investigated. Unless stated otherwise, conditions from the literature values are assumed to be the same as the experimental conditions (0.1 M NaCl, pH 7.4, 295 K)

Pharmaceutical	Total emission log*K*	Literature log*K* values
Methadone	4.96 (±0.02)	5.60 (±0.08)[112,c]
Disopyramide	4.59 (±0.01)	3.47[121,d] , 5.87 (±0.09)[178,c]
Imatinib	5.54 (±0.02)	6.38 (±0.2)[126]

The log*K* values that were determined in these experiments (Table 2.2) clearly differ from those found in literature, by approximately an order of magnitude. In the cases of disopyramide and methadone, this can be explained by the varying conditions in the experiments. For example, the first disopyramide value reported in the literature (log*K* = 3.47) was calculated at pH = 4.0, where binding to the complex may be significantly different depending on the levels of protonation of both the complex and the drug. The log*K* values for methadone, and the second disopyramide value quoted, were calculated at 37 °C, which may also explain why the literature values were different than those found in this experiment.

However, it does not explain the difference in log*K* values in imatinib. As imatinib replaces the complex in the binding site, it is in competitive equilibrium. Hence, the value calculated from total emission experiments, where imatinib replaces the complex in the binding site of the protein maybe smaller than if there was nothing bound to α_1-AGP already. Furthermore, in the same paper that found a log*K* value of 6.38 (±0.2), when calculating via displacement of imipramine, an apparent log*K* value of 5.30 was found, which is much closer to the value calculated from total emission.[126]

2.2.2 CPL Studies of Drug Binding

Circularly polarised luminescence is rarely used to monitor changes in europium emission. However, it is slowly gaining popularity as more CPL spectrometers are being built and bought, allowing greater advancement in its understanding. In this example, the drugs compete with the complex to bind to α_1-AGP. [Eu.**L**$^{\mathbf{1}}$]$^+$ returns back into the bulk solution, with no preference for either enantiomer which causes the CPL signal of the complex to decrease with increasing concentration of drug.

[c] 37 ˚C
[d] pH 4.0

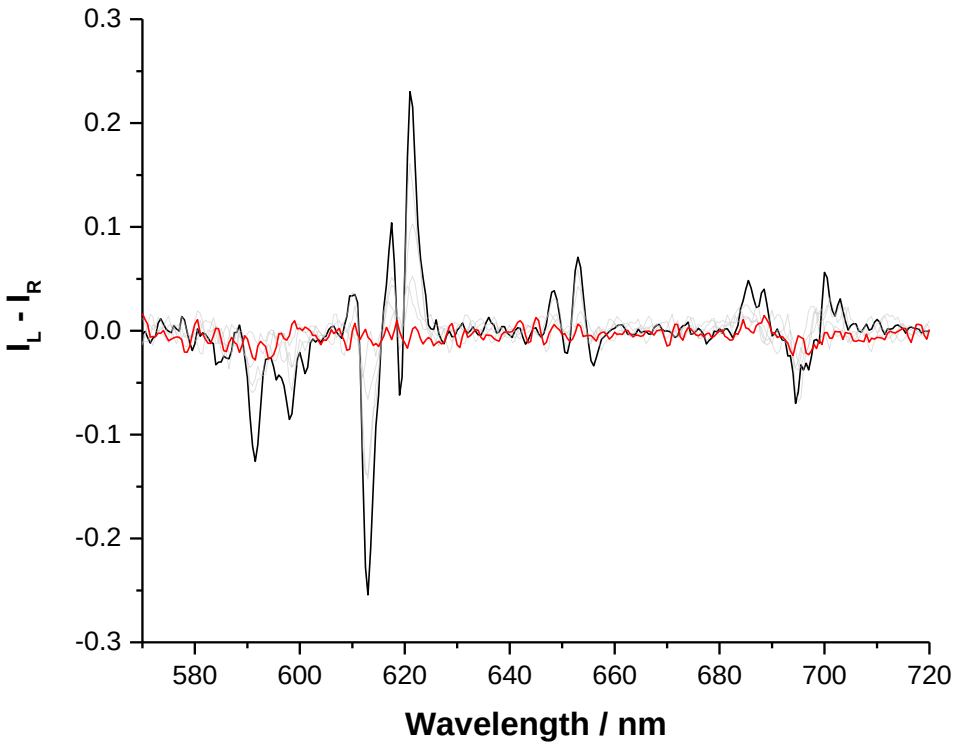

*Figure 2.11 - CPL spectrum of [Eu.**L**^{1}]$^+$:α_1-AGP (black) (30 μM, 1:1, 0.1 M NaCl, pH = 7.4, 295 K) with increasing concentrations of methadone, up to 0.3 mM (red), showing a decrease in CPL signal*

The two largest CPL signals, and hence the easiest to follow, are found in the $\Delta J = 2$ transition at 613 and 621 nm. The strong signal is not unsurprising as to attain maximum intensity in CPL, both the magnetic and electric dipole transition should be allowed, which is the case for this transition.

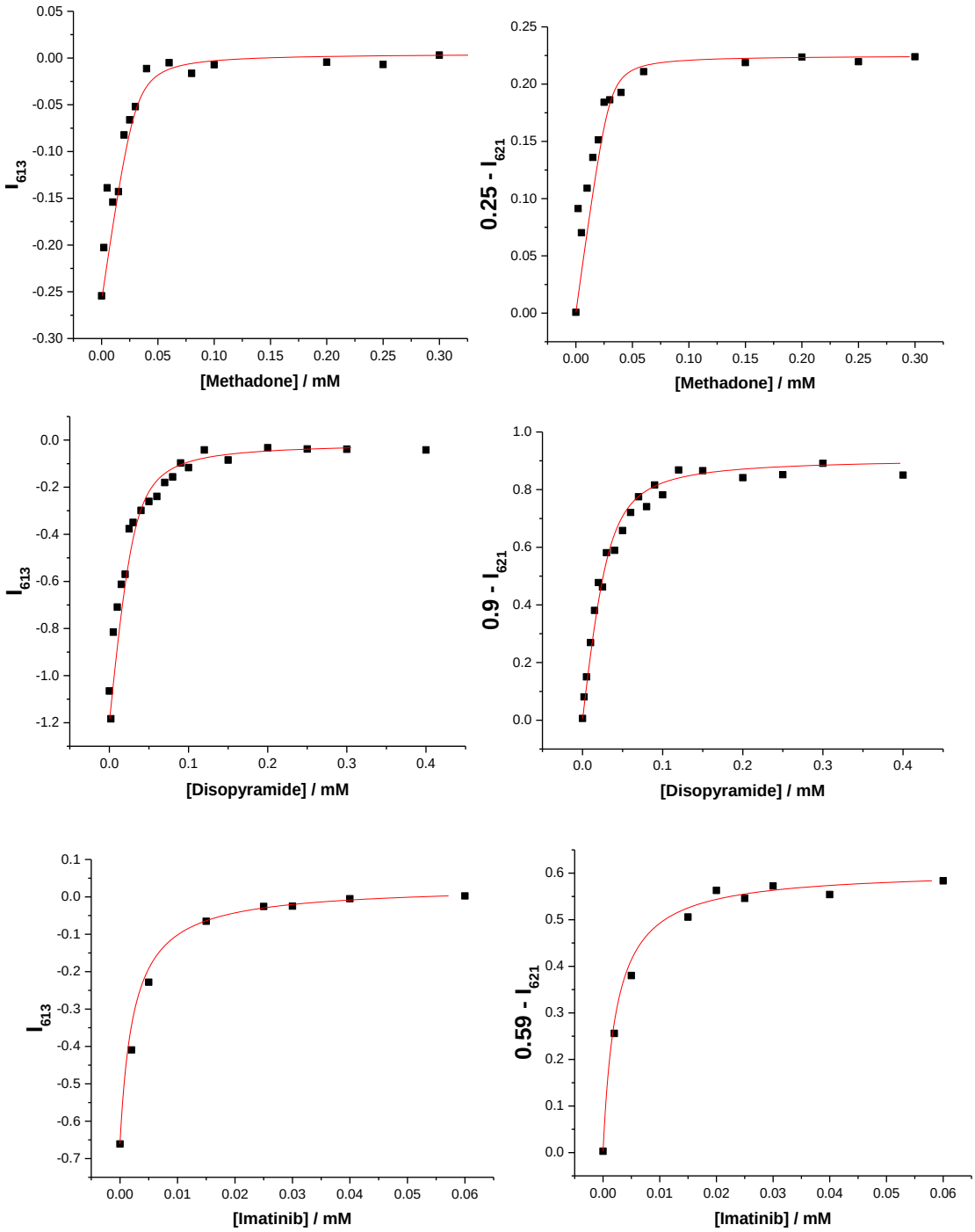

*Figure 2.12 - The change in intensity of the CPL signal of [Eu.**L**^{1}]$^{+}$:α_1-AGP (30 μM, 1:1, 0.1 M NaCl, pH = 7.4, 295 K) at 613 nm (left) and 621 nm (right) with added methadone (top), disopyramide (middle) and imatinib (bottom)*

In each case, the pharmaceutical was added to a [Eu.**L**^{1}]$^{+}$:α_1-AGP solution until the CPL signal had been completely lost. Hence, the binding curve reaches a limit. Both CPL signals at 613 and 621 nm were used, (Figure 2.12) and iterative least square fitting to a 1:1 binding model was used to determine an apparent log*K* value.

*Table 2.3 - The logK values calculated for the binding of each pharmaceutical to [Eu.**L**^{1}]$^{+}$:α_1-AGP (30 μM, 1:1, 0.1 M NaCl, pH = 7.4, 295 K) at 613 and 621 nm with total emission and literature values for reference*

Pharmaceutical	log*K* at 613 nm	log*K* at 621 nm	Total emission log*K*	Literature log*K* value
Methadone	5.66 (±0.07)	5.88 (±0.06)	4.96 (±0.02)	5.60 (±0.08)[112,e]
Disopyramide	5.27 (±0.04)	5.12 (±0.06)	4.59 (±0.01)	3.47[121,f], 5.87 (±0.09)[178,e]
Imatinib	5.63 (±0.01)	5.63 (±0.04)	5.54 (±0.02)	6.38 (±0.2)[126]

For methadone, the CPL derived values were significantly closer to the literature values, compared to the log*K* values calculated from analysis of total emission changes. Indeed, the binding constant calculated from data at 613 nm is the same as the literature value within the statistical error of the fit. However, as the experiments were performed under different experimental conditions, more specifically, at different temperatures, these log*K* values should not be the same. A binding constant calculated at the same temperature would be more useful.

There is a similar story for disopyramide. The two literature binding constants are very different, due to the differing conditions used in each. For example, at pH 4.0, the log*K* value is significantly smaller, but the one calculated at physiological temperature is slightly higher. Although the two binding constant from the CPL are not within the stated error, they are more similar compared to the binding constant of 4.59 (±0.01) derived from total emission data. Again, although it is difficult to compare due to the variation in conditions, the CPL binding constants are more in agreement with literature values than the total emission constants.

Lastly, imatinib still gives log*K* values that are almost an order of magnitude different from the literature value, and is only a little higher than the value 5.54 (±0.02), calculated from total emission. The CPL values are in agreement with each other, but they should be within error of both the total emission and literature. Evidently, this is not the case.

[e] 37 ˚C
[f] pH 4.0

2.2.3 Emission Lifetime Analysis

The lifetime of europium was measured at the end of each titration. Using analogous methods to gain the lifetimes after α_1-AGP titrations, the readings were initially taken in H_2O, the solution lyophilised and subsequently re-dissolved in D_2O. The removal of solvent was repeated three times to ensure complete removal of H_2O as residual levels could affect the emission decay data. The sample was dissolved again in D_2O, to obtain the second lifetime necessary for the calculation of the *q* value.

Table 2.4 - Lifetimes of $[Eu.\mathbf{L^1}]^+$:α_1-AGP (1:1) with methadone, disopyramide, and imatinib in H_2O and D_2O and the relevant q value

Pharmaceutical	Lifetime in H_2O (τ_1) (ms)	Lifetime in D_2O (τ_1) (ms)	*q* value
Methadone	0.45	1.46	1.5
Disopyramide	0.45	1.48	1.5
Imatinib	0.40	1.39	1.8

In all three cases, the lifetimes were extracted, and using Equation **2.1** the *q* values were calculated. The *q* values increase back to levels similar to those seen with the complex in the absence of α_1-AGP. Again, this behaviour suggests that the pharmaceutical binds to the protein, displacing the complex. When this process occurs, the glutamate arm from the binding site of α_1-AGP is no longer bound and the complex is removed from the hydrophobic pocket of the protein. This allows for a solvent water to bind directly to the metal ion, which decreases the lifetime as water promotes a pathway for non-radiative decay. Not only does this affect the lifetime, but also decreases the overall intensity of the europium spectrum.

2.3 Enantiomer Resolution of the Drug

Of the drugs chosen for this investigation, two are available as a racemic mixture. In many examples, pharmacological drugs existing as two enantiomers have very different effects on biological systems. The most famous example of this is thalidomide, a drug originally given to alleviate morning sickness during early pregnancy and thought to be safe.[179] However, it was soon found to be the cause of phocomelia, the disfigurement in developing foetuses. Research later found that *S*-thalidomide is responsible for this effect, with *R*-thalidomide being the enantiomer with sedative properties.[180] It has also been suggested that if only *R*-thalidomide was prescribed, then it would still be

effective. However, due to the acidic proton at the chiral carbon centre, enantiomeric interconversion occurs rapidly in the body. Although the drug is still used today in frontline cancer treatment, the risk associated with pregnancy means it is carefully controlled.

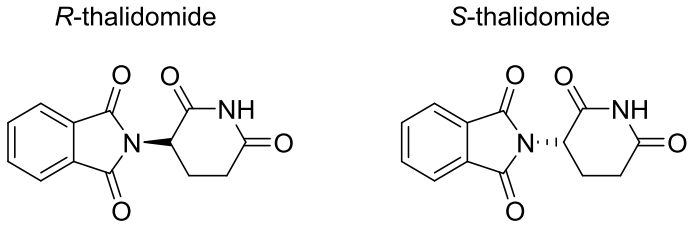

Figure 2.13 - The structure of (R)- (left) and (S)-thalidomide (right)

There are numerous other examples of one enantiomer working more efficiently, or one enantiomer being liable for certain side-effects. Methadone is no exception; the *R*-enantiomer being a better MOR (μ-opioid receptor) than *S*-, with the *S*- enantiomer thought to be responsible for the arrhythmia problems which are sometimes noted in methadone treatment.[181]

It is possible that with both methadone and disopyramide, the two enantiomers interact differently with α_1-AGP. This aspect is important, as if one enantiomer binds more strongly to the protein, it will be less bioavailable which could potentially affect the efficacy of the medicine. This situation is of particular note if the more strongly bound enantiomer is more active.

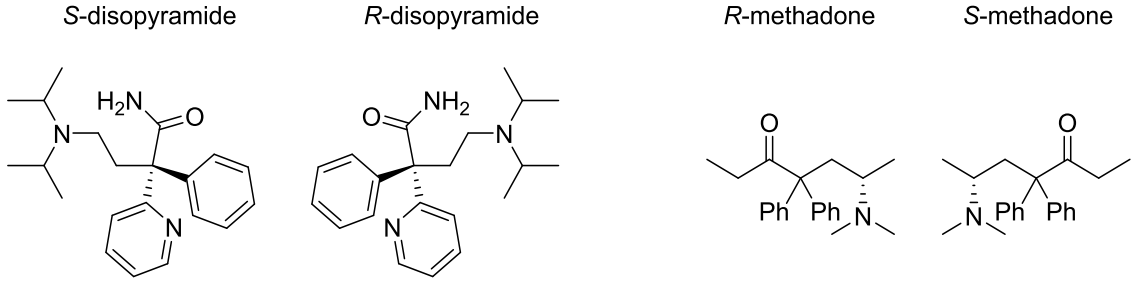

Figure 2.14 - Structures of the two enantiomers of disopyramide (left) and methadone (right)

Both disopyramide and methadone were obtained as racemic mixtures and their resolution was studied.

2.3.1 Disopyramide Enantiomers

Disopyramide was selected initially, and separation of its enantiomers was attempted on a series of chiral HPLC columns, with different solvent systems. Base line separation

was successfully achieved with a CHIRALPAK-IC analytical column in hexane:DCM:methanol (65:30:5) adding 0.05% diethylamine (DEA) to stop the tailing of the peaks, by inhibiting N-protonation.

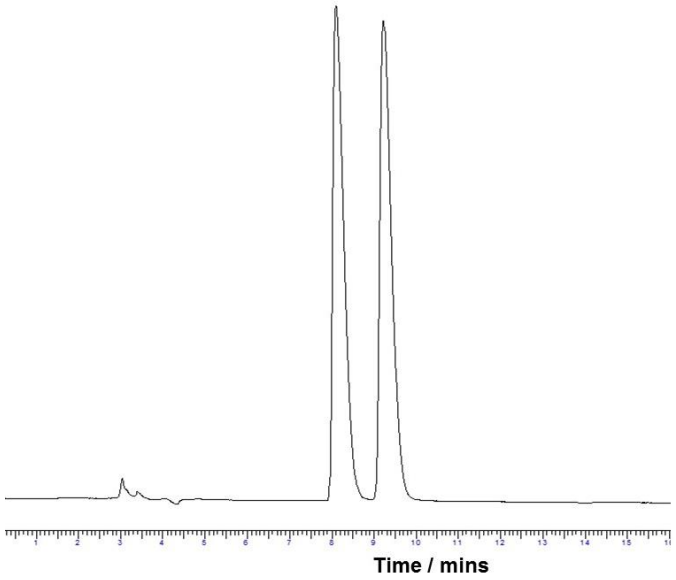

Figure 2.15 - Resolution of the two enantiomers of disopyramide (CHIRALPAK-IC, hexane:DCM:methanol (65:30:5) with 0.05% DEA, 295 K, λ_{em} = 260 nm)

Once separated on a larger scale, using the same conditions, but with a semi-prep CHIRALPAK-IC column, the two enantiomers could be tested separately and the binding constants compared. However, once the two enantiomers were separated, there was no way of detecting which enantiomer was which. The amount obtained from HPLC were too low to use a polarimeter, and even after attempts at recrystallisation, only a powder was obtained and as such, the absolute configuration of the enantiomer could not be determined through crystallography. As such, they were labelled disopyramide one, which eluted from the column first, and the latter was named disopyramide two.

As with all previous experiments, the complex was dissolved in purite water at pH 7.4, with 0.1 M NaCl, until a concentration of 30 μM was achieved. α_1-AGP was then added to make a 1:1 solution with the complex. Disopyramide was sequentially added and the change in the europium emission spectrum was monitored.

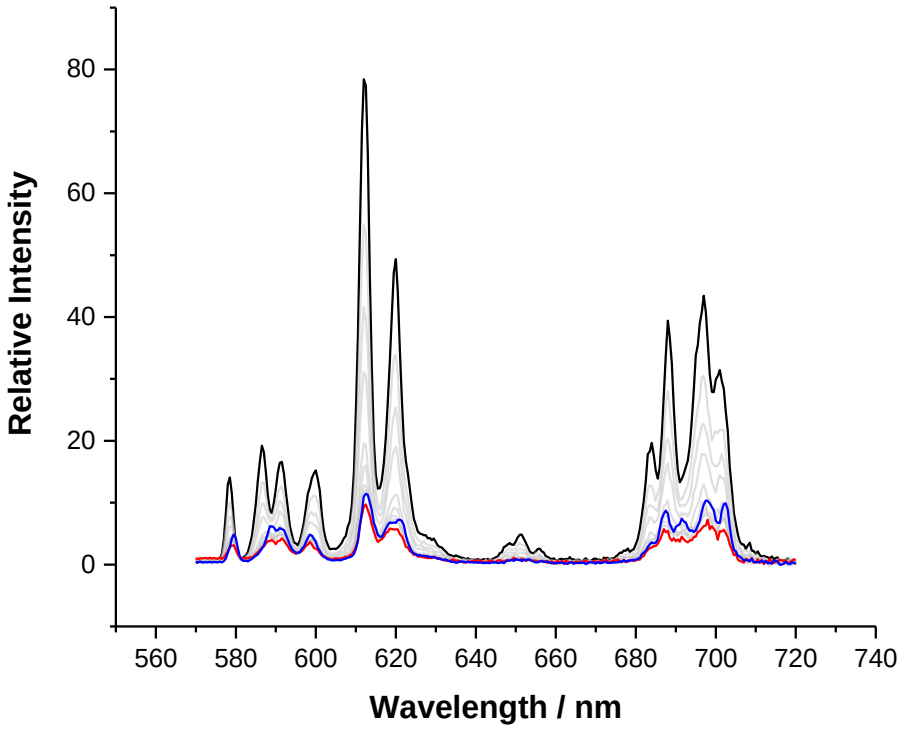

*Figure 2.16 - Change in the emission spectra of [Eu.**L**^{1}]$^{+}$:α_1-AGP (black) (30 μM, 1:1, 0.1 M NaCl, pH 7.4, 295 K) with increasing concentration of disopyramide 'one', up to 0.3 mM (red), with 0.3 mM of racemate for comparison (blue)*

As expected, the change in emission intensity and spectral form of both disopyramide one and two are similar to those of the racemic mixture.

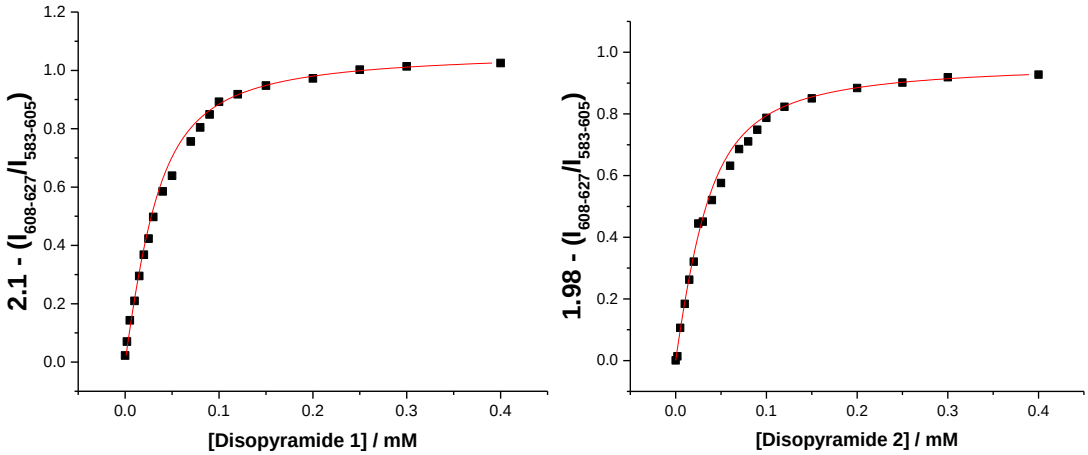

*Figure 2.17 - The binding curves of [Eu.**L**^{1}]$^{+}$:α_1-AGP (30 μM, 1:1, 0.1 M NaCl, pH = 7.4, 295 K) following the ratio 608-627 nm / 583-605 nm, with increasing concentrations of disopyramide 'one' (left) and 'two' (right)*

After plotting the binding curve, the binding constants were estimated by non-linear regression analysis were smaller than expected with log*K* values of 4.80 (±0.01) and 4.78 (±0.02) for 'one' and 'two' respectively. This is a magnitude lower than the quoted

literature value, and surprisingly, significantly smaller than the value calculated with the racemate.

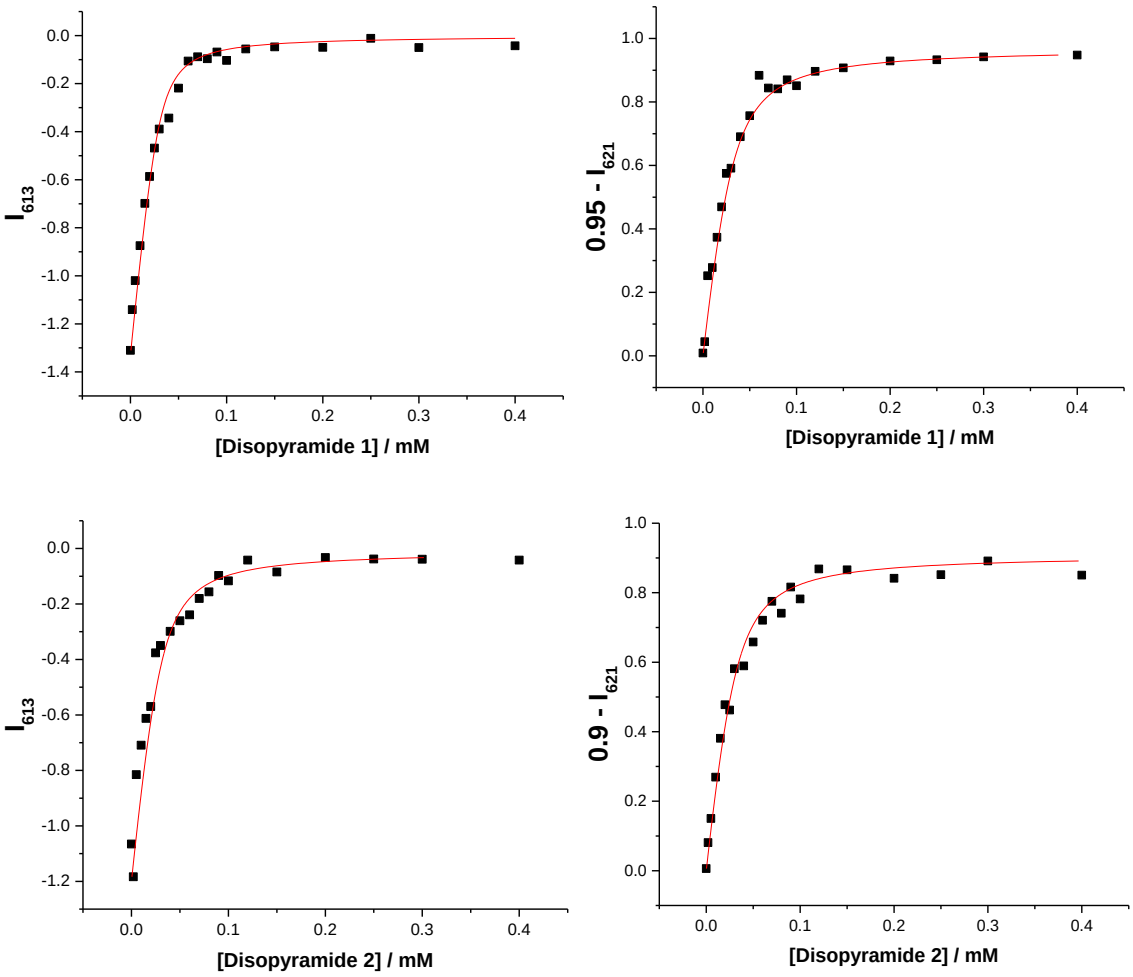

*Figure 2.18 - The fitted binding curved of [Eu.**L**^{1}]$^{+}$:α_1-AGP (30 μM,1:1, 0.1 M NaCl, pH 7.4, 295 K) with increasing concentrations of disopyramide one (top) and two (bottom) following the intensity of the CPL signal at 613 nm (left) and 621 nm (right)*

The analogous titration examined changes in CPL. As expected, there was a decrease in CPL signal, and the binding event was followed as in previous experiments, by analysing the changes in the two wavelengths that gave the strongest initial signal at 613 and 621 nm.

*Table 2.5 - The logK values of the two enantiomers of disopyramide with [Eu.**L**^{1}]$^{+}$:α_1-AGP (30 μM, 1:1, 0.1 M NaCl, pH 7.4, 295 K) using CPL and total emission*

	log*K* CPL (613 nm)	log*K* CPL (621 nm)	log*K* Total emission (608-627 nm / 583-605 nm)
Disopyramide 'one'	5.49 (±0.08)	5.09 (±0.01)	4.80 (±0.01)
Disopyramide 'two'	5.24 (±0.04)	5.12 (±0.06)	4.78 (±0.02)

For the first enantiomer, none of the three calculated log*K* values were within error, so it is impossible to determine the correct binding constant from these experiments. For disopyramide 'two' the range of log*K* values is not as broad, but again, they are not within the error of each other. Therefore, there is no definite conclusion to the correct binding constant of either enantiomer, and it cannot be confirmed if they have the same or different binding constants. However, they are sufficiently close that it suggests that each enantiomer binds with a similar affinity to α_1-AGP.

Again, experimental errors could play a part in these experiments, particularly in the readings from the CPL at high disopyramide concentration as there is poor signal to noise ratio and as such, liable to significant error. Other errors, such as change in pH could also play a role.

2.3.2 Methadone Enantiomers

To separate the two enantiomers of methadone, a different approach was necessary. Although it is possible to use chiral HPLC columns, the appropriate columns were not available. A classic way to differentiate between enantiomers is to recrystallise them. Louis Pasteur famously discovered molecular chirality after the discovery of mirror image forms of crystals in the sodium ammonium salt of paratartaric acid.[182] With methadone, the addition of one enantiomer of tartaric acid allows the crystallisation of one diastereoisomeric salt, from which methadone can be subsequently released by addition of base.

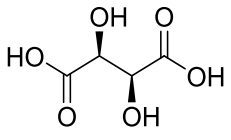

Figure 2.19 - The structure of D- or (S,S)-tartaric acid

Following the method of Larsen *et al*., a racemic mixture of methadone was dissolved in propanol with *D*-tartaric acid (Figure 2.19), and left in the fridge overnight.[183] A white powdery solid was filtered off, which was recrystallised again to ensure sample purity. The powder was dissolved in water and a few drops of ammonia were added to remove the tartaric acid. Methadone precipitated out, and was filtered, before a few drops of conc. HCl were added to make the hydrochloride salt. The separation of the pure enantiomer was confirmed by melting point analysis at each point in the separation, following values recorded in the literature.[183]

To retrieve the second enantiomer, the original solution was taken, and *L*-tartaric acid was added. Thus, following the same method as above, both enantiomers were successfully separated.

Although purification was confirmed through melting point analysis, particularly at the point of formation of their tartrate diastereoisomers, further confirmation of enantiomeric purity was achieved using a chiral solvating agent (CSA), (*R*)-(−)-*O*-acetylmandelic acid (Figure 2.20). This compound can be used to determine the enantiomeric purity of amines by ^{1}H NMR analysis of the diastereoisomeric salts formed *in situ*.[184]

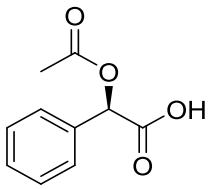

Figure 2.20 - The structure of (R)-(–)-O-acetylmandelic acid[184]

The amine in methadone interacts with the CSA in a non-polar solvent which causes ^{1}H NMR resonances of the different enantiomers to shift. The CSA was first added to the racemic mixture to see which resonances were affected and therefore, which were best to monitor.

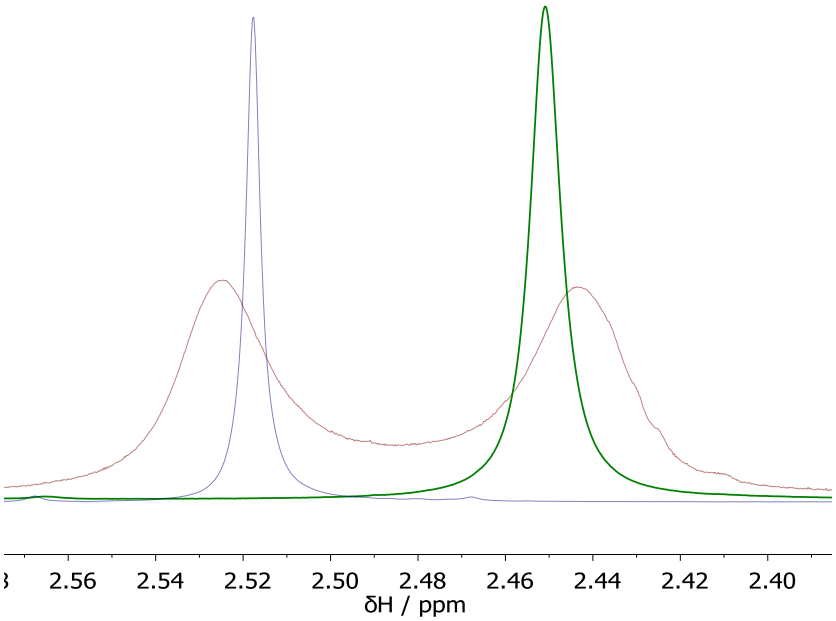

Figure 2.21 - Partial ^{1}H NMR (400 MHz, $CDCl_3$, 295 K, 2.39 – 2.57 ppm) spectrum of racemic methadone (red), (R)-methadone (green), (S)-methadone (blue) following the addition of (R)-(-)-O-acetylmandelic acid

The resonance at 2.15 ppm shifted to 2.48 ppm (Figure 2.21) and the splitting of this resonance from a singlet to a doublet for the two methyl groups attached to the nitrogen (H^6) was the most promising, along with some smaller splitting of methyl resonances in the 0-1 ppm region.

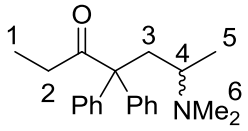

Figure 2.22 - The structure of racemic methadone

Upon addition of the CSA to the separated enantiomers, the resonance at 2.15 ppm was shifted to either 2.45 (*R*-) or 2.52 ppm (*S*-) but remained as a single peak. The splitting of the resonance of the methyl group at 0.54 ppm (H^5) also occurred. Two dimensional NMR methods, namely COSY, HSQC and HMBC were utilised to find out more about the full spectral assignment.

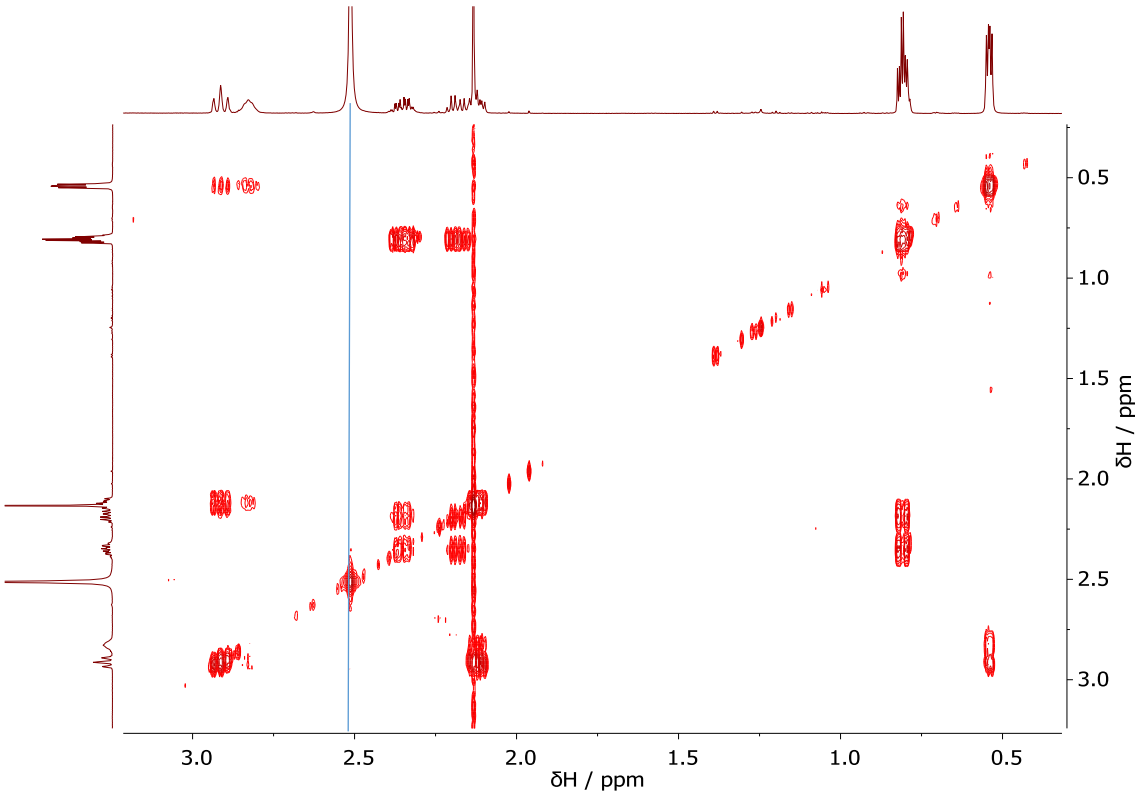

Figure 2.23 - ^{1}H NMR COSY (500 MHz, 295 K, $CDCl_3$) of (S)-Methadone in the presence of (R)-(−)-O-Acetylmandelic acid

From Figure 2.23, it is possible to see that the resonance at 0.54 ppm (H^4) is coupled to two resonances at 2.83 and 2.93 ppm (H^3). The two separate peaks for H^3 highlights that two protons are diastereotopic, which can be seen on NMR due to the more rigid structure of methadone when interacting with (*R*)-(−)-*O*-acetylmandelic acid.

There are other slight changes including the shifting of the two diastereotopic CH_2CO protons (H^2) to 2.20 ppm and 2.37 ppm; it was proven that they were on the same carbon using HSQC.

2.3.2.1 Binding studies of the enantiomers of methadone.

Following successful separation of the two enantiomers of methadone, titrations with $[Eu.\mathbf{L^1}]^+$:α_1-AGP were carried out at pH 7.4, with increasing concentration of the drug.

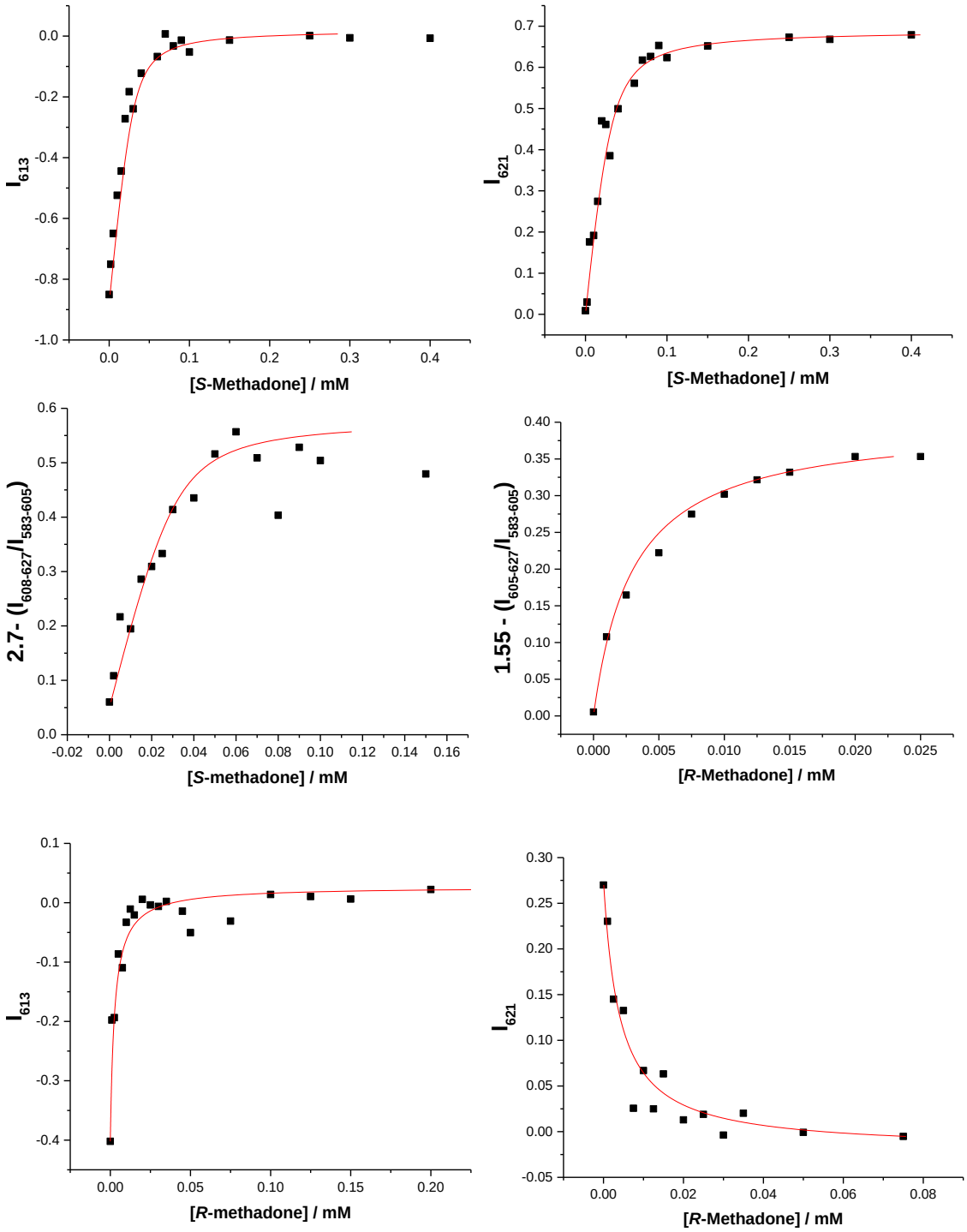

*Figure 2.24 - The binding curves of [Eu.**L**^{1}]$^{+}$:α_1-AGP (30 μM, 1:1 ratio, 0.1 M NaCl, pH 7.4, 295 K) with increasing concentration of S-methadone (top) and R-methadone (bottom) using both CPL and total emission (middle)*

The experiments were followed by analysis of CPL and total emission data (Figure 2.24), and the binding constants were calculated similarly to previous experiments. In the total emission experiments, the ratio of the bands at 608-627 nm / 583-605 nm were used, as it gave a slightly better data.

*Table 2.6 - The logK values of [Eu.**L**^{1}]$^{+}$:α$_1$-AGP (30 μM, 1:1 ratio, 0.1 M NaCl, pH 7.4, 295 K) with the two enantiomers of methadone, using CPL and total emission*

	log*K* CPL 613 nm	log*K* CPL 621 nm	log*K* total emission
R-Methadone	5.58(±0.05)	5.40 (±0.07)	5.52 (±0.01)
S-Methadone	5.42 (±0.09)	5.20 (±0.02)	5.41 (±0.13)

For *R*-methadone, the binding constants, ranged from log*K* 5.40-5.58, with the higher values being close to the literature value of 5.60 (±0.08) However, none of the values are within error of each other. For *S*-methadone, two log*K* values are close to 5.42, but with relatively large errors. The relevance of this being that it is still close to the literature value, and again suggests that both enantiomers have similar binding constants to α$_1$-AGP. However, the third log*K* value for *S*-methadone is smaller, with a value of 5.20 (±0.02). For both enantiomers, the calculated log*K* value at 621 nm were smaller than those at 618 and those calculated from the total emission. This lower value could also be a product of the poor shape of the graph, and the subsequent poor fit of the data. Furthermore, it could be related to the poor signal to noise ratio as the CPL gets smaller as the complex is removed from the binding site of α$_1$-AGP. More repetitions of this experiment could produce better results, with a smooth graph which could be fit to give a more accurate binding constant.

2.4 Conclusions and Further Work

The complex, [Eu.**L**^{1}]$^{+}$ was specifically selected because of previous reports detailing its ability to bind to α$_1$-AGP. The pharmaceuticals were chosen as they have demonstrated similar binding constants as the complex to α$_1$-AGP, which allows for competitive binding, as well as having a suitable absorption spectrum allowing selective excitation of the europium complex chromophore. This chapter highlights the use of this complex as a ratiometric probe, to calculate the drug concentration in solution, using both total emission and CPL spectroscopy. A binding curve was obtained for the complex with α$_1$-AGP, as well in the presence of the three competing drugs.

There are a number of previous examples which highlight the importance of enantiomeric drugs in biological systems, so the racemic mixtures of methadone and disopyramide were separated using crystallisation and chiral HPLC respectively. The separate enantiomers were also titrated into a [Eu.**L**^{1}]$^{+}$: α$_1$-AGP solution and the binding

constants determined to investigate whether they bound to the protein with different binding affinities.

The next step would be to construct a calibration curve for each drug in the medium of interest. Following this, there is the potential to test 'unknown' concentrations to determine whether [Eu.$\mathbf{L^1}$]$^+$ can be used analytically. Thus far, the complex has only been investigated in water. One of the next steps to take would be to look at how well the [Eu.$\mathbf{L^1}$]$^+$ works in more competitive media, with the aim being to analyse samples of the complex in human serum.

Furthermore, as mentioned in Section 1.4, α_1-AGP has a number of different polymorphs and previous research has shown that varying the polymorphs and levels of glycosylation can affect the binding behaviour of certain analytes. This is an important aspect for any type of personalised medicine, as concentrations of the polymorphs can differ from person to person.[185] It is possible to separate polymorphs into A and F1*S by chromatography.[127] Analogous binding experiments can be carried out on these two polymorphs to extract a binding constant to gather more information towards the main goal of creating a complex that may be suitable for more general use.

The complex has the potential to be tested on a greater number of pharmaceuticals. Work within Durham has examined this aspect. Four other drugs were examined, the anaesthetics lidocaine and bupivacaine, as well as the antidepressants nortriptyline and imipramine. Using the same complex, Ryan Waters MChem. looked at the CPL and total emission changes to calculate the binding constants.[111]

Table 2.7 - The logK values of [Eu.$\mathbf{L^1}$]$^+$:α_1-AGP (30 μM, 1:1, 0.1 M NaCl, pH = 7.4, 295 K) with four pharmaceuticals, from CPL, total emission, and quoted literature values[111]

	log*K* (Total emission)	log*K* (CPL)	log*K* (literature)
Bupivacaine	4.77 (±0.05)	5.38 (±0.03)	5.5-5.7[186,187]
Lidocaine	4.31 (±0.03)	4.38 (±0.04)	4.6-5.2[187,188,g]
Nortriptyline	3.60 (±0.01)	4.44 (±0.04)	4.3-5.1[189]
Imipramine	4.18 (±0.02)	4.90 (±0.04)	5.6[186]

[g] log*K* calculated at 37 °C

Again, promising results were obtained, both in analysing the total emission and CPL data. Any further work suggested for the three drugs in chapter two, can also be applied to these. Bupivacaine is another racemic drug so the separation of the two enantiomers and subsequent titrations was considered a logical next step. *S*-Bupivacaine is commercially available, and therefore, titrations were also performed with this enantiomer, to give log*K* values that are reported in the range 5.41 (±0.04) and 5.46 (±0.01) for total emission and CPL respectively. This value was very close to the literature value of 5.4-5.8.[187,190] However, the *R*- enantiomer was never isolated. Although this is the case, as *S*-bupivacaine has a very similar binding constant to α_1-AGP as the racemate, it is suggestive that *R*-bupivacaine would also have the same or a similar log*K* value. There is no reason however, to limit such analysis to these drugs. Any alkaline drugs with a known binding constant of approximately log*K* = 5 to α_1-AGP could be suitable for analysis provided they do not absorb strongly above 300nm.

3. Eu(III) Complexes for the Detection of Glyphosate

Due to the popularity of glyphosate, and the ever growing resistance against its usage, the low cost 'in-house' detection of glyphosate is of increasing interest. The initial and current methods of detection are through HPLC and mass spectrometry, which requires derivatisation of glyphosate, adding time and money to the process.

This chapter will consider a number of complexes that were selected base on their particular absorption and chemical properties. It will examine complexes that upon binding to glyphosate, give rise to an emission spectral profile that allows ratiometric methods of analysis to be used. The ratio can be simply used by comparison to a calibration curve to calculate the concentration of the herbicide in a variety of solvent media, from experiments in water, to river water, and grain background.

The first example is an azaxanthone based complex which has previously been reported to bind citrate selectively with a log*K* value of 4.36 (±0.01); citrate itself is unlikely to be a competitive interferent when looking at river water or drinking water samples.[52] It is hypothesised that it would bind to glyphosate through the phosphate oxygen.

3.1 Synthesis and Overview

The synthesis of [Eu.$\mathbf{L^2}$]$^+$ was undertaken following a previously published method.[52] The first step in the synthesis is the same as for [Eu.$\mathbf{L^1}$]$^+$, i.e., the *trans* disubstitution of cyclen, **1** (Scheme 3.2). An alkylation step followed, involving addition of the α-bromoamide, **8**, to the remaining secondary amine sites on the ring to yield **9**. The amino acid arm was synthesised in a single step involving the reaction of alanine ethyl ester with bromoacetyl bromide to yield a yellow oil which was crystallised from DCM and petroleum ether to give a white crystalline solid (Scheme 3.1).

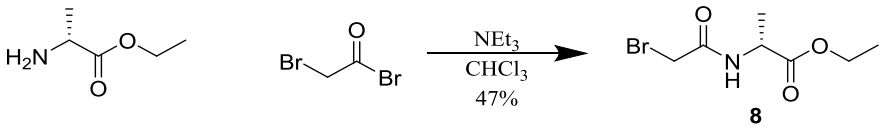

8

Scheme 3.1 - Synthesis of the α-bromo amide

The protecting groups of **9** were selectively removed by hydrogenation to yield **10**, before the addition of a single chromophore moiety. The separation of **11** from dialkylated material was achieved by column chromatography on alumina. The remaining secondary amine on cyclen was methylated, by boiling under reflux with

formic acid and formaldehyde to give **12**. This step was followed by hydrolysis of the ester groups to give $\mathbf{L^2}$. The hydrolysis reaction was carried out using NaOD in D_2O to allow the reaction to be tracked by ^1H NMR. The ligand was then complexed with $Eu(OAc)_3$, at pH 5.5 to yield the desired complex as a pale yellow solid.

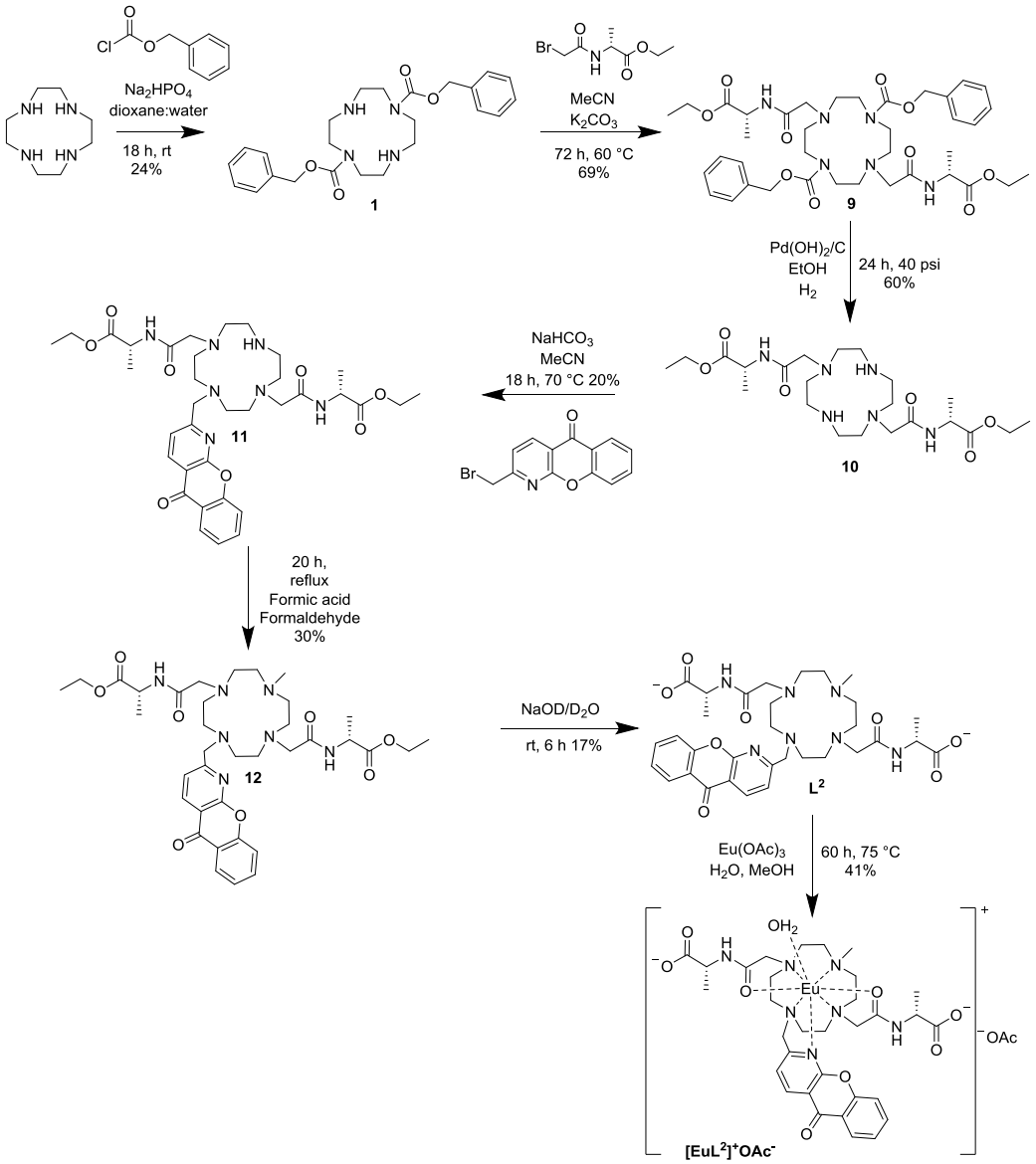

Scheme 3.2 - Synthesis of $[Eu.\mathbf{L^2}]^+$

The organic chromophore in this complex is the same as that used in $[Eu.\mathbf{L^1}]^+$ (Scheme 2.2). The synthesis of the complex was confirmed by mass spectrometry and characterised by its luminescence emission spectrum.

3.2 Initial Tests of Glyphosate Detection in Buffer

Titrations with glyphosate were undertaken. Initial tests were carried out in aqueous solution, as one of the key aims of this project is the ability to test for glyphosate in

water. An aqueous solution of 0.1 M NaCl was chosen to ensure constant ionic strength throughout the titrations. The pH of each titration was maintained at 5.9 with a 0.1 M MES buffer solution. The pH of 5.9 was specifically chosen due to the differing pK_a values of glyphosate and one of its main interferents, inorganic phosphate. The pK_a of dihydrogen phosphate is known to be 7.21,[191] whereas the equivalent proton in glyphosate has a pK_a of 5.58.[192] Therefore, at 5.90, glyphosate is predominately a di-anion, whereas phosphate is a mono-anion, and enhanced selectivity for the doubly charged species is expected, based on the primary electrostatic interaction.

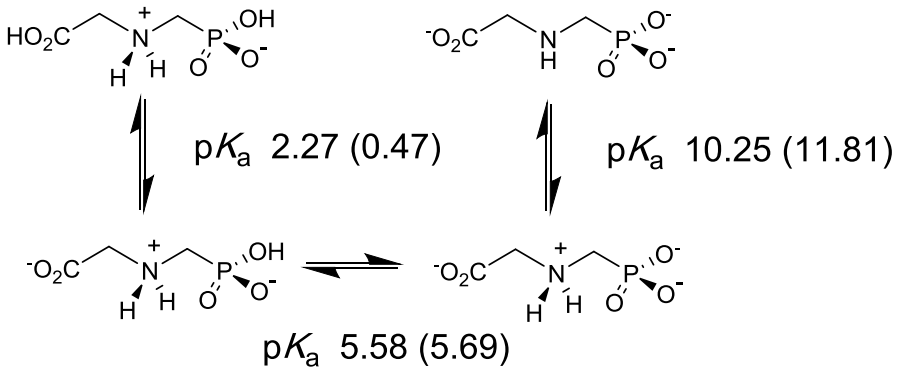

Figure 3.1 - The experimental pK_as of glyphosate[193] (0.1 M NaCl) and in parentheses, the corresponding calculated values[192] (I = 0)

The long lifetime of europium luminescence allows for time-gating to be utilised effectively. In 'real world' samples of grain extract, and even possibly river water, the presence of certain components may give rise to unwanted short lived auto-fluoresce, following excitation at 365 nm. In the instrumental set up used throughout this project, a 365 nm LED, operating at 330 mW was used as the excitation source, and each sample was irradiated for 2 ms during excitation. The time-gated spectrometer then collected data 0.01 ms after the excitation pulse, to ensure it is solely the long-lived lanthanide luminescence that is being monitored, with a 7 ms intergration time.

Throughout these titrations, a 2 mL solution of $[Eu.\mathbf{L^2}]^+$ was used and incremental additions of an analyte solution, were made which was also dissolved in solution containing 0.1 M NaCl and 0.1 M MES at pH 5.9.

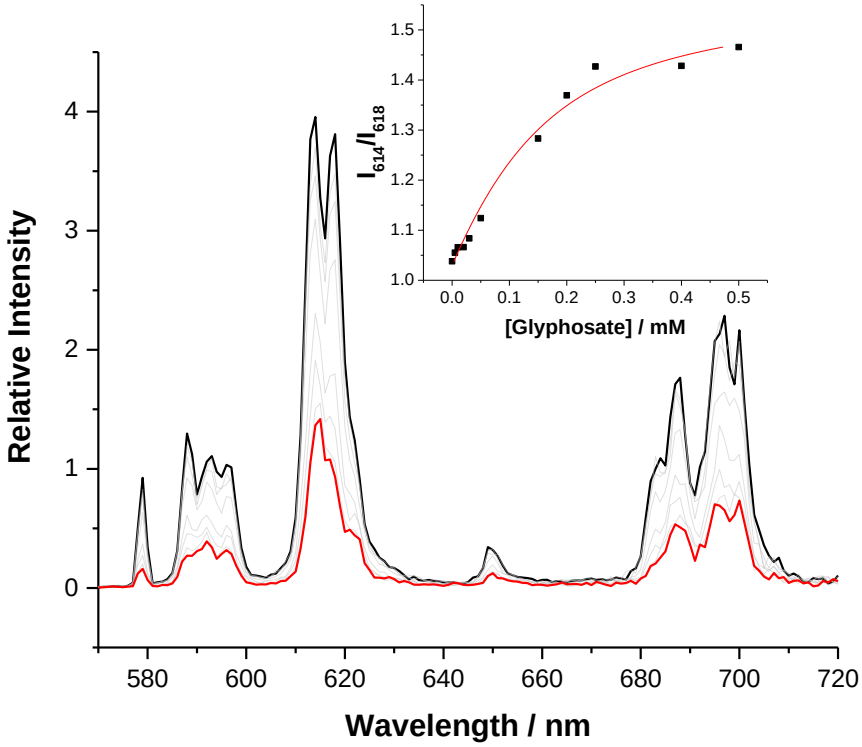

*Figure 3.2 - Changes in the emission spectrum of [Eu.**L**^{2}]$^+$ (black) (0.1 mM, 0.1 M NaCl, 0.1 M MES, pH 5.9, 295 K) with increasing concentration of glyphosate up to 0.5 mM (red). (Inset) The binding curve of [Eu.**L**^{2}]$^+$ as a function of increasing glyphosate concentration following the intensity ratio of 614 nm / 618 nm*

Following the titration, an overall decrease in emission intensity was observed. Binding of glyphosate could be tracked by examining the ratio of emission intensity at 614 nm / 618 nm in the hypersensitive $\Delta J = 2$ manifold, and could be used to calculate an apparent binding constant, following iterative least-squared fitting to a 1:1 binding model. A log$K$ value of 4.02 (±0.02) was extracted, consistent with the relatively strong binding expected with a phosphate group to a europium complex.

The log$K$ value was calculated using Equation **5.2** and the error stated in parenthesis is the statistical error of the fit to the data. Other experimental errors could play a role, with slight changes in concentration of either the complex or glyphosate would effect this value. The pH was controlled using buffer, but the reading from a pH meter is 0.02, and although the experiments were conducted in a temperature controlled room, there was still some fluctuations throughout all the experiments.

To test the efficiency of the complex, four samples (A-D) of 'unknown' concentration were made up by weighing out glyphosate, making a stock solution and then diluting further to get four samples of varying concentration. These were then analysed by the Durham University Geography Department, who from a stock solution of glyphosate were able to create a calibration curve of glyphosate using a Dionex LC system. From

this calibration curve, the four unknown samples were examined and their concentration calculated. These values were then compared to the 'weighed' values and those deduced by emission spectroscopic analysis.

Table 3.1 - Four samples of 'unknown' concentration, and the concentration calculated from Dionex LC, and via europium emission analysis. The values for Dionex LC are 95% confidence intervals. For the weighed complex there is 0.05% error and with the emission of the complex, there is a 10% error

Sample	Weighed conc. (μM)	Dionex LC (μM)	$[Eu.\mathbf{L^2}]^+$ (μM)
A	6.0	3.4	8.0
B	12.0	11.6	11.1
C	23.0	21.3	22.0
D	44.0	44.6	40.2

At lower concentrations, both the Dionex LC column and the complex are not the most accurate. Furthermore, at the highest concentration, the complex gives a smaller value compared to both the weight and LC column. The other two samples give values in a very similar range to the LC column which gives some confidence in the accuracy of the complex determination in this range. The USA is one of the only places to set an MRL in drinking water of 4.1 μM. This is slightly below sample 'A', but if the level of glyphosate was above this limit, the use of $[Eu.\mathbf{L^2}]^+$ would allow its detection.

3.3 Testing Competitive Analytes

Although initial results are promising, in more complex media there are more likely to be analytes which compete in binding to the complex and therefore inhibit accurate detection of glyphosate. Therefore, potential competitors should be studied to note the effect on binding and minimise interference risks.

3.3.1 Inorganic Phosphate

The titration was repeated, this time with inorganic phosphate at pH 5.9, in place of glyphosate. This competitive binding study observed little change in the 614 nm / 618 nm intensity ratio consistent with little or no interference. At the end of the titration, the pH was raised to 8.0 and a final emission spectrum was taken.

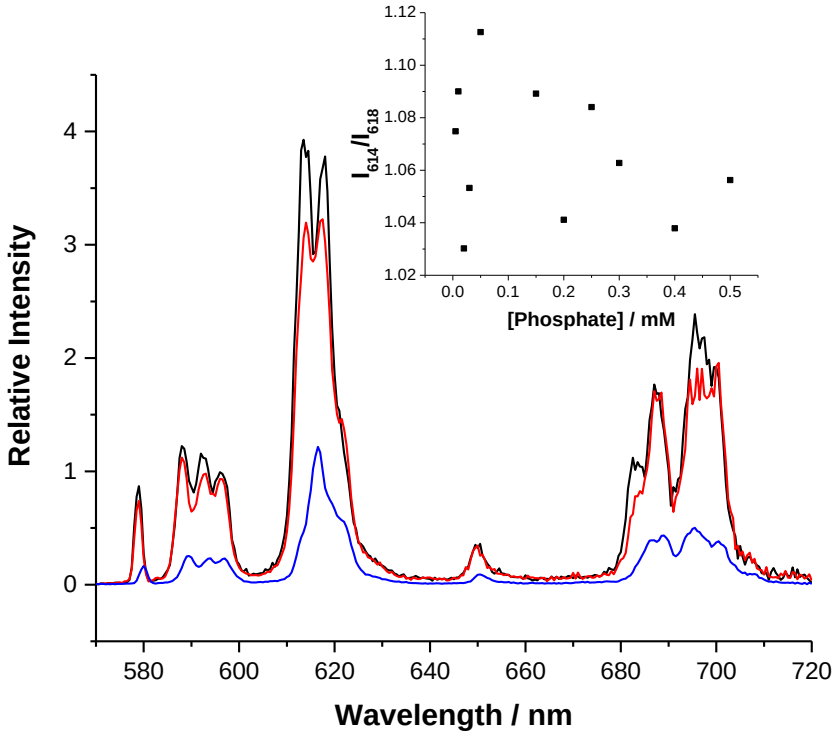

*Figure 3.3 - The emission spectrum of [Eu.**L**^{2}]$^+$ (0.1 mM, 0.1 M NaCl, 0.1 M MES, 295 K) with (red) and without (black) phosphate at pH 5.9 and with phosphate (0.5 mM) at 8.00 (blue). (Inset) The intensity ratio of 614 nm / 618 nm of [Eu.**L**^{2}]$^+$ at pH 5.9 as a function of increasing phosphate concentration*

At pH 8.0, the phosphate di-anion was expected to bind to the complex in a similar way to glyphosate. Indeed, the intensity ratio of 614 nm / 618 nm showed a significant change from 1.05 at pH 5.9 to 0.63 to pH 8.0, suggesting that binding of inorganic phosphate indeed occurs under these conditions.

The change in spectral form and intensity at pH 8.0 confirms that although phosphate has the potential for significant interference, the control of pH should minimize this effect. Phosphate is expected to bind in a monodentate fashion, with a water molecule still in the inner sphere, as deduced through lifetime measurements.[10] This is in line with previously reported data that phosphate acts as a monodentate ligand to single metal centres, with the possibility of bridging to multiple centres.[194,195] However, phosphate does still bind significantly better to the metal centre at pH 8.00, due to the stronger coulombic interactions.

To show that phosphate binds as a monodentate ligand, lifetime measurements were taken for [Eu.**L**^{2}]$^+$ in D_2O and H_2O, at the beginning and end of the glyphosate titration. These measurements were input into Equation **2.1** to obtain the relevant *q* values.

*Table 3.2 - The lifetimes and q values of [Eu.**L**^{2}]$^+$ with and without glyphosate in H_2O and D_2O*

	Lifetime in H_2O (τ_1 ms)	Lifetime in D_2O (τ_1 ms)	*q* value
[Eu.**L**^{2}]$^+$	0.58	1.42	0.9
[Eu.**L**^{2}]$^+$ + Glyphosate	0.52	1.33	1.1

Table 3.2 clearly shows little change in emission decay rates following the addition of glyphosate in both H_2O and D_2O. Both give a *q* value of one, within error, which proves that the inner sphere water in not lost upon glyphosate binding. If a chelate were formed, an inner sphere water would be lost to allow room for this type of binding. However, there is no evidence in the Cambridge Crystallography Database Centre for phosphate chelation to a lanthanide centre.

3.3.2 *N*-Methyl Glyphosate

To delve deeper into the type of binding that occurs, further tests with other analytes were considered useful. Through simple methylation of the glyphosate amine by refluxing with formic acid and formaldehyde, methyl glyphosate was synthesised. This can give a good indication as to whether the secondary amine plays a role in binding, or whether the binding is purely through the phosphate group.

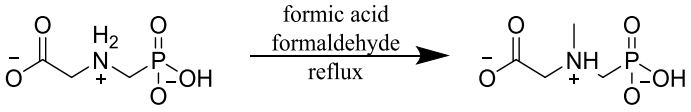

Scheme 3.3 - Synthesis of N-methyl Glyphosate

A titration similar to glyphosates was carried out with *N*-methyl glyphosate. Increments of *N*-methyl glyphosate were added to a buffered solution of [Eu.**L**^{2}]$^+$ and the emission intensity ratio at 614 nm / 618 nm was monitored, as a function of added analyte.

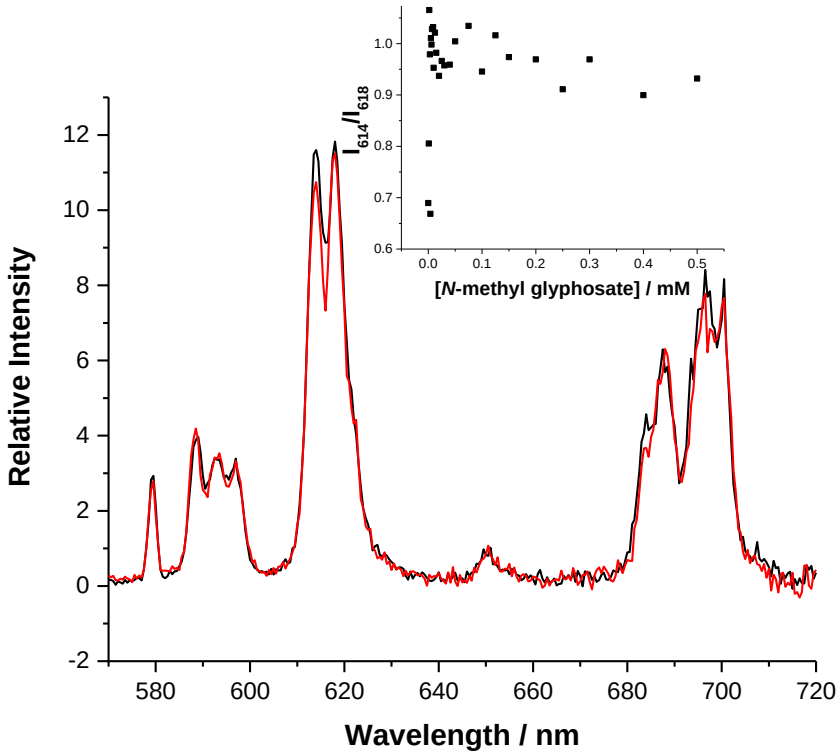

*Figure 3.4 - The emission spectrum of [Eu.**L**^{2}]$^+$ (57 μM, 0.1 M NaCl, 0.1 M MES, 295 K, pH 5.9) with (red) and without (black) N-methyl glyphosate. (Inset) The intensity ratio of 614 nm / 618 nm, as a function of increasing N-methyl glyphosate concentration*

Following addition of *N*-methyl glyphosate (0.5 mM), no major change in either spectral form or emission intensity was observed (Figure 3.4). This lack of change suggests that in this system, the central nitrogen plays a surprisingly significant role in the binding of glyphosate to the europium centre, and the absence of binding maybe steric in origin.

3.3.3 Glufosinate

Glufosinate is a naturally occurring broad-spectrum, systemic herbicide, which has a structure that is not dissimilar to that of glyphosate. It has a phosphinate group, an amine, and a carboxylate group. However, with a phosphinate rather than phosphonate group, it was predicted not to bind as well as glyphosate as phosphorus O atom is much less basic and a much poorer donor to a metal ion. However, glufosinate is an herbicide that is produced by some species of soil bacteria, and is a possible competitor of glyphosate, particularly in 'real-world' samples.[196]

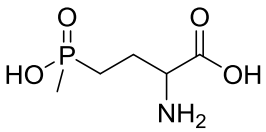

Figure 3.5 - Structure of glufosinate

Incremental additions of glufosinate were added to a buffer solution of [Eu.$\mathbf{L}^2$]$^+$ and was monitored by observing total emission intensity ratio changes, at 614 nm / 618 nm.

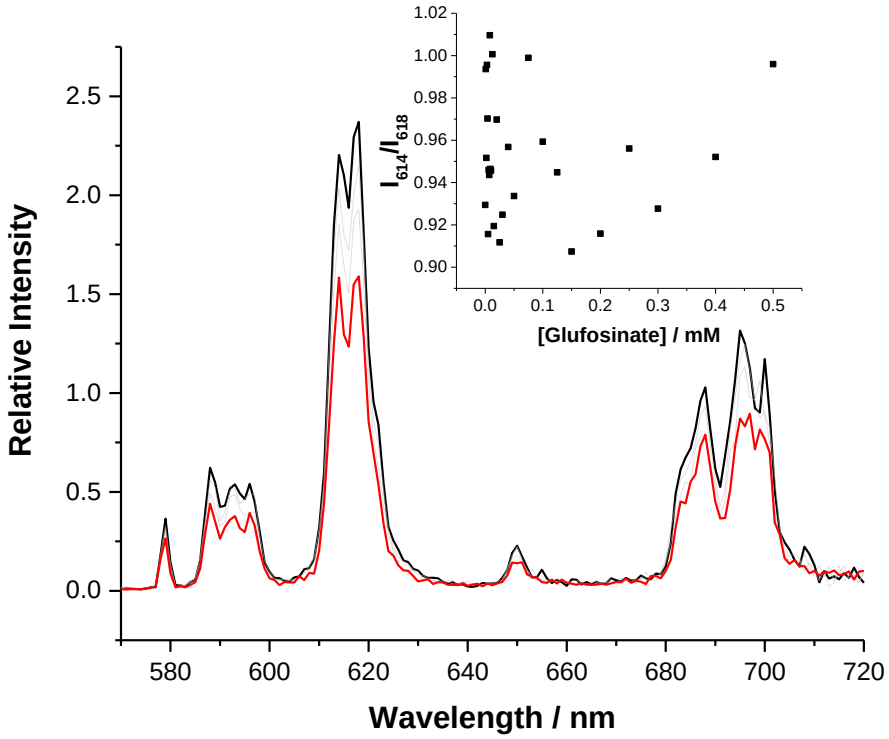

Figure 3.6 - Changes in the emission spectrum of [Eu.$\mathbf{L}^2$]$^+$ (black) (57 μM, 0.1 M NaCl, 0.1 M MES, 295 K, pH 5.9) with increasing concentration of glufosinate, up to 0.5 mM (red). (Inset) The change in emission ratio of 614 nm / 618 nm as a function of increasing glufosinate concentration

As is evident from the intensity ratio (inset, Figure 3.6), there was no significant change of spectral form upon increasing glufosinate concentration. It is therefore a clear indication that glufosinate does not bind to the complex in the same manner as glyphosate. However, there was an overall decrease in emission that was used to assess binding (Figure 3.7).

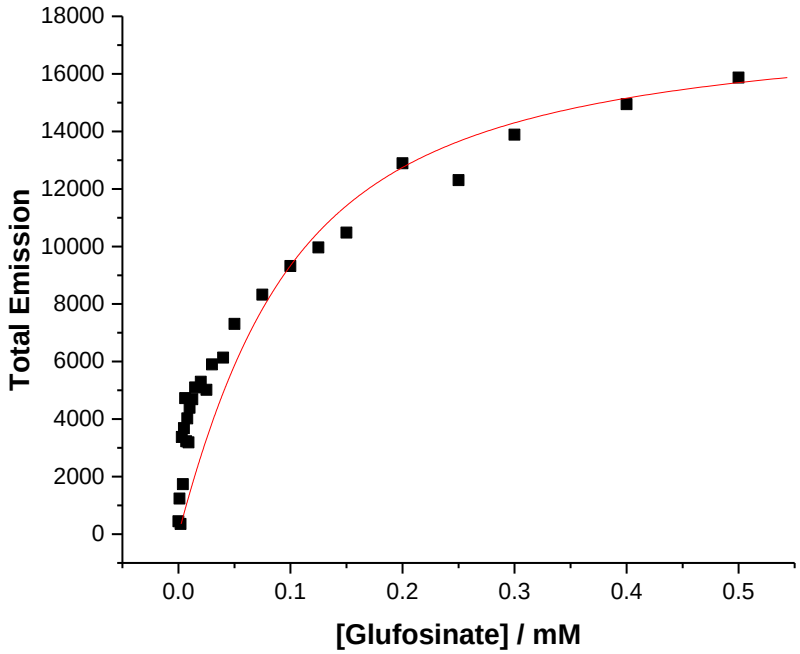

*Figure 3.7 - The fitted binding curve following the total emission of [Eu.**L**^{2}]$^+$ (57 μM, 0.1 M NaCl, 0.1 M MES, 295 K, pH 5.9) as a function of increasing glufosinate concentration*

Following the change in total emission, an apparent log*K* value of 4.17 (±0.02) was extracted. Although this is roughly equivalent to glyphosate, the detection of glyphosate is through the change in ratio which glufosinate does not impact significantly. The issues could arise if there was a very low glyphosate concentration or an excess of glufosinate binds more strongly to the complex. However, the concentration of glufosinate is never likely to be high enough that it would affect the emission ratio hugely.

3.3.4 Quenching Studies

As well as competitive binding, there are other factors that can also affect the complex emission spectrum which need to be monitored. For example, as [Eu.**L**^{2}]$^+$ uses an electron-poor azaxanthone chromophore, it can be susceptible to quenching by electron rich species. The issue lies with the intermediate triplet state of the chromophore, which can undergo non-radiative decay when an exciplex is formed. As the goal of this research is to find uses in biological systems, this may be a problem as electron rich species are common. Uric acid and catechol were chosen, as they are readily found in these systems and are well known quenchers with such azaxanthone Eu complexes.[175]

3.3.4.1 Uric Acid

The first to be examined was uric acid, which is a natural component of urine, but is also found in the blood. It is the product of the metabolic breakdown of purine

nucleotides. Purine can be found in higher plants, and some are capable of this degradation step.[197] Therefore, this may be found in some biological systems tested.

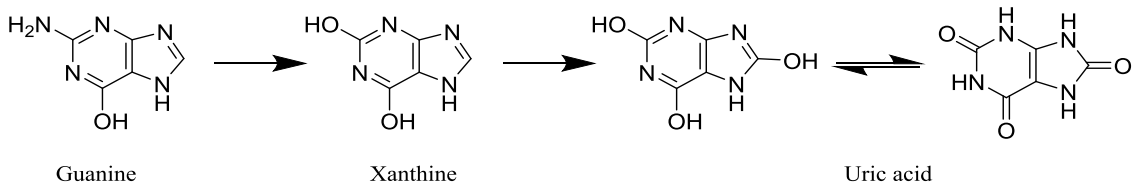

Figure 3.8 - The breakdown of guanine into uric acid

The concentration of uric acid in human blood is approximately 14 μM, and several plants can be found to contain 100-500 mg of uric acid per 100 g of food (6 - 30 μM). It is therefore possible that some uric acid could be present in food-stuff tested with the complex. Titrations were carried out starting at these levels and increasing to much higher concentrations.

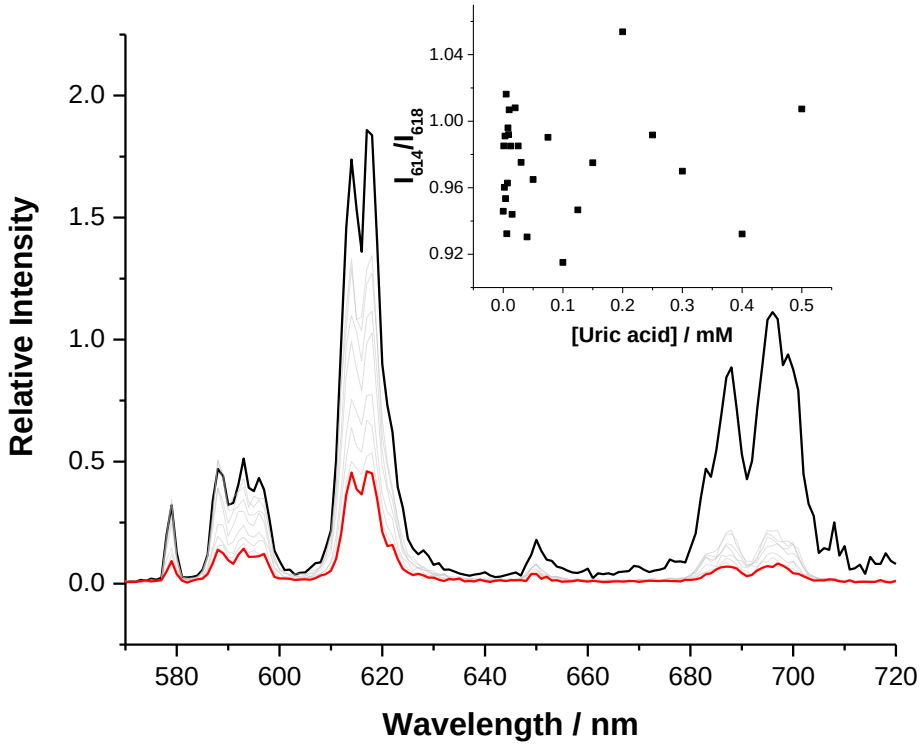

Figure 3.9 - Changes in the emission spectrum of $[Eu.\mathbf{L}^2]^+$ (black) with increasing concentrations of uric acid, up to 0.5 mM (red) (57 μM, 0.1 M NaCl, 0.1 M MES, 295 K, pH 5.9). (Inset) The intensity ratio of 614 nm / 618 nm as a function of increasing uric acid concentration

The ratio used to track the binding of glyphosate is devoid of any trend, so unlikely to compete directly (Figure 3.9, inset). There appears to be no other change in spectral form, suggesting that uric acid does not bind to the complex. However, there is a change in emission intensity.

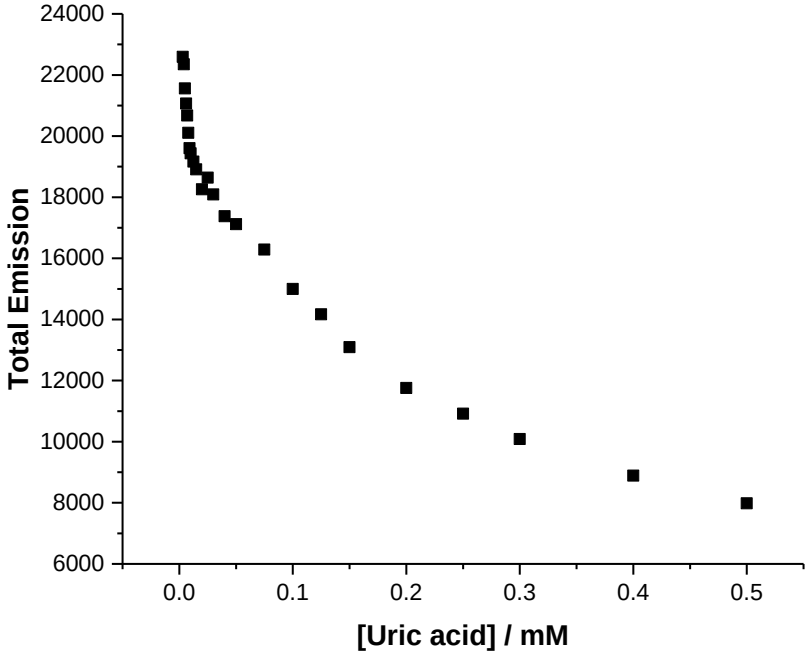

Figure 3.10 - The change in total emission of [Eu.$\mathbf{L}^2$]$^+$ (57 μM, 0.1 M NaCl, 0.1 M MES, 295 K, pH 5.9) as a function of increasing uric acid concentration, up to 0.5 mM

Figure 3.10 highlights that there is a significant decrease in intensity upon addition of the first 0.05 mM of uric acid. This is suggestive that uric acid interacts strongly in a 1:1 fashion with the complex, likely forming an exciplex to allow non-radiative decay. Hence, a much less intense europium signal is observed. This could be an issue as if there are relatively high levels of uric acid in samples being tested with [Eu.$\mathbf{L}^2$]$^+$, quenching effects could decrease the europium signal sufficiently for the signal-to-noise ratio to effect accurate glyphosate detection.

3.3.4.2 Catechol

Another potential quencher is catechol, which occurs naturally in fruit and vegetables. Although catechol itself is usually only found in trace amounts, the catechol moiety is found widely in the natural world, as well as synthetic catechols being used in the production of pesticides, and pharmaceuticals.[198,199] It is therefore likely that either catechol or more complex derivatives could be present in food samples.

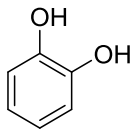

Figure 3.11 - The structure of catechol

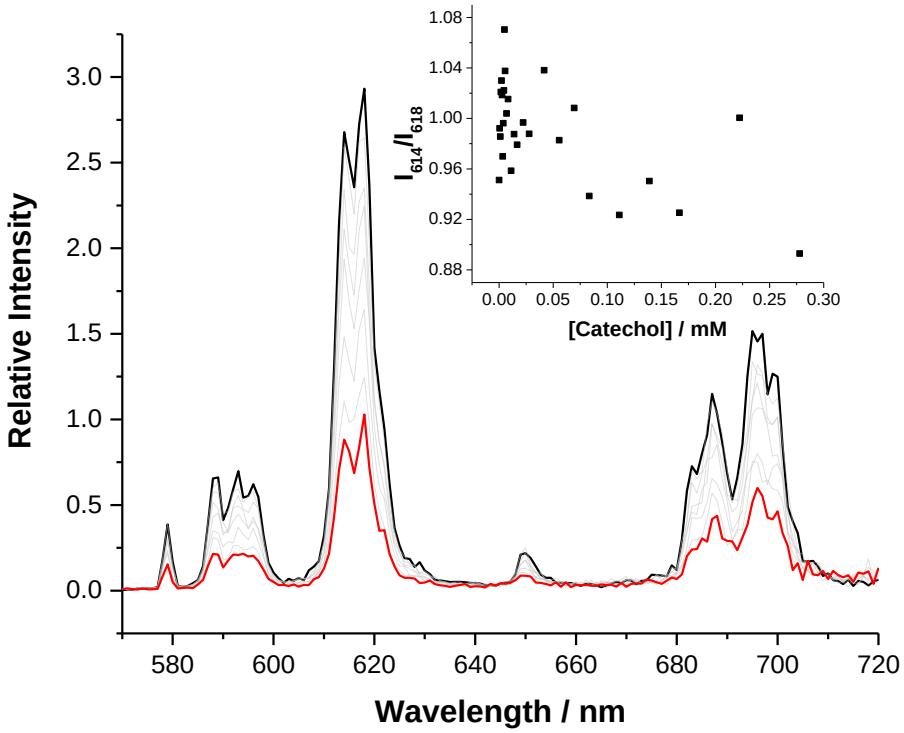

*Figure 3.12 - Changes in the emission spectrum of [Eu.**L**^{2}]$^+$ (black) with increasing concentrations of catechol, up to 0.3 mM (red) (57 μM, 0.1 M NaCl, 0.1 M MES, 295 K, pH 5.9). (Inset) The intensity ratio of 614 nm / 618 nm as a function of increasing catechol concentration*

The intensity ratio of 614 nm / 618 nm of [Eu.**L**^{2}]$^+$ shows a slight decrease (Figure 3.12, inset). However, there is no clear and smooth trend. Furthermore, the change in ratio is small in comparison to the change seen upon addition of glyphosate. However, if catechol or another compound which bound this moiety was present at 0.5 mM, the change seen in the emission would be significant enough to affect the glyphosate reading, likely suggesting that there was a lower concentration. This is obviously an issue, particularly if levels were close to MRLs.

Although there is comparatively little change in spectral form in comparison to the addition of glyphosate, the change in emission intensity decreases upon addition of catechol.

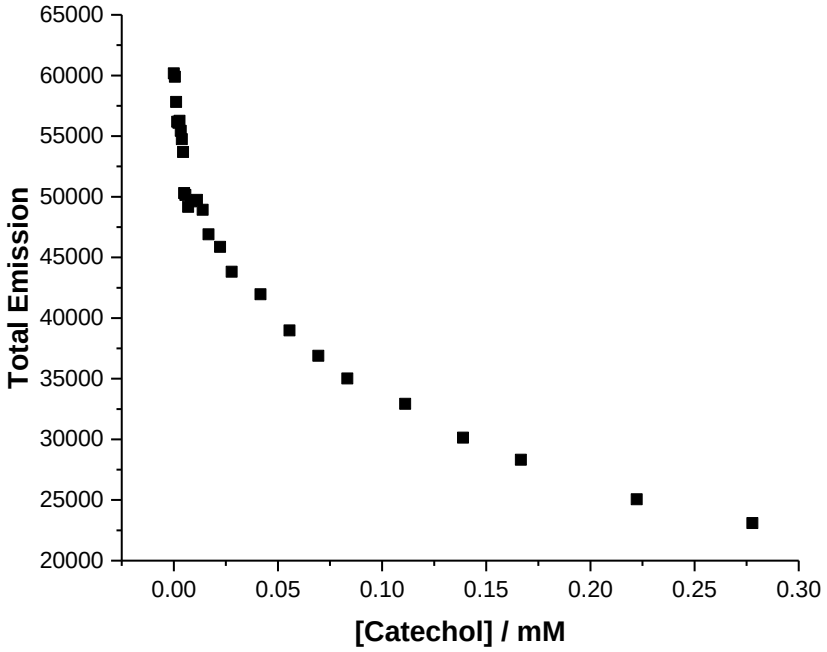

Figure 3.13 - The change in total emission of [Eu.$\mathbf{L^2}$]$^+$ (57 μM, 0.1 M NaCl, 0.1 M MES, 295 K, pH 5.9) as a function of increasing catechol concentration, up to 0.3 mM

The emission intensity is more than halved upon addition of catechol. This decrease is problematic as the binding of glyphosate in biological systems is also expected to be coupled with a decrease in intensity. Hence, if there are high concentrations of both catechol and glyphosate, or perhaps another quencher, the europium emission intensity may be insufficient to extract a ratio, and therefore would not be able to detect an accurate level of glyphosate.

3.4 Testing in River Water

Due to its widespread use in agriculture, glyphosate has been found in river water.[200] Therefore, it was imperative to check whether the complex was viable for analysing samples in this background medium, or if there is interference from other species present in the water. To do this, a sample of river water was taken from the River Wear in January 2017. The level of glyphosate in the river was assumed to be minimal, if present at all, as the spraying of glyphosate generally stops over the winter months when fewer crops are grown.

The Dionex LC medium of analysis was again used to investigate the river water sample. The water had to be filtered through 0.2 μM filters to remove any solids from the sample which could block the column. It was tested for a number of common anions such as chloride or nitrate. Bromide was also tested for, but none was detected.

Table 3.3 - Concentration of anions found in river water, with the detection limit from Dionex LC, with 95% confidence intervals

Anion	Fluoride	Chloride	Sulfate	Phosphate	Nitrite	Nitrate
Concentration detected (mg/L)	0.70	23.27	9.91	0.01	0.03	0.87
Detection limit (mg/L)	0.01	0.03	0.02	0.02	0.02	0.04

The UV trace of the river water alone was taken to see if anything in the sample absorbs at, or close to, the complex excitation wavelength. There is a strong maximum absorbance at 228 nm (A_{228} = 0.558). The absorbance does decrease slowly, but by the time is reaches 365 nm (A_{365} = 0.137), where the complex will be excited, the absorbance has not yet reached zero. It is therefore clear that something else competitively absorbs at that wavelength. However, the complex should still be able to be excited sufficiently to see a spectrum. It is also clear that the use of a time-gated method is necessary as there is potentially a lot of background luminescence from fluorescent species present in the water.

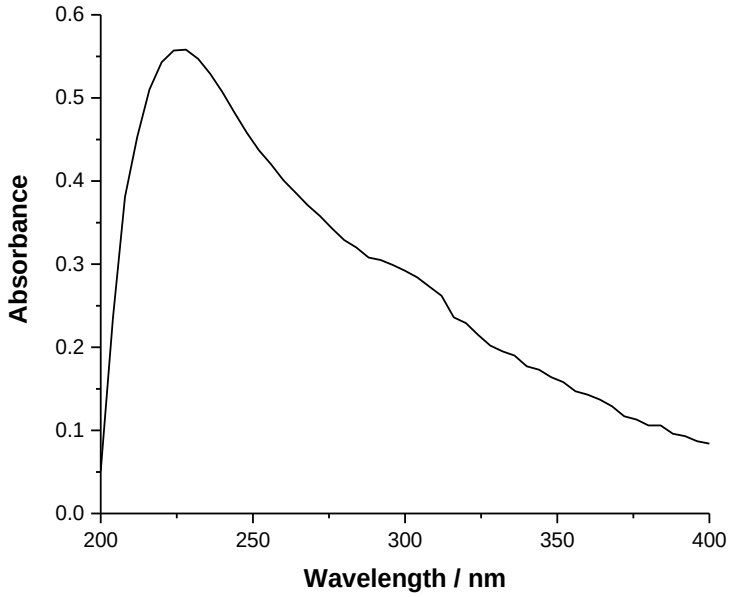

Figure 3.14 - The absorption spectrum of the river water collected from the river Wear (295 K)

The titrations carried out in river water were analogous to those in buffer. The difference stems only from the fact that the solvent changed from purite water to river water. Although a number of ions are clearly present in river water, 0.1 M NaCl was added, to ensure minimal change in ionic strength, and the pH was maintained at 5.9 with 0.1 M MES.

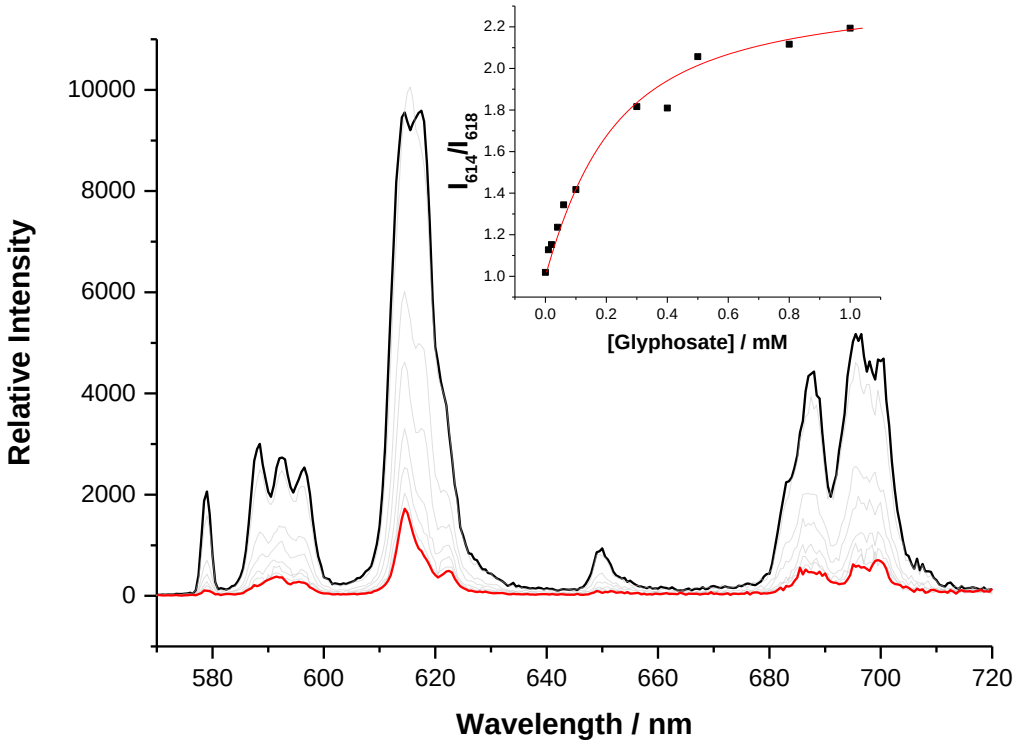

Figure 3.15 - Changes in the europium spectrum of $[Eu.\mathbf{L}^2]^+$ *in river water (black) (1.1 mM, 0.1 M NaCl, 0.1 M MES, pH 5.9, 295 K) with increasing concentration of glyphosate, up to 1 mM (red). (Inset) The binding curve, following the intensity ratio of 614 nm / 618 nm as a function of increasing glyphosate concentration*

The same intensity ratio of 614 nm / 618 nm was used and gave an apparent log*K* value of 3.81 (±0.02) which is below the binding constant found in purite water. It is suggestive of a more competitive media, but the log*K* value, and the change in spectral form implies it should still be able to act as 'real-life' probe in river water without significant interference from other analytes at pH 5.9. However, a problem arises with the significant decrease in overall emission intensity, leading to the observed signal being weaker, causing issues in getting accurate readings from the measured ratio.

3.5 Testing in Rice Samples

The next step of the investigation was to see if the level of glyphosate could be detected in biological samples, particularly plant extract. Rice was selected as a test grain due to its high absorbency, so it was thought likely to be able to absorb the water and glyphosate. The experiments were also used as a study to compare the speed and accuracy of different methods.

The first step was to take 30 grains of long-grain rice and soak it in glyphosate. The herbicide selected was 'Resolva' which is commercially available, and therefore, likely to be widely used by the public. It contained 0.81% *w/w* glyphosate giving an

approximate aqueous concentration of 5 mM. The grains were split into three groups of ten and each group were soaked in 5 mL of glyphosate for 24 h before being dried. From this point, each group of grain samples were treated differently. While the rice had been soaking in glyphosate, three identical solutions of $[Eu.\mathbf{L}^{2}]^{+}$ (2 mL, 50 μM) were made up, in 0.1 M NaCl and MES, pH 5.9 and then left to lyophilise overnight.

The first set of ten (A) were washed with 2 mL of tap water and the water was immediately added to a cuvette with the complex, salt and buffer, and used to take an emission spectrum. Another set of ten (B) were soaked in 2 mL of water for 24 h, before this water was added to the second cuvette of complex and used to take an emission spectrum. The final ten grains (C) were frozen in liquid nitrogen and crushed using a mortar and pestle. The sample was then soaked for 24 h in water. To collect the water from group 'C', the mixture has to be filtered through a syringe filter before being added to a cuvette to take the final emission spectrum. This process ensured that all the pieces of floating rice had been removed which have the potential to affect the emission spectrum.

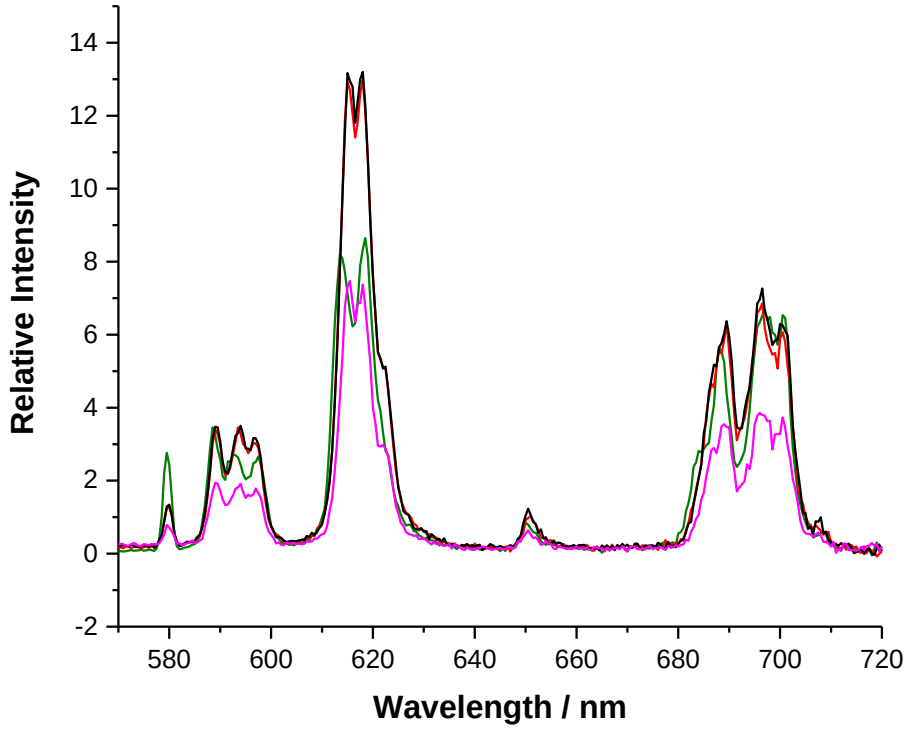

Figure 3.16 - The variation in the emission spectrum of $[Eu.\mathbf{L}^{2}]^{+}$ (1.1 mM, 0.1 M NaCl, 0.1 M MES, pH 5.9, 295 K) (green), with different treatments of rice, 'A' (red), 'B' (black) and 'C' (pink)

It was found that the ratio of intensity at 614 nm / 618 nm decreased from 0.9 in the complex alone, to 0.76 (A), 0.74 (B), and 0.73 (C) for the three different rice treatments.

There is also an increase in emission intensity for ‘A’ and ‘B’. This behaviour is interesting, as an increase in emission intensity has not previously been seen for this complex upon binding glyphosate. Nevertheless, the binding event is tracked using the ratio of 614 nm / 618 nm. In each case, the ratio dropped, rather than increased as occurred in buffer solution and river water. Such behaviour is indicative of competition from another analyte, which may perturb the results. Sample set ‘B’ gives a lower ratio value than ‘A’ suggesting the addition of soaking time extracts other species from the grain, which may include glyphosate.

Although set ‘C’ gave a lower ratio value than either ‘A’ or ‘B’, the additional steps in the protocol makes the system inaccessible to most people, who do not have access to liquid nitrogen, and adds time to the process. Furthermore, one issue with glyphosate in food is that it is sprayed during the drying process and unlikely to be taken up by fruit or grain. Indeed, the majority of glyphosate is expected to be on the outside of food. This step of crushing the sample also may add other competitive compounds, which could massively interfere with the complex binding glyphosate.

Taking this into account, the next step of this study is testing for glyphosate in grains. This initial result in rice suggested that a calibration curve for grain extract was necessary as it appears as though there are other compounds that also bind to the complex. To take this into account, the binding curves in buffer solution or river water are not sufficient to also work in biological media. This work suggests that the best way, for the most accurate results, would be to leave the grains soaking in water for 24 hours to ensure all the glyphosate is extracted. If a rough calculation is needed, simple washing may be sufficient. However, as we strived to be rigorous, subsequent work was carried out after soaking for 24 hours before testing.

3.6 Analysis of Grain Samples

The next step to test whether complex $[Eu.\mathbf{L^2}]^+$ was able to detect glyphosate in ‘real-life’ samples, was to obtain grains which have been treated with different levels of glyphosate, to test whether it is possible to calculate the concentration using the methods described above. From the initial tests with rice, it was clear that a calibration curve using water that had soaked grains, which had not been treated with glyphosate, was necessary.

To establish the calibration curve, untreated cordiale wheat grains were soaked in purite water for 24 h. The water was then lyophilised prior to regenerating in 2 mL solution of complex in 0.1 M MES and NaCl. Glyphosate (1mM solution) was added in incremental steps to the complex mixture to produce a calibration curve.

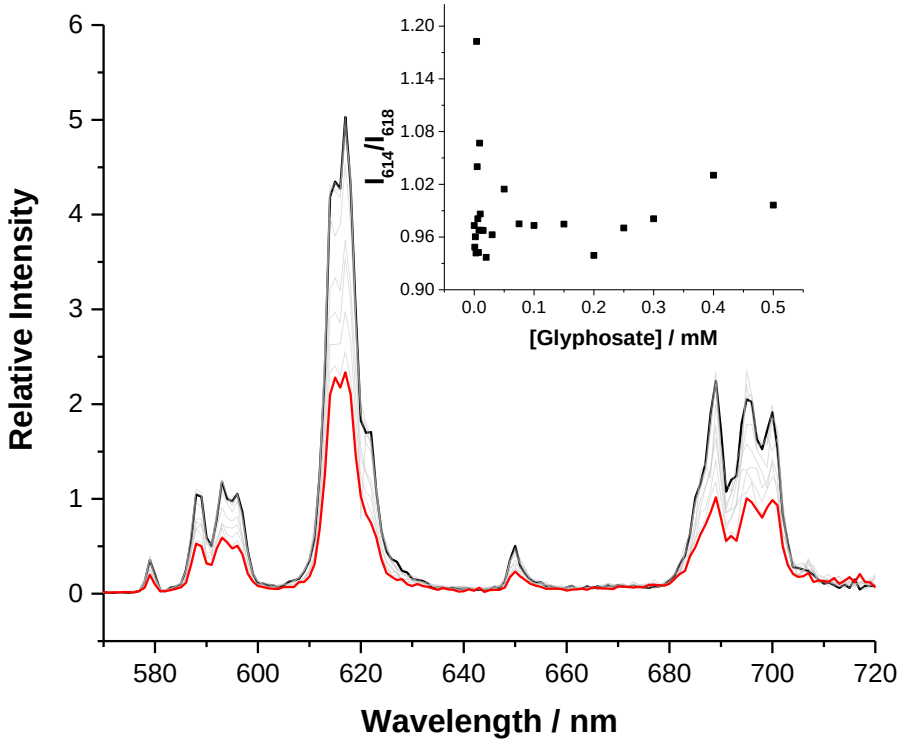

Figure 3.17 - Changes in the emission spectrum of $[Eu.\mathbf{L}^2]^+$ (black) (51 μM, 0.1 M NaCl, 0.1 M MES, pH 5.9, 295 K) with increasing concentration of glyphosate up to 0.5 mM (red) in grain extract. (Inset) The ratio of emission intensity at 614 nm / 618 nm as a function of increasing glyphosate concentration

In previous experiments, there were several ratios which could have been chosen to track changes in spectral form as a function of the change in concentration of glyphosate. In Figure 3.17, it can be seen that the ratio used thus far with $[Eu.\mathbf{L}^2]^+$ clearly does not give rise to a smooth binding curve. Indeed, the ratio decreases which is unlike the analogous experiments in buffer and tap water. Other ratios that could have been used, such as comparing the $\Delta J = 2$ and the $\Delta J = 1$ manifolds were of similarly poor quality, and it was impossible to retrieve an apparent binding constant. The only spectral response change that gave a curve that could possibly be used was the total emission.

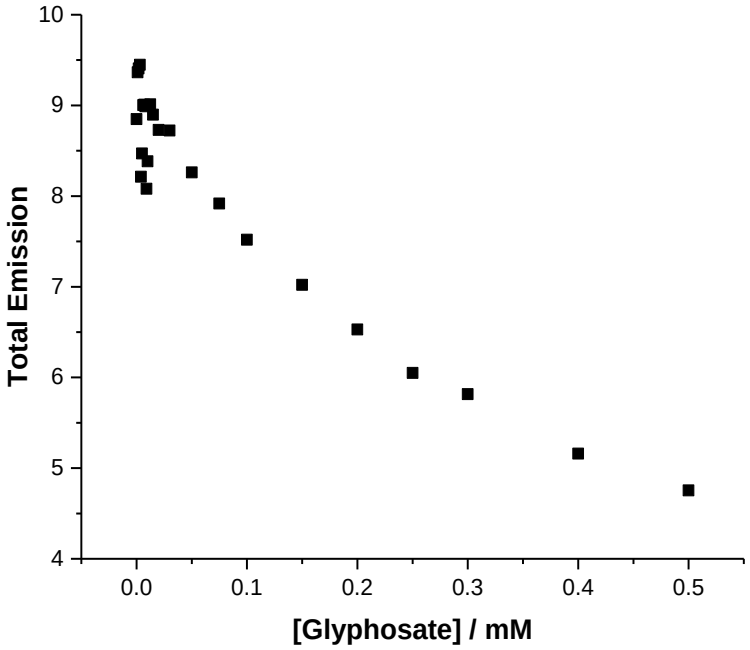

*Figure 3.18 - The change in total emission of [Eu.**L**^{2}]$^+$ (51 μM, 0.1 M NaCl, 0.1 M MES, pH 5.9, 295 K) as a function of increasing glyphosate concentration, up to 0.5 mM*

In this grain extract experiment, the overall emission intensity decreased. However, using the total emission in place of a ratio to calculate a binding constant is not ideal. The advantage of a ratiometric method, rather than looking at change in the overall emission is that ratios are not as dependent on the concentration of the complex. Variations in total emission may also be subject to interference from unrelated signal quenching process.

Following the addition of the first 50 μM of glyphosate, a significant amount of noise is present, as highlighted by the curve tracking overall intensity (Figure 3.18). As this is the region in which glyphosate is likely to be detected in grains, and the MRL in the EU is 59 μM, it constitutes a difficult problem. It appears as though the complex is bound to something other than glyphosate present in grains, which glyphosate is replacing. The unknown analyte is interfering with the results.

There are two potential solutions to consider in an attempt to circumnavigate this problem. Firstly, something could be added to the initial solution which could bind to the chemical responsible for the loss of a ratiometric response. The second option was to consider the use of another complex that showed higher affinity yet maintained selectivity for glyphosate, and functioned in a range of media.

3.7 Removing the Quenching Species

As this complex has already been synthesised and showed initial promise, the first choice of attack to overcome this problem was to attempt to remove the compound or compounds in the grain which causes the issues. However, grains are complex biological entities and therefore, it is difficult to predict exactly what is causing the effect.

Therefore, instead of concentrating initially on the grains themselves, the complex was examined to determine possible interactions. As the chromophore is electron poor and π- conjugated and the problem is a decrease in intensity, there is a possibility of π- π stacking. This interaction would diminish the activity of the probe as instead of energy transfer to the europium, non-radiative decay is more likely occur. Polyphenols are regularly found in biological media, which would be prime candidates for π- π stacking with the chromophore, and a consequent of quenching of emission via charge transfer.

The UV spectrum of the background grain showed a strong absorption band at around 200 nm. However, the tail is long and there is still strong absorption at 336 nm, the wavelength at which the chromophore is excited. Even at 365 nm where the time-gated experiments are excited, there is still 0.5 abs, i.e. the light used to excite the complex is also being absorbed by the endogenous chromophore.

3.7.1 Activated Charcoal

The first attempt to remove the endogenous chromophores in the hope of returning to a ratiometric response of $[Eu.\mathbf{L}^{2}]^{+}$ with varying concentrations of glyphosate, was to use activated charcoal which has been known for decades to remove impurities through chemical filtration.[201] Charcoal (20 mg) was initially added to the solution extracted from the grain, before the complex was added. The mixture was stirred at room temperature for 2 h, the charcoal removed by centrifuge and the absorption spectrum was taken. The process was repeated multiple times, eventually stirring for 24 h when no further change was seen in the absorption spectrum. Although it was clear that the treatment reduced the absorption at 336 nm, it did not decrease to zero, only to 0.17 abs which is still more than half of the 0.30 abs which is the target of absorption for the complex. However, this is still a significant decrease from 0.71 abs.

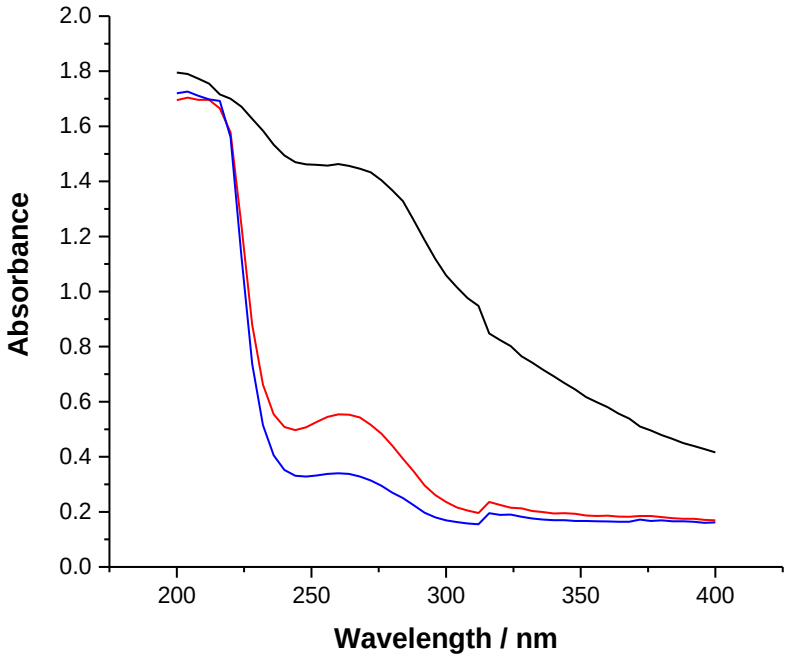

Figure 3.19 - The absorbance spectrum of grain extract stirring in activated charcoal at 0 h (black), 2 h (red) and 24 h (blue)

After this reduction in absorbance by grain extract, a titration was attempted to see if stirring with activated carbon had helped. The titration was performed, exciting at 336 nm with $[Eu.\mathbf{L}^{2}]^{+}$.

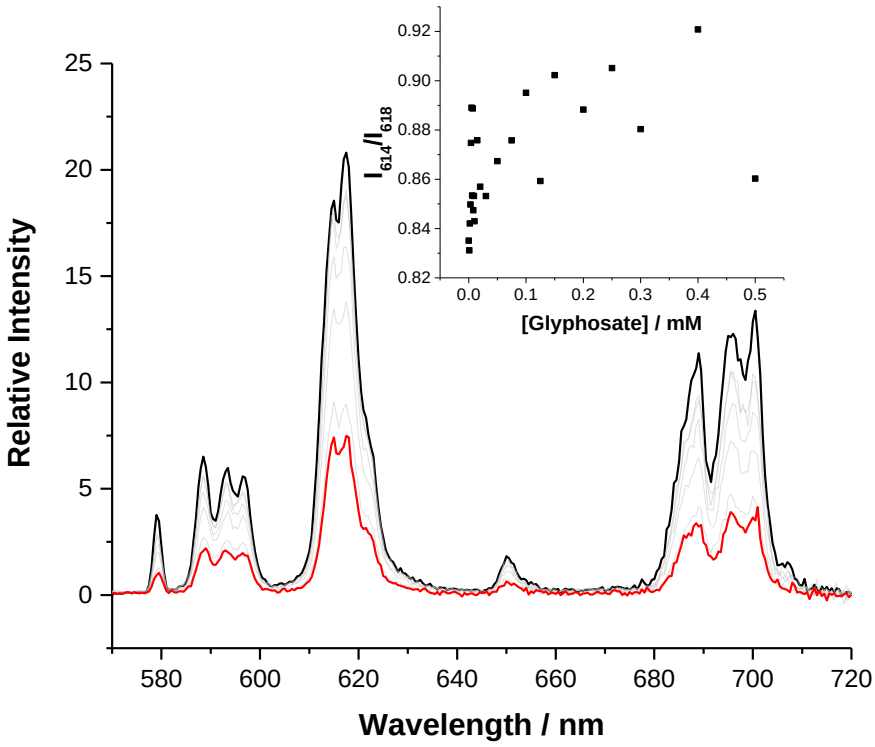

Figure 3.20 - Changes in the emission spectrum of $[Eu.\mathbf{L}^{2}]^{+}$ (black) in grain extract that has been treated with activated carbon with increasing concentration of glyphosate up to 0.5 mM (red) (46 μM, 0.1 M NaCl, 0.1 M MES, pH 5.9, 295 K). (Inset) The intensity ratio of 614 nm / 618 nm as a function of increasing concentration of glyphosate

Following treatment with charcoal, there was still an overall decrease in emission intensity .The ratio used in buffer solution, 614 nm / 618 nm, increased upon addition of glyphosate (Figure 3.20). However, it was not a smooth increase, and still not one that would be suitable to be used to calculate either an apparent binding constant of glyphosate under these conditions, or the concentration of glyphosate in unknown samples.

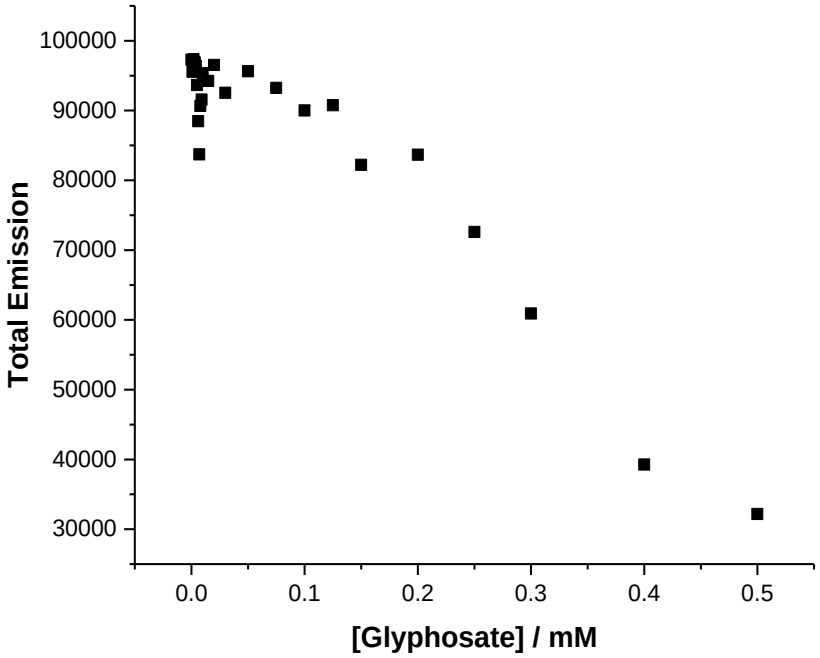

*Figure 3.21 - The change in total emission of [Eu.**L**^{2}]$^+$ (46 μM, 0.1 M NaCl, 0.1 M MES, pH 5.9, 295 K) with increasing concentration of glyphosate*

Furthermore, looking at the changes in total emission of [Eu.**L**^{2}]$^+$ with increasing concentration of glyphosate, the start of the titration still has a lot of noise which has not been removed by treatment of activated carbon. The compound that binds to the complex which is replaced by glyphosate is clearly still present. Although activated carbon has helped to remove some compounds in the grain, not enough of the competitors have been removed to make this complex good enough to work in complex biological media.

3.7.2 Silver Nitrate

Another additive used was silver nitrate. It was theorised that a small amount of silver nitrate would interact with some biological molecules, especially proteins and cause them to precipitate out of solution and allow them to be easily filtered off. Solid was expected to form almost instantaneously but even after treating the solution and stirring for 24 h, no solid could be observed.

3.7.3 Acid Bath Treatment

It was hypothesised that under acidic conditions many large biological molecules, including proteins, would denature and therefore no longer interact with the complex. Glyphosate has been detected in urine, meaning it has survived the rigour and pH swings of human digestion.[202,203] As the stomach is approximately pH 2.0, glyphosate should be stable under these conditions. After stirring at room temperature for 24 h at pH 2.0, the pH of the background solution was raised back up to 5.9 followed by a titration which monitored europium emission as a function of glyphosate concentration.

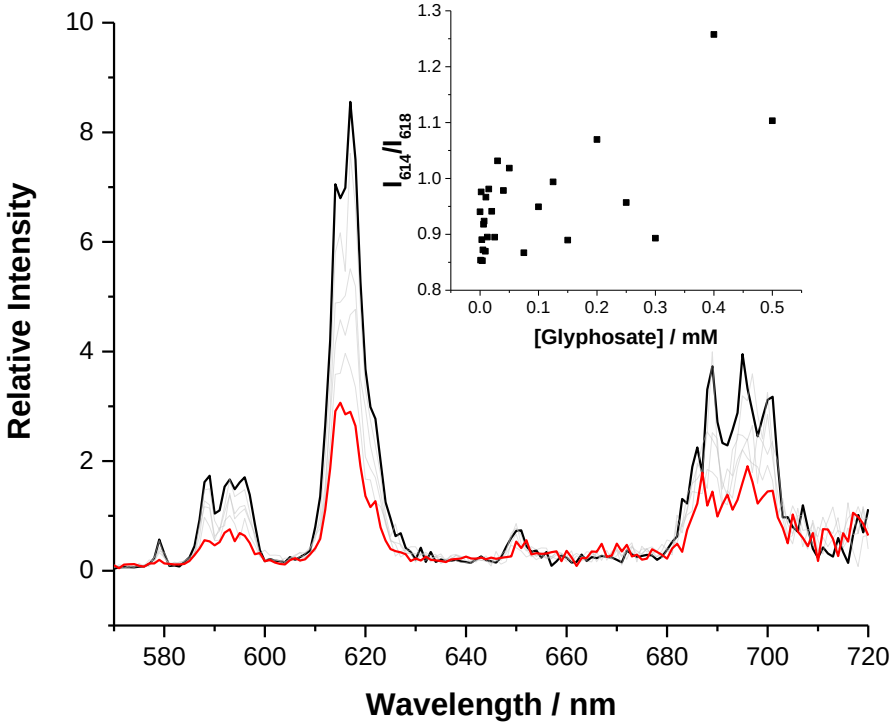

Figure 3.22 - Changes in the emission intensity of $[Eu.\mathbf{L}^2]^+$ (black) (46 μM, 0.1 M NaCl, 0.1 M MES, pH 5.9, 295 K) in acid treated grain extract with increasing concentration of glyphosate, up to 0.5 mM (red). (Inset) The intensity ratio of 614 nm / 618 nm of $[Eu.\mathbf{L}^2]^+$ as a function of increasing glyphosate concentration

Upon addition of glyphosate, the emission intensity decreased, as expected, coupled with a change in spectral form (Figure 3.22). Using the ratio 614 nm / 618 nm there was an increase upon addition of glyphosate. However, there is a lack of a distinct curve to utilise. Following the changes in total emission, however, there is a decrease in intensity, which showed a comparatively smooth curve.

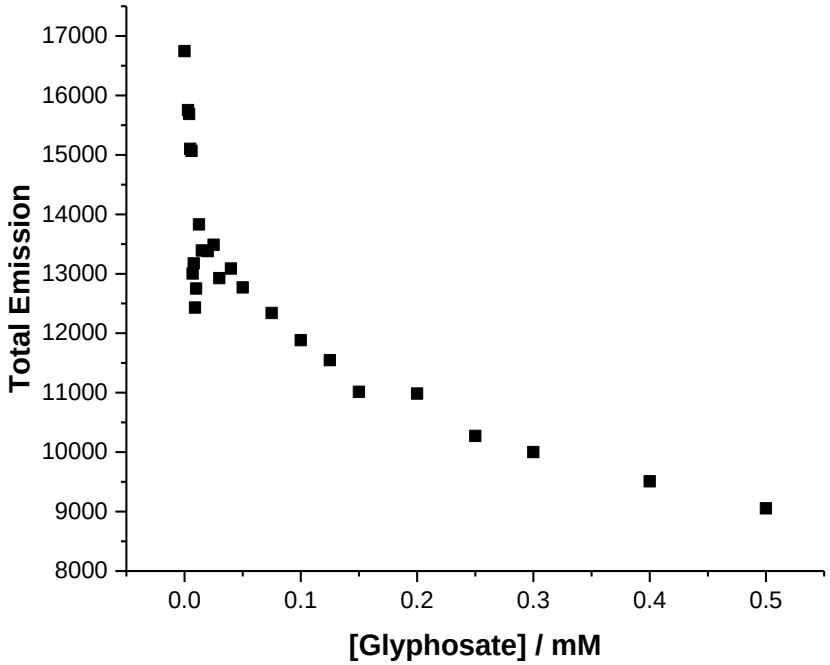

*Figure 3.23 - The changes in total emission of [Eu.**L**^{2}]$^+$ (46 μM, 0.1 M NaCl, 0.1 M MES, pH 5.9, 295 K) in acid treated grain extract following an increase in glyphosate concentration*

Despite the clear trend of decreasing intensity, there is still noise close to the beginning of the titration, suggestive that the compound that binds to the complex has not been removed by the treatment of acid. Outside of this initial range, the smooth curve suggests that the acid treatment of the grain extract has aided in removing some unwanted competition.

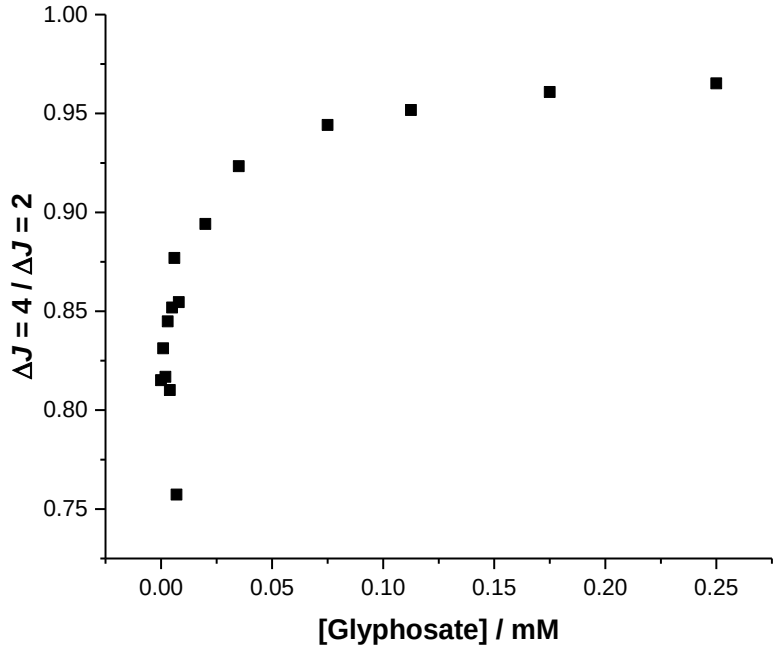

*Figure 3.24 - Following the intensity ratio of ΔJ = 4 / ΔJ = 2 (681-704 nm / 608-629 nm) of [Eu.**L**^{2}]$^+$ (46 μM, 0.1 M NaCl, 0.1 M MES, pH 5.9, 295 K) as a function of increasing glyphosate concentration*

A better example highlighting the removal of some interference follows the ratio of $\Delta J = 4$ / $\Delta J = 2$ (681-704 nm / 608-629 nm), two hypersensitive transitions. The binding curve has little noise at the start with a steep response at low glyphosate concentrations, over the concentration range 0-50 μM. However, a 1:1 binding curve could not be fit, suggesting that glyphosate isn't binding to $[Eu.\mathbf{L^2}]^+$ as expected, particularly since the 614 nm / 618 nm ratio also does not give a good curve.

3.8 Other Azaxanthone Based Complexes Screened

Although the acid digestion of the grains showed some promise, the problems which arose upon testing in grain extract were not overcome. Therefore, the second route using alternative complexes was taken to find a complex which would continue to work in biological media.

3.8.1 The Tri-positive Complex $[Eu.\mathbf{L^3}]^{3+}$

The next complex examined was very similar in structure to $[Eu.\mathbf{L^2}]^+$. The difference stems from the lack of the N-Me group on the cyclen ring and the ester group on the alanine arm, meaning the overall charge of the complex is now +3, rather than +1. Synthesis is analogous to $[Eu.\mathbf{L^2}]^+$, up to compound **11** (Scheme 3.2). Then instead of methylation of the final nitrogen on the amine, and deprotection of the esters, the ligand is immediately complexed to give $[Eu.\mathbf{L^3}]^{3+}$. The lifetimes in H_2O and D_2O were measured for this complex, giving values for τ_1 of 0.27 and 0.63 ms respectively. Inserting these values into Equation **2.1**, gave a q value of 2.3, which fits with the observation that the ligand is seven coordinate, leaving two spaces for solvent molecules.

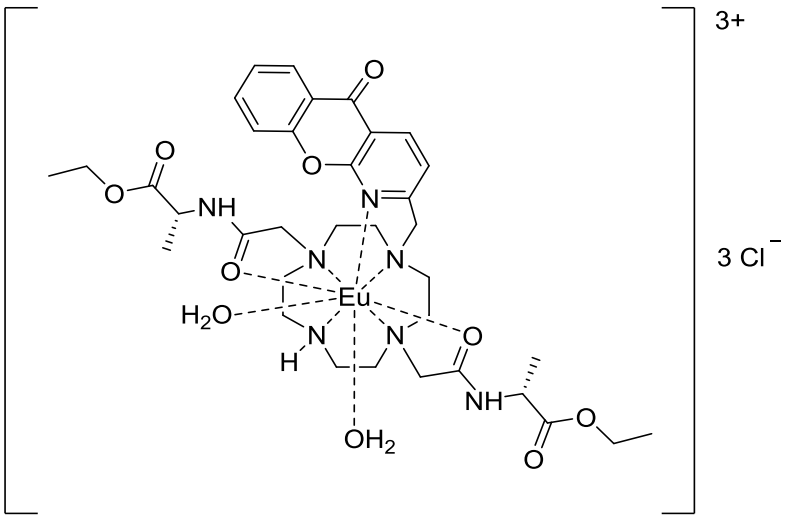

Figure 3.25 - The structure of $[Eu.\mathbf{L^3}]Cl_3$

Modification of the N-Me group in [Eu.$\mathbf{L}^{2}$]$^{+}$ to N-H in [Eu.$\mathbf{L}^{3}$]$^{3+}$ changes the steric demand around the europium centre. The ester groups protecting the carboxylic acid group of the alanine moiety means the overall charge of the complex has changed, as there is no negative charge on the ligand to balance the +3 charge from the europium ion. Each of these points was expected to influence binding and, as such, a different log*K* value needed to be determined experimentally.

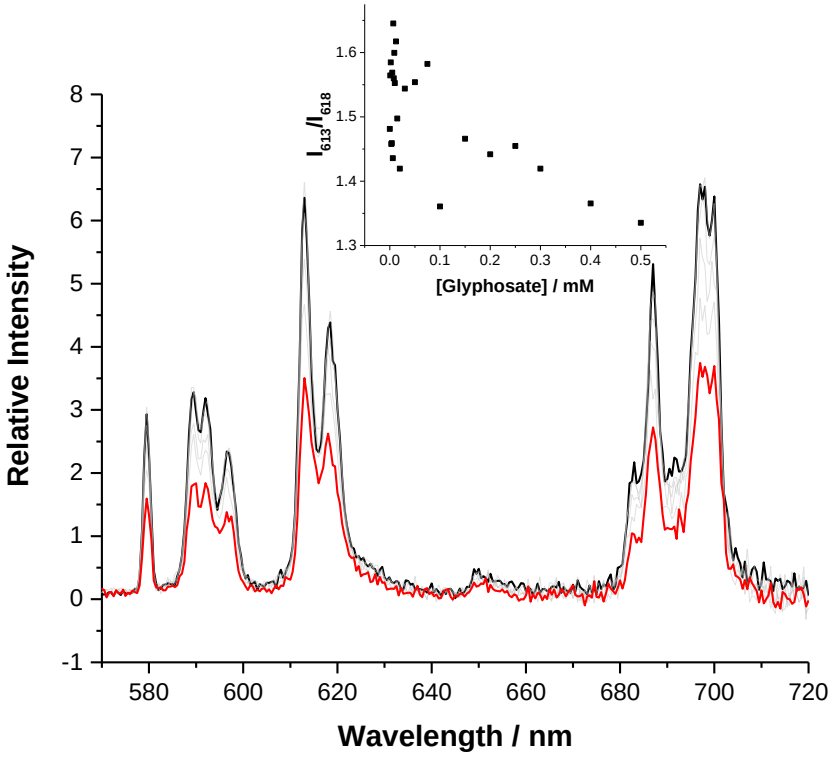

Figure 3.26 - Changes in the emission spectrum of [Eu.$\mathbf{L}^{3}$]$^{3+}$ (40 μM, 0.1 M NaCl, 0.1 M MES, pH 5.9, 295 K) upon addition of glyphosate, up to 0.5 mM. (Inset) The intensity ratio of 613 nm / 618 nm as a function of increasing glyphosate concentration

The addition of glyphosate can be seen to decrease the overall total emission. However, no ratio could be found in which a smooth binding curve could be attained. Even following the total emission a curve could not be found. The lack of any useful spectral change makes it difficult to glean any information about binding constants. The absence of a useful ratio meant that this complex was not used in further experiments.

3.8.2 Azathioxanthone Complex

The complex, [Eu.$\mathbf{L}^{4}$]$^{3+}$, (synthesised by R. Pal) utilises an azathioxanthone group rather than an azaxanthone as a sensitiser. It was used to see if [Eu.$\mathbf{L}^{4}$]$^{3+}$ would still bind to glyphosate, as it is structurally similar to previous complexes, and whether the slight change in chromophore structure would have any effect on the quenching of the emission state in grain background.

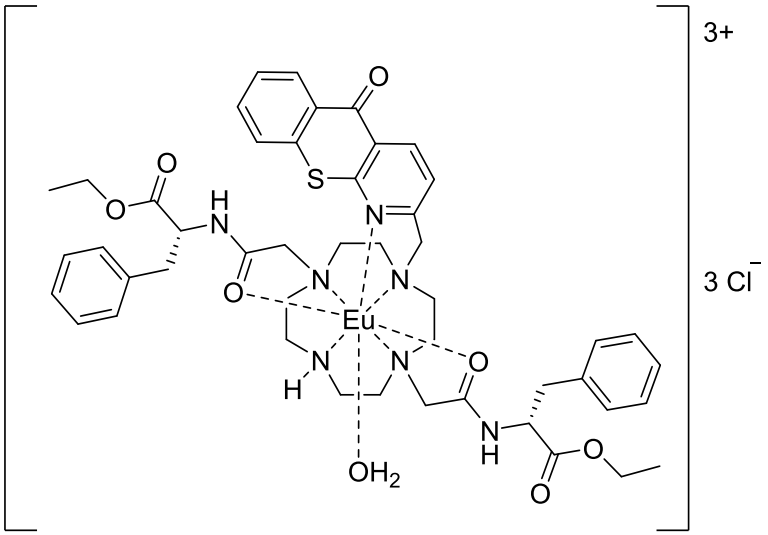

*Figure 3.27 - The structure of [Eu.**L**^{4}]Cl$_3$*

There is again no N-Me group on the cyclen ring and there is a change in the amide arm, from a methyl group to a phenyl moiety; i.e. the arm is derived from phenylalanine rather than alanine. The lifetimes in both H_2O and D_2O were calculated and gave values for τ_1 of 0.30 and 0.45 ms respectively. Putting these values in Equation **2.1**, a *q* value of 1.1 was obtained. This is slightly different from the value calculated in [Eu.**L**^{3}]$^{3+}$ which had two inner sphere waters. The difference in *q* value could be to do with the more bulky arms, which increase steric hindrance sufficiently to stop the second water molecule binding, meaning this complex is eight coordinate.

After seeing little binding in the grain extract, a change in chromophore was thought to be necessary, in order to permit longer wavelength excitation, where there is less absorbance by endogenous chromophores in grains. With azathioxanthone, excitation can occur at 385 nm. However, there is still the risk of quenching by electron-rich species in more complex media. Titrations were carried out in purite water, with the addition of 0.1 M NaCl and MES to maintain ionic strength and pH respectively.

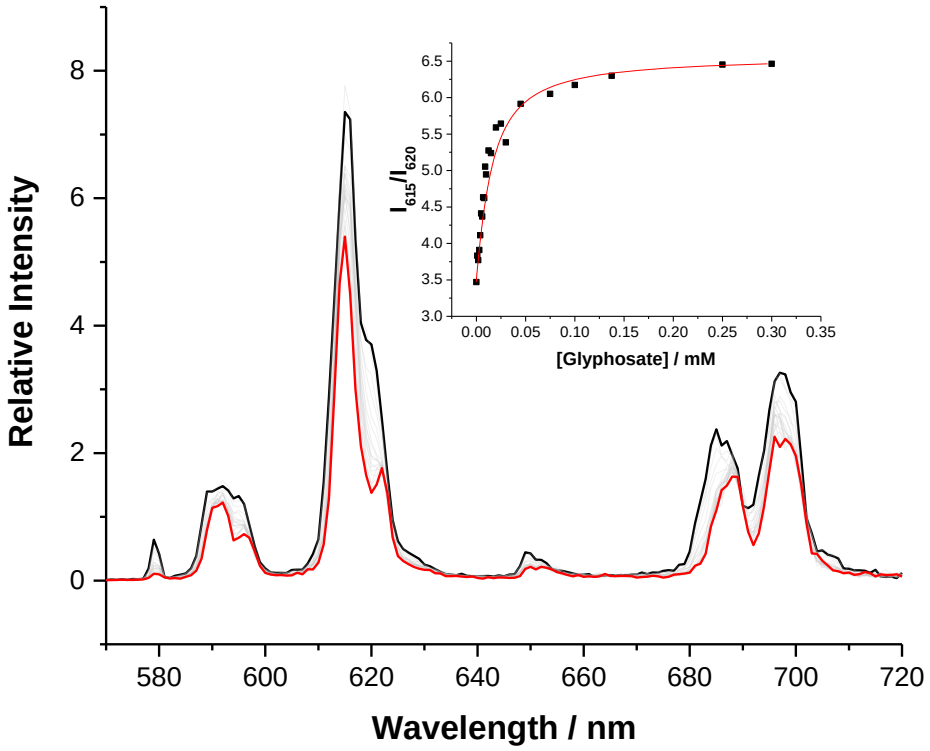

*Figure 3.28 - Change in the total emission of [Eu.**L**^{4}]$^{3+}$ (90 μM, 0.1 M NaCl, 0.1 M MES, pH = 5.9, 295 K) (black) with increasing glyphosate concentration, up to 0.3 mM (red). (Inset) The intensity ratio of 615 nm / 620 nm as a function of increasing glyphosate concentration*

From Figure 3.28, it is clear the complex has bound to glyphosate with a significant change in spectral form observed, revealed particularly in the ΔJ = 2 manifold around 620 nm. From the fitted curve, an apparent log$K$ value of 4.95 (±0.01) was determined which is greater by nearly a factor of 10 than [Eu.**L**^{2}]$^{+}$ (4.01). This greater log$K$ value suggests from initial experiments that this complex is a better glyphosate probe.

Lifetime experiments were also performed to see any change in lifetimes, and what this could tell us about binding. In H_2O, the Eu emission lifetime was 0.39 ms, with D_2O giving a slightly longer lifetime of 0.48 ms. These are both longer than found without glyphosate, and gave a q value of 0.30 suggesting the inner sphere water has been displaced. This behaviour is expected as it is theorised that glyphosate will bind to the metal directly, through its phosphate oxygen, and hence replace the most labile ligand, which in this case is the water molecule.

3.8.2.1 Titration of [Eu.L^{4}]$^{3+}$ with Inorganic Phosphate

It is likely that as this complex is highly charged, other analytes may interfere with glyphosate binding. As it again binds through the phosphate group, one of the main competitors was expected to be inorganic phosphate. A control experiment was undertaken to see if the complex binds phosphate in buffered solution.

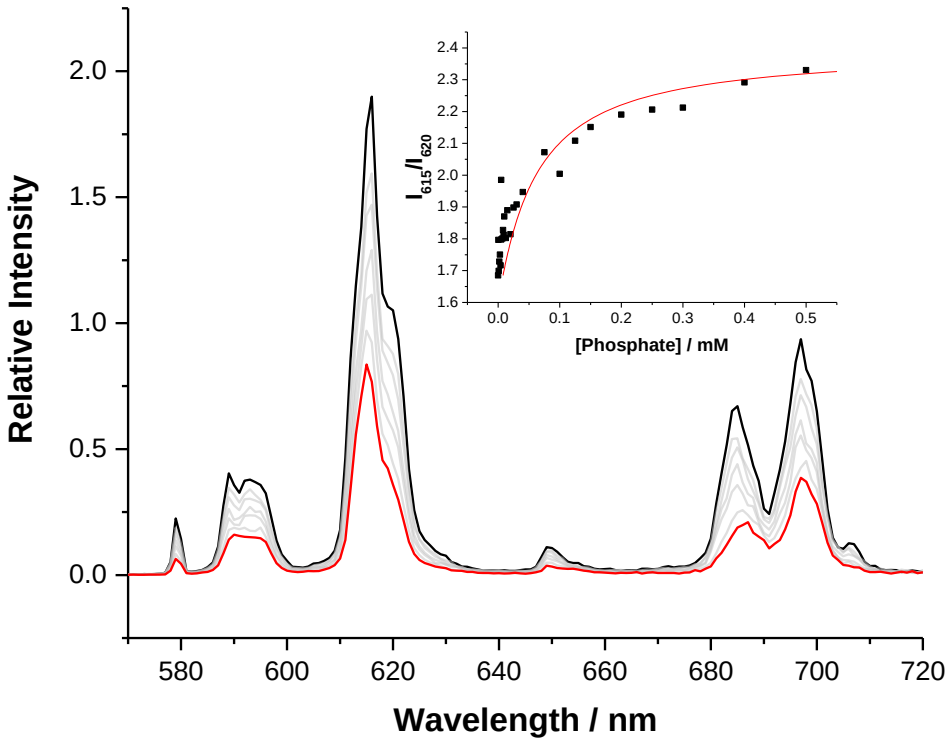

*Figure 3.29 - Changes in the emission spectrum of [Eu.**L**^{4}]$^{3+}$ (black) (90 μM, 0.1 M NaCl, 0.1 M MES, pH = 5.9, 295 K) following incremental additions of phosphate, up to 0.5 mM (red). (Inset) The intensity ratio of 615 nm / 620 nm as a function of increasing concentration of phosphate*

A decrease in emission intensity was observed and the change in spectral form appeared very similar to that seen with glyphosate. Indeed, following the ratio as before of 615 nm / 620 nm, an apparent log*K* value of 4.26 (±0.02) was calculated, which is less than a factor of ten smaller than glyphosate. However, the fit is clearly not perfect. The conclusion which can be drawn from this is that although glyphosate has a higher binding constant, phosphate is likely to interfere with the intensity ratio and may be the reason why the complex is not suitable for use in river water samples.

3.8.2.2 Titration of [Eu.L^{4}]$^{3+}$ with AMPA

AMPA (Figure 3.30) is a metabolite of glyphosate, which still contains the phosphonate group and hence it was theorised that it could still bind to the Eu complex.

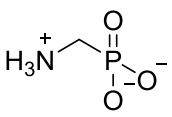

Figure 3.30 – The structure of AMPA

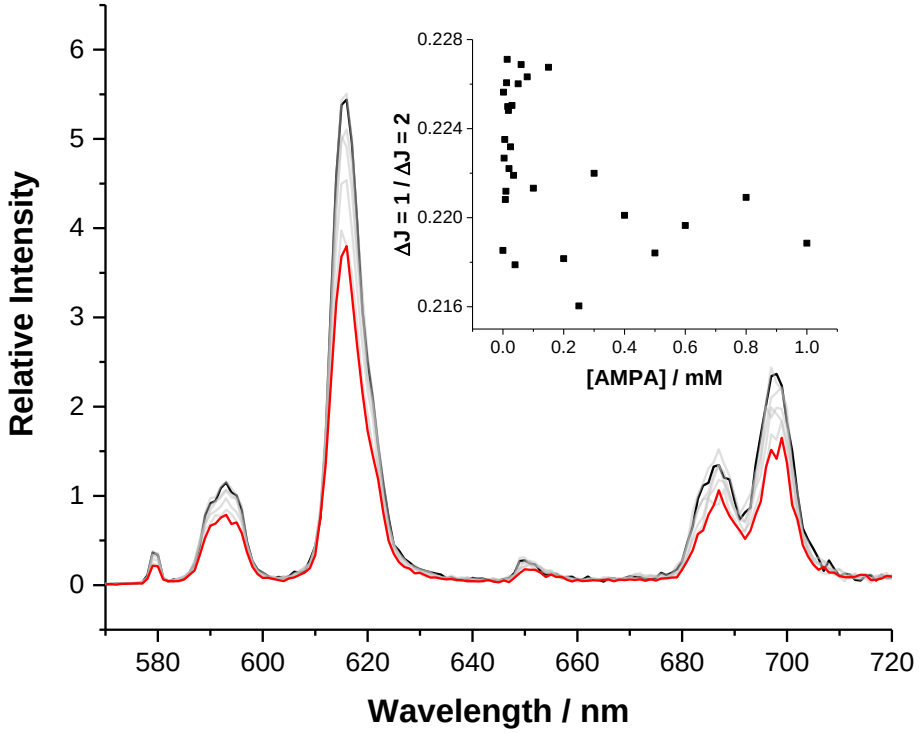

*Figure 3.31 - Changes in the emission spectrum of [Eu.**L**^{4}]$^{3+}$ (black) (80 μM, 0.1 M NaCl, 0.1 M MES, pH = 5.9, 295 K) following incremental additions of AMPA, up to 1 mM (red). (Inset) The intensity ratio of ΔJ = 1 / ΔJ = 2 following increasing concentration of AMPA*

Unexpectedly, following the ratio of intensities of the manifolds $\Delta J = 1$ / $\Delta J = 2$, as well as the intensities at 615 nm / 620 nm, a distinct change upon addition of AMPA was not observed. Even after adding up to 1 mM, the changes in ratios were noisy and not easy to follow. However, there is a decrease in emission intensity. These results suggest that the complex may interact with AMPA, but not bind to the metal centre in the same manner as both glyphosate and phosphate.

3.8.2.3 River Water

Following on from the successful titration in buffer, the next step was to see how the complex functioned in the slightly more complex medium of river water, using the same sample introduced in Section 3.4.

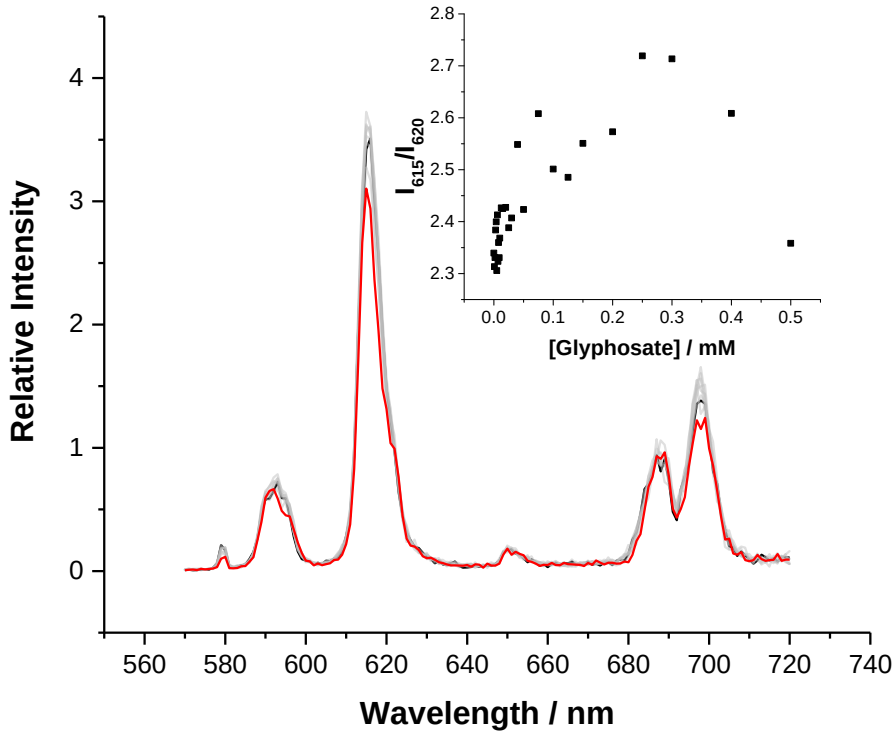

*Figure 3.32 - Changes in the emission spectrum of [Eu.**L**^{4}]$^{3+}$ (black) (90 μM, 0.1 M NaCl, 0.1 M MES, pH = 5.9, 295 K) with increasing levels of glyphosate in river water, up to 0.5 mM (red). (Inset) The intensity ratio of 615 nm / 620 nm as a function of increasing glyphosate concentration*

Initial results in river water were not promising, with Figure 3.32 showing little change in spectral form, and the intensity ratio originally used of 615 nm / 620 nm gave a poor correlation. There is also very little change in emission intensity.

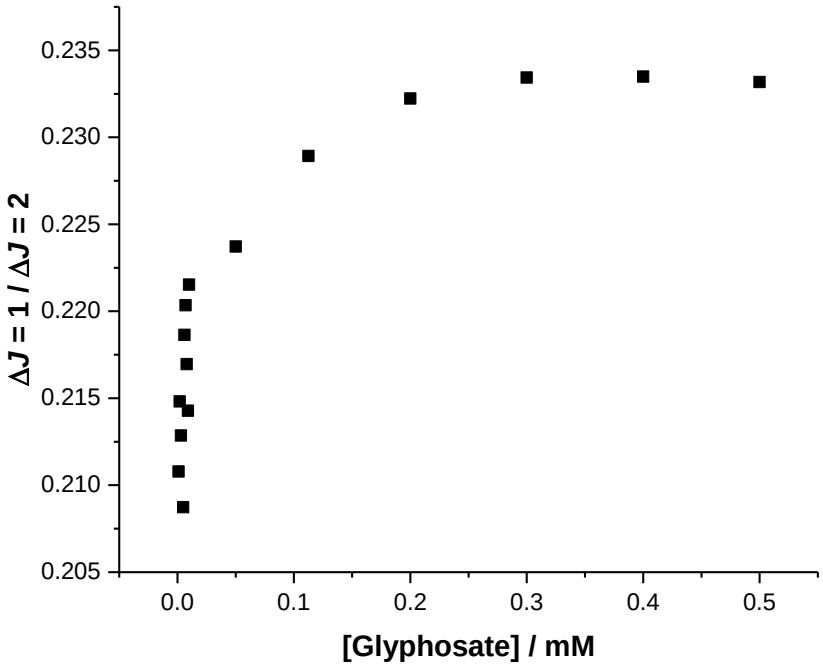

*Figure 3.33 - The change in the intensity ratio of ΔJ = 1 / ΔJ = 2 of [Eu.**L**^{4}]$^{3+}$ (90 μM, 0.1 M NaCl, 0.1 M MES, pH = 5.9, 295 K) following incremental additions of glyphosate in river water, up to 0.5 mM*

However, different ratios were investigated and it was found that a ratio of bands, namely $\Delta J = 1$ / $\Delta J = 2$ was found to produce a more useful apparent binding curve (Figure 3.33). Although this provided a smooth curve, a 1:1 binding model did not give rise to a binding constant. As river water contains phosphate, it is possible this is interfering with glyphosate binding.

3.8.2.4 Testing the Complex in Grain Extract

The next step was to test how efficient [Eu.$\mathbf{L^4}$]$^{3+}$ was at detecting glyphosate in 'real-life' samples. Following the river water titration, the change in spectral form in the $\Delta J = 2$ band itself was not as obvious, so the binding event was followed using two transitions, $\Delta J = 1$ and $\Delta J = 2$.

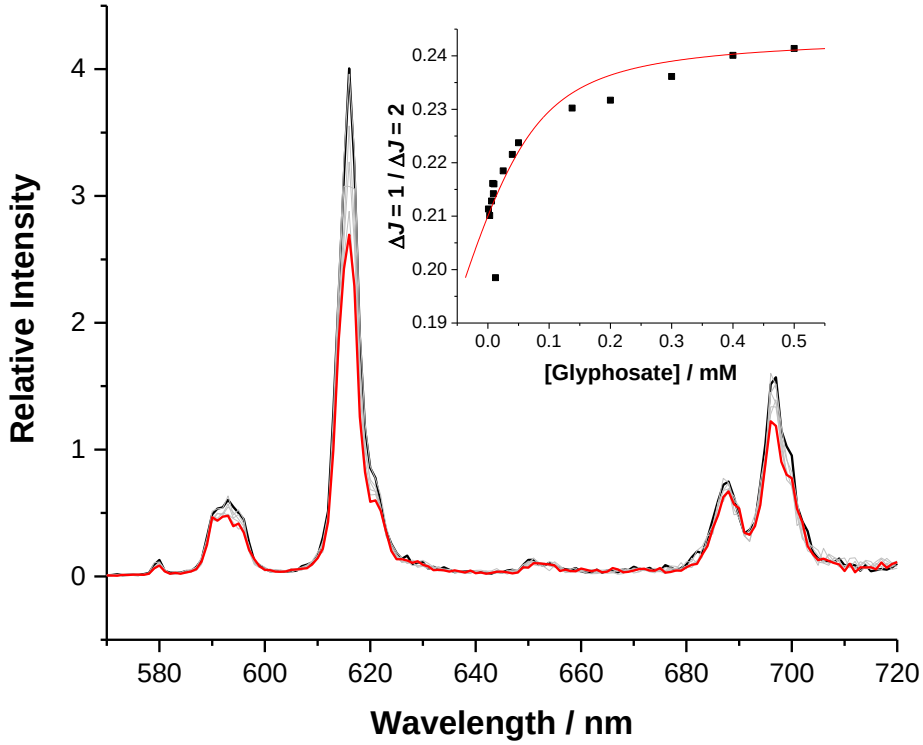

Figure 3.34 - Changes in the emission spectrum of [Eu.$\boldsymbol{L^4}$]$^{3+}$ (black) (90 μM, 0.1 M NaCl, 0.1 M MES, pH = 5.9, 295 K) in grain extract with increasing glyphosate concentration, up to 0.5 mM (red). (Inset) The intensity ratio of ΔJ = 1 / ΔJ = 2 as a function of increasing glyphosate concentration

Comparing the start of this titration in grain extract to that in buffer solution clearly highlights the difference in spectral form, particularly in the $\Delta J = 2$ band. The band in grain extract is already a single peak, compared to two distinct ones at the start of the buffer titration. This behaviour suggests that there is something in grain extract which has already bound to the complex to cause this change in form, perhaps something containing a phosphate group. An issue that arose from this conjecture is that the ratio

followed in the buffered solution, of 615 nm / 620 nm did not show any correlation, upon addition of glyphosate.

A binding curve was found, however, by comparing the $\Delta J = 1$ and $\Delta J = 2$ transition intensities, giving an apparent log$K$ value of 4.39 (±0.03). As can be seen in Figure 3.34, the binding curve is not a perfect fit, and therefore, this value is subject to error, and the further use of this curve to calculate the concentration of glyphosate is not ideal. Furthermore, using this ratio is not as useful compared to the ratio 615 nm / 620 nm due to the significantly smaller change. The binding curve in the ratio of bands is in the range 0.208-0.234 compared to 3.4-6.3 as seen in 615 nm / 620 nm. The significantly smaller range with the bands could lead to much greater error, with any noise potentially having great effect on the reading of glyphosate concentration.

In addition, the use of azathioxanthone as a chromophore has the significant disadvantage of having a smaller extinction coefficient than the azaxanthone, meaning more complex is needed to see change and the binding curve it is then more susceptible to noise fluctuations.

3.8.3 Cationic Complex, $[Eu.\mathbf{L^5}]^{3+}$

The next complex (synthesised by S. Shuvaev) utilises a new chromophore used previously within the Parker group.[204] It utilises an extended chromophore system as opposed to the fused ring moiety previously used. If the quenching arose in the aforementioned complexes from π-π stacking, it is less likely to affect $[Eu.\mathbf{L^5}]^{3+}$. The use of the same phenylalanine based arm over the alanine arm was partly due to the higher log$K$ value of $[Eu.\mathbf{L^4}]^{3+}$ over $[Eu.\mathbf{L^2}]^{+}$. It may encourage selective binding of glyphosate, but, for this to occur, disassociation of one pyridine nitrogen atom must take place. This process may lead to decreases in the overall emission intensity but may also give rise to a large change in spectral form.

The extended chromophore with the push-pull system means europium is excited through the ICT state of the ligand. The extended conjugation shifts the excitation wavelength to 340 nm, but the broad absorption band means that there is still significant absorbance at the LED wavelength of 365 nm.

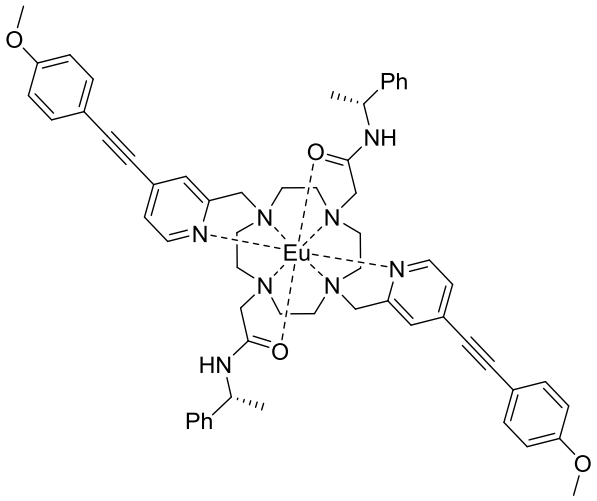

*Figure 3.35 - The structure of [Eu.**L**^{5}]$^{3+}$*

As expected, there was a decrease in emission intensity. However, there is not the predicted change in spectral form, and as such, finding intensity ratios capable of following the binding event becomes increasingly difficult (Figure 3.36).

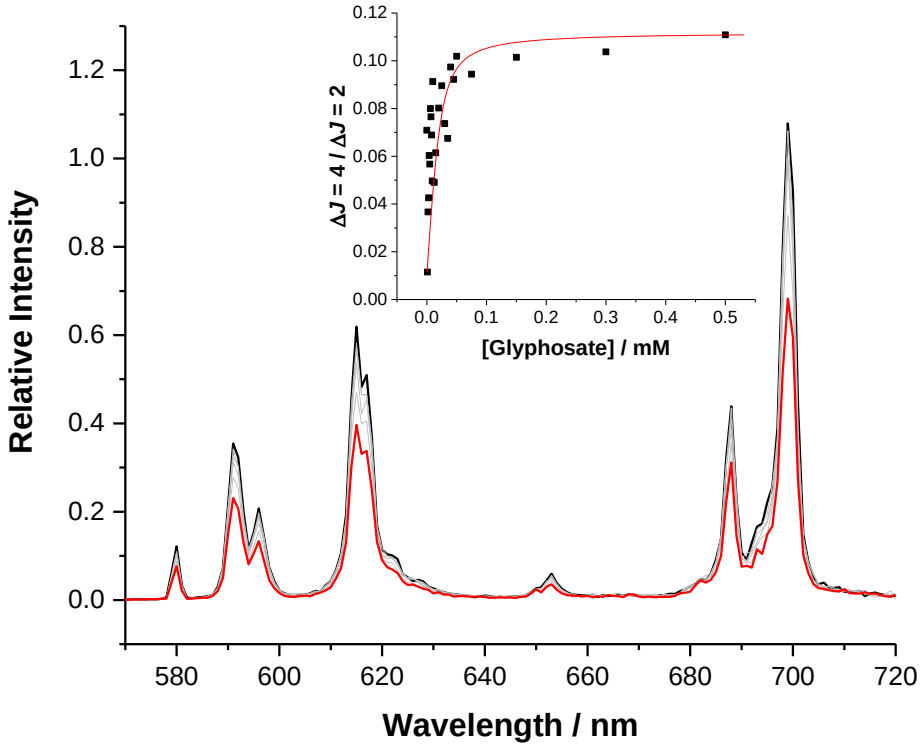

*Figure 3.36 - Changes in the emission spectrum of [Eu.**L**^{5}]$^{3+}$ (black) (20 μM, 0.1 M NaCl, 0.1 M MES, pH 5.9) with increasing concentration of glyphosate, up to 0.5 mM (red). (Inset) The intensity ratio of (1.8 - (ΔJ = 4 / ΔJ = 2)) with increasing glyphosate concentration*

The change in ratio that gave the most promising results involved the comparison of the $\Delta J = 4$ / $\Delta J = 2$ transition. A binding constant was calculated using an iterative least-square fitting to a 1:1 binding model, giving an apparent log$K$ value of 5.24 (±0.04), the highest value found thus far.

The titration was also carried out using a time-gated instrument, as the relatively high absorbance at 365 nm meant that the europium emission signal was sufficiently large to allow use of this method. It also means going forward, this technique can be used to remove fluorescence from the grain extract, as it removes the first 0.01 ms of emission. Following promising glyphosate results, the next step would be to look at the effect of possible interferents, such as phosphate.

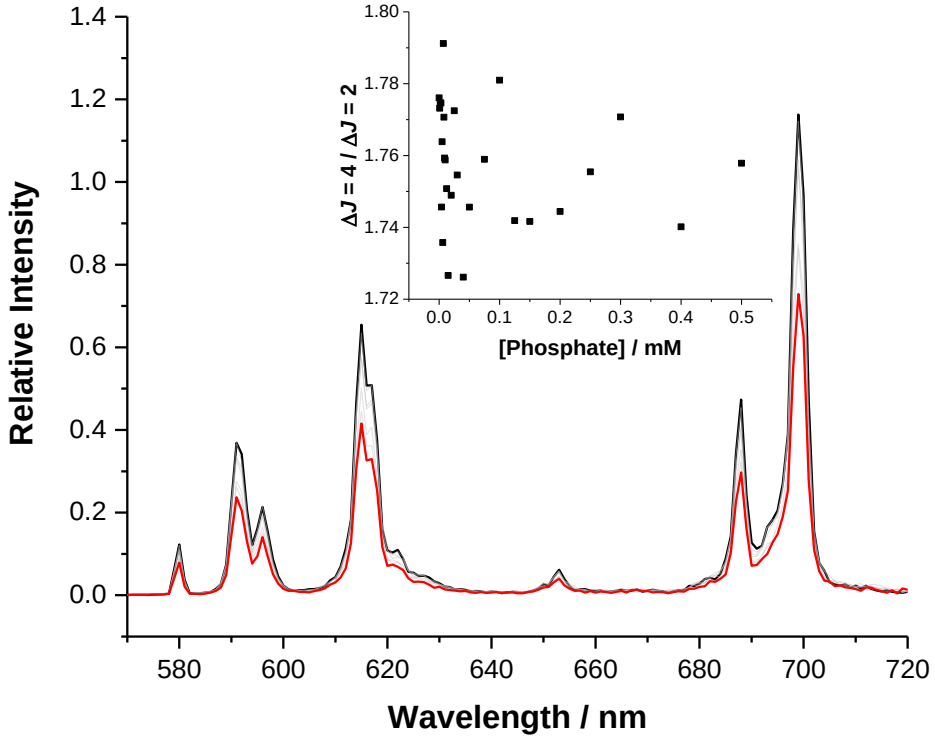

*Figure 3.37 - Changes in the emission of [Eu.**L**^{5}]$^{3+}$ (black) (20 μM, 0.1 M NaCl, 0.1 M MES, pH 5.9) with increasing concentration of phosphate, up to 0.5 mM (red). (Inest) The intensity ratio of ΔJ = 4/ΔJ = 2 as a function of increasing concentrations of phosphate*

A 15% decrease in emission intensity upon addition of phosphate was observed (Figure 3.37). However, the intensity ratio did not produce any meaningful variation.

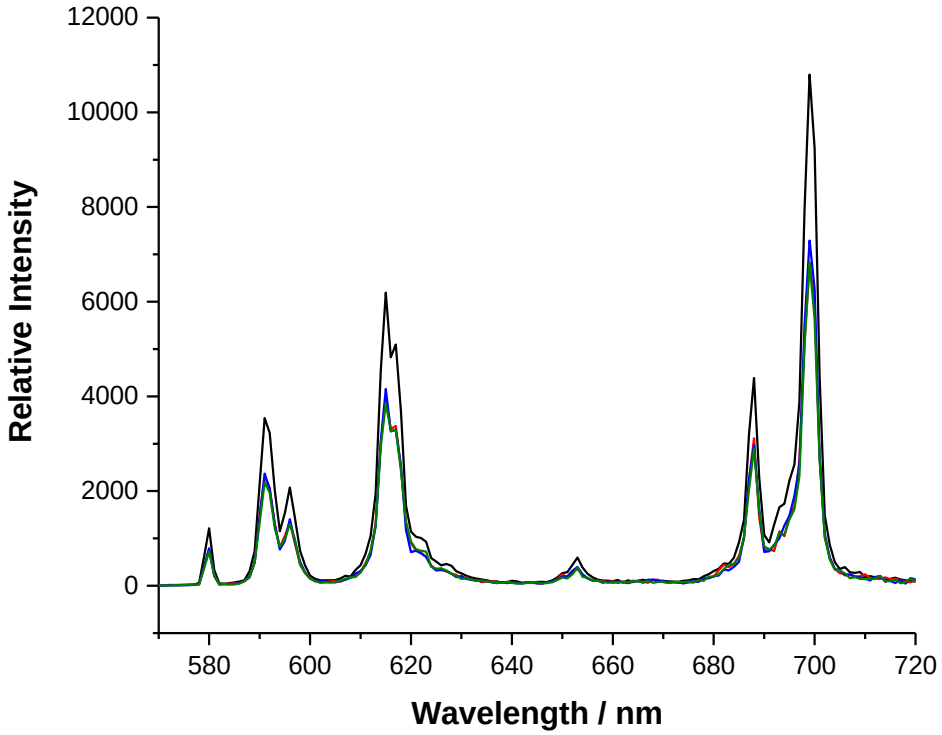

*Figure 3.38 - The emission spectrum of [Eu.**L**^{5}]$^{3+}$(black) (20 μM, 0.1 M NaCl, 0.1 M MES, 295 K) with 0.5 mM of glyphosate (red), 0.5 mM of phosphate at pH = 5.9 (blue) or pH 8.0 (green)*

The effect of pH on phosphate was also investigated. After altering the pH of the complex and phosphate (0.5 mM) to 8.0, there was no change in emission intensity or spectral form suggesting that the deprotonation of the second phosphate oxygen does not affect the binding. Furthermore, the overlaid emission spectrum of glyphosate, phosphate at pH 5.9 and 8.0, all showed almost exactly the same emission intensity and spectral form. This could potentially be a huge issue in 'real-world' samples as there would be no way to distinguish between a signal from phosphate and a signal from glyphosate.

Testing in grain extract will give an indication of whether this complex will be able to function in more complex media. It may be possible that there is endogenous phosphate-bearing material in the group which could interfere with glyphosate binding to the complex.

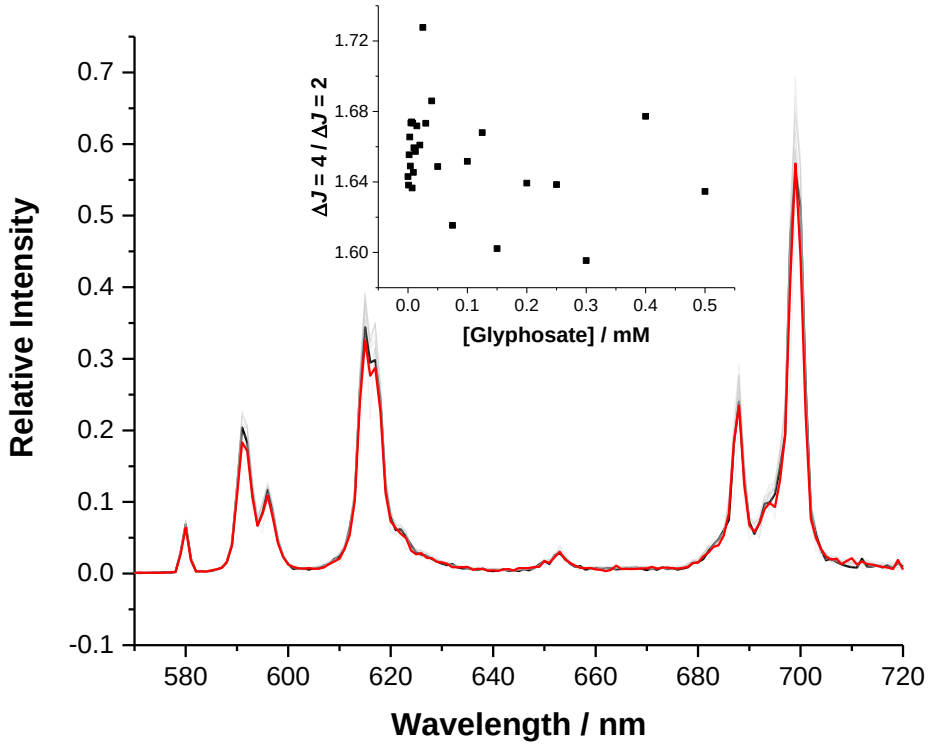

Figure 3.39 - Changes in the emission spectrum of $[Eu.\mathbf{L}^{5}]^{3+}$ *(black) in grain extract (20 μM, 0.1 M NaCl, 0.1 M MES, pH 5.9, 295 K) with increasing concentration of glyphosate, up to 0.5 mM (red). (Inset) The intensity ratio of ΔJ = 4 / ΔJ = 2 following incremental additions of glyphosate*

Again, a distinct lack of change in spectral form meant that no ratio was found which could be used to follow the binding event. To highlight this, the ratio of two bands in Figure 3.39 shows no correlation between $\Delta J = 4$ / $\Delta J = 2$ and glyphosate concentration. Furthermore, the unusual change in spectral form suggests that something is bound to the complex which competes with glyphosate which could explain why the emission intensity initially increases, and then decreases back to almost the original intensity.

To further test this complex, the grains were treated with acid, as in Section 3.7.3. To see if this could improve the response of the complex with glyphosate.

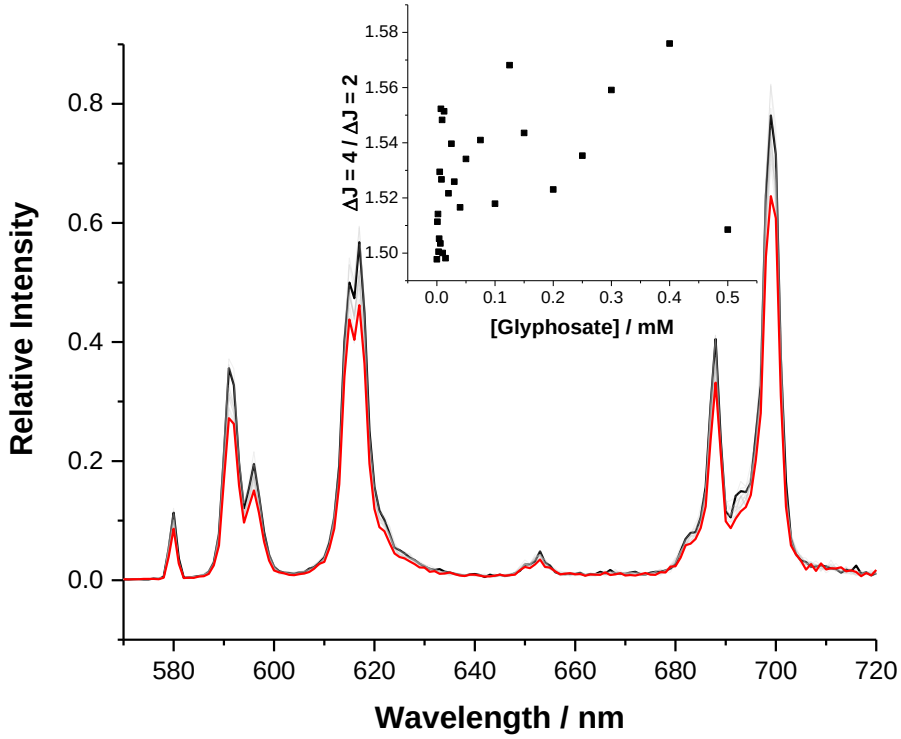

*Figure 3.40 - Changes in the emission spectrum of [Eu.**L**^{5}]$^{3+}$ (black) (20 μM, 0.1 M NaCl, 0.1 M MES, pH 5.9, 295 K) in acid treated grain extract with increasing glyphosate concentrations, up to 0.5 mM (red). (Inset) The intensity ratio of ΔJ = 4/ ΔJ = 2 with incremental additions of glyphosate*

The treatment of acid appeared to help the change in emission intensity to return to a more typical trend of a decrease with increasing glyphosate concentrations. However, even at the beginning of the titration, the spectral form of $\Delta J = 2$ was still different from the titration which was performed in buffer solution. It suggests that even with the acid treatment, there is still something in the grain extract which binds to the complex.

The complex binds to unwanted analytes, which may be due to the +3 charge. Hence, there is a suggestion that this would be less selective for glyphosate as other negatively charged compounds within biological media are likely to bind to the complex, through simple electrostatic interactions. Therefore, going forward, a complex that does not have such a large charge may be required to increase selectivity for glyphosate.

3.9 Conclusion and Further Work

The four compounds tested in this chapter utilised the alanine or phenylalanine arm in the detection of the herbicide, glyphosate. The complexes also differed through the variation of the chromophore structure, and systems with an azaxanthone, azathioxanthone and an extended chromophore were examined.

With the exception of [Eu.**L**^{3}]$^{3+}$, all complexes were found to bind glyphosate in buffer solution, showing that in non-competitive media, the complexes have some merit, and

most bound at a rate that would be useful if looking at the detection limits set by the EU and US EPA of glyphosate in food. However, the complexes were often not selective for glyphosate, as seen in the titrations with phosphate in particular. The pH was specifically set at 5.9 to attempt to overcome this competition but this strategy did not seem to be successful in every case.

Furthermore, once the titrations were carried out in more complex media, it became evident that the complexes were affected by the presence of other species which made the selective detection of glyphosate impossible.

Both the azaxanthone and azathioxanthone systems are sensitive to quenching of the intermediate triplet state due to the electron deficient nature of the chromophores. This aspect was highlighted by the titrations run with $[Eu.\mathbf{L^2}]^+$ and potential electron rich quenchers. They all showed a dramatic decrease in emission intensity upon addition of the quencher and as these were switch-off probes anyway, this behaviour only exacerbated the problems related to glyphosate binding.

The complex, $[Eu.\mathbf{L^5}]^{3+}$, binds glyphosate but the change in spectral form and indeed emission, was limited. Therefore, any interference from other species stopped efficient detection of glyphosate, as was seen in the grain extract. Although once the grains were treated with acid, the ability of the complex to detect glyphosate was enhanced, it was not sufficient for the complex to be useful.

This chapter showed the types of system that would not work in 'real-life' samples. For example, no further work should be done in the detection of glyphosate in grain extract with azaxanthones or azathioxanthones lanthanide probes, as they are too easily quenched by electron-rich species.

Although the use of the extended chromophore stopped this interference, $[Eu.\mathbf{L^5}]^{3+}$ was not selective for glyphosate, perhaps due to the +3 charge associated with the complex. Therefore, by changing the charge of the complex, for example by the addition of a carboxylate group, phosphonate or phosphinate group on the 6-position of the pyridines which would decrease the positive charge to +1. Furthermore, the comparison between these groups could further develop the probe.

4. Further Development on Europium Sensors for Glyphosate Detection

A series of complexes were synthesised, the first of which was originally designed as a zinc sensor, building on work by Pope *et. al.*.[205] The tripicolylamine group binds to a zinc ion through the four exocyclic nitrogen atoms. It was found more recently to bind strongly to ATP and ADP with the aid of zinc, which interestingly induced opposite chirality into the probe complex.[206] It was therefore possible to distinguish between the nucleotides and allowed the determination of the relative concentrations in a mixture of the two. As it binds to ATP and ADP, it was hypothesised that the complex could potentially bind to glyphosate directly through the phosphonate group.

4.1 Synthesis of [Eu.L^6]

The complex, [Eu.**L**^{6}], was synthesised from cyclen, and follows Scheme 2.1 giving rise to the intermediate diester, **3**. Preparation of the chromophore used in this complex required a six step synthesis (Scheme 4.1). Starting from chelidamic acid, the hydroxyl group is converted to a chloride atom and the carboxylate groups were protected as methyl esters, **13**, before halide exchange to provide the iodo compound, **14**. Controlled reduction of a single ester to the hydroxyl group (**15**) was followed by a Sonogashira cross-coupling reaction with 4-ethynylanisole to form the extended chromophore system, **16**. The final step in the chromophore synthesis is mesylation to give the intermediate, **17**.

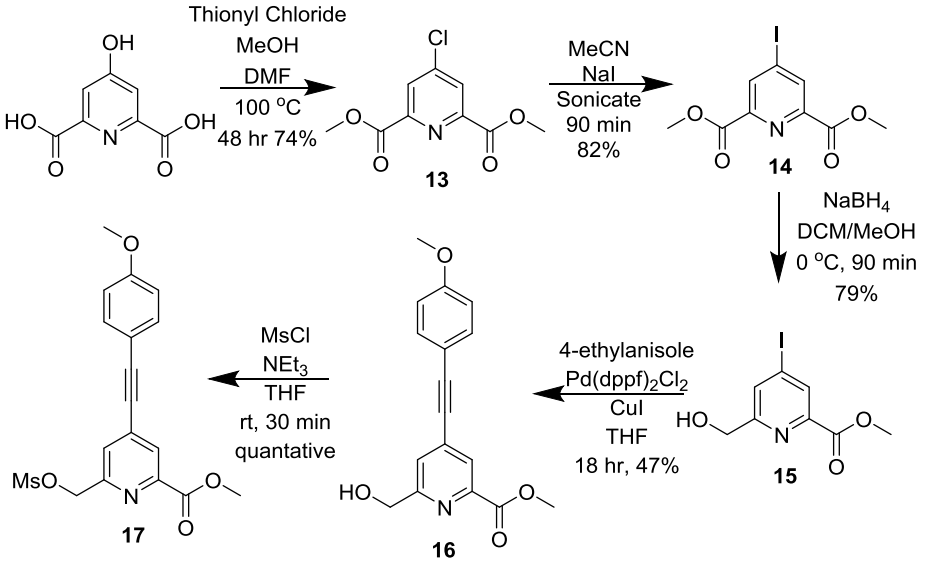

*Scheme 4.1 - Synthesis of the extended chromophore, **17***

Synthesising the tripicolylamine was conducted in a single step from commercially available starting materials, following a previously published method (Scheme 4.2). [205] A modified purification step was utilised with an alumina column being found to be more effective than a silica column.

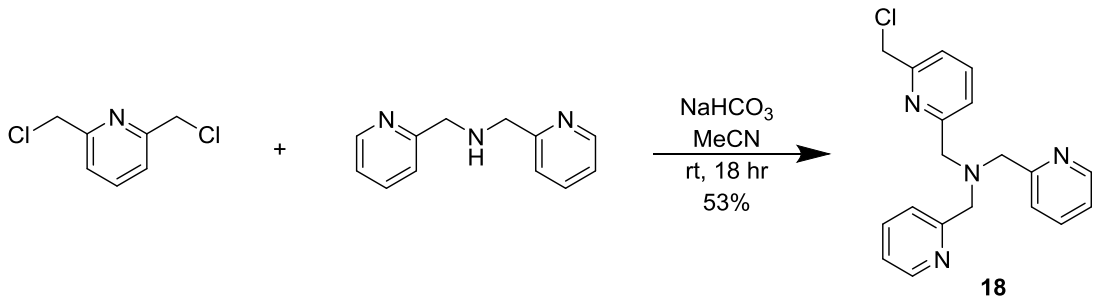

*Scheme 4.2 - Synthesis of the tripicolylamine arm, **18***

Stepwise alkylation of **3** with **17** gave first **19**, followed by addition of the tripicolylamine arm, **18**, to yield **20** (Scheme 4.3). Hydrolysis of the peripheral ester groups was undertaken using basic conditions and subsequent complexation gave [Eu.$\mathbf{L^6}$].

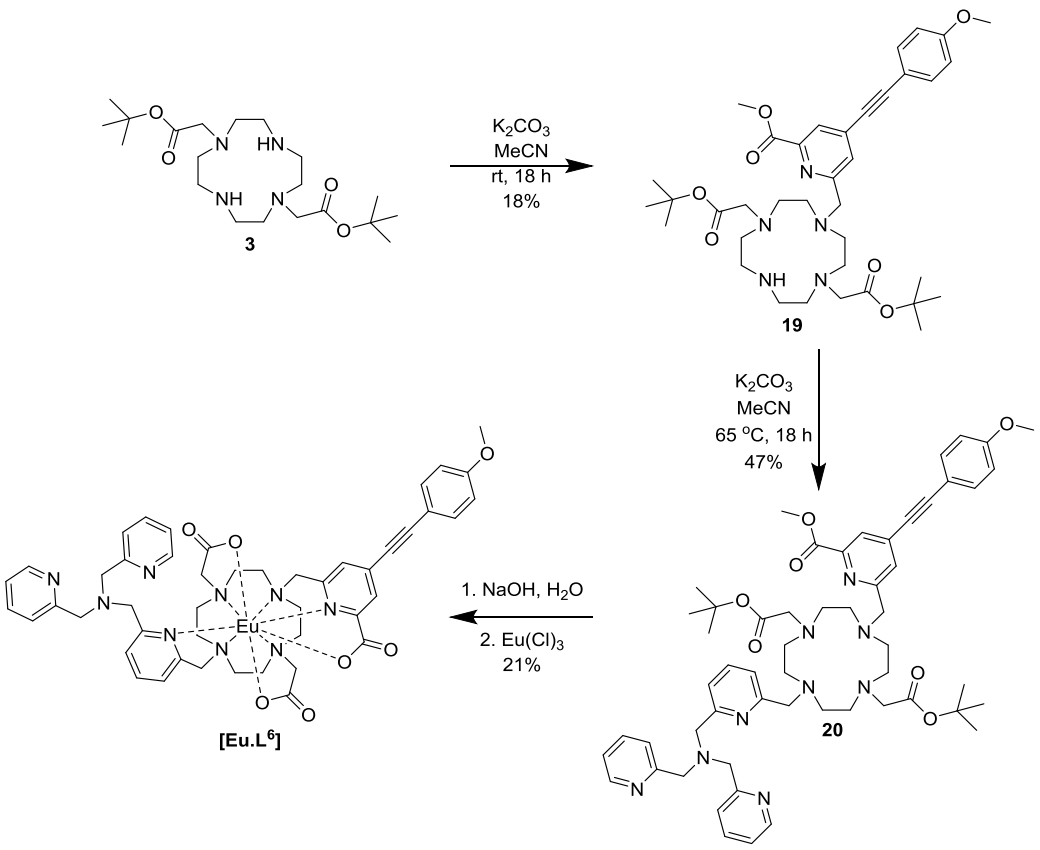

*Scheme 4.3 - Synthesis of [Eu.**L**^{6}]*

It was not found possible to purify the complex itself either by column chromatography or HPLC. However, purification of the ligand was achieved using HPLC and the complex was dialysed to remove any unwanted salt, which is an inevitable by-product in this complexation reaction. Complexation was monitored using both mass spectrometry and emission spectroscopy. Complete consumption of the ligand was confirmed by the absence of any residual ligand fluorescence.

4.2 Luminescence Studies on [Eu.L^6]

Following successful synthesis of [Eu.**L^6**], a titration was set up in purite water with 0.1 M NaCl and 0.1 M MES at pH 5.9. Incremental additions of glyphosate were followed through changes in europium emission, following excitation at 365 nm. Although this is not the maximum absorbance of this complex (λ_{max} = 340 nm), 365 nm is a commercially available LED laser and there is still adequate absorbance at this wavelength to achieve a sufficiently intense signal. Some initial titrations were performed without time-gated methods for more efficient collection of data.

4.2.1 Buffer Solution

In a buffer solution, there should be no binding competition from unwanted species and the pH is controlled, so glyphosate binding to the complex should be easily followed through the change in emission and spectral form. It is hypothesised that in the presence of glyphosate, the pyridine carboxylate on the chromophore would be displaced from the metal centre to allow glyphosate to bind through the phosphate oxygen. A significant change in spectral form is expected which should be easy to track through the use of a variety of wavelength ratios.

The first titration was performed without time-gating. The complex was excited at its absorbance maximum, i.e. 340 nm. Initial testing was extremely promising; a ‘switch-on’ effect was observed and multiple ratios could potentially be used to monitor the binding of glyphosate to the complex. Two bands in the hypersensitive $\Delta J = 2$ manifold, 604-614 nm and 614-633 nm became the chosen ratio to following the emission of the europium complex with increasing concentrations of glyphosate.

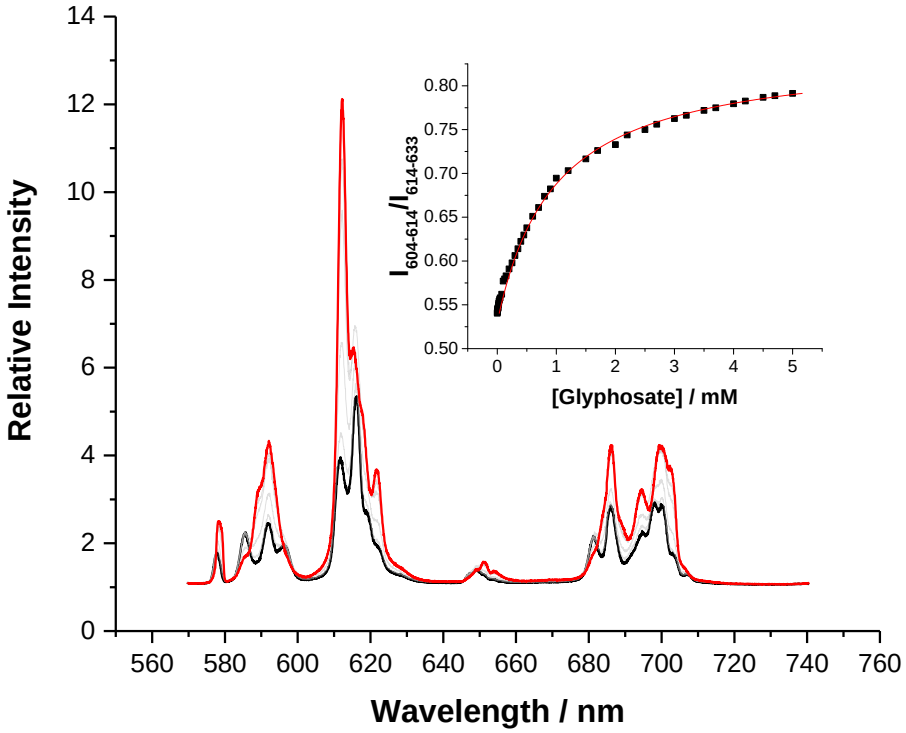

*Figure 4.1 - The change in the emission intensity of [Eu.**L**^{6}] (black) (7 μM, 0.1 M NaCl, 0.1 M MES, pH 5.9, 295 K) with incremental additions of glyphosate, up to 5 mM (red) with no stirring after addition. (Inset) The intensity ratio of 604-614 nm / 614-633 nm as a function of increasing glyphosate*

Upon repeating these titrations, discrepancies between what should be the same titrations were found, after using different instruments. After initial testing on a fluorolog where each scan takes approximately 10 seconds per scan, they were repeated on a time-gated instrument which takes close to 5 minutes per spectrum. They were found to have different log*K* values of 3.09 and 4.11 respectively. The differences between the two titrations were time and wavelength. Having changed the excitation wavelength on the fluorolog to 365 nm, a binding constant within error of the original was found. It was therefore hypothesised to be due to time.

An experiment which followed the change in spectral form after the addition of a small increment of glyphosate over time was performed. It was found that after stirring for 10 minutes, there was no further change in spectral form. Therefore, all subsequent titrations with [Eu.**L**^{6}] were performed after stirring for ten minutes.

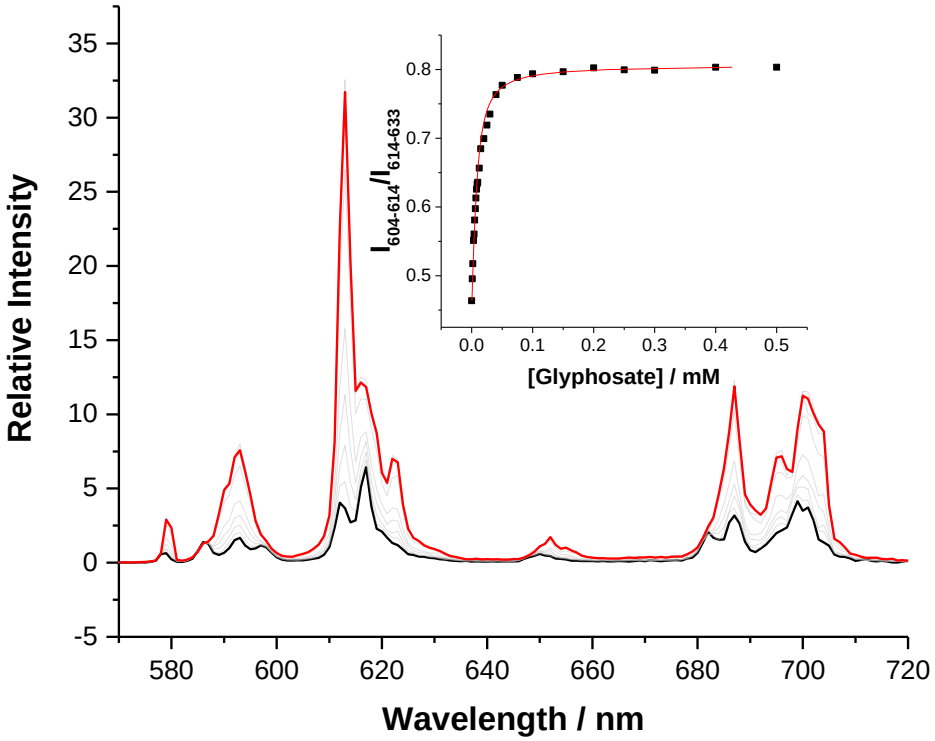

*Figure 4.2 - Changes in the emission intensity of [Eu.**L**^{6}] (black) (6 μM, 0.1 M NaCl, 0.1 M MES, pH 5.9, 295 K) with incremental additions of glyphosate, up to 0.5 mM (red). (Inset) The intensity ratio of 604-614 nm / 614-633 nm as a function of increasing glyphosate*

The apparent log*K* value of the addition of glyphosate to [Eu.**L**^{6}] with ten minutes stirring after each increment gave an apparent log*K* value of 5.36 (±0.02), significantly larger than found without stirring. There is a strong change in emission intensity and the spectral form is visually different upon addition of glyphosate, particularly in the hypersensitive $\Delta J = 2$ manifold. The linear range is also well within the MRLs of glyphosate, so potentially could be used as a probe.

The log*K* value was calculated using Equation **5.2** and the value in parenthesis is the statistical error of the fit to the data. Errors in these titrations are similar to those in the previous chapter. The experiments were carried out in a buffered solution throughout to minimise any change in pH which could affect the binding of glyphosate and other species such as phosphate. It was also carried out in a temperature controlled room, but there would be some slightly fluctuations throughout the titration and even comparing two separate titrations. Although these errors have been minimised, they could still have some influence on the log*K* values calculated. Titrations were repeated to minimise random error.

The lifetimes were recorded at the start and end of the titration in both H_2O and D_2O to allow a *q* value to be calculated.

*Table 4.1 - The lifetimes of [Eu.**L**^{6}] with and without glyphosate in H_2O and D_2O, as well as the equivalent q values*

	Lifetime in H_2O (τ_1) (ms)	Lifetime in D_2O (τ_1) (ms)	q
[Eu.**L**^{6}]	0.55	0.73	0.2
[Eu.**L**^{6}] + glyphosate	0.79	1.36	0.3

In both cases, the q value is approximately zero showing that there is no water in the inner sphere, which would be expected as the coordination number around the europium ion is already predicted to be nine.

The positive results obtained, with the high binding constant for glyphosate, the selectivity of the complex also needed to be probed. A number of relevant compounds will be tested, which will investigate both selectivity and the binding mode of glyphosate to the complex.

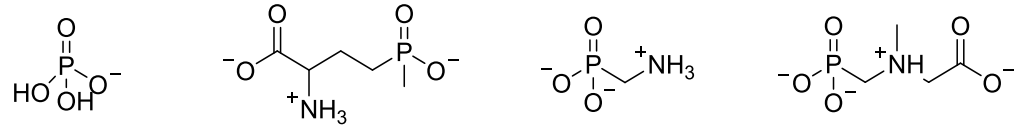

Figure 4.3 - The structures of four compounds which will be investigated

As discussed in previous sections, phosphate is expected to be the main competitor due to glyphosate binding through the phosphate group.

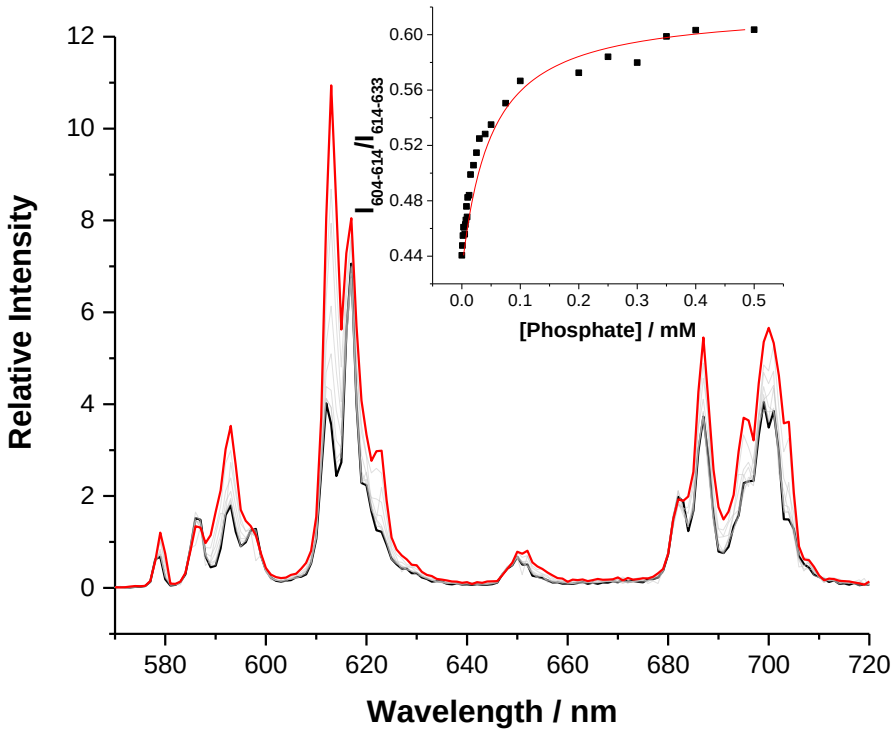

*Figure 4.4 - Changes in the emission intensity of [Eu.**L**^{6}] (black) (6 μM, 0.1 M NaCl, 0.1 M MES, pH 5.9, 295 K) with incremental additions of phosphate, up to 0.5 mM (red). (Inset) The intensity ratio of 604-614 nm / 614-633 nm as a function of increasing phosphate concentration*

Unfortunately, the complex did bind to phosphate, suggesting that monitoring phosphate levels in subsequent media is required. A change in spectral form is observed, analogous to that of glyphosate binding, suggestive of a similar binding mode. However, the log*K* value in buffer solution is 4.35 (±0.01), almost one order of magnitude smaller than found with glyphosate, in addition to a smaller intensity ratio.

The herbicide glufosinate was also tested as the presence of the phosphinate group could potentially allow it to bind to [Eu.**L**^{6}] in such a way that would mimic the change in spectral form found with phosphate and glyphosate.

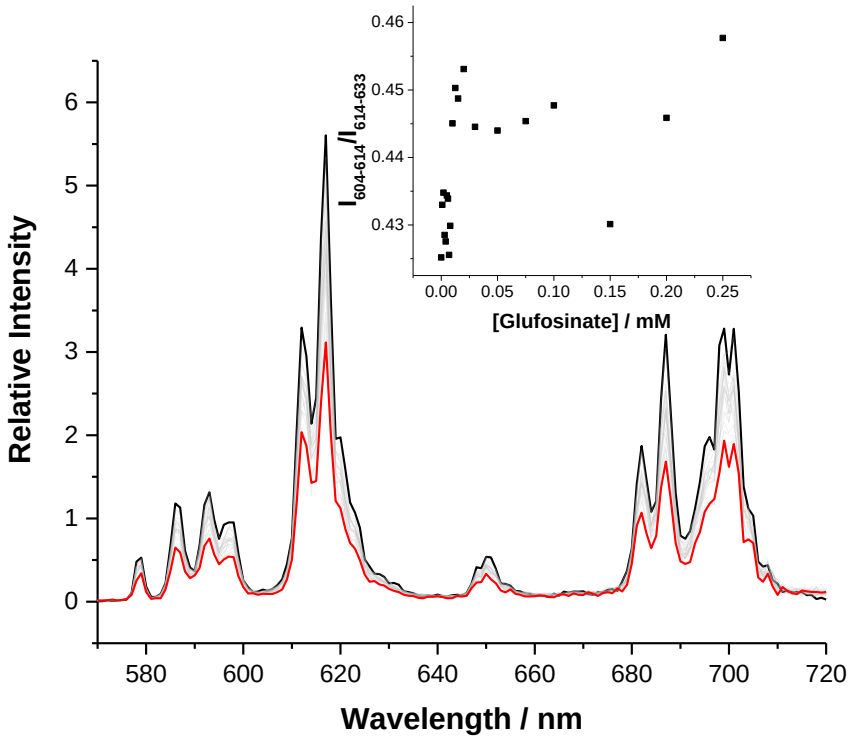

*Figure 4.5 - Changes in the emission intensity of [Eu.**L**^{6}] (black) (7 μM, 0.1 M NaCl, 0.1 M MES, pH 5.9, 295 K) with increasing concentration of glufosinate, up to 0.25 mM (red). (Inset) The intensity ratio of 604-614 nm / 614-633 nm as a function of increasing glufosinate concentration*

For this compound, a decrease in emission intensity was observed, which has not been witnessed for this complex thus far. Furthermore, there is no distinct change in spectral form, highlighted by the lack of correlation in the intensity ratio of 604-614 nm / 614-633 nm with increasing glufosinate concentration. The range of the ratio change was only 0.425-0.460, which is small in comparison to that observed upon addition of glyphosate. Therefore, it is likely that glufosinate does not bind to the complex through the phosphinate group and is unlikely to interfere if it were present in 'real-world' samples.

Glyphosate can decompose into the derivative, AMPA, which has been detected in some soil samples that also contain the herbicide. It retains the phosphate group and consequently its presence may interfere with glyphosate binding.

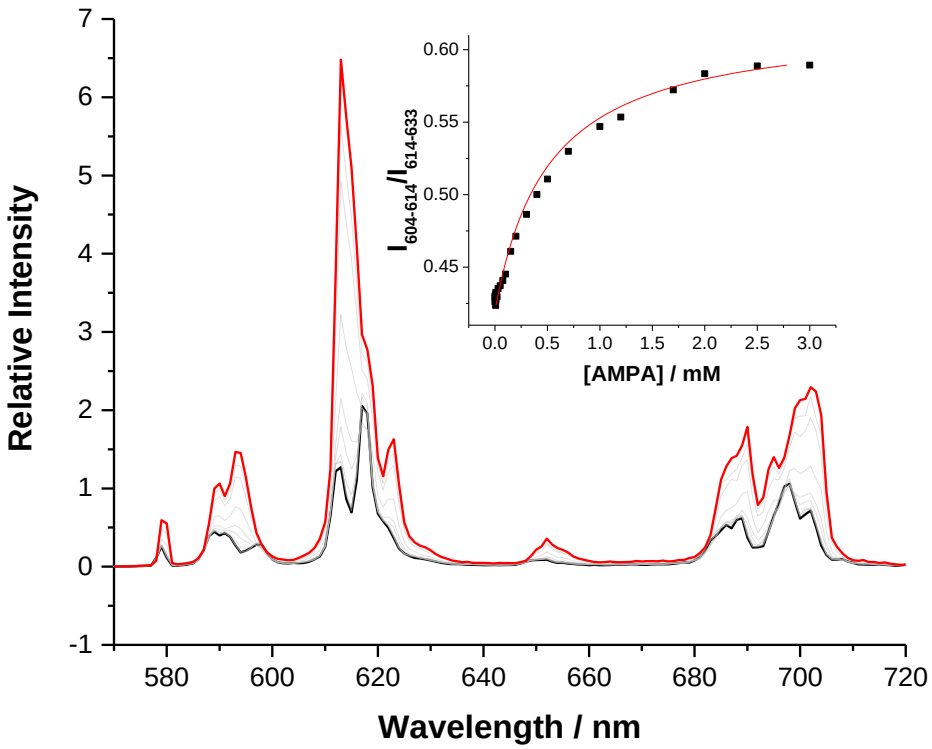

*Figure 4.6 - Changes in the emission intensity of [Eu.**L**^{6}] (7 μM, 0.1 M NaCl, 0.1 M MES, pH 5.9, 295 K) with increasing concentration of AMPA, up to 3 mM (red). (Inset) The intensity ratio of 604-614 nm / 614-633 nm as a function of increasing AMPA concentration*

Following addition of AMPA, an increase in emission intensity was observed. There was also a change in spectral form, particularly in the hypersensitive $\Delta J = 2$ band, with the two bands merging into one and the growth of the shoulder band. Following the change in this transition, with increasing concentrations of AMPA, a binding curve could be produced and fitted to obtain an apparent log$K$ value of 3.30 (±0.01). This is almost exactly two log units smaller than that obtained with glyphosate. The suggestion is that the binding involves the carboxylate group, which may hydrogen bond to the complex. This is a significant contribution to the binding, so studies analysing the carboxylate group could be carried out to establish how much this contributes to binding.

Many of the competitive studies focus on the phosphate moiety, but glyphosate can be considered as a glycine residue with a phosphate tag. Therefore, a titration of glycine with [Eu.**L**^{6}] was undertaken to determine if any significant interactions exist between the europium centre and glycine.

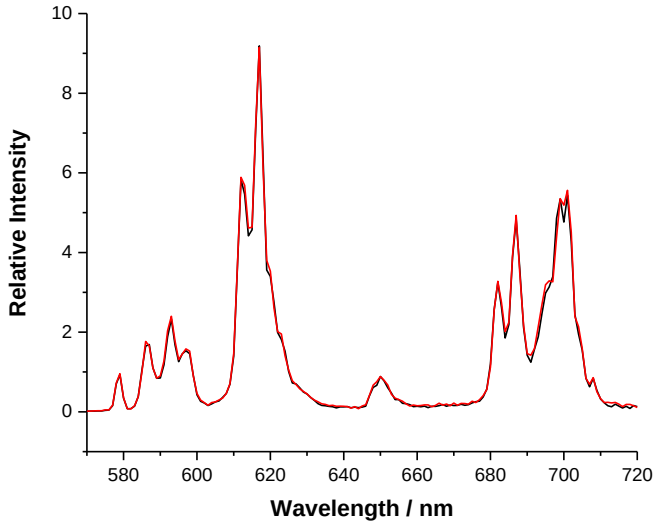

*Figure 4.7 - The emission of [Eu.**L**^{6}] (7 μM, 0.1 M NaCl, 0.1 M MES, pH 5.9, 295 K) with (red) and without (black) 0.5 mM glycine*

As revealed in Figure 4.7 the addition of glycine changed neither the emission intensity nor the spectral form. This lack of change confirms the hypothesis that glyphosate binds through the phosphonate group and any interactions with the rest of the molecule are significantly less important.

Methylation of the central amine on glyphosate is simply achieved by refluxing with formic acid and formaldehyde. Titrations performed with this compound can give more information about the importance of a secondary amine in comparison to a tertiary amine.

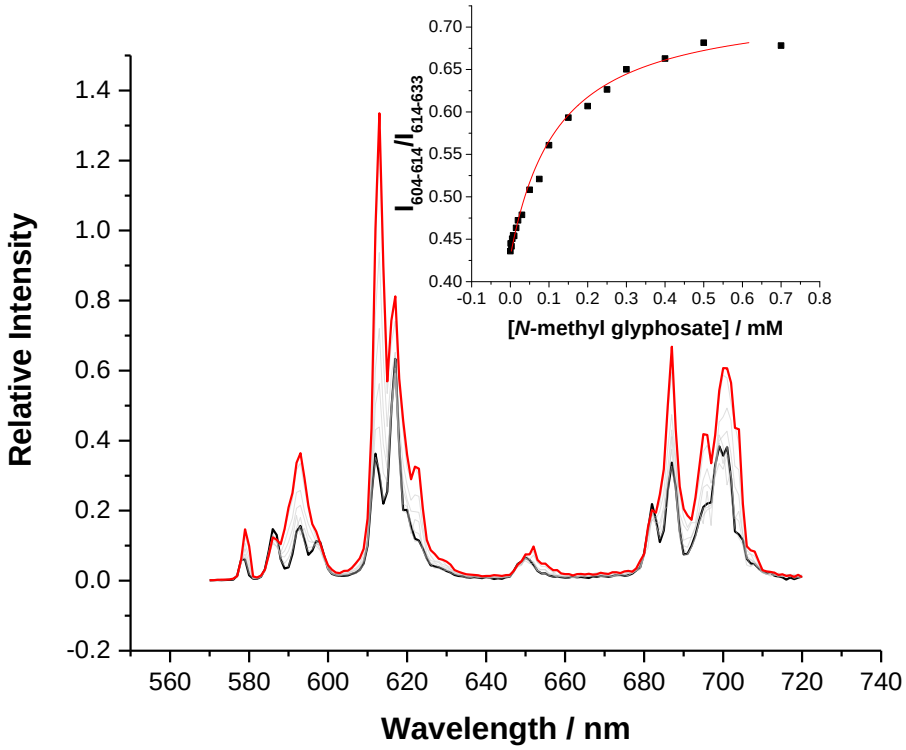

*Figure 4.8 - Changes in the emission intensity of [Eu.**L**^{6}] (7 μM, 0.1 M NaCl, 0.1 M MES, pH 5.9, 295 K) with increasing concentration of N-methyl glyphosate, up to 0.7 mM (red). (Inset) The intensity ratio of 604-614 nm / 614-633 nm as a function of increasing N-methyl glyphosate concentration*

Upon addition of *N*-methyl glyphosate, an increase in emission intensity and change in spectral form can be observed. Following the change in the intensity ratio of 604-614 nm / 614-633 nm with increasing glyphosate concentration, a binding constant was estimated using non-linear regression analysis to obtain an apparent log*K* value of 3.93 (±0.02). This value is smaller than that obtained with glyphosate and phosphate. It suggests that the binding of glyphosate to [Eu.**L**^{6}] either involved two hydrogen bonds with both hydrogens on the central amine on glyphosate, or the addition of the methyl group causes a steric effect which stops *N*-methyl glyphosate binding to the crowded complex.

4.2.2 Titrations in Different Media

Following the promising results of the competitive studies, work in more competitive media was carried out. The first study used local tap water, although there is no detection limit imposed in the EU, the US EPA have advised an MRL. Glyphosate has been known to decompose in chlorinated water, but it has been detected in some samples, albeit very rarely.[207]

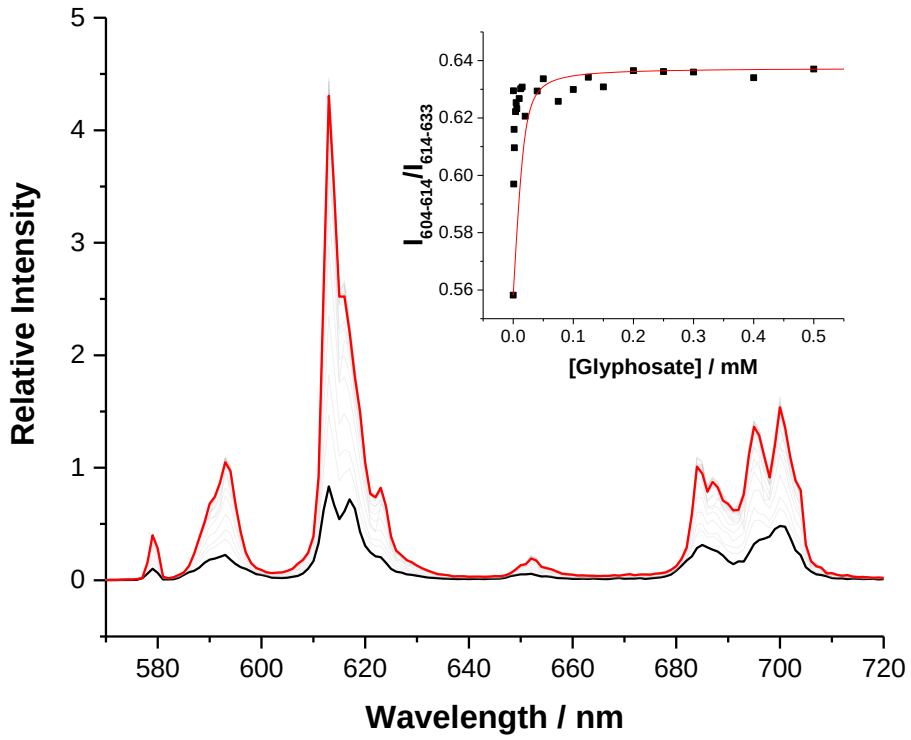

*Figure 4.9 - Changes in the emission intensity of [Eu.**L**^{6}] in tap water (black) (18 μM, 0.1 M NaCl, 0.1 M MES, pH 5.9, 295 K) with increasing concentration of glyphosate, up to 0.5 mM (red). (Inset) The intensity ratio of 604-614 nm / 614-633 nm as a function of increasing glyphosate concentration*

Indeed, there was an increase in emission intensity and change in spectral form observed that was similar to that found in buffer solution. Following the intensity ratio used throughout the studies on this complex, an increase similar to that for glyphosate was observed, suggesting that glyphosate decomposition into phosphate occurs on a timescale greater than the length of the titration. An apparent log*K* value of 5.52 (±0.05) was calculated, not dissimilar to that in buffer solution. However, the final ratio is not as high as that observed in glyphosate.

Therefore, another experiment was conducted to assess the possibility of glyphosate decomposition in tap water throughout the initial titration. An emission spectrum was taken of the complex itself, immediately upon addition of 0.5 mM of glyphosate, after equilibration, and then after 48 h.

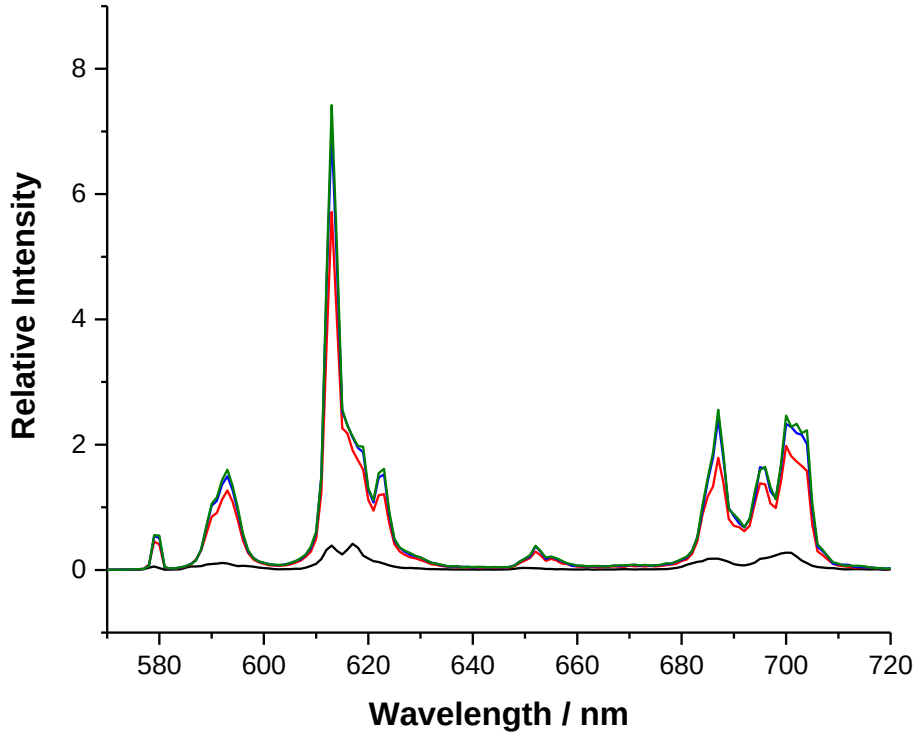

*Figure 4.10 - The emission spectrum of [Eu.**L**^{6}] (black) (12 μM, 0.1 M NaCl, 0.1 M MES, pH 5.9, 295 K) in tap water after addition of glyphosate (0.1 M) after 0 h (red), 0.5 h (blue) and 48 h (green)*

It is evident that the decay with the complex does not occur after 48 h and the possibility of glyphosate decay on the timescale of the titration can be discounted. However, the spectral response measured in tap water is not as smooth as that found in buffer solution, suggesting that the small amount of phosphate present in tap water might be interfering.[208]

Using the same river water as the sample in Section 3.4, with 0.1 M NaCl and 0.1 M MES to ensure the pH was maintained at 5.9, a glyphosate solution was again titrated into a solution containing [Eu.**L**^{6}].

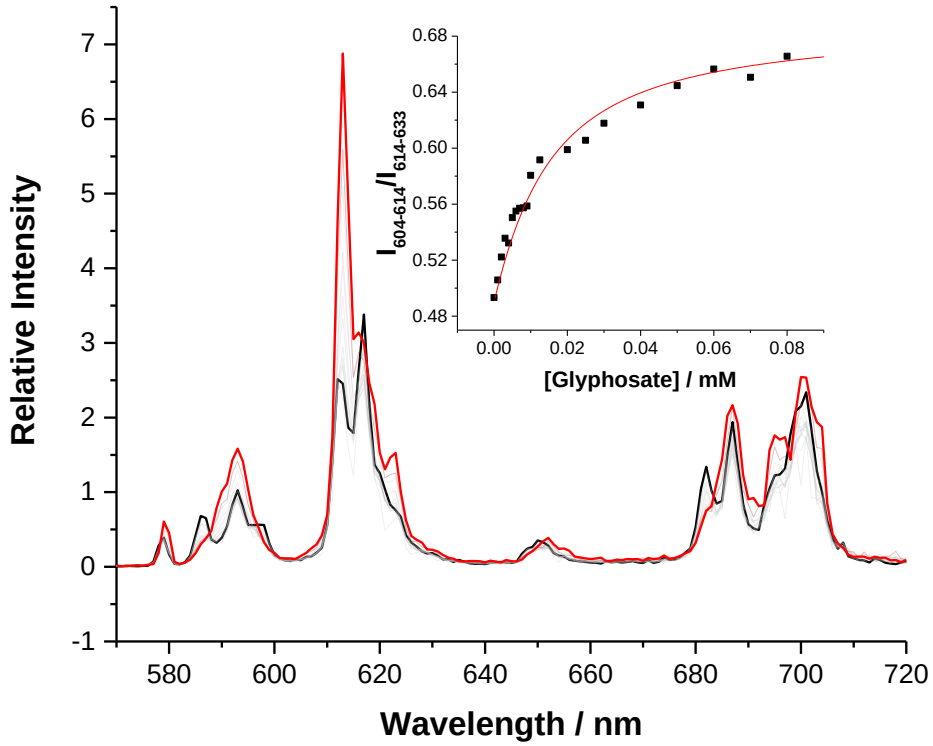

*Figure 4.11 - The change in emission intensity of [Eu.**L**^{6}] in river water (black) (6 μM, 0.1 M NaCl, 0.1 M MES, pH 5.9, 295 K) with increasing concentration of glyphosate, up to 0.08 mM (red). (Inset) The ratio of 604-614 nm / 614-633 nm with increasing glyphosate concentration*

Following the addition of glyphosate, a significant increase in emission intensity and a change in spectral form were observed. The change could be tracked using the intensity ratio 604-614 nm / 614-633 nm. From Figure 4.11 it can be clearly seen that the two bands in the ΔJ = 2 manifold invert in emission intensity. The binding constant was estimated using non-linear regression analysis to obtain an apparent log$K$ value of 4.92 (±0.02), lower than the binding constant observed in buffer. It is therefore likely that additional species in the river water interact with the complex. However, as the increase in emission intensity is maintained and the ratio gives a smooth curve, this probe is still appropriate for use with river water samples. This complex would be suitable for the detection of glyphosate in samples where the concentration is close to the limit, particularly as in the USA, the EPA MRL for drinking water is 0.7 μg/mL (4 μM).

Another medium in which glyphosate has been found is in urine. This could be concentrations remain below potentially dangerous levels.

The urine was collected from a healthy 24 year old male for initial investigations, to test if the complex could be a viable probe in this medium.

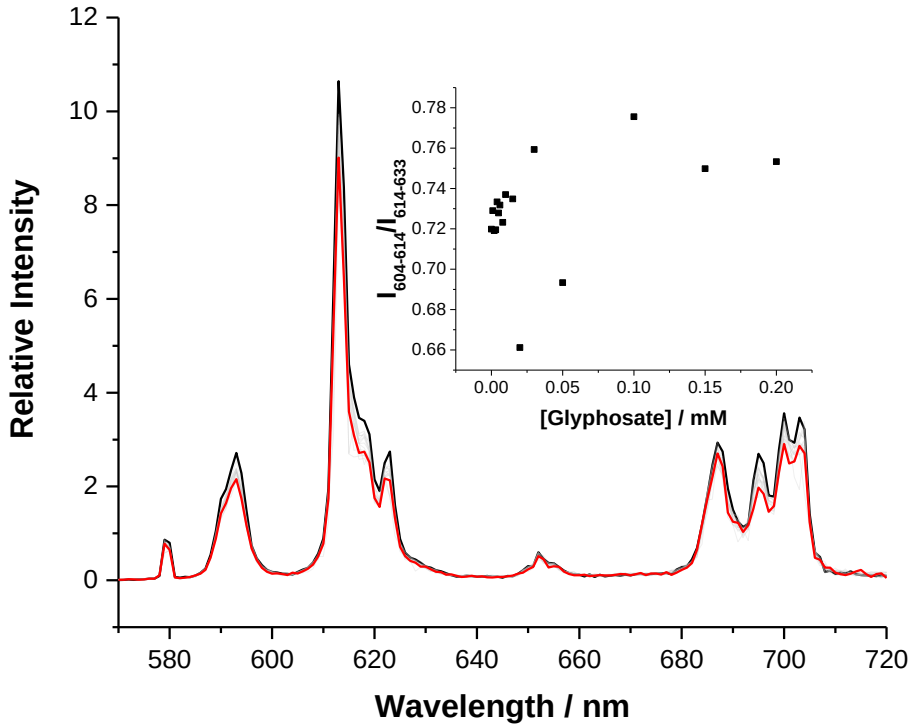

*Figure 4.12 - Changes in the emission intensity of [Eu.**L**^{6}] in urine (black) (7 μM, 0.1 M NaCl, 0.1 M MES, pH 5.9, 295 K) with increasing concentration of glyphosate, up to 0.2 mM (red). (Inset) The intensity ratio of 604-614 nm / 614-633 nm as a function of increasing glyphosate concentration*

Before addition of glyphosate, the spectral form in urine was observed to be very different from that in buffer. This implied an unknown species was already bound.

Upon addition of glyphosate there is minimal change in both emission intensity and spectral form. This is suggestive that the species bound to the complex in urine binds more strongly than glyphosate, and hence, no real change in the emission spectrum was observed. This was confirmed by the lack of change in the intensity ratios which can be used to track any binding event. There could be a number of compounds in urine which cause this behaviour, but these initial results confirm that this probe cannot be used in this medium.

The next background solution to be tested was oat extract. The MRL set by the EU is 0.1 mM and therefore detection around this point is important. Oat extract was made using a similar method to the wheat grain extract but with an important difference. Sainsbury's Scottish oats were obtained and soaked in water. However, upon addition of water to soak the oat, a thick suspension was formed, akin to porridge. A practical issue arose when trying to remove the oats. The best method involved centrifugation to remove the majority of the oats, followed by membrane filtration to remove any remaining solid traces of oat.

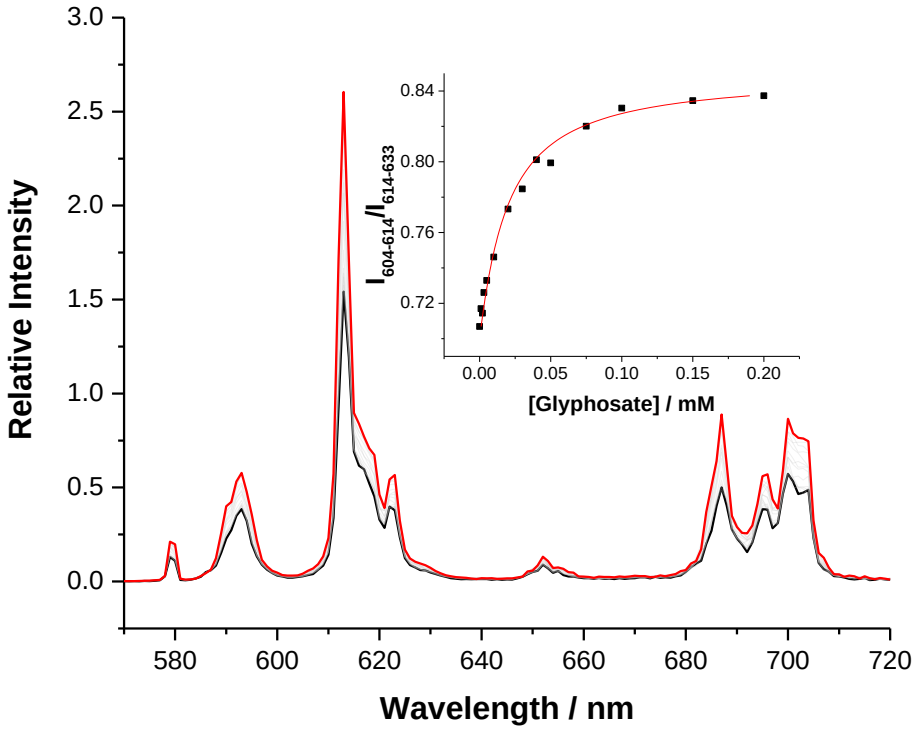

*Figure 4.13 - Changes in the emission intensity of [Eu.**L**^{6}] in oat extract (black) (5 μM, 0.1 M NaCl, 0.1 M MES, pH 5.9, 295 K) with increasing concentration of glyphosate, up to 0.2 mM (red). (Inset) The intensity ratio of 604-614 nm / 614-633 nm as a function of increasing glyphosate concentration*

The spectral form at the beginning of the titration resembled that seen with the urine sample, rather than buffer solution. The changes in spectral form were only small. However, by plotting the intensity ratio 604-614 nm / 614-638 nm as a function of glyphosate concentration, a clear, smooth curve was obtained. The binding constant was estimated using non-linear regression analysis, giving an apparent log*K* value of 4.77 (±0.01), similar to the value found in river water.

Next, a wheat grain extract was prepared in an analogous method to that described in Section 3.6, with an MRL of 59 μM set by the EU.

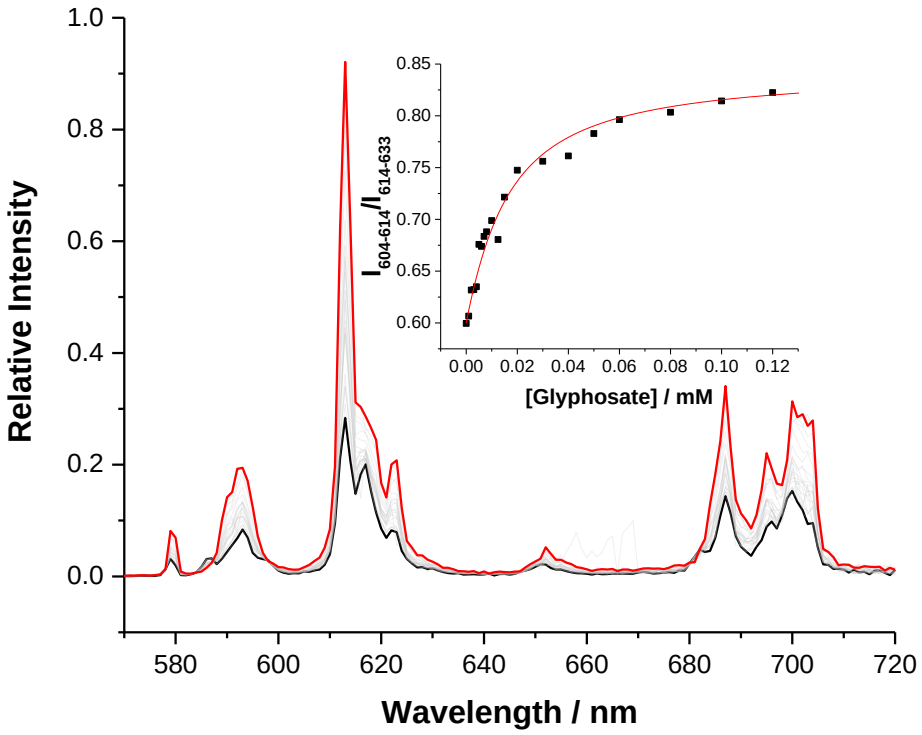

*Figure 4.14 - Changes in the emission intensity of [Eu.**L**^{6}] in grain extract (black) (7 μM, 0.1 M NaCl, 0.1 M MES, pH 5.9, 295 K) with increasing concentration of glyphosate, up to 0.12 mM (red). (Inset) The intensity ratio of 604-614 nm / 614-633 nm as a function of increasing glyphosate concentration*

The initial emission spectrum taken in grain extract with no glyphosate present was not dissimilar to that in buffer, suggesting that the species bound to the complex in oat extract was not found in grains. Upon addition of glyphosate, an increase in emission intensity of approximately three fold was found, with an observable change in spectral form, as expected for this complex. Following the intensity ratio of 604-614 nm / 614-633 nm, a curve was extracted. The binding constant was estimated using non-linear regression analysis, and an apparent log*K* value of 4.42 (±0.02) was obtained, similar to the values for oats and river water.

In summary, the results with this complex are encouraging; not only can the complex bind glyphosate selectively in a variety of media, but the levels in which glyphosate can be detected falls in the range of MRL values set in grains and oats by both US EPA and EU. Furthermore, as the complex is an effective probe in these media, it is possible that the complex would be able to function in a wide range of food stuffs.

Although it is not completely selective for glyphosate over phosphate or AMPA, the complex does not bind to glufosinate or glycine showing it does have some degree of selectivity. The ratio of log*K* values for glyphosate over phosphate is 5.36/4.35 = 1.23 and for glyphosate over AMPA is 5.36/3.30 = 1.62.

*Table 4.2 - The logK values of [Eu.**L**^{6}] of different analytes and glyphosate in different media (295 K, pH 5.9, 0.1 M NaCl, 0.1 M MES)*[h,i]

	Glyphosate					Phosphate	AMPA
	Purite water	River water	Oat extract	Grain Extract	Tap water		
[Eu.**L**^{6}]	5.36 (±0.02)	4.92 (±0.02)	4.77 (±0.01)	4.42 (±0.02)	5.52 (±0.05)	4.35 (±0.01)	3.30 (±0.01)

4.2.3 Testing [Eu.L^{6}] with Zinc

As the tripicolylamine arm was originally used as zinc sensor, and the ADP/ATP probe also functions in the presence zinc ions, a study to examine the effect of zinc on the binding of glyphosate was undertaken. It is possible that the presence of added zinc may increase the log*K* value for the association of glyphosate with [Eu.**L**^{6}].

4.2.3.1 DFT Experiments

Density Functional Theory (DFT) is a computational method that among other uses, can identify and allow theoretical comparisons of putative low energy structures of compounds. Dr. Mark Fox (Durham University) modelled the [Eu.**L**^{6}] complex with glyphosate in the presence and absence of zinc. The alkynyl substituent in the chromophore was removed and Y was used in place of Eu for simplicity.

[h] The complex was also tested in urine but a binding constant could not be calculated
[i] Errors given represent statistical error on the fit

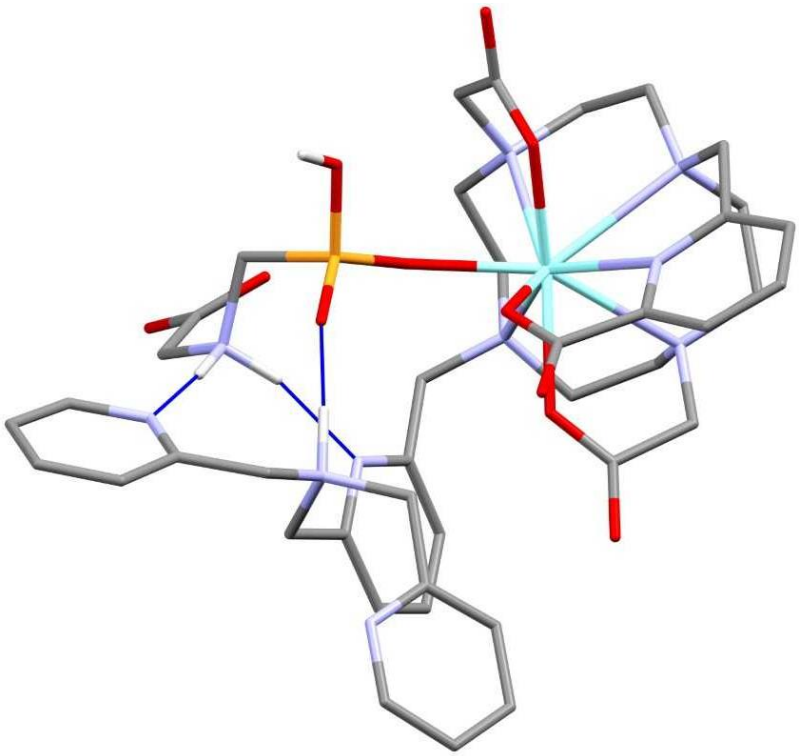

*Figure 4.15 - The DFT of [Y.**L**^{6}] with glyphosate in the absence of zinc, using the hydrid-DFT B3LYP and the 3-21G* basis set*

Glyphosate was bound to the metal centre of the complex through the phosphate oxygen. Furthermore, a network of stabilising intramolecular hydrogen bonds were also defined. The optimised model geometry for {[Y.**L**^{6}]*glyphosate} revealed a N-H…O interaction with a H…O distance of 1.47 angstroms and two N-H…N interactions with H…N distances of 1.84 and 1.88 angstroms. The phosphate oxygen hydrogen bonds to the protonated central amine. Furthermore, each NH in the protonated amine group in glyphosate can act as an H-bond donor to the pyridine N atom; at pH 5.9 it is expected to be protonated. These stabilising secondary interactions help to explain the differences in log*K* values compared with AMPA and phosphate, where such secondary hydrogen binding interactions cannot occur.

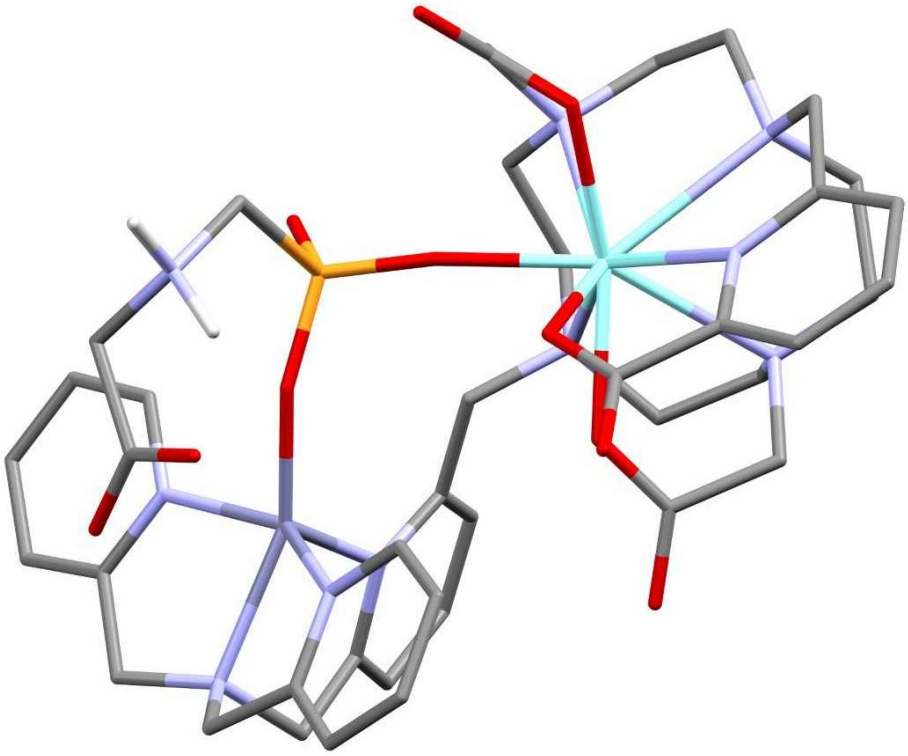

*Figure 4.16 - The DFT of [Y.**L**^{6}] with zinc and glyphosate, using the hydrid-DFT B3LYP and the 3-21G* basis set*

In the presence of zinc, the tripicolylamine arm encapsulates the zinc ion and changes how glyphosate binds. It binds to the metal centre in the same manner, through the phosphate oxygen. However, it is no longer stabilised through a number of hydrogen bonds. Instead, the remaining deprotonated phosphate oxygen binds to the zinc ion generating a phosphate bridge between the two metal ions. Such an interaction with zinc should be sufficiently strong to compensate for the loss of free energy associated with hydrogen bonding.

4.2.3.2 Binding with Zinc

A titration was performed involving the incremental additions of a zinc chloride solution to [Eu.**L**^{6}] in 0.1 M NaCl, 0.1 M MES buffer solution. Although this titration had been carried out at pH 7.4,[206] the titration at 5.9 was thought to be necessary as the change of pH could have an effect both on the free energy of binding of glyphosate, and of the zinc ion.

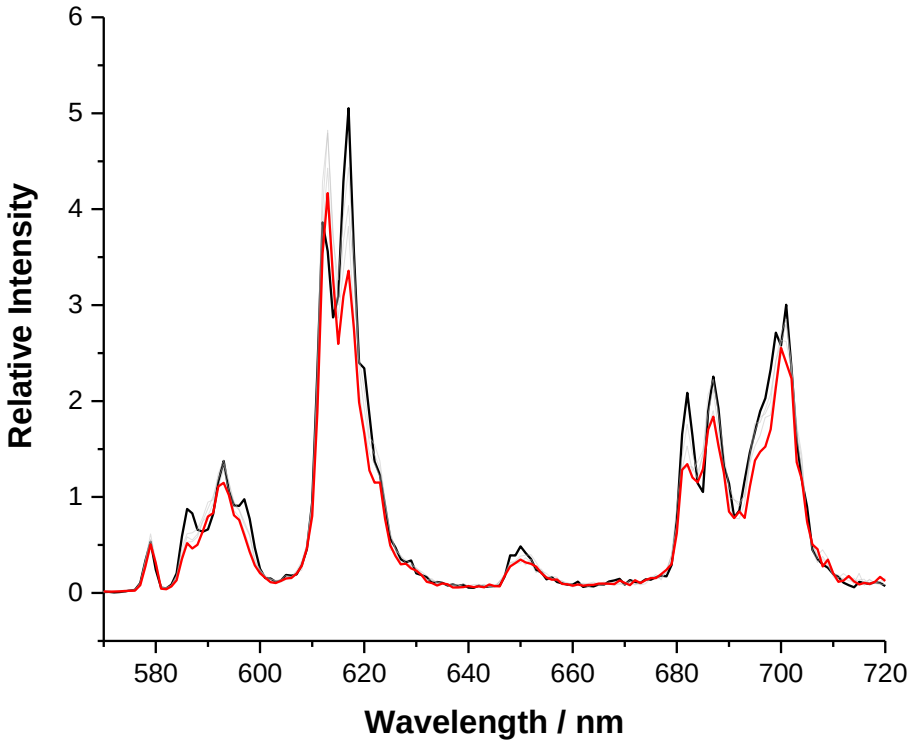

*Figure 4.17 - Changes in the emission spectrum of [Eu.**L**^{6}] (black) (6 μM, 0.1 M NaCl, 0.1 M MES, pH 5.9, 295 K) with increasing concentration of zinc chloride, up to 10 equivalents (red)*

Upon addition of excess of zinc, a change in spectral form was observed, particularly noticeable in the $\Delta J = 2$ manifold. The intensity ratio of 604-614 nm / 614-633 nm was used to track this change, and a smooth binding curve was obtained. However, a simple 1:1 binding curve was not able to fit this. This was not unexpected as previous studies, although done at pH 7.4, had also found this and used a 2:1 binding curve, suggesting two complexes, in particular two tripicolylamine moieties, encapsulate the zinc metal ion.

4.2.3.3 Glyphosate Binding in the Presence of Zinc

From the DFT study it is possible that in the presence of zinc, a different log*K* value for glyphosate could be obtained. Experiments in which one or two equivalents of zinc were added to the complex solution were prepared, before glyphosate was titrated in.

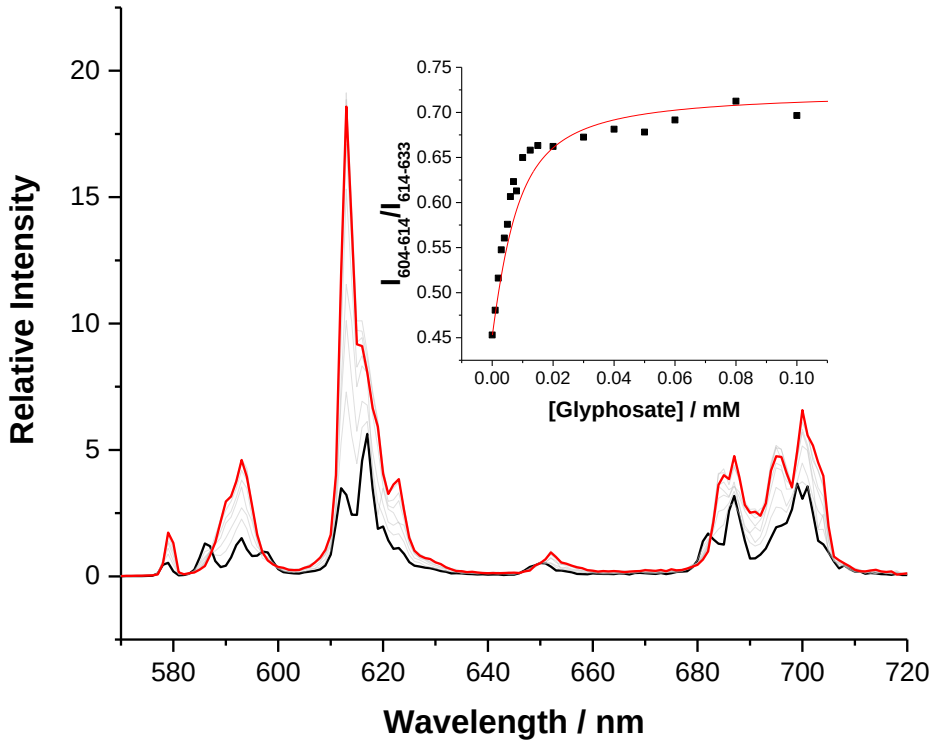

*Figure 4.18 - Changes in the emission spectrum of [Eu.**L**^{6}] with one equivalent of zinc chloride (black) (6 μM, 0.1 M NaCl, 0.1 M MES, pH 5.9, 295 K), with increasing glyphosate concentration, up to 0.1 mM (red). (Inset) The intensity ratio of 604-614 nm / 614-633 nm with incremental additions of glyphosate*

In the presence of one equivalent of zinc, addition of glyphosate led to an increase in emission of almost four-fold. There was also a distinct change in spectral form in almost all transitions. These changes were very similar to those observed in the absence of zinc. The ratio which has previously been used in glyphosate titrations for [Eu.**L**^{6}] was again utilised, and a 1:1 bind curve was fitted to the data. From this analysis, a log*K* value of 5.33 (±0.05) was obtained, which is within error of the log*K* value achieved in the absence of zinc.

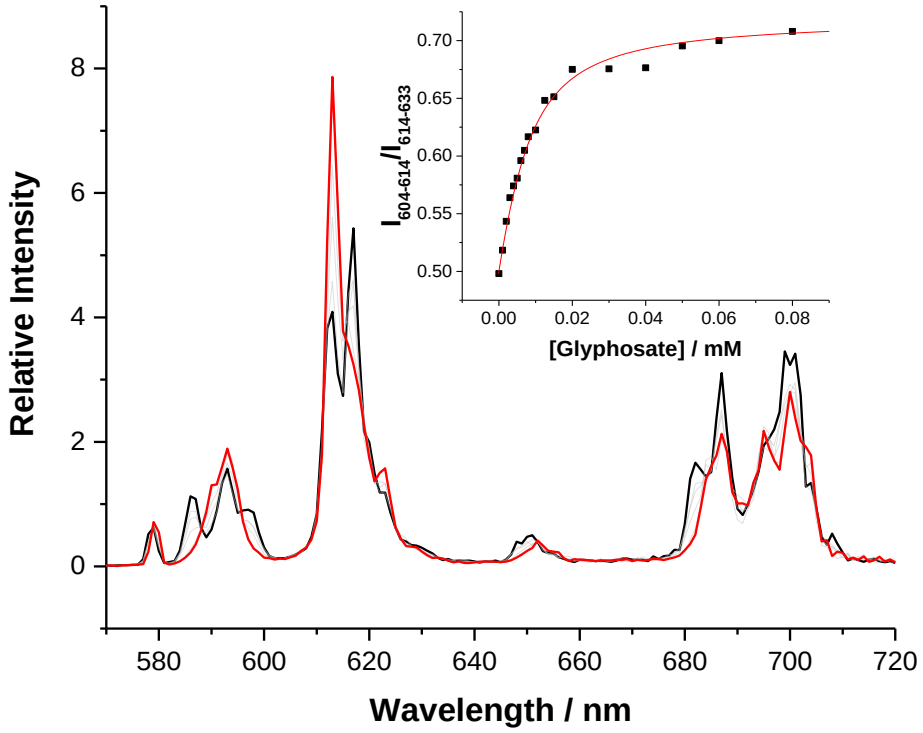

*Figure 4.19 - Changes in the emission spectrum of [Eu.**L**^{6}] with two equivalents of zinc chloride (black) (6 μM, 0.1 M NaCl, 0.1 M MES, pH 5.9, 295 K), with increasing concentration of glyphosate, up to 0.08 mM (red). (Inset) The intensity ratio of 604-614 nm / 614-633 nm with incremental additions of glyphosate*

In the presence of two equivalents of zinc, a log*K* value of 5.31 (±0.02) was estimated, i.e., within error of both one equivalent of zinc, and in the absence of zinc. An interesting note in these titrations are that the overall increase in emission intensity is much smaller compared to that of one equivalent, which is in turn smaller than that observed with no zinc. The reasons behind these traits are unknown. However, what these titrations state is that zinc does not increase the apparent binding constant for glyphosate to [Eu.**L**^{6}]. Therefore, all further work does not include the addition of zinc chloride.

4.3 Modifying the Tripicolylamine Arm

The next step in this series of experiments would be to test spiked grains, but improvement on the binding ability of glyphosate and selectivity, without the need to stir for ten minutes before recording would be preferable. Building on [Eu.**L**^{6}], there are a number of ways the complex could be adapted to improve binding.

The first step is to look at the tripicolylamine. As this moiety was designed to bind zinc, it was thought that this arm was not important in the binding of glyphosate, particularly as zinc was observed not to improve on the log*K* value. Therefore, with this in mind, the removal of one and two of these picolyl groups was tested.

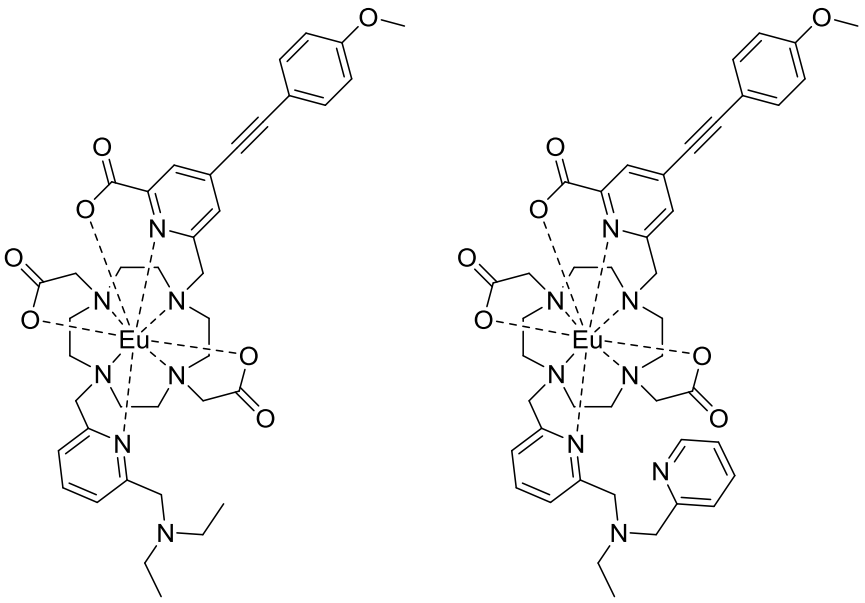

*Figure 4.20 - The structure of [Eu.**L**^{7}] (left) and [Eu.**L**^{8}] (right)*[j]

The synthesis of these complexes followed the Scheme 4.3 up to **19**. The arm for [Eu.**L**^{7}] was synthesised by reacting 2,6-*bis*(chloromethyl)pyridine with diethylamine. This arm was then introduced onto the ring, followed by deprotection of the esters groups, and complexation. The remaining pendant arm for [Eu.**L**^{8}] was synthesised similarly, using *N*-(pyridin-2-ylmethyl)ethanamine in place of diethylamine, followed by alkylation, deprotection and complexation in an analogous fashion to Scheme 4.3.

The same titrations as those described for [Eu.**L**^{6}] in buffer solutions were performed on [Eu.**L**^{7}], to test what effect the picolyl groups have on the binding of glyphosate.

The europium emission lifetimes were also recorded at the beginning and end of each titration in H_2O and D_2O so that a *q* value could be calculated.

*Table 4.3 The lifetimes and q value of [Eu.**L**^{7}] and [Eu.**L**^{8}] in H_2O and D_2O at the beginning and end of the glyphosate titrations*

	Lifetime in H_2O (τ_1) (ms)	Lifetime in D_2O (τ_1) (ms)	*q*
[Eu.**L**^{7}]	0.61	0.80	0.2
[Eu.**L**^{7}] + glyphosate	0.65	1.16	0.5
[Eu.**L**^{8}]	0.44	0.64	0.5
[Eu.**L**^{8}] + glyphosate	0.99	1.28	0.0

[j] Both synthesised by S. Shuvaev

The *q* values for both complexes with and without glyphosate are all close to zero. Such behaviour is not wholly unexpected as [Eu.**L**^{6}] also shows *q* values around zero, and the binding around the europium centre has not changed, as the initial complex is nine coordinate.

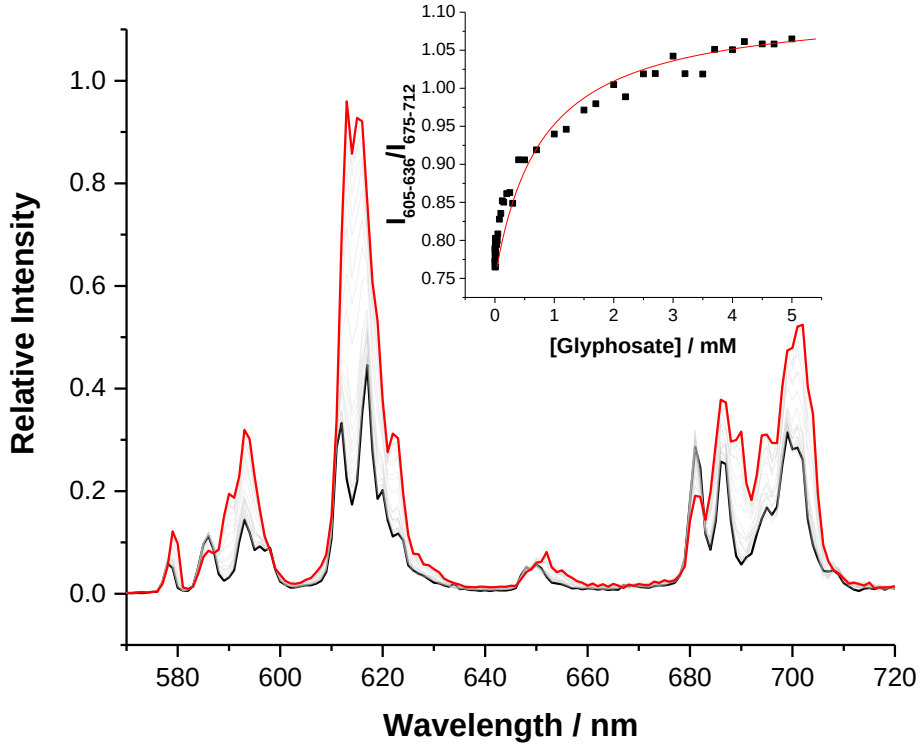

*Figure 4.21 - Changes in the emission spectrum of [Eu.**L**^{7}] (black) (7 μM, 0.1 M NaCl, 0.1 M MES, pH 5.9, 295 K) with increasing concentration of glyphosate, up to 5 mM (red). (Inset) The intensity ratio of ΔJ = 4 / ΔJ = 2 as a function of increasing glyphosate concentration*

An increase in emission intensity and a distinct change in spectral form was observed upon addition of glyphosate to [Eu.**L**^{7}]. The change in spectral form is similar to that of [Eu.**L**^{6}], although not as marked. The binding could also be tracked using the intensity ratio of the two bands in the $\Delta J = 2$ transition, using 602-615 nm / 615-638 nm. What was somewhat unexpected was the large decrease in log*K* compared to [Eu.**L**^{6}]. From the fit of the binding a curve, using non-linear regression analysis an estimated value of 3.11 (±0.01) was obtained, which corresponds to a *K* value a factor of 100 smaller than the tripicolylamine equivalent. Clearly the exchange of two picoylyamine arms for two ethyl groups has a deleterious effect on the binding of glyphosate.

Further experiments were performed to give more information about the binding. For example, the binding of phosphate will give an indication if the picoylyamine groups interact in any way with the phosphate group itself.

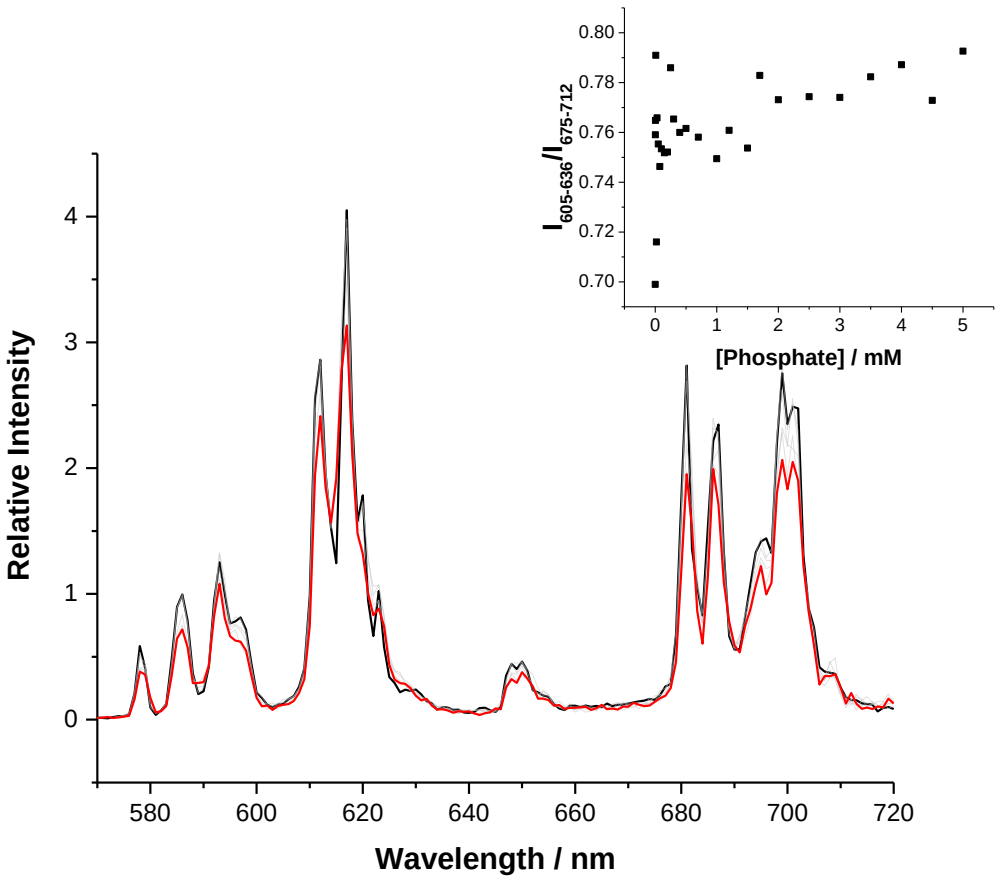

*Figure 4.22 - Changes in the emission spectrum of [Eu.**L**^{7}] (black) (7 μM, 0.1 M NaCl, 0.1 M MES, pH 5.9, 295 K) with increasing concentration of phosphate, up to 5 mM (red). (Inset) The intensity ratio of ΔJ = 2 / ΔJ = 4 as a function of increasing phosphate concentration*

Upon addition of hydrogen phosphate, there is little evidence of binding; only a slight decrease in emission intensity was observed but no discernible change in spectral form. This is highlighted in the intensity ratio at 605-636 nm / 675-712 nm, or the ΔJ = 2 / ΔJ = 4 manifolds. The change in ratio is small, between the values 0.74 to 0.80, particularly when compared to the change in ratio upon addition of glyphosate which increases up to 1.10. Another point to note, is that this is the change upon addition of 5 mM of phosphate, compared to the 0.3-0.5 mM used in glyphosate titrations. Due to the lack of distinct change in ratio with increasing phosphate concentration, it was not possible to fit this to a binding curve to obtain a log$K$ value. These results suggest that at pH 5.9 this complex does not bind phosphate in a significant manner.

However, AMPA is slightly different to phosphate, with a relevant pK_a of 5.36.[209] Hence, at pH 5.9, the second phosphonate oxygen is deprotonated, as in glyphosate, and therefore it may compete in binding to [Eu.**L**^{7}].

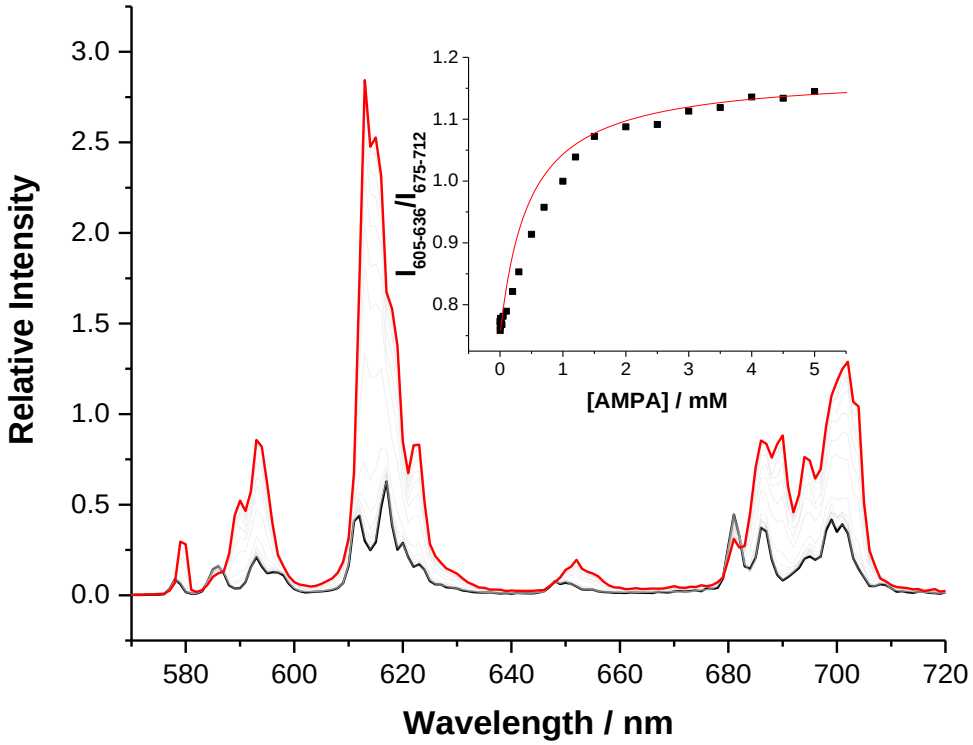

*Figure 4.23 - Changes in the emission of [Eu.**L**^{7}] (black) (10 μM, 0.1 M NaCl, 0.1 M MES, pH 5.9, 295 K) with increasing concentration of AMPA, up to 5 mM (red). (Inset) The intensity ratio of ΔJ = 2 / ΔJ = 4 as a function of increasing AMPA concentration*

When AMPA is added to a sample of [Eu.**L**^{7}] there is an increase in emission intensity and a change in spectral form. The change is form was analogous to that seen with glyphosate, as one would expect. It therefore affords a ratio which can be used to track the binding event, which is assumed to be similar in nature to that of glyphosate. Following the variation of the intensity ratio 605-636 nm / 675-712 nm an apparent log*K* value of 3.35 (±0.02) was found. This value is slightly larger than found for glyphosate; this complex is not selective for the herbicide over its metabolite. Inspection of the fit however, suggests that this value is not perfect, so although it may not bind AMPA better than glyphosate, it is sufficiently close that it will not be possible to detect glyphosate in its presence. Further evidence of the similar overall response comes from looking at the range of ratios which vary from 0.75 to 1.10, very similar to the range obtained upon addition of glyphosate. This titration also suggests that the carboxylate groups are involved in binding to the picolyl groups in [Eu.**L**^{6}], which is why AMPA and glyphosate behave similarly in this system. As hydrogen phosphate itself does not behave in the same manner, it suggests that either the comparative pK_as of AMPA/glyphosate vs phosphate plays a crucial role, or that the nitrogen on the analyte plays an important role in binding to the complexes.

The complex was tested with glufosinate, which showed no change in spectral form or emission intensity, suggesting that it interacts minimally with glufosinate. Glufosinate should therefore not be considered as a competitor for glyphosate with this complex.

N-methyl glyphosate was also tested, which had little effect on the emission spectrum of [Eu.**L**^{7}]. It therefore suggests that the addition of the methyl group disrupts the hydrogen bonding as seen in the DFT models (Section 4.2.3.1), and may also make the analyte too sterically hindered to bind to the metal centre effectively.

[Eu.**L**^{7}] was then tested in different media to see how this would affect the binding capabilities. The first medium to be tested was urine, in which thus far, no complex had been successfully found to work.

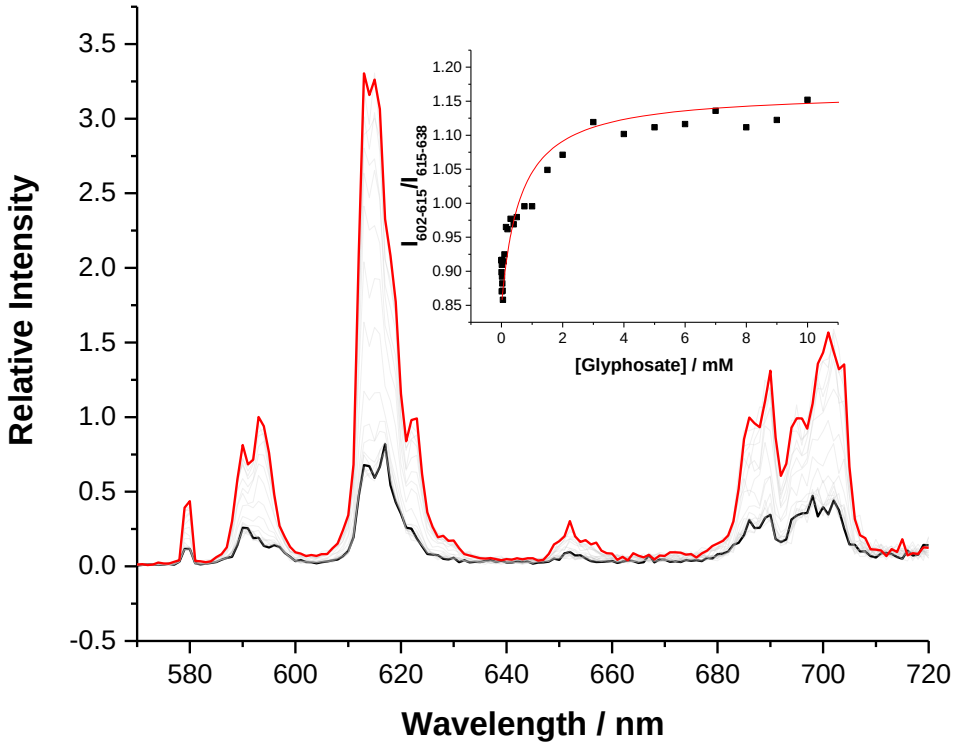

*Figure 4.24 - Changes in the emission spectrum of [Eu.**L**^{7}] in urine (black) (5 μM, 0.1 M NaCl, 0.1 M MES, pH 5.9, 295 K) with increasing concentration of glyphosate, up to 10 mM (red). (Inset) The intensity ratio of 605-615 nm / 615-638 nm as a function of increasing glyphosate concentration*

Surprisingly, a change in spectral form and a remarkable increase in emission intensity were observed in urine. What was even more interesting was the fact that the ratio led to a relatively smooth increase upon incremental additions of glyphosate. An apparent log*K* value of 3.21 (±0.05) was found, very close to the binding constant found for glyphosate in buffer solution. However, an important point to note is that the binding curve in Figure 4.24 is upon addition of 10 mM of glyphosate in total. Most other titrations with glyphosate with this complex usually involve addition up to 0.5 - 1.0

mM. Although this has given by far the best response thus far, the range of concentrations in which glyphosate is likely to be present in urine, is lower than the detection limit with this complex.

The next medium to be tested was aqueous grain extract. For complex [Eu.$\mathbf{L}^{6}$], a response could be tracked in this background, and it is therefore, a similar result should be seen with [Eu.$\mathbf{L}^{7}$].

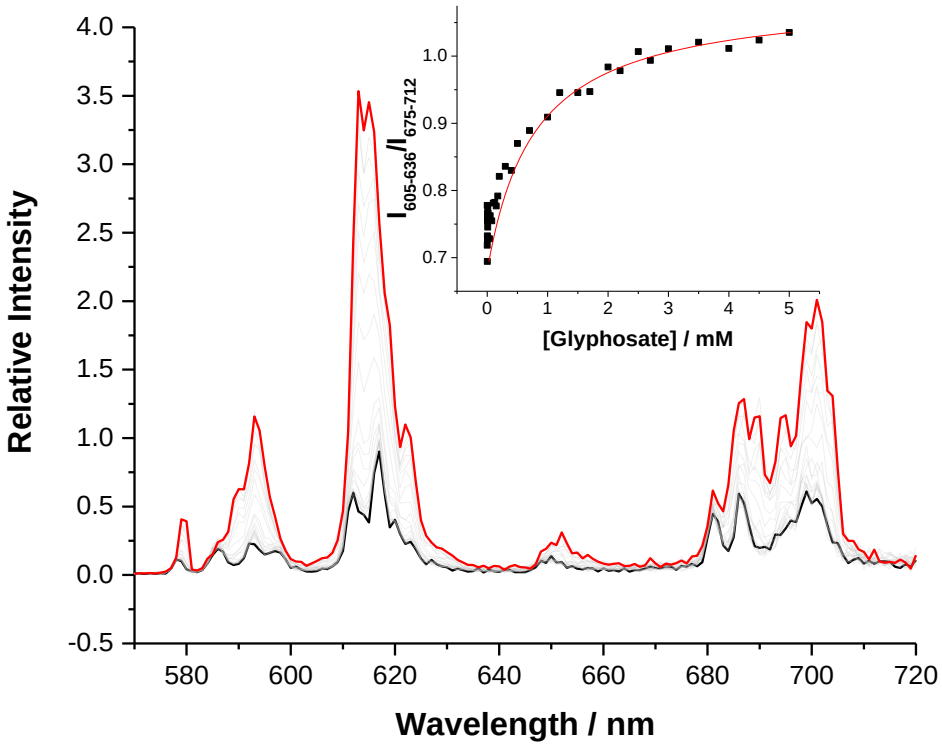

Figure 4.25 - Changes in the emission of [Eu.$\mathbf{L}^{7}$] (black) in grain extract (6 μM, 0.1 M NaCl, 0.1 M MES, pH 5.9, 295 K) with increasing concentration of glyphosate, up to 5 mM (red). (Inset) The intensity ratio of ΔJ = 2 / ΔJ = 4 as a function of increasing glyphosate concentration

As found in urine, there was both an increase in emission intensity and a change in spectral form. The spectral form at the start of this titration in grain extract is similar to that in buffer solution, which may not be expected on comparison with [Eu.$\mathbf{L}^{6}$] in the same medium. The change in spectral form was tracked using the intensity ratio of 605-636 nm / 675-712 nm as a function of increasing glyphosate concentration, to give an estimated log*K* value of 3.11 (±0.01). This is identical to the value in buffer solution suggesting this complex is not affected by other species in grain extract, which is a very useful trait. However, the glyphosate added to get this response is ten times more than that used with [Eu.$\mathbf{L}^{6}$]. This sensitivity issue means that unless the sample volume is pre-concentrated prior to analysis, the concentration this complex can detect is not close to any MRL.

Oats were then tested to check if a similar situation is found in this background, to see the effect this medium has on [Eu.$\mathbf{L}^7$].

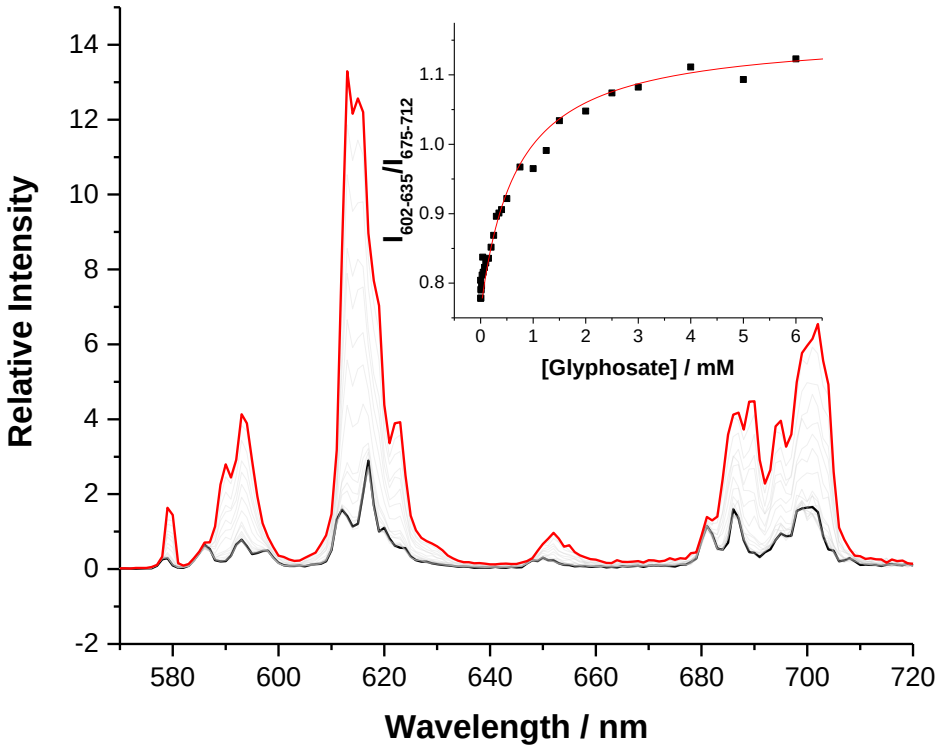

Figure 4.26 - Changes in the emission spectrum of [Eu.$\mathbf{L}^7$] in oat extract (black) (6 μM, 0.1 M NaCl, 0.1 M MES, pH 5.9, 295 K) with increasing concentration of glyphosate, up to 6 mM (red). (Inset) The intensity ratio of ΔJ = 2 / ΔJ = 4 as a function of increasing glyphosate concentration

The spectral form at the beginning of the titration is again not dissimilar to that found in buffer solution, suggesting that the complex doesn't bind anything in oat extract to a significant degree. Furthermore, upon addition of glyphosate, there was an increase in emission intensity and the same change in spectral form as previously seen for this complex. Following the intensity ratio of $\Delta J = 2$ / $\Delta J = 4$ as a function of glyphosate concentration, an apparent log$K$ value of 3.18 (±0.01) was estimated. This is slightly higher than achieved in buffer solution, again suggesting that the complex is somewhat unaffected by the media it is in. However, it retains the same sensitivity issues observed in grain extract.

It is evident that the two ethyl groups have a dramatic impact on the efficacy of the complex to bind glyphosate. The lack of apparent binding at the beginning of titrations or any interference from complex media such as grain or oat extract may be related to the fact that binding to the complex seems to be less efficient. The lower log$K$ values compared to [Eu.$\mathbf{L}^6$] suggests that it may still have the potential to bind to the compounds in grain and oat, but the concentrations of these species is not sufficiently high enough to cause a change in spectral form.

The next complex examined looked at comparing whether both of these picolyl groups are necessary for the binding of glyphosate, or if one is sufficient.

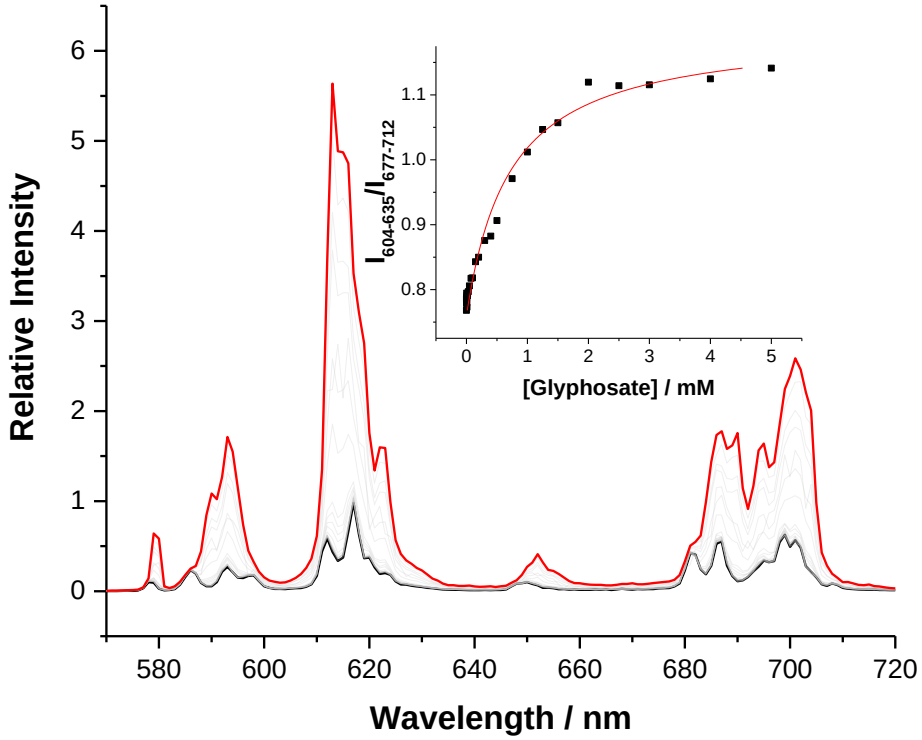

*Figure 4.27 - Changes in the emission spectrum of [Eu.**L**^{8}] (black) (18 μM, 0.1 M NaCl, 0.1 M MES, pH 5.9, 295 K) with increasing concentration of glyphosate, up to 5 mM (red). (Inset) The intensity ratio of 604-635 nm / 677-712 nm as a function of increasing glyphosate concentration*

From initial observations, it is clear that upon addition of glyphosate to [Eu.**L**^{8}], in 0.1 M MES and 0.1 M NaCl, there is an increase in emission intensity and change in spectral form, as is expected from related titrations. The intensity ratio of $\Delta J = 2$ / $\Delta J = 4$ (604-635 nm / 677-712 nm) can be used to follow the binding event, to yield an apparent log*K* value of 3.16 (±0.01), similar to that found for [Eu.**L**^{7}]. The comparatively poor sensitivity compared to [Eu.**L**^{6}] suggests that both picolyl groups are necessary for efficient binding to glyphosate.

Upon addition of phosphate to a buffer solution of [Eu.**L**^{8}], similar results compared to [Eu.**L**^{7}] were obtained, albeit with a greater change in spectral form and emission intensity. However, this increase is not smooth and appears to be two binding events so a log*K* value cannot be extracted. Phosphate clearly interacts with the complex but, at relevant concentrations in most media, the change in the ratio is not large. This behaviour suggests that both picolyl groups interact with phosphate and encourage its binding to the complex, but will not be a major competitor for glyphosate detection with this complex.

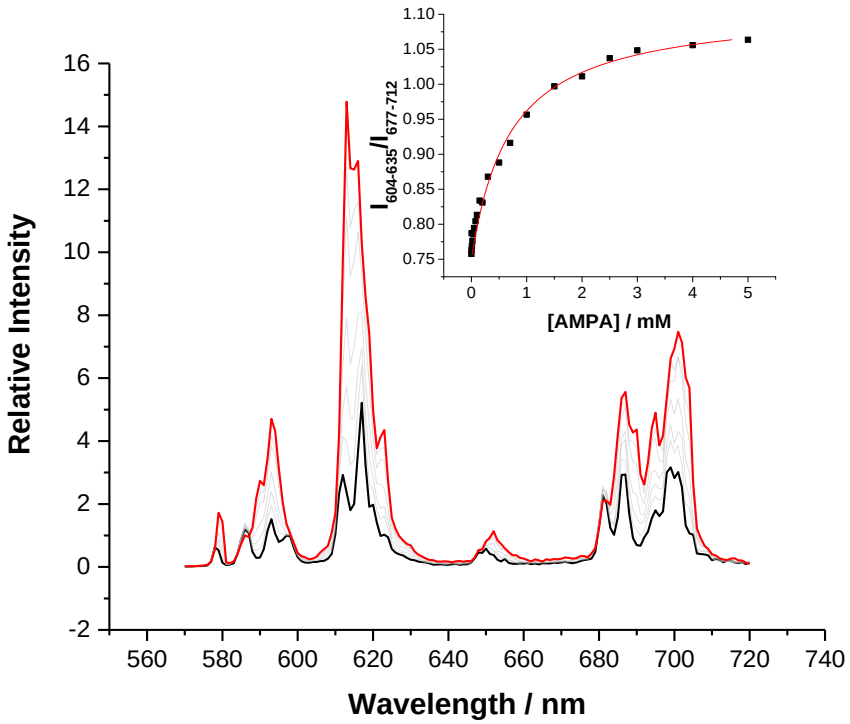

*Figure 4.28 - Changes in the emission spectrum of [Eu.**L**^{8}] (black) (9 μM, 0.1 M NaCl, 0.1 M MES, pH 5.9, 295 K) with increasing concentration of AMPA, up to 5 mM (red). (Inset) The intensity ratio of 604-635 nm / 677-712 nm as a function of increasing AMPA concentration*

As might be expected, the complex does bind to AMPA, with a change in spectral form and emission intensity similar to that seen with glyphosate (Figure 4.28). Again looking at the intensity ratio of $\Delta J = 2$ / $\Delta J = 4$ bands, the binding event can be followed with increasingly concentrations of AMPA, to give an apparent log$K$ value of 3.16 (±0.01). This value is significant, as there is no selectivity between AMPA and glyphosate for either [Eu.**L**^{7}] or [Eu.**L**^{8}]. It therefore hypothesised that the increase in glyphosate binding and its selectivity over AMPA is related to the interactions of the carboxylate group of glyphosate and both picolyl groups. As the binding constant is so similar to that obtained for [Eu.**L**^{7}] as well as [Eu.**L**^{6}] it is consistent with the hypothesis that that AMPA does not interact with the picolyl groups. Moreover, the fact that glyphosate has a higher binding constant for [Eu.**L**^{6}] means that the carboxylate groups must interact favourably with both picolyl groups in the ternary adduct.

Although AMPA binds to [Eu.**L**^{8}], glufosinate is not a competitor for glyphosate with this complex. There was a minor decrease in emission intensity and the change in spectral form is minimal upon addition of glufosinate highlighted by the lack of trend in intensity ratios with increasing concentrations.

To further probe the binding of glyphosate to the complex, titrations with *N*-methyl glyphosate could highlight the interactions of the central nitrogen atom on glyphosate with the complex.

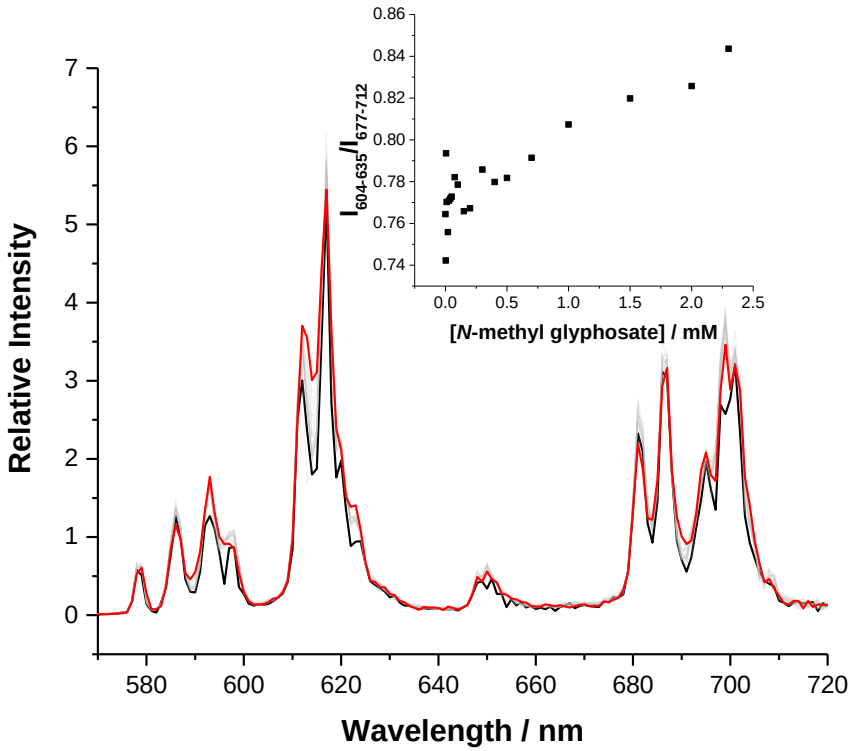

*Figure 4.29 - Changes in the emission spectrum of [Eu.**L**[8]] (black) (8 μM, 0.1 M NaCl, 0.1 M MES, pH 5.9, 295 K) with increasing concentration of N-methyl glyphosate, up to 2.5 mM (red). (Inset) The intensity ratio of 604-635 nm / 677-712 nm as a function of increasing methyl glyphosate concentration*

The spectral change observed upon addition of *N*-methyl glyphosate is very similar to that of phosphate, albeit with a greater increase in emission intensity. The ratio of the two hypersensitive bands shows an increase, but not a smooth one from which a log*K* value could be extracted. This behaviour suggests that the two hydrogens on the amine on glyphosate must be involved in stabilising hydrogen bond interactions (as H-bond donors) to the two picolyl nitrogen acceptors, as seen in the DFT structure, otherwise a binding response similar to that of phosphate would be observed

This complex was then tested in different media to observe how it interacts with potentially competitive species that exist in them. The medium tested first was urine.

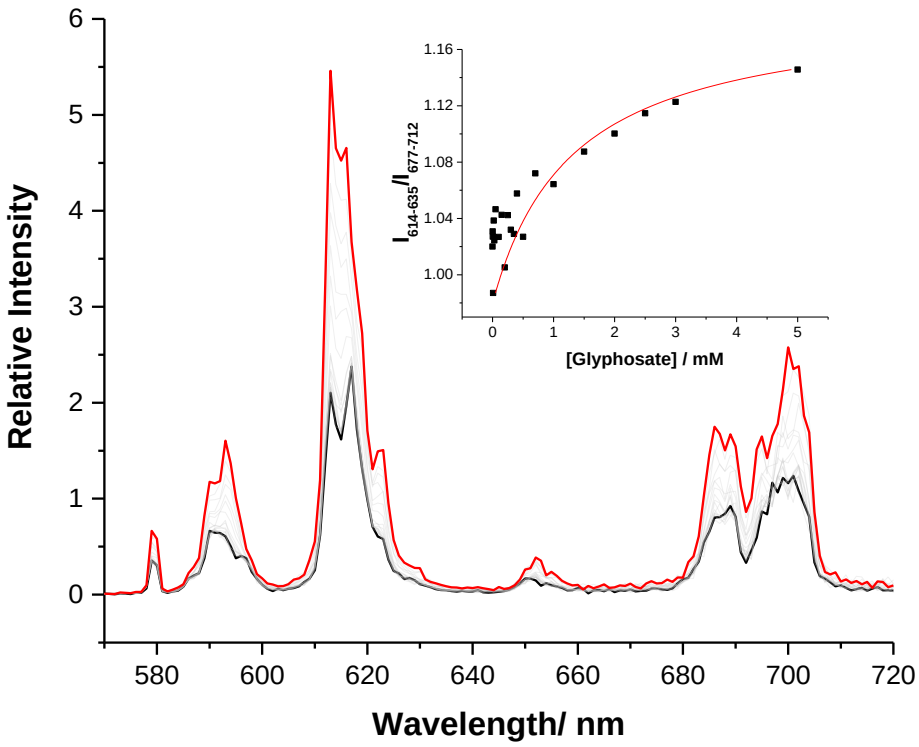

*Figure 4.30 - Changes in the emission spectrum of [Eu.**L**^{8}] (black) in urine (9 μM, 0.1 M NaCl, 0.1 M MES, pH 5.9, 295 K) with increasing concentration of glyphosate, up to5 mM (red). (Inset) The intensity ratio of 604-635 nm / 677-712 nm as a function of increasing glyphosate concentration*

Again, an increase in emission intensity and change in spectral form was observed. However, the increase is not as distinctive as it was with [Eu.**L**^{7}]. This was affirmed by looking at the ratio of $\Delta J = 2$ / $\Delta J = 4$. A binding constant could be estimated using non-linear regression analysis to give an apparent log*K* value of 2.89 (±0.01), lower than that found in buffer and for [Eu.**L**^{7}] in urine. Furthermore, there is a lot of 'scatter' at the beginning of the titration, so even if there was an unnaturally high concentration of glyphosate in urine, the confidence in the value calculated working from this binding constant would be low. This scatter is likely due to a species in urine which bound to the [Eu.**L**^{8}] and is replaced by glyphosate.

Grain extract was then tested, which was predicted to give similar results to that observed with [Eu.**L**^{7}].

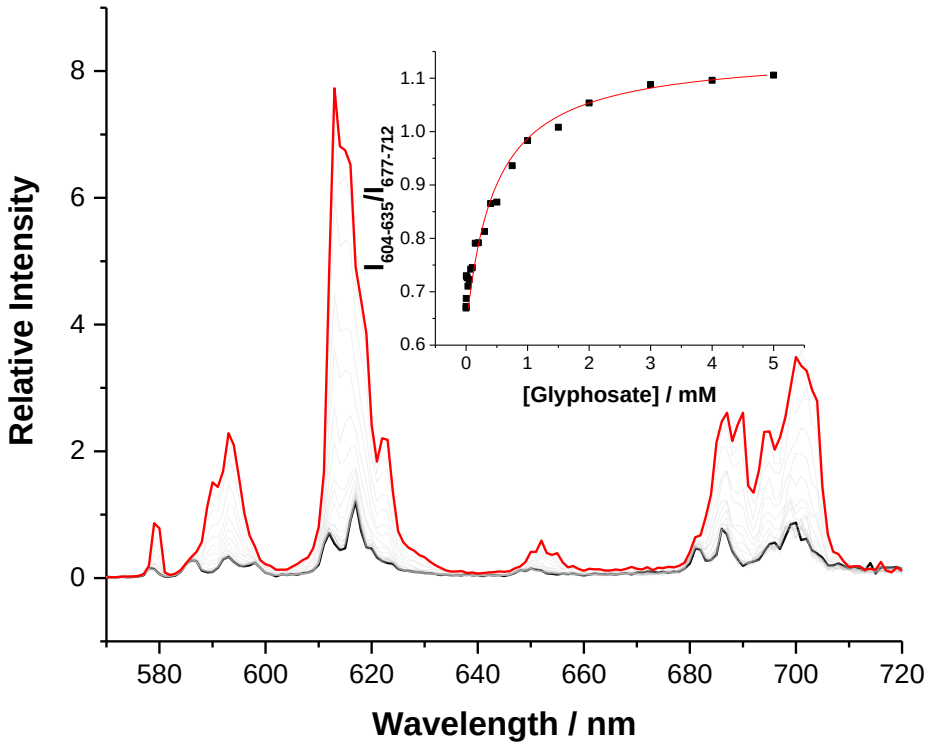

*Figure 4.31 - Changes in the emission spectrum of [Eu.**L**^{8}] (black) in grain extract (18 μM, 0.1 M NaCl, 0.1 M MES, pH 5.9, 295 K) with increasing concentration of glyphosate, up to 5 mM (red). (Inset) The intensity ratio of 604-635 nm / 677-712 nm as a function of increasing glyphosate concentration*

A change in spectral form was observed upon addition of glyphosate in grain extract, and the emission intensity greatly increased (Figure 4.31). The change in spectral form allowed a binding curve to be fitted using non-linear regression analysis of the emission ratio of $\Delta J = 2$ / $\Delta J = 4$, to give an apparent log$K$ value of 3.34 (±0.01). This binding constant is larger than the value found in buffer solution, suggesting that this complex is less sensitive to other species in grain extract compared to [Eu.**L**^{6}]. It is also slightly larger than the value found for [Eu.**L**^{7}] in grain, indicating that this complex in marginally better behaved, but not with sufficiently avidity to allow its use in grains with levels of glyphosate close to MRLs in grains as set by the EU.

A titration in oat extract is expected to give very similar results to that found in grain extract, as the complex thus far has behaved in a very similar manner to that of [Eu.**L**^{7}].

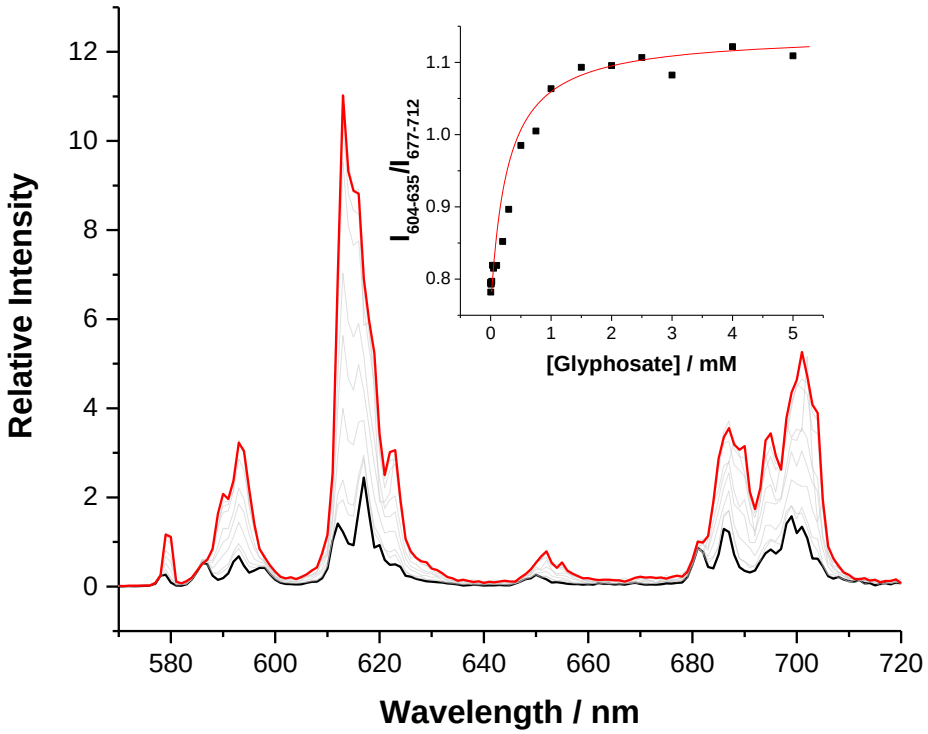

*Figure 4.32 - Changes in the emission of [Eu.**L**^{8}] (black) in oat extract (9 μM, 0.1 M NaCl, 0.1 M MES, pH 5.9, 295 K) with increasing concentration of glyphosate, up to 5 mM (red). (Inset) The intensity ratio of 604-635 nm / 677-712 nm as a function of increasing glyphosate concentration*

The changes in emission intensity and the spectral form were almost identical to those seen in buffer solution, with an apparent log*K* value of 3.57 (±0.04) estimated. This value is greater than that found in buffer solution, which was 3.16 (±0.01). However, to achieve these changes, a high concentration of glyphosate is needs to be added to the titration, and therefore, this complex would not be useful at detecting at or close to expected levels of glyphosate in oat. Looking at the inset graph in Figure 4.32, there is little to no noise at the beginning of the titration, which is uncommon for complexes in this medium. This may be due structural difference of the complexes means it no longer binds strongly to these species in these backgrounds so they are not in sufficiently high enough concentration to allow a notable change in spectral form, or for a competitive displacement process.

4.4 Further Modification of the Tripicolylamine Arm Utilising 1,2,3 - triazole

Following the observation of the importance of the two picolyl groups, another way the complex can be altered structurally is through the insertion of a 1,2,3-triazole, replacing the pyridine ring closest to the heart of the complex.

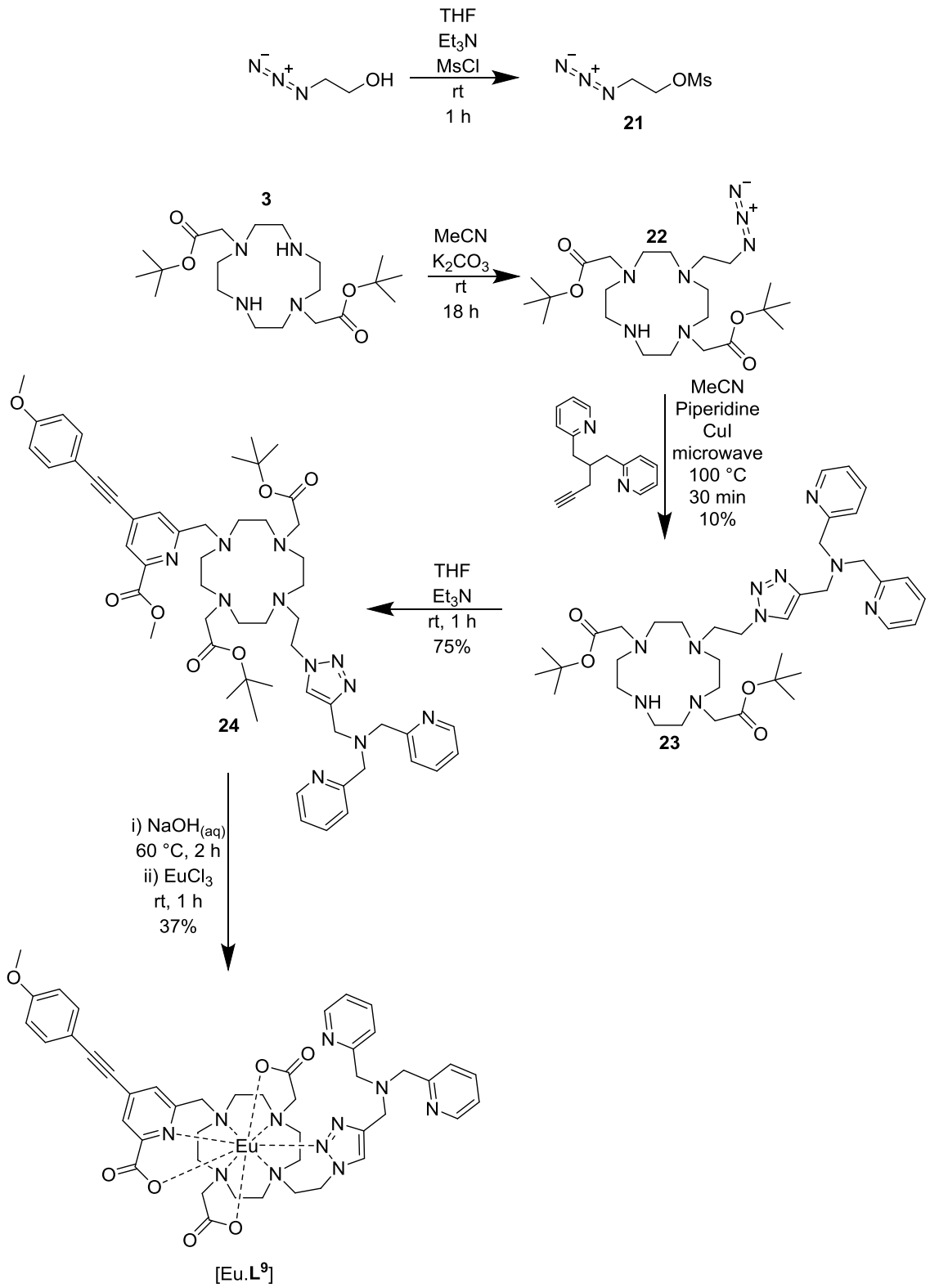

*Figure 4.33 - The synthetic route to [Eu.**L**^{9}]*[k]

The synthesis followed Scheme 2.1 up to the preparation of compound **3**. The mesylate, **21**, is formed through reaction of 2-azidoethanol with mesyl chloride, which is alkylated onto cyclen (**22**). The pendant arm is synthesis through 'click chemistry' with *N*,*N*-

[k] Synthesised by S. Shuvaev

bis(pyridin-2-ylmethyl)prop-2-yn-1-amine, to form the triazole moiety (**23**). The chromophore, **17**, is alkylated onto the final amine on the cyclen ring, **24**, before deprotection and complexation to give [Eu.**L**^{9}]. The lifetime of the complex was recorded in H_2O and D_2O at the beginning and the end of the titration with glyphosate.

*Table 4.4 - The lifetimes and q values of [Eu.**L**^{9}] with and without glyphosate*

	Lifetime in H_2O (τ_1) (ms)	Lifetime in D_2O (τ_1) (ms)	*q*
[Eu.**L**^{9}]	0.61	0.80	0.2
[Eu.**L**^{9}] + glyphosate	0.65	1.16	0.5

In both cases, the *q* values were close to zero, suggesting no inner sphere water is bound. This is perhaps not unexpected as the complex is already 9-coordinate and therefore there would be no space for the water, as seen with previous complexes in this chapter.

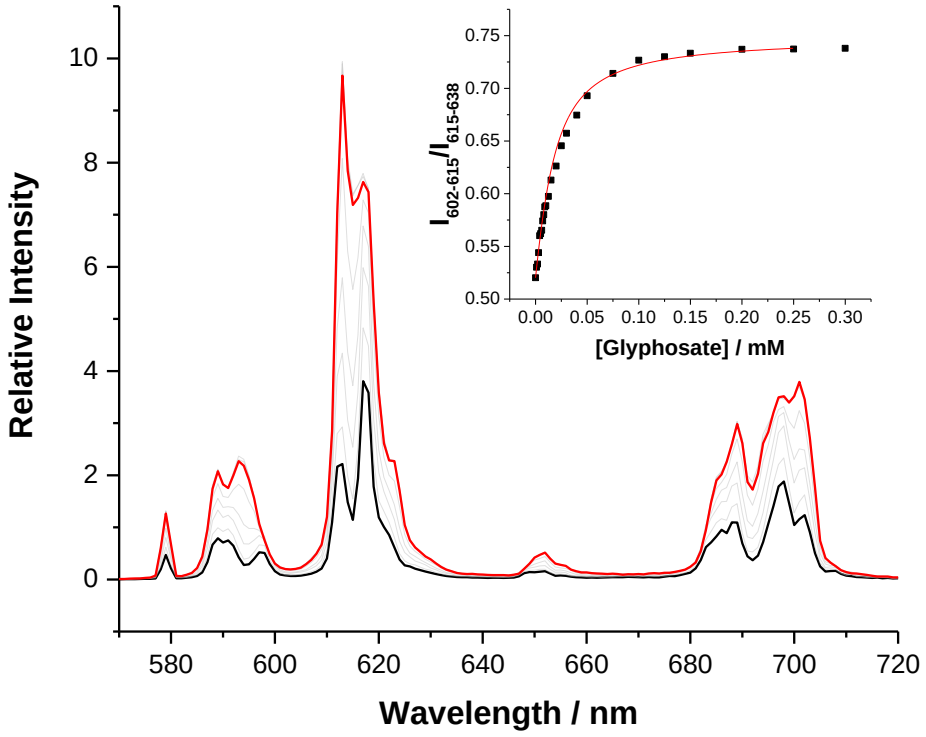

*Figure 4.34 - Changes in the emission spectrum of [Eu.**L**^{9}] (black) (21μM, 0.1 M NaCl, 0.1 M MES, pH 5.9, 295 K) with increasing glyphosate concentration, up to 0.3 mM (red). (Inset) The intensity ratio of 602-615 nm / 615-638 nm as a function of increasing glyphosate concentration*

The complex bound glyphosate with an increase in emission intensity and a change in spectral form, similar to those observed in [Eu.**L**^{6}]. The binding event could be followed through a variety of ratios, and the one chosen for this complex was 602-615 nm / 615-

638 nm. Fitting this intensity ratio to a 1:1 binding curve using non-linear regression analysis gave an apparent log*K* value of 4.92 (±0.01). This value is in between the log*K* value calculated for [Eu.**L**^{6}], and [Eu.**L**^{7}] and [Eu.**L**^{8}]. This information is consistent with notion that the tripicolylamine arm plays a key role in the binding of glyphosate, but the tertiary aliphatic amine that binds directly to the metal centre is less important than the remaining two pyridine groups. Furthermore, experiments which looked at the rate in which glyphosate binds were undertaken. The binding of glyphosate was seen instantaneously in the change in spectral form. Therefore, although this complex had a slightly less favourable log*K* value, the lack of needing to wait for equilibration gives [Eu.**L**^{9}] an advantage.

Following the confirmation of the detection of glyphosate, separate studies were carried out, with phosphate, AMPA and glufosinate.

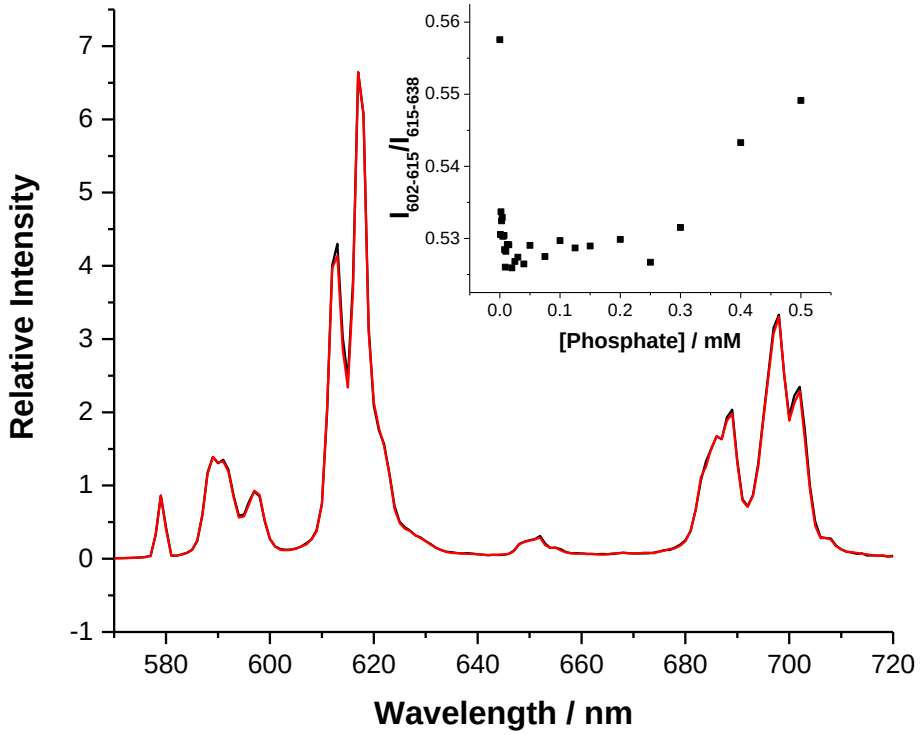

*Figure 4.35 - The emission spectrum of [Eu.**L**^{9}] (black) (12 μM, 0.1 M NaCl, 0.1 M MES, pH 5.9, 295 K) with 0.5 mM of phosphate (red). (Inset) The intensity ratio of 602-615 nm / 615-638 nm as a function of increasing phosphate concentration*

[Eu.**L**^{9}] was the first complex tested which was not affected by the addition of phosphate. There was no change in spectral form or emission intensity, and the ratio used previously in the detection of glyphosate showed no correlation with phosphate concentration. This is the first complex in this study which the decision to maintain the pH at 5.9 has been effective, as phosphate does not bind, unless the pH is changed to 8.0 which deprotonates the second phosphate oxygen. This is another very desirable quality

of this complex as it is expected that inorganic phosphate would be one of the main competitors.

However, AMPA has bound in this set of compounds, each with a log*K* value of around three. Following the most promising result with phosphate, the complex was titrated with AMPA.

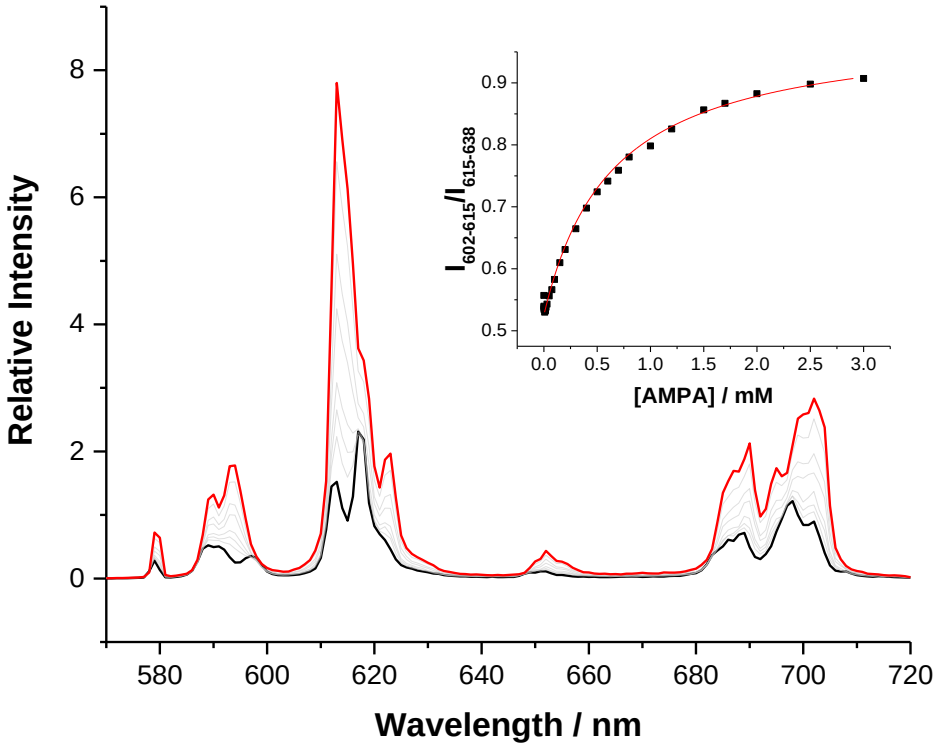

*Figure 4.36 - Changes in the emission spectrum of [Eu.**L**^{9}] (black) (8 μM, 0.1 M NaCl, 0.1 M MES, pH 5.9, 295 K) with increasing AMPA concentrations, up to 3 mM (red). (Inset) The intensity ratio of 602-615 nm / 615-638 nm as a function of increasing AMPA concentration*

Following addition of AMPA, a change in spectral form and emission intensity was found. Following the ratio of the two bands in the $\Delta J = 2$ manifold, an apparent log*K* value of 3.20 (±0.01) was obtained, which again is similar to the previous three complexes. This is significantly smaller than the value obtained with glyphosate, but still has the potential to interfere with the ratio used in glyphosate binding.

As expected, glufosinate does not bind to the complex in the same way as glyphosate, as highlighted by the lack of overall change in spectral form and a lack of distinct change in emission intensity. Again, glufosinate is not a competitor for glyphosate in this system. The same can also be said for *N*-methyl glyphosate, which also showed no change in spectral form or emission intensity.

The complex was then tested in more complex media. The first was urine, in which the complex [Eu.**L**^{6}] was unsuccessful in positively detecting glyphosate. The change in

spectral form for [Eu.$\mathbf{L}^{9}$] showed only a vague correlation, which was not sufficient to determine a binding constant. The increase in emission intensity was also small indicating that this complex does not work well in urine, perhaps having already bound to a species that exists in urine which competes with glyphosate in binding to [Eu.$\mathbf{L}^{9}$].

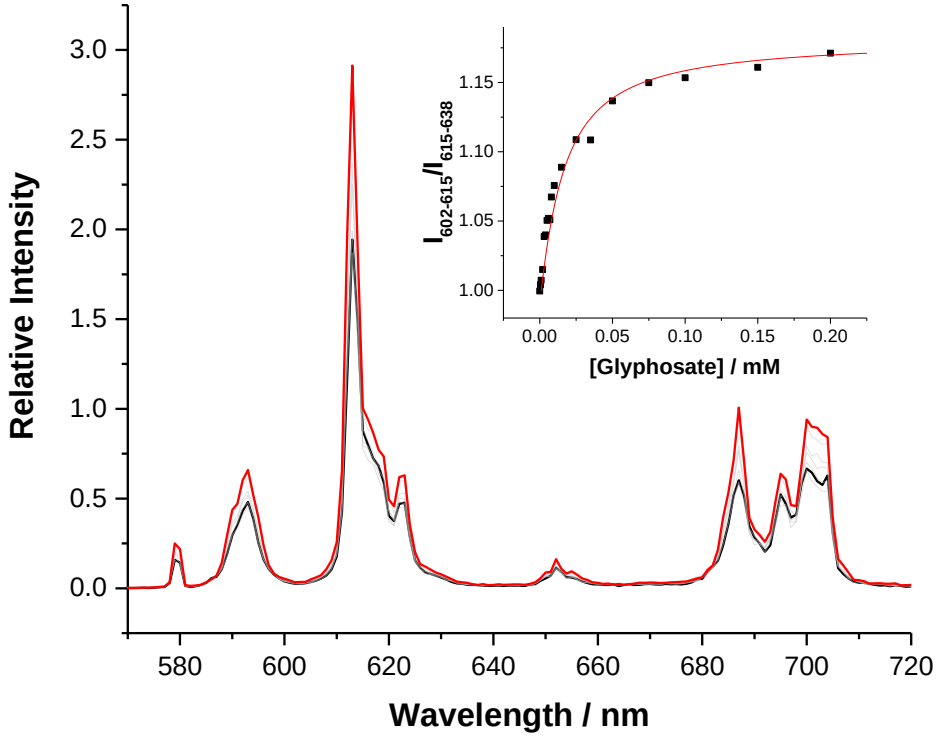

Figure 4.37 - Changes in the emission spectrum of [Eu.$\boldsymbol{L}^{9}$] in oat extract (black) (9 μM, 0.1 M NaCl, 0.1 M MES, pH 5.9, 295 K) with increasing glyphosate concentration, up to 0.2 mM (red). (Inset) The intensity ratio of 602-615 nm /615-638 nm as a function of increasing glyphosate concentration

At the beginning of the titration in aqueous oat extract solution, the spectral form was notably different compared to that at the start of the titration in aqueous buffer. This behaviour suggests that there is a species in oats which binds to the complex to causes this change in spectral form. Upon addition of glyphosate, an increase in emission intensity was observed, although this change is not as large as others observed upon addition of glyphosate with [Eu.$\mathbf{L}^{9}$]. Furthermore, only a slight change in the spectral form was noted in the $\Delta J = 2$ manifold, and this can be tracked using the ratio 602-615 nm / 615-638 nm. When plotted as a function against increasing glyphosate concentration, it yields a binding curve which can be fitted using non-linear regression analysis to give an apparently log$K$ value of 4.88 (±0.02). This is marginally smaller than the log$K$ value achieved in buffer solution, i.e., this medium does little to affect the binding of glyphosate. Another point to note is the lack of noise at low concentrations of glyphosate as seen inset in Figure 4.37. It suggests that whichever species causes the

change in spectral form compared to buffer solution does little to affect the binding of glyphosate.

After positive results in oat extract, the complex was then tested in grain extract. Again looking back at [Eu.$\mathbf{L}^{6}$], it may be expected that the complex will have a similar binding constant to that found in oats.

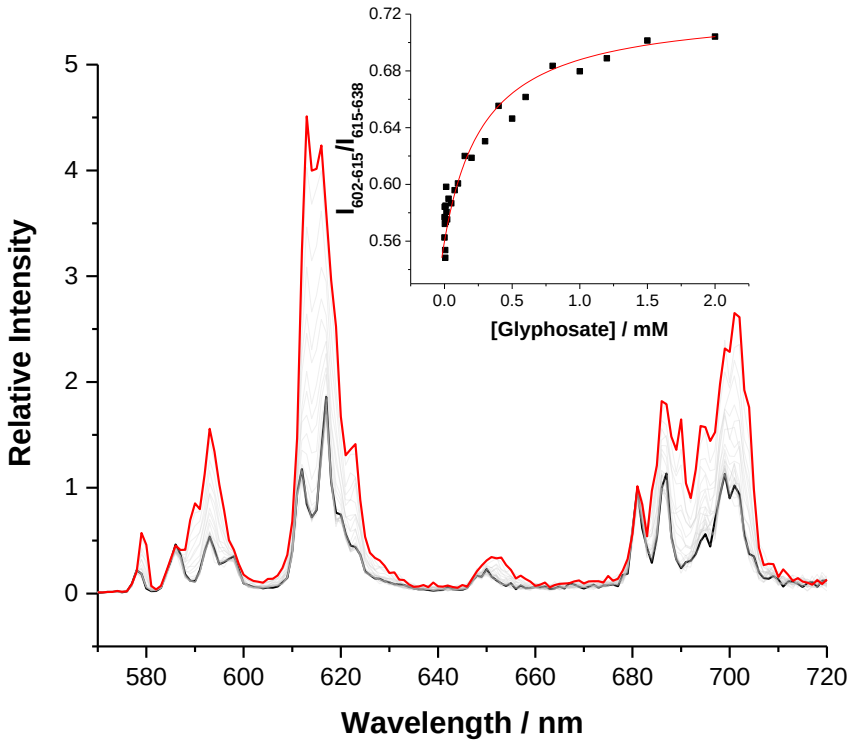

Figure 4.38 - Changes in the emission spectrum of [Eu.$\mathbf{L}^{9}$] in grain extract (black) (10 μM, 0.1 M NaCl, 0.1 M MES, pH 5.9, 295 K) with increasing glyphosate concentration, up to 2 mM (red). (Inset) The intensity ratio of 602-615 nm / 615-638 nm as a function of increasing glyphosate concentration

A large increase in emission intensity was evident, with distinct and definite changes in almost all transitions. The binding event was tracked following the changes in the ΔJ = 2 manifold, with the intensity ratio of 602-615 nm / 615-638 nm giving an apparent log$K$ value of 3.54 (±0.01). This is small compared to the log$K$ value of [Eu.$\mathbf{L}^{6}$] as well as this complex in buffered water and in oats.

This behaviour suggests that something that is present in wheat grain solution, which is not present in oat extract, interferes with the binding of glyphosate to decrease the log$K$ value by almost 100 fold. As the initial spectral form is similar to that observed in buffer solution, it suggests that the species which interferes does not bind to the complex in a similar manner to glyphosate. Therefore, this complex would be suitable for the detection of glyphosate in oats, but not grains. As such, if a sensor which could

be used in a wide range of media was desired, this complex may not be the best choice, although further tests should be done in a number of different samples to confirm this.

Thus far, four complexes have been tested to see if they bind to glyphosate, as well as a number of other competitors. The complexes have also been tested to investigate if they are capable of detecting glyphosate in a range of media.

Table 4.5 - The logK values of the complexes with analytes and glyphosate in a range of media (295 K, pH 5.9, 0.1 M NaCl, 0.1 M MES)[l]

	Glyphosate				Phosphate	AMPA
	Purite Water	Urine	Oat Extract	Grain extract		
[Eu.**L**^{6}]	5.36 (±0.02)	-	4.77 (±0.01)	4.42 (±0.02)	4.35 (±0.01)	3.30 (±0.01)
[Eu.**L**^{7}]	3.11 (±0.01)	3.21 (±0.05)	3.18 (±0.01)	3.11 (±0.01)	-	3.35 (±0.02)
[Eu.**L**^{8}]	3.16 (±0.01)	2.89 (±0.01)	3.57 (±0.04)	3.34 (±0.01)	-	3.16 (±0.01)
[Eu.**L**^{9}]	4.92 (±0.01)	-	4.88 (±0.02)	3.54 (±0.01)	-	3.20 (±0.01)

[l] Errors given represent statistical error on the fit

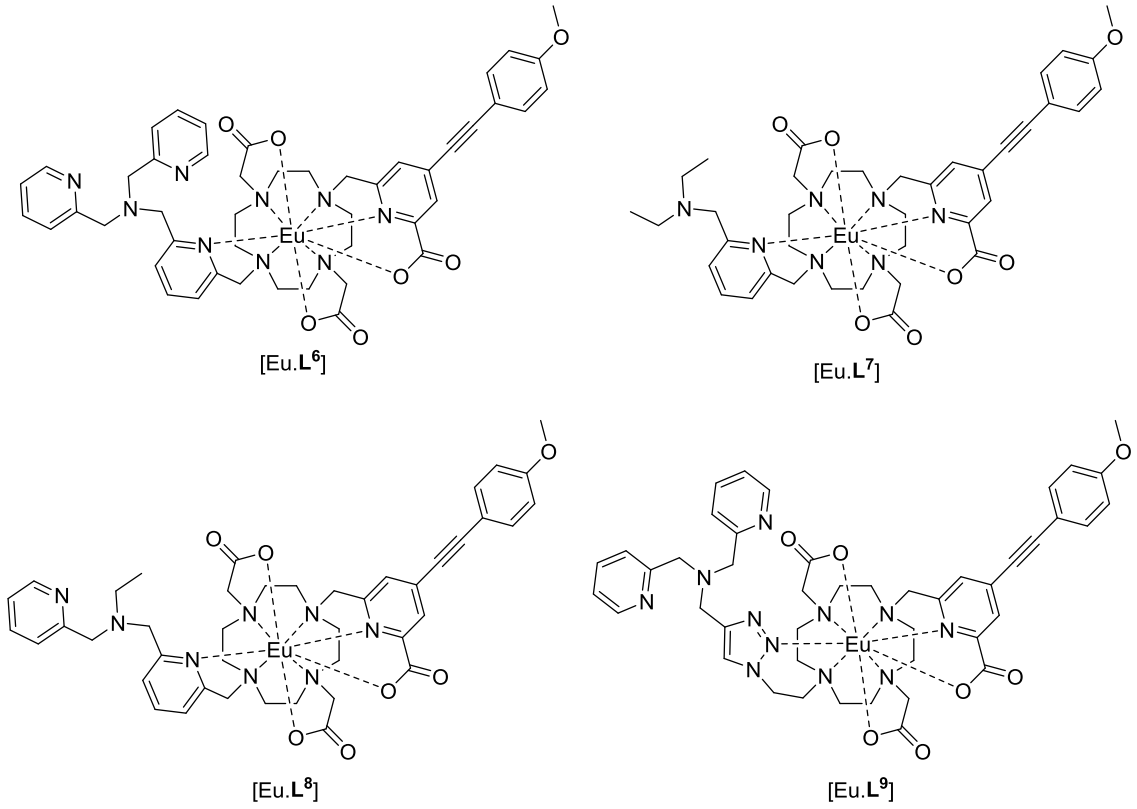

*Figure 4.39 - The structures of [Eu.**L**$^{6-9}$]*

The complex, [Eu.**L**^{6}] gives the highest log*K* value for glyphosate. However, phosphate and AMPA also bind to the complex, albeit slightly more weakly. The reason why phosphate only binds to [Eu.**L**^{6}], and seemingly no other complexes may be due to the poorer binding abilities of [Eu.**L**$^{7-8}$] in particular. A slight response can be seen with these complexes, but nothing of any significance. The electrostatic interaction of phosphate is smaller than that of glyphosate or AMPA, due to the titrations being performed at 5.9 may also contribute to the lack of binding. Furthermore, the complex performs well in both oat and wheat extract, but not in urine. The two complexes which do give well-defined curves in urine, do so with too low an affinity to detect glyphosate in the concentration range at which the herbicide has been found in this medium.

4.5 Changing the Charge

The final complex synthesised also includes the tripicolylamine moiety, as this entity is clearly important in the binding event of glyphosate. The last alteration was to modify the chromophore itself. By removing the carboxylate group at the 6-position of the pyridine group, the coordination environment around the europium centre was varied, as well as changing the overall charge of the complex.

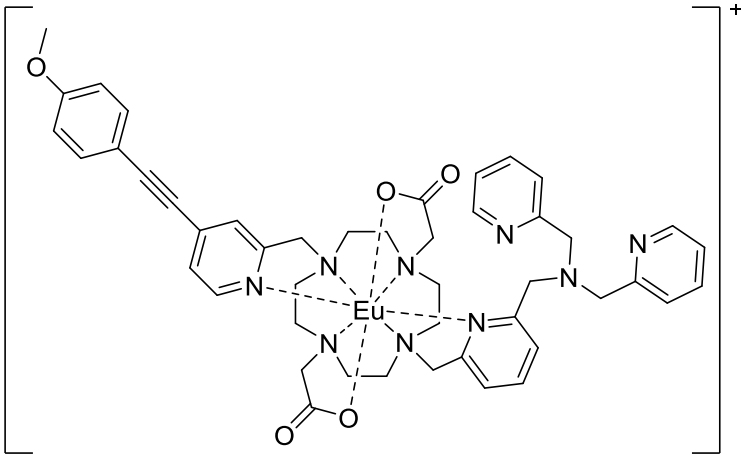

*Figure 4.40[m] - The structure of [Eu.**L**[10]]$^+$*

Synthesis of the conjugated chromophore began by coupling commercially available (4-bromopyridin-2-yl)methanol and 4-ethynylanisole in THF.[210] The alcohol was then converted into the mesylate ester using mesyl chloride, before an alkylation reaction which formed the C-N bond to the 12-N_4 cyclen ring, following the analogous synthesis in Scheme 4.3.

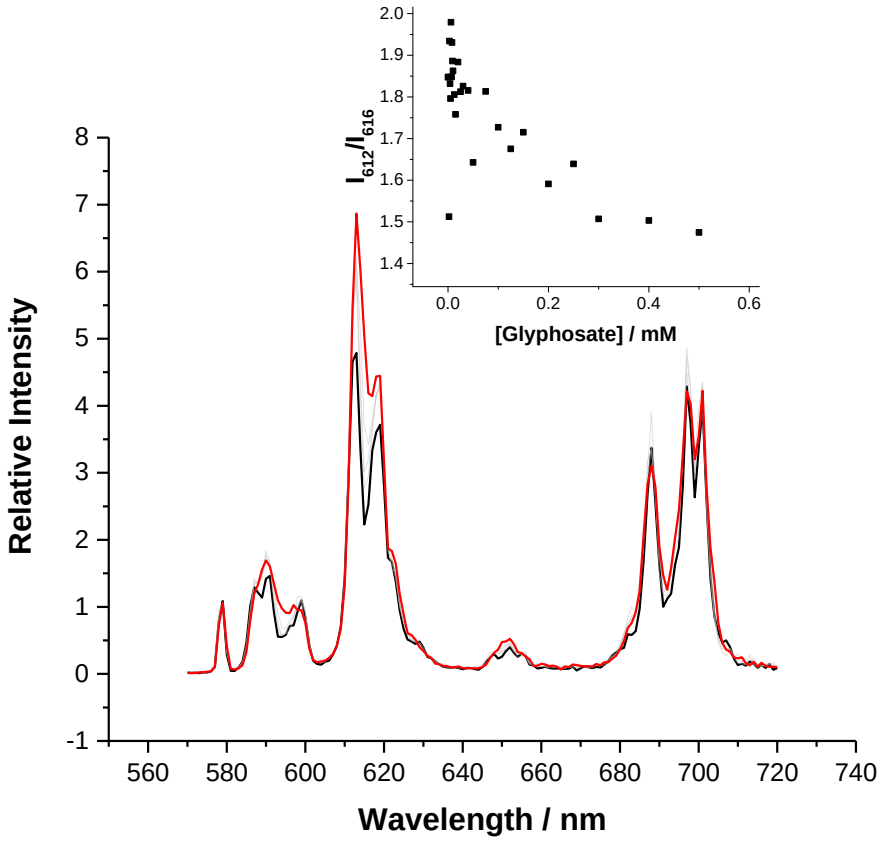

*Figure 4.41 - Changes in the emission spectrum of [Eu.**L**[10]]$^+$ (black) (20 μM, 0.1 M NaCl, 0.1 M MES, pH 5.9, 295 K) with increasing concentration of glyphosate, up to 0.5 mM (red). (Inset) The intensity ratio of 612 nm /616 nm as a function of increasing glyphosate concentration*

[m] Synthesised by S. Shuvaev

A minor increase in emission intensity was observed with little change in spectral form. Finding an intensity ratio to track proved difficult, but 612 nm / 616 nm was used which showed that with increasing glyphosate concentration, there is a decrease in the intensity ratio. This decrease is not smooth, with a lot of scatter, to the extent that fitting a binding curve is impossible.

Furthermore, a month after the synthesis of the complex, a different spectral form was observed when dissolved in buffer, and mass spectrometry confirmed that the complex had started to decompose. Following these poor results, no further experiments were undertaken with this complex.

4.6 pK_a Experiments

When trying to rationalise the difference in binding between these complexes and glyphosate, one key factor to consider is the pK_a values of the complexes themselves. The pK_a of a pyridine N atom is expected to approximately 5.3 which is close to the pH in which the titrations were performed (5.9).[211] It is necessary, therefore, to consider the protonation state of the sp^2 and sp^3 nitrogen atoms that lie close to the europium centre. Hence, studies of the complexes were carried out in which the pK_a values for four of the complexes were determined in 0.1 M NaCl. For [Eu.**L**^{9}], as the triazole is closest to the europium centre it is expected to have a pK_a of approximately 1.

*Table 4.6 - The pK_a of complexes [Eu.**L**$^{6-9}$] (295 K, 0.1 M NaCl)*[n]

	Pyridine pK_a	Amine pK_a
[Eu.**L**^{6}]	5.67 (±0.04)	11.97 (±0.02)
[Eu.**L**^{7}]	7.60 (±0.06)	11.26 (±0.02)
[Eu.**L**^{8}]	6.99 (±0.05)	11.36 (±0.02)
[Eu.**L**^{9}]	< 2.5	11.11 (±0.02)

The lower pK_a value for [Eu.**L**^{9}] could not be determined, having started the pK_a titration at pH 3.5. This is expected due to the low pK_a values of triazole moieties. The pK_a value of [Eu.**L**^{6}], which has the highest affinity for glyphosate, was 5.67 (±0.04) and therefore, is around 80% deprotonated under the pH conditions of the titrations, which were held at 5.9.

[n] Errors given represent statistical error on the fit

The p*K*a's were determined in H_2O at 295 K and the data reported was pH vs the intensity ratio 604-614 nm / 614-633 nm. The curved were fitted using non-linear least-square iterative analysis by Boltzmann using OriginPro 2015 software, producing approximate p*K*a values. The values stated in parenthesis were statistical errors from the fit to the data. Other errors could arise from the pH meter which has an error of ±0.02, or in temperature and therefore the experiments were carried out in a temperature controlled room.

However, upon modification of the tripicolylamine arm, by successively replacing the picolyl groups with ethyl groups, the pK_a value of the pyridine N atom closest to the europium centre was raised to 6.99 (±0.05) for the complex with one ethyl group and 7.60 (±0.06) with two. Hence, in each of these cases, the pyridine N atom will be > 90 and 97% protonated at pH 5.9, strongly affecting the binding capabilities of the complex.

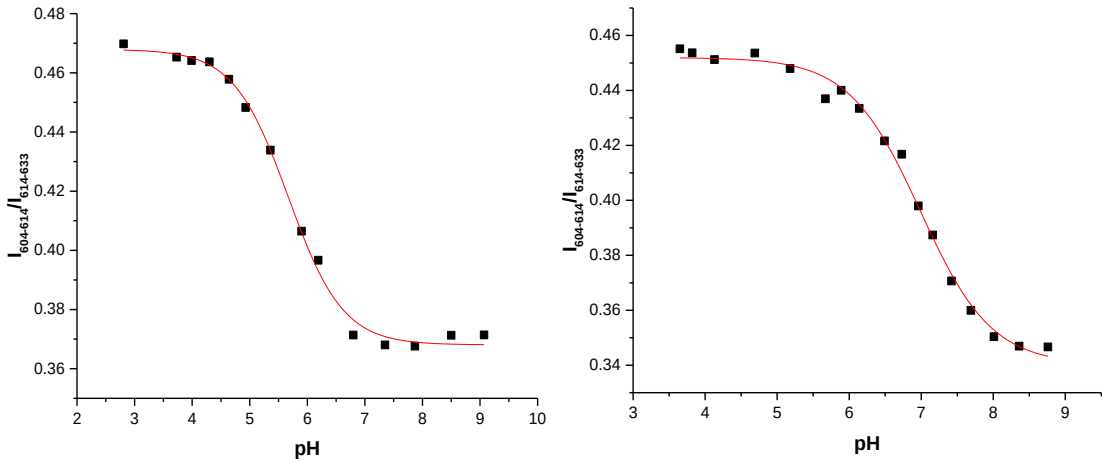

*Figure 4.42 - The variation of the europium emission intensity ratio (604-614 nm / 614-633 nm) with pH for [Eu.**L**^{6}] and [Eu.**L**^{8}] (7 μM, 0.1 M NaCl, 295 K, λ_{ex} = 340 nm), showing the fit to the experimental data points*

Considering the DFT figures (Section 4.2.3.1), the protonation of the pyridine N atom means it cannot act as a hydrogen bond acceptor to the protonated amine in glyphosate.

The pK_a of the central sp^3 hybridised nitrogen atom was expected to be much higher and found to be between 11 and 12 in each case, as expected for this type of aliphatic amine group, when close to another protonated ammonium centre that can form a stabilising hydrogen bond. Around this pH, the change in spectral form is dramatic, suggesting a change in coordination. This could be due to the central aliphatic nitrogen atom coordinating to the complex, perhaps replacing the carboxylate group. By raising the pH of the titration, it might be argued that these 'ethyl' complexes may bind more strongly

to glyphosate. However, under higher pH conditions, phosphate is a major competitor, as its pK_a value is around 7.2.

4.7 Spiked Grain Experiments

The complex which gave the best overall binding results was [Eu.$\mathbf{L}^{\mathbf{6}}$] and it was chosen to assess its performance in a further series of experiments. Following the successful detection of glyphosate in grain extract, a logical step was to use spiked grains with measured amounts of glyphosate and check the known concentration versus the values measured using the europium emission complex. Wheat grain was initially chosen, rather than oat or urine; the complex did not function well in urine, and handling oat extract proved more difficult, but gave similar results.

The wheat grains were spiked using stock solutions of glyphosate which had been diluted down to appropriate concentrations at which this complex would be used. Ten grains were then selected and 0.01 mL of a glyphosate solution was added and left for 24 h in a closed system. The grains absorbed the glyphosate infused water, and the grains were subsequently freeze-dried and then soaked for 24 h. The water was removed by lyophilisation and remade up to a standard 2 mL in a solution of complex of known concentration and 0.1 M MES plus 0.1 M NaCl. A stock solution of the complex was made up for these experiments to minimise the risk that difference could arise from minor fluctuations in complex concentration or pH.

After an initial emission spectrum was measured, further increments of a standard solution of glyphosate were added to the complex solution, to ensure that a change in spectral form ensued. The variation in emission intensity was plotted on the calibration curve in grain extract.

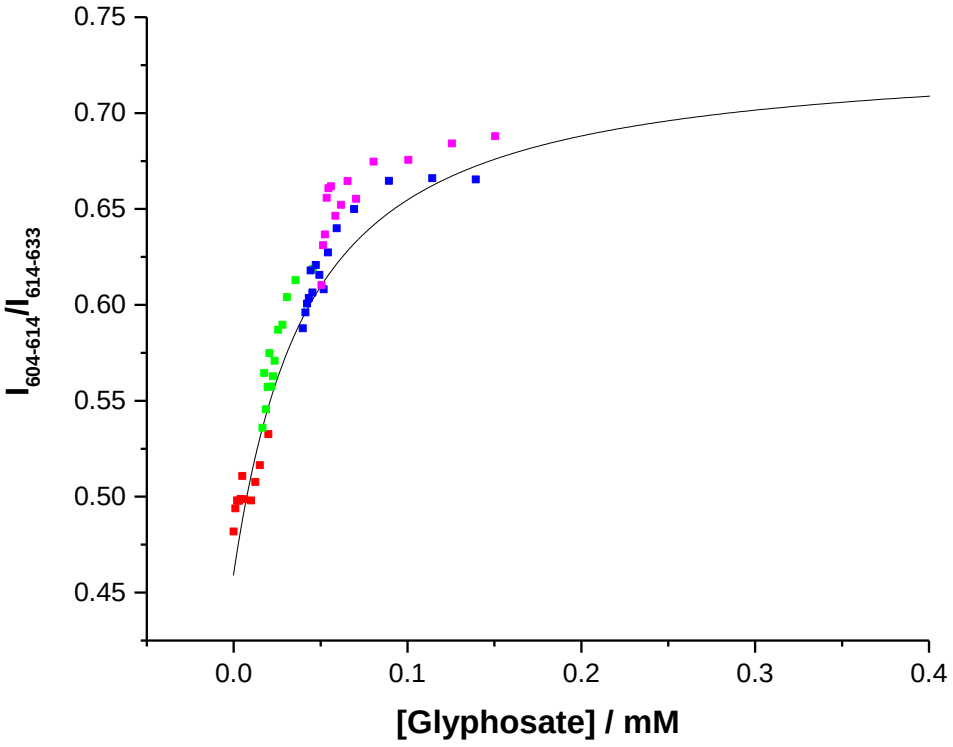

*Figure 4.43 - The calibration curve (solid line) of [Eu.**L**^{6}](7 μM, 0.1 M NaCl, 0.1 M MES, 295 K, pH 5.9) with increasing glyphosate concentrations, with spiked grain at different concentrations at 60 μM (purple), 30 μM (blue), 15 μM (green), 7.5 μM (red)*

What is initially clear from Figure 4.43 is that upon addition of more glyphosate, the curve that is produced in each case (colour coded) do not faithfully follow the initial calibration curve (shown as a solid line), with perhaps the exception of 7.5 μM (Figure 4.43, red). Some remain fairly close, but others notably, such as 60 μM (Figure 4.43, purple), do not stay very close to what might have been expected.

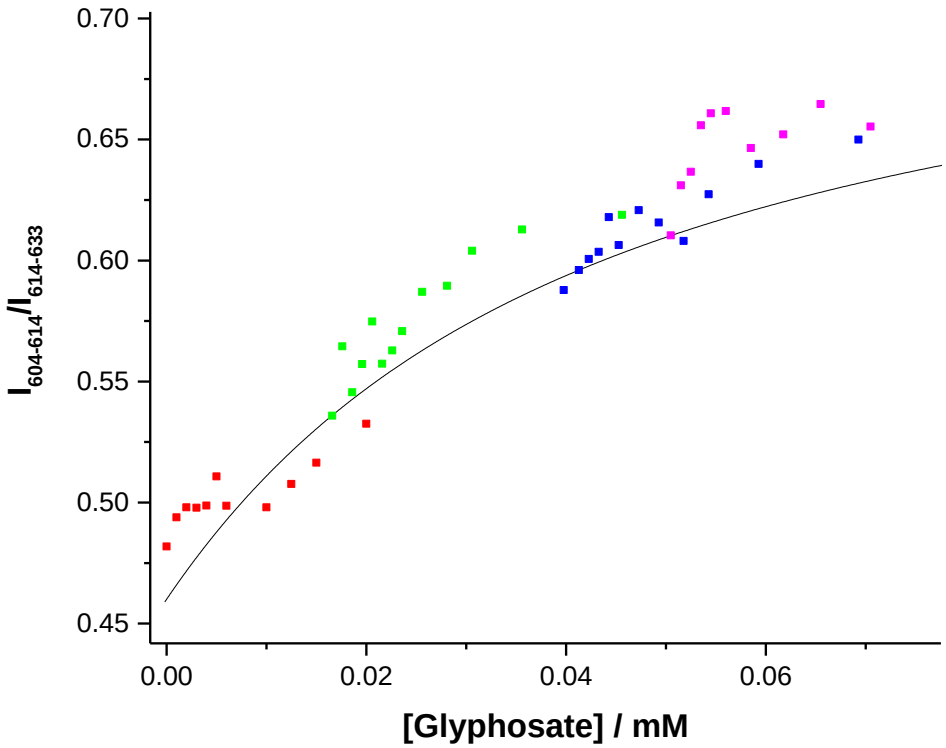

*Figure 4.44 - The calibration curve (solid line) of [Eu.**L**^{6}](7 μM, 0.1 M NaCl, 0.1 M MES, 295 K, pH 5.9) with increasing glyphosate concentrations between 0-0.06 mM, with spiked grain at different concentrations at 60 μM (purple), 30 μM (dark blue), 15 μM (green), 7.5 μM (red)*

However, over the range from zero to 60 micromolar added glyphosate, there is a pseudo-linear section with a 35% modulation of the intensity ratio that could be regarded as a 'working' calibration curve.

*Table 4.7 - The concentration of glyphosate in the spike grains, the calculated values from [Eu.**L**^{6}] calibration curve with the percentage recovered*

Spiked grain	[Glyphosate] added / μM	Calculated [Glyphosate] / μM	Percentage recovered
1	60.0	50.5	84%
2	30.0	39.2	132%
3	15.0	15.6	104%
4	7.5	3.9	52%

For the 1st spike grain, an 84% percentage recovery is not unexpected, as the concentration of glyphosate in the grain itself is unknown, as it is impossible to know whether the grain took up all of the glyphosate when spiking the grains. However, both

grains ‘2’ and ‘3’ gave a percentage recovery of over 100%. The same logic therefore cannot be applied to these. Grain set ‘3’ was only 104% which could potentially be within error, taking into account errors in initial glyphosate curve, the errors in this reading, as well as errors associated with the solution itself. A percentage recovery of 132% on the other hand cannot be justified in the same manner, and is anomalous. Grains ‘4’ give a much lower percentage recovery of approximately 50% which is worryingly low. It suggests either the grains did not soak in all the glyphosate, or the complex is not very good at detecting glyphosate at this level.

Furthermore, the data points in Figure 4.43 mostly occur above the calibration curve determined in grain extract. Therefore, the spiked grain data set was fitted using non-linear regression analysis, to calculate a new binding constant in grain extract.

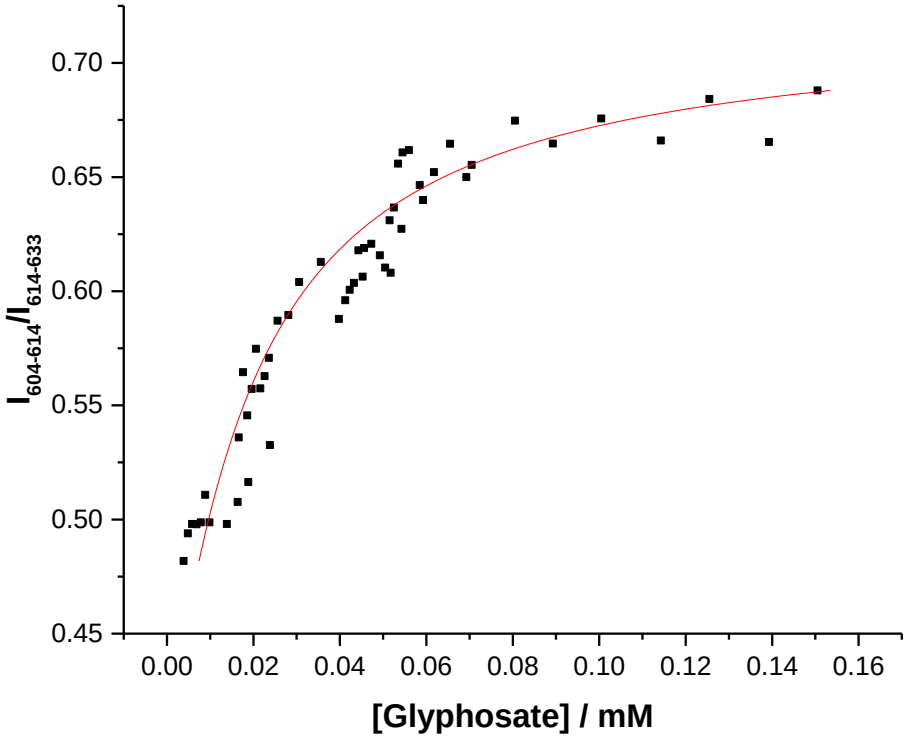

Figure 4.45 - Data from the spiked grains fitted using non-linear regression analysis

Although there is some scatter from the various examples, a binding curve could be fitted to this data in Figure 4.45 to give an apparent log*K* value of 4.97 (±0.01). This is slightly higher than found for the original calibration curve (log*K* = 4.42 (±0.02)), suggesting that the complex binds to glyphosate in grain extract slightly more strongly than originally surmised. However, owing to the difference between the calibration curve originally calculated, and that found using the ‘spiked grain’ data, it suggests that there is still some error in the readings which need to be addressed. Some data points have been removed from those presented above as they appeared anomalous.

A reasonable explanation for the overall behaviour is that grain extract is a very complex medium. Each grain may vary in concentrations of species which can bind to the complex, or interact with it in some way. For example, how close the grain is to germination could affect the concentration of a number of different compounds.

The easiest way to work around this problem is to do these tests on a greater sample size of grains. Clearly, ten grains are not sufficient to get an average background reading, but for this project, the limit was the number of grains available. For future studies, collecting a greater number of grains and concentrating experiments specifically on this complex will increase the number of grains possible to use in each experiment.

4.8 Conclusion and Further Work

A series of five complexes was synthesised, based on a complex that has previously been shown to detect ATP and ADP. The tripicolylamine moiety was shown to be a critical structural feature, as any alteration of it resulted in a lower log*K* value. However, the alteration of one of the pyridines for a triazole group resulted in a complex that did not bind to phosphate at 5.9 and did not require an equilibration period, after addition of glyphosate. The complex [Eu.$\mathbf{L}^{\mathbf{9}}$] also bound strongly to AMPA, resulting in interference of the glyphosate reading. Furthermore, it was not as effective as [Eu.$\mathbf{L}^{\mathbf{6}}$] in oat and grain extract. It was also found that the carboxylate group on the pyridine of the chromophore was necessary for good binding behaviour.

Following the pK_a experiments, it would be interesting to determine the effect of the pH of the titrations on the binding capabilities of the complexes. This could be done through repetition of the titrations of [Eu.$\mathbf{L}^{\mathbf{7\text{-}8}}$] with glyphosate at a higher pH, above the pK_as of both complexes. Although this would likely make phosphate a much more important competitor, it would give an indication as to how much binding occurs through the picolyl groups themselves, or if glyphosate binding is effected by the level of protonation in the complex itself.

Overall, complex [Eu.$\mathbf{L}^{\mathbf{6}}$] was found to be the best complex for binding glyphosate selectively in a range of media, and no structural alteration of this complex was found to improve the log*K* value. It is a ‘switch-on’ sensor, with a number of emission intensity ratios which can be used to track the binding event.

After ascertaining the best complex, further experiments in grain extract were conducted in which the grains were spiked with a known concentration of glyphosate. However,

[Eu.$\mathbf{L}^{6}$] did not perform consistently, with percentage recoveries ranging from 50-134%.

To improve on these results, repeats with a greater number of grains in the sample are required. Furthermore, tests with the Dionex column could be used as a control, to see how much the complex does take up when it is spiked with the glyphosate.

Changes on the chromophore structure may also be possible, for example, the effect of changing a carboxylate for a phosphinate. Furthermore, it is also possible to change the methoxy group on top of the chromophore to a wide range of other substituents. Changing the size of this group or the electronic nature of it affects the absorption wavelength, so care must be taken, but could also potentially avert some of the non-specific binding issues with aromatic species in the extracts.

5. Experimental Details

5.1 General Experimental

5.1.1 Materials

Commercially available reagents and solvents were used without further purification, from Sigma Aldrich, Fischer Scientific or Fluorochem. The exception to this was the recrystallisation of *N*-bromosuccinimide (NBS). NBS (10 g) was dissolved in water (100 mL) and heated to just below boiling until a clear solution was formed. It was then placed in an ice bath for 3 h. The white solid that precipitated out was collected by filtration and dried under vacuum. m.p. 176-178 ˚C (lit.[212] 174 ˚C).

5.1.2 LC analysis

The river water and 'spiked' glyphosate samples were run through a Dionex LC column at 308 K. The column was an IonPac AS18 (2mm) with an ASRS 300 (2mm) suppressor. The ECD detector was an ICS series ECD and the UV/vis detector was an ICS series VWD. The eluent used throughout was aqueous KOH (30 mM) at a flow rate of 0.32 mL/min. This was run by the Durham University Geography Department.

5.1.3 HPLC analysis

Preparative HPLC was performed at 298 K using a Shimadzu system consisting of a Degassing Unit (DGU-20A_{5R}), a Prominence Preparative Liquid Chromatograph (LC-20AP), a Prominence UV/Vis Detector (SPD-20A) and a Communications Bus Module (CBM-20A). An XBridge C18 OBD 19 x 100 mm, i.d. 5 µM column was used, with a flow rate of 17 mL/min. Fractions were collected by hand. The solvent system was H_2O and MeOH + 0.1% formic acid or H_2O and MeCN (gradient elution see Table 5.1, Table 5.2 and Table 5.3). The UV detector was set at 336 nm and fraction collection was performed manually.

Table 5.1 - HPLC conditions for Method A

Step	Time / min	Flow / mL min^{-1}	%MeOH (+0.1% FA)	%H_2O (+0.1%) FA
0	0	17	10	90
1	0.7	17	10	90
2	11	17	95	5
3	14	17	95	5
4	14.5	17	10	90
5	16.5	17	10	90

Table 5.2 - HPLC conditions for Method B

Step	Time / min	Flow / mL min^{-1}	%MeCN	%H_2O
0	0	17	10	90
1	3	17	10	90
2	13	17	50	50
3	15	17	50	50
4	18	17	10	90
5	20	17	10	90

Table 5.3 - HPLC conditions for Method C

Step	Time / min	Flow / mL min^{-1}	%MeCN	%H_2O
0	0	17	10	90
1	3	17	10	90
2	13	17	100	0
3	15	17	100	0
4	18	17	10	90
5	20	17	10	90

Chiral HPLC was carried out at 290 K on a Perkin Elmer Series 200 system consisting of a Perkin Elmer series 200 pump, Perkin Elmer 200 auto-sampler and Perkin Elmer series 200 UV/vis detector. A CHIRALPAK-IC 250 × 4.6 mm column was used, with a flow rate of 1 mL/min for analytic, and 250 x 10 mm, 5μm semi-prepatory column with a flow rate of 4.4 mL/min. A solvent system of hexane:DCM:etheanol (65:30:5) with 0.1 % DEA was used. The UV detector was set at 260 nm. Fraction collection was performed manually.

5.1.4 Analytical Methods

NMR spectra were recorded on Varian Mercury-400 (^{1}H 399.945 MHz and ^{13}C 100.566 MHz) at 298 K or an Appleby VNMRS-600 (^{1}H 599.832 MHz and ^{13}C 150.828 MHz) for 2D experiments. Spectra were recorded in commercially available deuterated solvents from Apollo Scientific and Cambridge Isotope Laboratories. ^{13}C and ^{1}H chemical shift values are quoted in ppm relative to trimethylsilane and all coupling constants are given in Hz. Abbreviations when quoting NMR data are as follows: singlet (s), doublet (d), triplet (t), quartet (q), multiplet (m), broad (br).

Electrospray mass spectra were obtained on a TQD mass spectrometer equipped with an Acquity UPLC, an electrospray ion source and an Acquity photodiode array detector (Waters Ltd, UK). Methanol or acetonitrile were used as the carrier solvent. For LC-MS analyses a 2.1 x 100 mm 1.7 micron Acquity UPLC BEH C18 column was used. LC-MS analyses were performed on a Waters system comprising a 3100 Mass Detector and a 2998 Photodiode array detector.

Accurate masses were recorded on a QTOF Premier mass spectrometer equipped with an Acquity UPLC, a lock-mass electrospray ion source and an Acquity photodiode array detector (Waters Ltd, UK). Methanol was used as the carrier solvent.

Thin layer chromatography was carried out on neutral aluminium silica plates (Merck 5554) or neutral aluminium oxide plates (Merck 5550) and visualised under UV irradiation (254 or 365 nm). Preparative column chromatography was performed using silica gel (Merck Silica Gel 60, 230-400 mesh) or neutral aluminium oxide (Merck 90, 70-320 mesh).

Melting points were recorded using Sanyo Gallenkamp melting point apparatus and are uncorrected.

5.1.5 Optical Techniques

All samples for optical analyses were contained in quartz cuvettes with a path length of 1 cm and a polished base. Measurements were recorded at 295 K.

UV/Vis absorbance spectra were recorded on an ATI Unicam UV/Vis spectrometer (Model UV2) using Vision version 3.33 software. Samples were measured relative to a reference of pure solvent. Emission spectra were recorded on an ISA Joblin-Yvon Spex Fluorolog-3 luminescence spectrometer, or Horiba-Jobin Yvon Fluoromax-3 luminescence spectrometer equipped with an iHR320 module, which selects either a HORIBA FL-1073 (Hammatsu R928P) photomultiplier tube or a HORIBA Synapse BIDD CCD for detection of emitted light, using FluorEssence software (based on Origin® software). Increments of 2 nm were used, with slit widths of 1.5 nm for both excitation and emission.

Lifetime measurements were carried out on a Perkin Elmer LS55 spectrometer using FL Winlab software version 4.00.02. The complexes were excited at λ_{max}, emission monitoring at 612.5 or 614 nm, during a fixed gate time of 0.1 ms, after a delay time. The lifetimes were taken between 0.1 and 3 ms or 6 ms delay times, dependant on the solvent. The excitation and emission slits were set to 10 nm. The observed decays were plotting in Origin® using Equation **5.1**.

$$I = A_0 + A_1 e^{-kt} \qquad \textbf{(5.1)}$$

The measured excited state lifetime, τ, is the inverse of the radiative decay rate constant, *k*.

CPL spectra were recorded on a custom built spectrometer consisting of a laser driven light source (Energetiq EQ-99 LDLS, spectral range 170 to 2100 nm) coupled to an Acton SP2150 monochromator (600 g/nm, 300 nm Blaze) that allows excitation wavelengths to be selected with a 6 nm FWHM band-pass. The collection of the emitted light was facilitated (90º angle set up, 1 cm path length quartz cuvette) by a Lock-In Amplifier (Hinds Instruments Signaloc 2100) and Photoelastic Modulator (Hinds Instruments PEM-90). The differentiated light was focused onto an Acton SP2150 monochromator (1200 g/nm, 500 nm Blaze) equipped with a high sensitivity cooled Photo Multiplier Tube (H10723-20 Extended red-multialkali). Spectra were recorded using a 5 spectral average sequence in the range of 570-720 nm with 1 nm spectral intervals and 500 μs integration time.

All data fitting and plotting were performed using Origin® software. Binding constants were calculated by fitting to Equation **5.2**. The numbers given in parenthesis following the binding constants are error in the fit of line to the data.

$$[X] = \frac{\frac{F - F_0}{F_1 - F_0}}{K} + [Eu] \times \left(\frac{F - F_0}{F_1 - F_0}\right) - [Eu] \times \left(\frac{F - F_0}{F_1 - F_0}\right)^2 \quad \textbf{(5.2)}$$
$$1 - \frac{F - F_0}{F_1 - F_0}$$

Where [X] is the total concentration of the selected analyte in solution, [Eu] is the total concentration of the complex, F is either intensity ratio of selected emission transitions or I_L - I_R values, F_0 is the initial ratio and F_1 is the final ratio. *K* is the binding constant, derived in Equation **5.3,** where [EuX] is the concentration of the analyte-coordination complex, $[X_f]$ is the concentration of free analyte and $[Eu_f]$ is the concentration of free complex.

$$K = \frac{[EuX]}{[X_f][Eu_f]} \quad \textbf{(5.3)}$$

Time gated experiments were carried out in a custom built time-gated spectrophotometer. It comprised of a 365 nm 330 mW pulsed LED with 2 ms per pulse in a 10 Hz cycle sequence. This was connected to a cuvette holder and an Acton 2155 scanning monochromator with a 1200 blaze grating, tuned between 400 and 750 nm, and a Hamamatsu 7155 red corrected PMT. This was operated using custom written Labview software.

5.1.6 DFT Computations

The model geometries for [Y.**L**^{6}]*Gly and [Y.**L**^{6}]*Zn^{2+}*Gly adducts in this study were fully optimised without symmetry constraints using the hybrid-DFT B3LYP functional[213,214] and the 3-21G* basis set[215–220] for all atoms with the Gaussian 09 package.[221] The 4-methoxyphenylethynyl group in ligand **L**^{6} was replaced with a hydrogen atom in the model geometries to reduce computational efforts. The paramagnetic Eu(III) complexes are very difficult to model computationally so Y(III) has been used instead of Eu(III) in calculations elsewhere.[222–225] Optimised geometries of Y(III) complexes with the B3LYP/3-21G* functional/basis set have been demonstrated previously to be suitable models for Eu(III) complexes.[85,90] The Gaussian09 default polarisation continuum solvent model (IEFPCM)[226] was applied to

all calculations using water as solvent. The figures of optimised model geometries were generated using Mercury software.[227]

5.1.7 Grain/Oat Extracts

Ten grains were selected and soaked in 2 mL of purite water for 24 hr. The water was then filtered and lyophilised. The residue was taken up in 2 mL of purite water with complex (7 μM) in 0.1 M NaCl, 0.1 M MES at pH 5.9.

To spike the grains, ten cordiale grains were taken and a 0.01 mL of a glyphosate solution (0.15-1.2 mM) was added and the container sealed for 24 hr to allow the grains to soak up the glyphosate. After lyophilised to remove any water, the grains were soaked for 24 hr in 2 mL of purite water. The solution was filtered and lyophilised again, before the residue was taken up in 2 mL of the complex (7 μM) solution with 0.1 M NaCl, 0.1 M MES at pH 5.9.

5.2 Synthetic Procedures

1,4,7,10-Tetraaza-cyclododecane-1,7-dicarboxylic acid dibenzyl ester, 1[228]

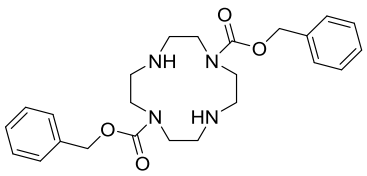

1,4,7,10-Tetraazacyclododecane (2.5 g, 14.5 mmol) and disodium hydrogen phosphate (7.0 g, 49.3 mmol) were dissolved in a solution of distilled water:dioxane (35 mL, 25:10). The pH was adjusted to 2.5 with addition of HCl. Benzyl chloroformate (5.0 mL, 35.0 mmol) in dioxane (10 mL) was added dropwise over 2 h, and the solution was stirred at room temperature for 18 h. The solvent was evaporated under reduced pressure and the residue re-dissolved in water (100 mL). The pH was adjusted to 7.0 using conc. KOH. The aqueous phase was then washed with diethyl ether (2 x 100 mL) and then extracted with DCM (2 x 100 mL). The DCM layers were combined, dried with magnesium sulfate and the solvent evaporated under reduced pressure to give a clear oil. The oil was crystallised from DCM and diethyl ether to give a white powder (1.54 g, 24%). m.p. 116-118 °C (lit.[229] 113-116 °C). ^{1}H NMR (400 MHz, $CDCl_3$) δ_H (ppm): 7.35 (10H, m, Ar), 5.18 (4H, s, C$\underline{H}_2$-Ar), 3.39-4.01 (8H, s, br, cyclen), 2.75-3.25 (8H, m, br, cyclen), 1.65 (2H, s, br, N$\underline{H}$). LCMS (ESI^+) *m/z*: 441 $[M+H]^+$.

4,10-Bis-(tert-butoxycarbonylmethyl)-1,4,7,10-tetraazacyclododecane-1,7-dicarboxylic acid dibenzyl ester, 2[228]

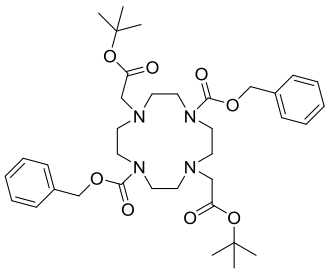

1,4,7,10-Tetraaza-cyclododecane-1,7-dicarboxylic acid dibenzyl ester (1.50 g, 3.41 mmol), *tert*-butyl bromoacetate (1.13 mL, 7.67 mmol) and Cs_2CO_3 (3.34 g, 10.24 mmol) were dissolved in anhydrous acetonitrile (25 mL). The mixture was heated under reflux for 18 h. The mixture was filtered and the solvent removed under reduced pressure to yield a yellow oil, that was purified using column chromatography (silica, 100% DCM → 2% MeOH) to yield a light yellow oil (1.73 g, 76%). ^{1}H NMR (400 MHz, $CDCl_3$) δ_H (ppm): 7.33 (10H, m, Ar), 5.12 (4H, s, C$\underline{H}_2$-Ar), 3.14-3.58 (16H, m, br, cyclen), 2.88 (4H, s, C$\underline{H}_2$CO), 1.42 (18H, s, br, ^{t}Bu). LCMS (ESI$^+$) *m/z*: 689 $[M+H]^+$.

1,7-Bis-(tert-butoxycarbonylmethyl)-1,4,7,10-tetraazacyclododecane, 3[228]

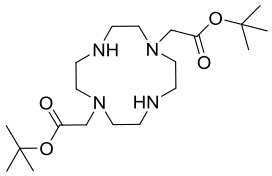

4,10-Bis-(tert-butoxycarbonylmethyl)-1,4,7,10-tetraazacyclododecane-1,7- dicarboxylic acid dibenzyl ester (2.00 g, 2.99 mmol) was dissolved in absolute ethanol (20 mL) with a catalytic amount of $Pd(OH)_2$/C (10%). The mixture was agitated in a Parr hydrogenation apparatus for 24 h under 40 bar of hydrogen. The catalyst was filtered and the solvent removed under reduced pressure to yield a white solid (1.05 g, 2.63 mmol, 88%). ^{1}H NMR (400 MHz, $CDCl_3$) δ_H (ppm): 3.30 (4H, s, C$\underline{H}_2$CO), 2.79 (8H, s, br, cyclen), 2.58 (8H, s, br, cyclen), 1.44 (18H, s, ^{t}Bu). LCMS (ESI$^+$) *m/z*: 401 $[M+H]^+$.

6-Methyl-2-phenoxynictonic acid, 4[51]

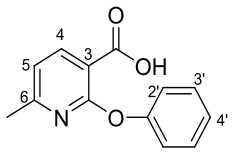

Sodium metal (840 mg, 36.5mmol) was slowly dissolved in dry methanol (20 mL). 2-Chloro-6-methylnicotinic acid (2.5 g, 14.6 mmol) and phenol (6.52 g, 69.4 mmol) were added to the solution and stirred for 15 min. The solvent was removed and the remaining liquid was refluxed at 180 ˚C for 18 h. The resultant mixture was cooled to room temperature and dissolved in water (20 mL) which was washed with diethyl ether (3 × 20 mL). The pH of the aqueous layer was adjusted to 4.0 and a white precipitate formed. The solvent was removed under reduced pressure to yield a white solid (2.47 g, 74 %). m.p. 154-156 ˚C (lit.[230] 155-156 ˚C). ^{1}H NMR (400 MHz, $CDCl_3$) δ_H (ppm): 8.40 (1H, d, $^{3}J_{H\text{-}H}$ = 8.0 Hz, H^4), 7.45 (2H, t, $^{3}J_{H\text{-}H}$ = 8.0 Hz, H^3), 7.30 (1H, t, $^{3}J_{H\text{-}H}$ = 8.0 Hz, $H^{4'}$), 7.21 (2H, d, $^{3}J_{H\text{-}H}$ = 8.0 Hz, $H^{2'}$), 7.05 (1H, d, $^{3}J_{H\text{-}H}$ = 8.0 Hz, H^5), 3.01 3H, s, CH3). LCMS (ESI^+) *m/z*: 234 $[M+H]^+$.

2-Methyl-1-azaxanthone, 5[51]

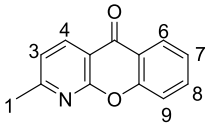

6-Methyl-2-phenoxynicotinic acid (2.47 g, 10.9 mmol) was added to polyphosphoric acid (80 g) and stirred at 120 °C for 18 h under argon. The mixture was then allowed to cool to room temperature before being poured onto ice water and stirred until the ice melted. The pH was adjusted to 12.0 with potassium hydroxide pellets and then extracted with DCM (3 × 100 mL). The organic layers were combined, and dried over K_2CO_3 before the solvent was removed under reduced pressure which yielded a yellow solid (1.14 g, 50%). m.p. 134-136 ˚C (lit.[231] (136-138 ˚C). ^{1}H NMR (400 MHz, $CDCl_3$) δ_H (ppm): 8.56 (1H, d, $^{3}J_{H\text{-}H}$ = 8.0 Hz, H^4), 8.28 (1H, dd, $^{3}J_{H\text{-}H}$ = 8.0 Hz, $^{4}J_{H\text{-}H}$ = 2.0 Hz, H^6), 7.75 (1H, ddd $^{3}J_{H\text{-}H}$ = 8.5, 7.0 Hz, $^{4}J_{H\text{-}H}$ = 2.0 Hz, H^8), 7.58 (1H, d, $^{3}J_{H\text{-}H}$ = 8.5 Hz, $^{4}J_{H\text{-}H}$ = 1.0 Hz, H^9), 7.40 (1H, ddd, $^{3}J_{H\text{-}H}$ = 8.0, 7.0 Hz, $^{4}J_{H\text{-}H}$ = 1.0 Hz, H^7), 7.28 (1H, d, $^{3}J_{H\text{-}H}$ = 8.0 Hz, H^3), 2.69 (3H, s, H^1). LCMS (ESI^+) *m/z*: 212 $[M+H]^+$, 234 $[M+Na]^+$.

2-Bromomethyl-1-azaxanthone, 6[51]

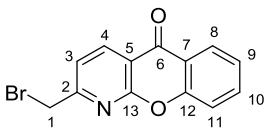

2-Methyl-1-azaxanthone (1.00 g, 4.74 mmol), was dissolved in carbon tetrachloride (25 mL) and heated with a 60 W tungsten lamp. *N*-bromosuccinimide (0.843 g, 4.74 mmol) and dibenzyl peroxide (15 mg, 0.05 mmol) were added and the solution was stirred under argon for 3 days, monitoring the reaction using TLC and ^{1}H NMR. The reaction was then allowed to cool to room temperature, filtered and the solvent removed under vacuum. The resulting solid was purified by column chromatography, with 1:1 DCM:toluene which yielded a white solid (0.4 g, 30%).

Alternative procedure:[232]

Diethylphosphite (1.11 mL, 8.59 mmol) and diisopropylamine (1.40 mL, 10.03 mmol) were added at 0 °C to a stirred solution of 2-dibromomethyl-1-azaxanthone (0.67 g, 1.82 mmol) in dry THF (30 mL) under argon. After 10 minutes the reaction was halted and poured onto iced water (50 mL), then extracted with chloroform (3 x 50 mL). The organic layer was backwashed with $NaHCO_{3(aq)}$ (50 mL) and water (50 mL) before it was dried and the solvent removed under pressure to give a white solid. The organic layer was purified by column chromatography (silica, 100% DCM → 3% MeOH) which yielded a white powder (0.407 g, 77%).

m.p. 164-166 ˚C (lit.[51] 169-170 ˚C). ^{1}H NMR (400 MHz, $CDCl_3$) δ_H (ppm): 8.72 (1H, d, $^{3}J_{H\text{-}H}$ = 8.0 Hz, H^4), 8.33 (1H, dd, $^{3}J_{H\text{-}H}$ = 8.0 Hz, $^{4}J_{H\text{-}H}$ = 1.5 Hz, H^8), 7.80 (1H, ddd, $^{3}J_{H\text{-}H}$ = 8.0, 7.0 Hz, $^{4}J_{H\text{-}H}$ = 1.5 Hz, H^{10}), 7.64 (1H, dd, $^{3}J_{H\text{-}H}$ = 8.0 Hz, $^{4}J_{H\text{-}H}$ = 1.0 Hz, H^{11}), 7.57 (1H, d, $^{3}J_{H\text{-}H}$ = 8.0 Hz, H^3), 7.46 (1H, ddd, $^{3}J_{H\text{-}H}$ = 8.0, 7.0 Hz, $^{4}J_{H\text{-}H}$ = 1.0 Hz, H^9), 4.62 (2H, s, H^1). ^{13}C NMR (100 MHz, $CDCl_3$) δ_C (ppm): 177.1 (C^6), 162.1 (C^2), 159.8, (C^{13}), 157.8 (C^{12}), 138.8, (C^4), 135.9 (C^{10}), 126.8 (C^7), 125.0 (C^9), 121.7 (C^8), 120.9 (C^3), 118.6 (C^{11}), 116.1 (C^5), 32.3 (C^1). LCMS (ESI^+) *m/z*: 298 $[M+H]^+$. R_f 0.29 (DCM, silica), R_f 0.51 (DCM:Toluene, silica).

1,7-Bis-(tert-butoxycarbonylmethyl)-4,10-bis[2-methyl-1-azaxanthone]-1,4,7,10-tetraazacyclododecane, 7[61]

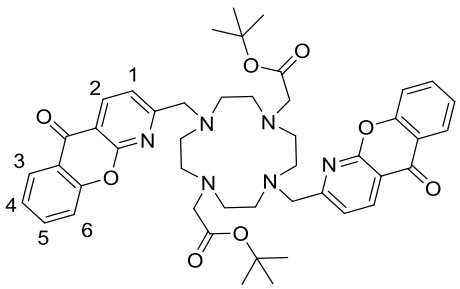

1,7-Bis-(tert-butoxycarbonylmethyl)-1,4,7,10-tetraazacyclododecane (107 mg, 0.27 mmol), 2-bromomethyl-1-azanthanthone (170 mg, 0.59 mmol) and Cs_2CO_3 (192 mg, 0.59 mmol) were dissolved in anhydrous acetonitrile (5 mL) and heated under reflux for 48 h under argon at 65 °C. The reaction was monitored by LCMS to ensure all the brominated material had been consumed. The mixture was allowed to cool to room temperature and gravity filtered before the solvent was removed under reduced pressure. The residue was dissolved in DCM (5 mL) and washed with water (3 x 5 mL) to remove caesium salts. The organic layer was dried and the solvent removed under reduced pressure to yield an orange oil (142 mg, 65%). ^{1}H NMR (400 MHz, $CDCl_3$) δ_H (ppm): 8.75 (2H, d, $^3J_{H\text{-}H}$ = 8.0 Hz, H^3), 8.32 (2H, d, $^3J_{H\text{-}H}$ = 8.0 Hz, H^2), 7.80 (2H, t, $^3J_{H\text{-}H}$ = 8.0 Hz, H^4), 7.63 (2H, d, $^3J_{H\text{-}H}$ = 8.0 Hz, H^1), 7.55 (2H, d, $^3J_{H\text{-}H}$ = 8.0 Hz, H^6), 7.45 (2H, t, $^3J_{H\text{-}H}$ = 8.0 Hz, H^5), 4.09 (4H, s, C$\underline{H}_2$), 1.57-3.52 (20H, m, cyclen, C$\underline{H}_2$CO), 1.47 (18H, s, ^{t}Bu). LCMS (ESI$^+$) *m/z*: 819 $[M+H]^+$.

$[Eu.L^1(OH_2)]^{+}$[61]

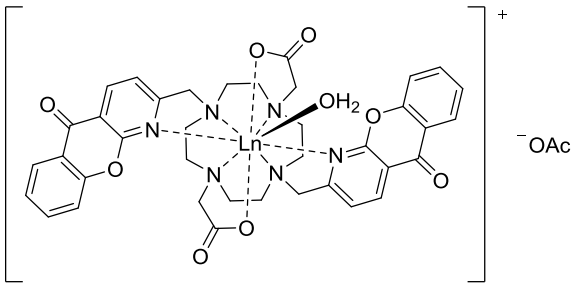

Trifluoroacetic acid (1 mL) was added to a solution of 1,7-bis-(tert-butoxycarbonylmethyl)-1,4,7,10-tetraazacyclododecane (14 mg, 0.017 mmol) in DCM (0.5 mL). The reaction mixture was stirred at room temperature for 60 h. The solvent was removed under reduced pressure, and the residue re-dissolved in DCM three times to ensure complete removal of the acid and *tert*-butyl alcohol, finally affording a pale

brown solid that was used in the following step without further purification. LCMS (ESI^+) *m/z*: 707 $[M+H]^+$.

The solid residue was dissolved in methanol:water (1 mL:2 mL, 3 mL). $Eu(OAc)_3$ (0.019 g, 0.057 mmol) was added and the pH was adjusted to 5.5 by addition of aqueous ammonia. The mixture was heated under reflux at 90 °C for 18 h. The reaction was cooled to room temperature, and then the pH was raised to 10.0 with aqueous ammonia. The solution was stirred for a further 1 h before filtering. The pH was adjusted to 5.5 with glacial acetic acid. The solvent was evaporated and lyophilised to yield a white solid which was purified by reverse phase HPLC (Method A, t_R = 6.8 min) to give a colourless solid (7 mg, 44%). HRMS (ESI^+) *m/z*: 871.1771 $[M+H]^+$ ($C_{38}H_{38}{}^{159}EuN_6O_9$ requires 871.1743). τ_{H2O}: 0.50 ms; τ_{D2O}: 1.69 ms; $\lambda_{abs}(H_2O)$: 336 nm.

(S)-Ethyl-N-bromoethanoyl-alanate, 8[233]

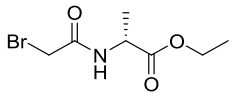

S-Alanine ethyl ester (1.5 g, 9.77 mmol), triethylamine (2.79 mL, 20mmol) and bromoacetyl bromide (0.85 mL, 9.77 mmol) were dissolved in chloroform and stirred at -30 °C in a dry ice/acetone bath for 3 h. The reaction was then warmed to room temperature and left to stir overnight. The mixture was washed with HCl (6 M, 15 mL) and water (4 x 10 mL). The organic layer was dried and the solvent removed under vacuum. The colourless oil was recrystallized with DCM and 40/60 pet. ether to give a white crystalline solid (1.10 g, 47%). m.p. 30-32 ˚C (lit.[233] 30-31 ˚C). ^{1}H NMR (400 MHz, $CDCl_3$) δ_H (ppm): 7.10 (1H, s, br, N<u>H</u>), 4.51 (1H, q, $^3J_{H-H}$ = 7.0 Hz, C<u>H</u>-CH_3, 4.18 (2H, q, $^3J_{H-H}$ = 7.0 Hz, O-C<u>H</u>$_2$), 3.85 (2H, s, br, Br-C<u>H</u>$_2$), 1.41 (3H, d, $^3J_{H-H}$ = 7.0 Hz, CH-C<u>H</u>$_3$), 1.28 (3H, t, $^3J_{H-H}$ = 7.0 Hz, O-CH_2-C<u>H</u>$_3$). LCMS (ESI^+) *m/z*: 238 $[M+H]^+$.

(*SS*)-1,7-Bis(benzyloxycarbonyl)-4,10-bis(ethoxycarbonyl-2-ethylcarbamoylmethyl)-1,4,7,10-tetraazacyclododecane, 9[233]

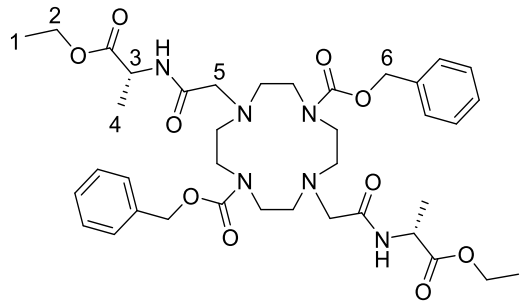

1,4,7,10-Tetraaza-cyclododecane-1,7-dicarboxylic acid dibenzyl ester (1.02 g, 2.3 mmol) and (*S*)-ethyl-*N*-bromoethanoyl-alanate (1.10 g, 4.6 mmol) were dissolved in anhydrous acetonitrile (25 mL) and potassium carbonate (2.25 g, 16 mmol) was added. The reaction mixture was heated to 60 °C and left to stir for 5 days, monitoring via LCMS to ensure all the alkyl halide was consumed. The mixture was filtered and the solvent removed under reduced pressure to yield an orange oil which was purified by column chromatography (alumina, DCM:MeOH, 98:2) to give a yellow oil (1.20 g, 69%). ^{1}H NMR (400 MHz, $CDCl_3$) δ_H (ppm): 7.33 (10H, m, br, Ar), 5.09 (4H, s, H^6), 4.51 (2H, br, H^3), 4.14 (4H, q, $^{3}J_{H\text{-}H}$ = 7.0 Hz, H^2), 3.73 (4H, s, br, H^5), 2.67-3.31 (18H, m, br, cyclen), 1.38 (6H, br, H^4), 1.25 (6H, t, $^{3}J_{H\text{-}H}$ = 7.0 Hz, H^1). LCMS (ESI^+) *m/z*: 755 $[M+H]^+$, 777 $[M+Na]^+$.

(*SS*)-1,7-Bis(ethoxycarbonyl-2-ethylcarbamoylmethyl)-1,4,7,10-tetraazacyclododecane, 10[233]

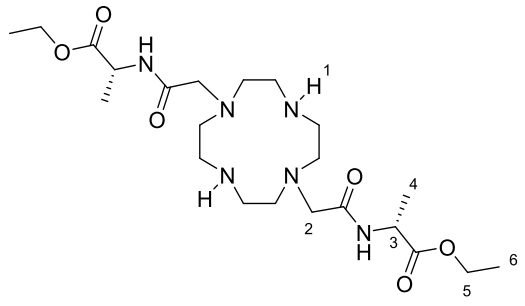

(*SS*)-1,7-Bis(benzyloxycarbonyl)-4,10-bis(ethoxycarbonyl-2-ethylcarbamoylmethyl)-1,4,7,10-tetraazacyclododecane was dissolved in absolute ethanol (20 mL) with a catalytic amount of $Pd(OH)_2/C$ (10%). The mixture was hydrogenated using a Parr hydrogenator (40 bar) overnight. The catalyst was filtered and the solvent removed to give a yellow oil which was used without further purification, (0.46 g, 60%). ^{1}H NMR

(400 MHz, $CDCl_3$) δ_H (ppm): 8.38 (2H, s, br, H^1), 4.55 (2H, m, H^3), 4.16 (4H, q, $^3J_{H\text{-}H}$ = 7.0 Hz, H^5), 3.22 (4H, m, H^2), 2.45-2.95 (18H, m, br, cyclen), 1.36 (6H, d, $^3J_{H\text{-}H}$ = 7.0 Hz, H^4), 1.26 (6H, t, $^3J_{H\text{-}H}$ = 7.0 Hz, H^6). LCMS (ESI^+) *m/z*: 488 $[M+H]^+$.

(*SS*)-1,7-Bis(ethoxycarbonyl-2-ethylcarbamoylmethyl)-4-[(1-azaxanthone)-2methyl]-1,4,7,10-tetraazacyclododecane, 11[52]

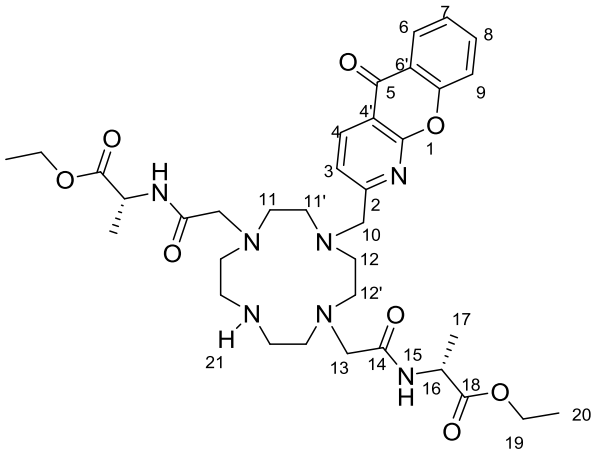

A mixture of (*SS*)-1,7-Bis(ethoxycarbonyl-2-ethylcarbamoylmethyl)-1,4,7,10-tetraazacyclododecane (301 mg, 0.619 mmol), and 2-bromomethyl-1-azaxanthone (179 mg, 0.619 mmol) was stirred in dry acetonitrile (10 mL) with sodium bicarbonate (50 mg, 0.619 mmol) at 70 ˚C for 18 h. The reaction was monitored using LCMS to confirm all the brominated starting material had been consumed. The solvent was removed under reduced pressure, the solid was re-dissolved in DCM (50 mL) and the sodium salts were filtered off. The solvent was removed and the solid was purified by a column chromatography (alumina, 100% DCM → 1% MeOH) to give an off-white solid (85 mg, 20%). ^{1}H NMR (400 MHz, $CDCl_3$) δ_H (ppm): 8.68 (1H, d, $^3J_{H\text{-}H}$ = 8.0 Hz, H^4), 8.25 (1H, dd, $^3J_{H\text{-}H}$ = 8.0 Hz, $^4J_{H\text{-}H}$ = 2.0 Hz, H^6), 7.81 (1H, ddd, $^3J_{H\text{-}H}$ = 8.0, 7.0 Hz, $^4J_{H\text{-}H}$ = 2.0 Hz, H^7), 7.62 (1H, dd, $^3J_{H\text{-}H}$ = 8.0 Hz, $^4J_{H\text{-}H}$ = 1.0 Hz, H^9), 7.46 (1H, ddd, $^3J_{H\text{-}H}$ = 8.0, 7.0 Hz, $^4J_{H\text{-}H}$ = 1.0 Hz, H^8), 7.41 (1H, d, $^3J_{H\text{-}H}$ = 8.0 Hz, H^3), 4.35 (2H, q, $^3J_{H\text{-}H}$ = 7.0 Hz, H^{16}), 4.11 (4H, q, $^3J_{H\text{-}H}$ = 7.0 Hz, H^{19}), 3.93 (2H, s, H^{10}), 2.80-3.40 (20H, m, cyclen, H^{13}), 1.24 (6H, d, $^3J_{H\text{-}H}$ = 7.0 Hz, H^{17}), 1.19 (6H, t, $^3J_{H\text{-}H}$ = 7.0 Hz, H^{20}). LCMS (ESI^+) *m/z*: 695 $[M+H]^+$.

(*SS*)-1,7-Bis(ethoxycarbonyl-2-ethylcarbamoylmethyl)-4-[(1-azaxanthone)-2methyl]-10methyl-1,4,7,10-tetraazacyclododecane, 12[52]

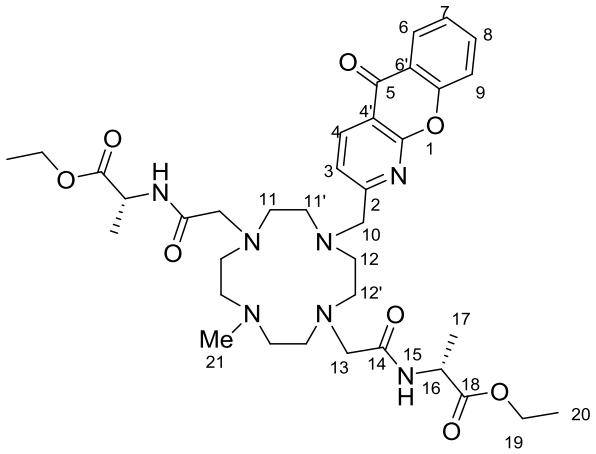

(*SS*)-1,7-Bis(ethoxycarbonyl-2-ethylcarbamoylmethyl)-4-[(1-azaxanthone)-2-methyl]-1,4,7,10-tetraazacyclododecane (85 mg, 0.12 mmol) was added to a solution of formic acid (2 mL) and formaldehyde (2 mL, 38% solution) and left to stir under reflux for 18 h. The solvent was removed under reduced pressure and the residue was re-dissolved in DCM:MeOH (10 mL, 10:1). The solid was filtered and the organic solvent was removed to yield a yellow solid (26 mg, 30%). ^{1}H NMR (400 MHz, $CDCl_3$) δ_H (ppm): 8.70 (1H, d, $^{3}J_{H\text{-}H}$ = 8.0 Hz, H^{4}), 8.27 (1H, dd, $^{3}J_{H\text{-}H}$ = 8.0, $^{4}J_{H\text{-}H}$ = 2.0 Hz, H^{6}), 7.75 (1H, ddd, $^{3}J_{H\text{-}H}$ = 8.0, 7.0 Hz, $^{4}J_{H\text{-}H}$ = 2.0 Hz, H^{7}), 7.61 (2H, m, $H^{3,9}$), 7.44 (2H, t, $^{3}J_{H\text{-}H}$ = 7.0 Hz, H^{8}), 4.33 (2H, q, $^{3}J_{H\text{-}H}$ = 7.0 Hz, H^{16}), 4.11 (2H, m, H^{10}), 4.07 (2H, q, $^{3}J_{H\text{-}H}$ = 7.0 Hz, H^{19}), 2.90-3.20 (20H, m, cyclen, H^{13}), 2.79 (3H, s, H^{21}), 1.41 (6H, d, $^{3}J_{H\text{-}H}$ = 7.0 Hz, H^{17}), 1.23 (6H, t, $^{3}J_{H\text{-}H}$ = 7.0 Hz, H^{20}). LCMS (ESI^{+}) *m/z*: 710 $[M+H]^{+}$.

(*SS*)-1,7-Bis(carboxy-2-ethylcarbamoylmethyl)-4-[(1-azaxanthone)-2-methyl]-10-methyl-1,4,7,10-tetraazacyclododecane, L^{2} [52]

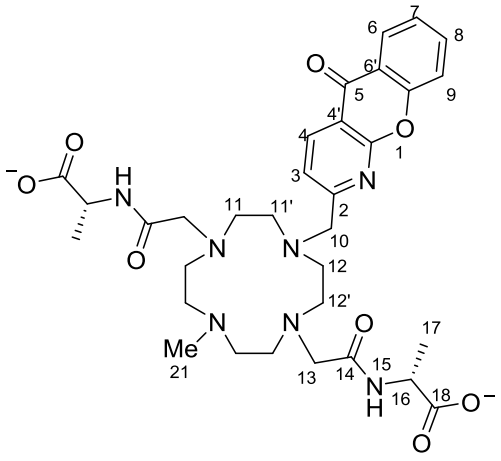

A solution of NaOD (5 mL, 0.1M) in D_2O was freshly made and (*SS*)-1,7-bis(ethoxycarbonyl-2-ethylcarbamoylmethyl)-4-[(1-azaxanthone)-2-methyl]-10-methyl-1,4,7,10-tetraazacyclododecane (26 mg) was added. The reaction was monitored by ^{1}H NMR. After 18 h, the pH was adjusted to 6.0 and the solvent was removed under reduced pressure and the resultant mixture was purified by HPLC (Method B, t_R = 9.2 min) to yield a yellow solid (4 mg, 17 %). ^{1}H NMR (400 MHz, D_2O) δ_H (ppm): 8.51 (1H, d, $^3J_{H\text{-}H}$ = 8.0 Hz, H^4), 8.16 (1H, dd, $^3J_{H\text{-}H}$ = 8.0 Hz, $^4J_{H\text{-}H}$ = 1.5 Hz, H^6), 8.00 (1H, ddd, $^3J_{H\text{-}H}$ = 8.0, 7.0 Hz, $^3J_{H\text{-}H}$ = 1.5 Hz, H^7), 7.62 (1H, t, $^3J_{H\text{-}H}$ = 7.5, H^9), 7.50 (1H, d, $^3J_{H\text{-}H}$ = 8.0 Hz, H^8) 7.27 (1H, d, $^3J_{H\text{-}H}$ = 8.0 Hz, H^3), 4.34 (2H, q, $^3J_{H\text{-}H}$ = 7.0 Hz, H^{16}), 1.65-2.15 (25H, m, cyclen, $H^{10, 13, 21}$), 1.07 (6H, d, $^3J_{H\text{-}H}$ = 7.0 Hz, H^{17}). LCMS (ESI^+) *m/z*: 807 $[M+H]^+$.

$[Eu.L^2(OH_2)]^{+}$ [52]

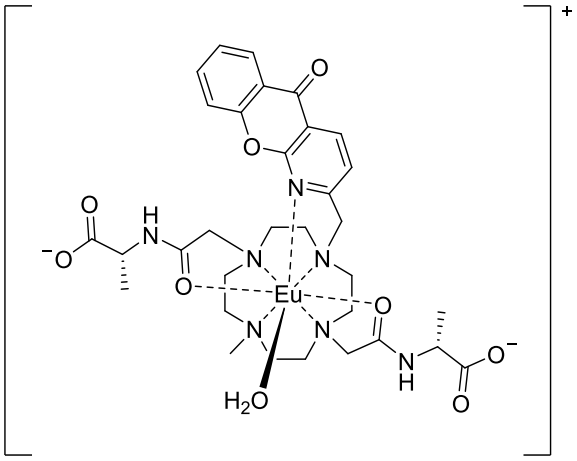

(*SS*)-1,7-Bis(carboxy-2-ethylcarbamoylmethyl)-4-[(1-azaxanthone)-2-methyl]-10-methyl-1,4,7,10-tetraazacyclododecane (4 mg, 6 μM) and $Eu(OAc)_3$ (2 mg, 6 μM) was dissolved in 50:50 H_2O:MeOH (1 mL) and was boiled under reflux for 4 days. The pH was adjusted to 10 and a white solid was removed with a centrifuge. The pH was adjusted to neutral and the solution was lyophilised to yield a yellow solid (2 mg, 41%). LCMS (ESI^+) *m/z*: 805 $[M\text{-}OAc]^+$. τ_{H2O}: 0.57 ms; τ_{D2O}: 1.42 ms; $\lambda_{abs}(H_2O)$: 336 nm.

Dimethyl 4-chloropyridine-2,6-dicarboxylate, 13[234] **CAS: 5371-70-0**

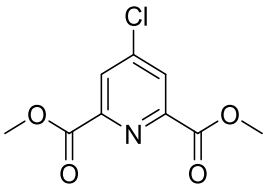

Chelidamic acid (1 g, 5.5 mmol) was dissolved in thionyl chloride (5.6 mL, 0.7 mol) and a few drops of DMF were added. The solution was stirred at 100 ˚C under argon for 48 h. The thionyl chloride was removed and the residue re-dissolved in dry DCM (3 mL). The solution was cooled to 0 ˚C before anhydrous MeOH (4 mL) was added dropwise. The solution was subsequently warmed to room temperature and the solvent removed under reduced pressure. The residue was washed with $NaHCO_3$ (20 mL) and extracted in to DCM (3 x 30 mL). The organic layers were combined and washed successively with water (50 mL), then brine (50 mL). The organic layer was dried with $MgSO_4$, filtered and the solvent removed yielding a yellow solid, (0.8 g, 74%). m.p. 145-147 °C (lit.[235] 139-140 °C). ^{1}H NMR (400 MHz, $CDCl_3$) δ_H (ppm): 8.30 (2H, s, py-H), 4.04 (6H, s, O-CH_3). ^{13}C NMR (100 MHz, $CDCl_3$) δ_C (ppm): 164.3 (C=O), 149.6 (py-C), 147.0 (py-C), 128.5 (py-C), 53.7 (O-CH_3). HRMS (ESI$^+$) *m/z*: 230.0231 $[M+H]^+$ ($C_9H_9NO_4Cl$ requires 230.0220). R_f (5% MeOH, silica) 0.61.

Dimethyl 4-iodopyridine-2,6-dicarboxylate, 14[234] CAS: 112776-84-8 221

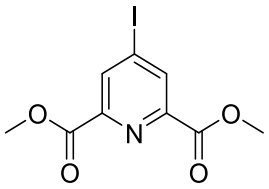

Dimethyl 4-chloropyridine-2,6-dicarboxylate (0.99 g, 3.4 mmol) was dissolved in dry acetonitrile (50 mL). Sodium iodide (6.49 g, 43.3 mmol) was then added and the mixture was sonicated for 30 min. Acetyl chloride (1 mL, 14.0 mmol) was subsequently added and the solution sonicated again, for 45 min. The solvent was removed and the residue re-dissolved in DCM (30 mL). The organic layer was extracted with $Na_2CO_{3(aq)}$ (25 mL), and the aqueous layer was re-extracted into DCM (2 x 30 mL). The organic layers were combined and washed with $NaS_2O_4.H_2O$ (50 mL), dried over $MgSO_4$, filtered and the solvent removed under reduced pressure. The orange solid was purified using column chromatography (silica, 100% DCM → 1% MeOH) to yield a white solid, (1.15 g, 82%). m.p. 184-185 ˚C (lit.[90] 179-180 °C). ^{1}H NMR (400 MHz, $CDCl_3$) δ_H (ppm): 8.66 (2H, s, py-H), 4.01 (6H, s, O-CH_3). ^{13}C NMR (100 MHz, $CDCl_3$) δc (ppm): 164.0 (C=O), 148.4 (py-C), 137.3 (py-C), 107.13 (py-C), 53.6 (O-CH_3). HRMS (ESI$^+$) *m/z*: 321.9658 $[M+H]^+$ ($C_9H_9NO_4I$ required 321.9576). R_f (5% MeOH, silica) 0.77.

Methyl 6-(hydroxymethyl)-4-iodopicolinate, 15[234] **CAS: 1247012-08-3 224**

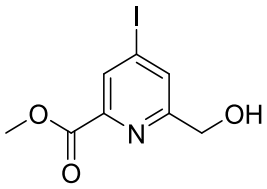

Dimethyl 4-iodopyridine-2,6-dicarboxylate was dissolved in DCM (6 mL) and MeOH (4 mL), and cooled to 0 °C. $NaBH_4$ was subsequently added and stirred for 1.5 hr. The reaction was quenched with HCl (4 mL, 1 M) and the volatile solvents removed under reduced pressure. The remaining aqueous solution was washed with ethyl acetate (3 x 30 mL). The organic layers were combined, dried with $MgSO_4$, filtered and the solvent removed yielding a yellow oil. This was purified using flash column chromatography (silica, 100% DCM → 1% MeOH) to give a white solid, (0.83 g, 79%). m.p. 139-140 ˚C (lit.[90] 140-141 °C). ^{1}H NMR: (400 MHz, $CDCl_3$) 8.39 (1H, s, py-H^3), 7.98 (1H, s, py-H^5), 4.83 (2H, s, CH_2-OH), 4.00 (3H, s, O-CH_3). ^{13}C NMR (100 MHz, $CDCl_3$) δc (ppm): 164.3 (C=O), 161.1 (py-C^6), 147.3 (py-C^2) 133.4 (py-C^5), 133.25 (py-C^3), 107.2 (py-C^4), 64.2 (CH_2-OH), 53.4 (CH_3). HRMS (ESI$^+$) *m/z*: 293.9593 $[M+H]^+$ ($C_8H_9NO_3I$ requires 293.9627). R_f (5% MeOH, silica) 0.30.

Methyl 6-(hydroxymethyl)-4-((4-methoxyphenyl)ethynyl)picolinate, 16[222]

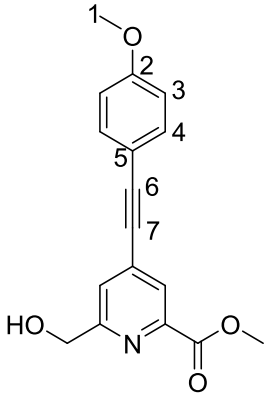

Methyl 6-(hydroxymethyl)-4-iodopicolinate (0.50 g, 1.7 mmol) was dissolved in dry THF (10 mL) and the solution degassed by three freeze-pump-thaw cycles. 4-Ethynylanisole (327μL, 2.5 mmol) and trimethylamine (1.19 g, 8.5 mmol) were added and the solution was degassed once more. [Bis(diphenylphosphino)ferrocene]dichloropalladium(II) (110 mg) and CuI (60 mg) were added and the mixture was stirred at 65 °C overnight. The solvent was removed under reduced pressure and purified by HPLC (Method C, t_R = 10.7 min), to yield a

white solid, (0.24 g, 47%). ^{1}H NMR (400 MHz, $CDCl_3$) δ_H (ppm) : 8.11 (1H, s, py-H^3), 7.62 (1H, s, py-H^5), 7.53 (2H, d, $^{3}J_{H\text{-}H}$ = 8.5 Hz, H^4), 6.93 (2H, d, $^{3}J_{H\text{-}H}$ = 8.5 Hz, H^3), 4.89 (2H, s, CH_2-OH), 4.04 (3H, s, $COOCH_3$), 3.87 (3H, s, H^1). ^{13}C NMR (100 MHz, $CDCl_3$) δ_C (ppm): 165.1 (C=O), 160.8 (C^2), 160.5 (py-C^6), 147.0 (py-C^2), 134.4 (C^4), 133.9 (C^5), 125.9 (py-C^3), 125.6 (py-C^5), 114.4 (C^3), 113.7 (py-C^4), 96.4 (C^6), 85.3 (C^7), 64.7 (CH_2-OH), 55.5 (O-CH_3), 53.3 (COO<u>C</u>H_3). HRMS (ESI$^+$) *m/z*: 298.1084 $[M+H]^+$ ($C_{17}H_{16}NO_4$ requires 298.1079).

1-(6-(Chloromethyl)pyridin-2-yl)-N,N-bis(pyridin-2-ylmethyl)methanamine, 18[205]

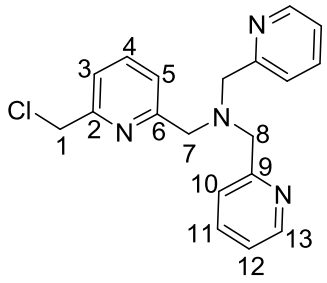

2,6 Bis(chloromethyl)pyridine (0.50 g, 2.8 mmol) and $NaHCO_3$ (0.24 g, 2.8 mmol) were dissolved in MeCN (20 mL). Di-picoylamine (0.56, 2.8 mmol) in MeCN (5 mL) was added dropwise and the resultant solution was stirred at room temperature overnight under argon. The mixture was then filtered and the solvent removed under reduced pressure to yield an orange solid. The compound was purified via flash column chromatography (alumina, 100% DCM) to yield a yellow solid, (0.5 g, 53%). m.p. 108-109 ˚C (lit.[236] 98 °C). ^{1}H NMR (400 MHz, $CDCl_3$) δ_H (ppm) : 8.53 (2H, m, H^{12}), 7.65 (3H, m, $H^{4, 13}$), 7.57 (2H, d, $^{3}J_{H\text{-}H}$ = 8.0 Hz, H^{10}), 7.52 (1H, d, $^{3}J_{H\text{-}H}$ = 8.0 Hz, H^5), 7.31 (1H, d, $^{3}J_{H\text{-}H}$ = 7.5 Hz, H^3), 7.14 (2H, ddd, $^{3}J_{H\text{-}H}$ = 8.0, 5.0 Hz, $^{4}J_{H\text{-}H}$ = 1.0 Hz, H^{11}), 4.63 (2H, s, H^1), 3.93 (4H, s, H^8), 3.92 (2H, s, H^7).^{13}C NMR (100 MHz, $CDCl_3$) δ_C (ppm): 159.0 (C^6), 158.9 (C^9), 156.0 (C^2), 149.1 (C^{12}), 137.6 (C^4), 136.7 (C^{13}), 123.3 (C^{10}), 122.4 (C^5), 122.3 (C^{11}), 121.2 (C^3), 60.1 (C^8), 59.9 (C^7), 46.9 (C^1). R_f (Alumina, DCM) 0.31. HRMS (ESI$^+$) *m/z*: 339.1385 $[M+H]^+$ ($C_{19}H_{20}ClN_4$ requires 399.1376).

Di-*tert*-butyl 2,2'-(4-((6-(methoxycarbonyl)-4-((4-methoxyphenyl)ethynyl)pyridine -2-yl)methyl)-1,4,7,10-tetraazacyclododecane-1,7-diyl)diacetate, 19[206]

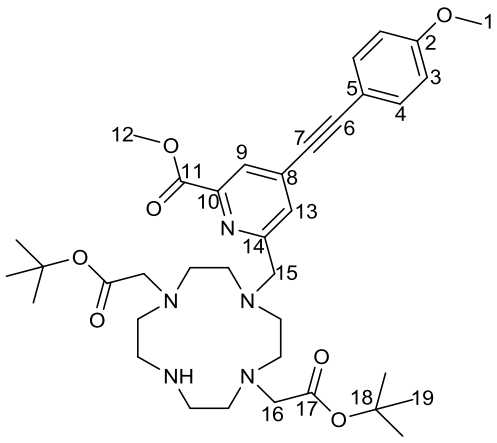

Methyl 6-(hydroxymethyl)-4-((4-methoxyphenyl)ethynyl)picolinate (0.24 g, 0.64 mmol) was dissolved in THF (10 mL). Trimethylamine (0.26 mL, 1.8 mmol) was added and the solution was cooled to 0 °C. Mesyl chloride (65 μL, 0.84 mmol) was added and the solution was allowed to warm to room temperature and stirred for 2 h, checking the progress of the reaction by TLC. Once the starting material was no longer visible, the solvent was removed and the residue was dissolved in DCM (30 mL). This solution was washed with water (30 mL) and the aqueous layer re-extracted with DCM (2 x 30 mL). The organic layers were combined, dried over potassium carbonate, filtered and the solvent removed to yield the mesylate ester as a viscous yellow glass that was used without purification in the subsequent alkylation reaction.

1,7-Bis-(tert-butoxycarbonylmethyl)-1,4,7,10-tetraazacyclododecane (1.11 g, 2.7 mmol) was stirred with K_2CO_3 (1.53 g, 11 mmol) in dry acetonitrile (20 mL) for 20 min under argon at room temperature and subsequently cooled to 0 °C. The mesylate was dissolved in dry MeCN (10 mL) and added dropwise to the cooled solution. The solution was then allowed to warm to room temperature and stirred under argon for 18 h. The solvent was removed under reduced pressure to yield a yellow solid (250 mg, 18%) which was purified using HPLC (Method C t_R = 9.1 min). ^{1}H NMR (400 MHz, $CDCl_3$) δ_H (ppm): 8.05 (1H, d, $^4J_{H\text{-}H}$ = 1.0 Hz , H^{13}), 7.52 (1H, d, $^4J_{H\text{-}H}$ = 1.0 Hz, H^9), 7.50 (2H, d, $^3J_{H\text{-}H}$ = 9.0 Hz, H^4), 6.92 (2H, d, $^3J_{H\text{-}H}$ = 9.0 Hz, H^3), 4.01 (3H, s, H^{12}), 3.84 (3H, s, H^1), 3.79 (2H, s, H^{15}), 3.23 (4H, s, H^{16}), 1.42 (18H, s, H^{19}). ^{13}C NMR (100 MHz, $CDCl_3$) δ_C (ppm): 170.4 (C^{17}), 165.6 (C^{11}), 160.8 (C^2), 158.6 (C^{14}), 147.7 (C^{10}), 134.2 (C^8), 133.7 (C^4), 128.5 (C^{13}), 125.8 (C^9), 114.3 (C^3), 113.3 (C^5), 96.9 (C^6), 84.8 (C^7), 81.6 (C^{18}), 58.4 (C^{15}), 56.5 (cyclen), 55.4 (C^1), 55.3 (cyclen), 53.3 (C^{12}), 51.2 (cyclen),

50.3 (cyclen), 46.1 (C^{16}), 28.3 (C^{19}). HRMS (ESI^+) *m/z*: 680.4023 $[M+H]^+$ ($C_{37}H_{54}N_5O_7$ requires 680.3698).

Di-*tert*-butyl 2,2'-(4-((6-((bis(pyridin-2-ylmethyl)amino)methyl)pyridin-2-yl)methyl)-10-((6-(methoxycarbonyl)-4-((4-methoxyphenyl)ethynyl)pyridin-2-yl)methyl)-1,4,7,10-tetraazacyclododecane-1,7-diyl)diacetate, 20[206]

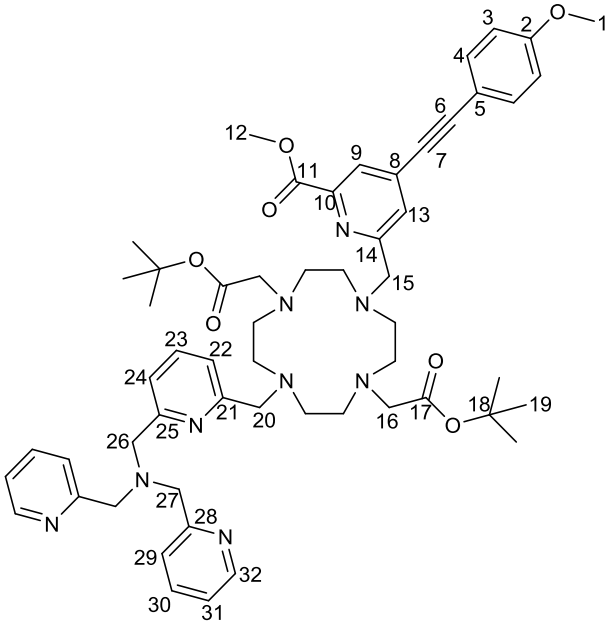

Di-*tert*-butyl 2,2'-(4-((6-(methoxycarbonyl)-4-((4-methoxyphenyl)ethynyl)pyridine-2-yl)methyl)-1,4,7,10-tetraazacyclododecane-1,7-diyl)diacetate (30 mg, 44 μmol) was dissolved in dry acetronitrile (10 mL). KI (20 mg, 0.12 mM), K_2CO_3 (50 mg, 0.36 mmol), and 1-(6-(chloromethyl)pyridin-2-yl)-N,N-bis(pyridin-2-ylmethyl)methanamine (31 mg, 91 μmol) were added and the solution was left to stir at 65 °C under argon for 18 h. The solvent was removed under reduced pressure and the resultant solid was purified through HPLC (Method C, t_R = 10.4 min), yielding a white solid (20 mg, 47%). ^{1}H NMR (400 MHz, $CDCl_3$) δ_H (ppm): 8.53 (2H, d, $^3J_{H\text{-}H}$ = 5.0 Hz, H^{32}), 8.07 (1H, d, $^4J_{H\text{-}H}$ = 1.0 Hz, H^9), 7.71 (3H, m, $H^{23, 30}$), 7.57 (4H, m, $H^{24, 29, 13}$), 7.48 (2H, d, $^3J_{H\text{-}H}$ = 9.0 Hz, H^4), 7.37 (1H, d, $^3J_{H\text{-}H}$ = 8.0 Hz, H^{22}), 7.20 (2H, ddd, $^3J_{H\text{-}H}$ = 8.0, 5.0 Hz, $^4J_{H\text{-}H}$ = 1.0 Hz, H^{31}), 6.89 (2H, d, $^3J_{H\text{-}H}$ = 9.0 Hz, H^3), 4.62 (2H, s, H^{20}), 4.22 (2H, s, H^{15}), 3.95 (3H, s, H^{12}), 3.89 (4H, s, H^{27}), 3.88 (2H, s, H^{26}), 3.83 (3H, s, H^1), 3.40 (6H, br, s, cyclen-H), 3.11 (2H, s, H^{16}), 2.94 (6H, s, cyclen-H), 1.40 (18H, s, H^{19}). ^{13}C NMR (100 MHz, $CDCl_3$) δ_C (ppm): 169.7 (C^{17}), 165.0 (C^{11}), 160.7 (C^2), 159.2 (C^{25}), 158.4 (C^{28}), 157.1 (C^{14}), 148.4 (C^{32}), 147.8 (C^{10}) 137.7 (C^{23}), 137.3 (C^{30}), 134.2 (C^8) 133.7 (C^4), 128.9 (C^{13}), 126.1 (C^9), 124.2 (C^{22}), 123.3 (C^{29}), 122.8 (C^{24}), 122.6 (C^{31}), 114.3 (C^3), 113.4 (C^5), 96.8 (C^6), 84.8 (C^7), 82.0 (C^{18}), 60.2 (C^{26}), 59.7 (C^{27}), 59.2 (C^{15}), 56.9 (cyclen),

56.8 (C^{20}), 55.4 (C^{1}), 53.0 (cyclen), 52.9 (C^{12}), 51.4 (cyclen), 50.4 (cyclen), 49.3 (C^{16}), 28.1 (C^{19}). HRMS (ESI^+) *m/z*: 982.5576 $[M+H]^+$ ($C_{56}H_{72}N_9O_7$ requires 982.5555)

$[Eu.\mathbf{L^6}]^{206}$

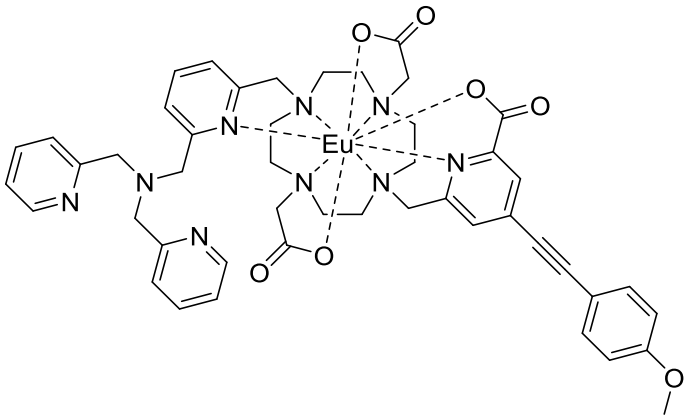

Di-*tert*-butyl 2,2'-(4-((6-((bis(pyridin-2-ylmethyl)amino)methyl)pyridin-2-yl)methyl)-10-((6-(methoxycarbonyl)-4-((4-methoxyphenyl)ethynyl)pyridin-2-yl)methyl)-1,4,7,10-tetraazacyclododecane-1,7-diyl)diacetate (30 mg, 0.03 mmol) was dissolved in $NaOH_{(aq)}$ (0.5 M, 6 mL) and stirred at 60 for 2 h, with the reaction being monitored via LCMS. The solution was neutralised with 1 M HCl (12 mL). $EuCl_3$ (30 mg, 0.12 mmol) was added and stirred at room temperature for a further 2 h. The solution was altered to pH 10.0 with ammonia solution. $Eu(OH)_3$ was centrifuged out, the remaining solution was neutralised and the solvent removed under reduced pressure. The resultant solid was dialysed to remove the salt yielding a white solid, (10 mg, 21%). HRMS (ESI^+) *m/z*: 1006.3148 $[M+H]^+$ ($C_{47}H_{50}{}^{159}EuN_9O_7$ requires 1006.3130). τ_{H2O}: 0.55 ms; τ_{D2O}:0.73 ms; $\lambda_{abs}(H_2O)$: 340 nm.

6. Bibliography

1 Aristotle, *De Anima, Book II, Part 7*.

2 E. N. Harvey, *A History of Luminescence from the Earliest Times until 1900*, The American Philosophical Society, New York, 1957.

3 S. D. Maind, S. A. Kumar, N. Chattopadhyay, C. Gandhi and M. Sudersanan, *Forensic Sci. Int.*, 2006, **159**, 32–42.

4 F. Suyver and A. Meijerink, *Chemisch2Weekblad*, 2002, 98, 12–13.

5 S. J. Butler, M. Delbianco, L. Lamarque, B. K. McMahon, E. R. Neil, R. Pal, D. Parker, J. W. Walton and J. M. Zwier, *Dalton Trans.*, 2015, **44**, 4791–803.

6 Q. You, M. Liu, Y. Liu, H. Zheng, Z. Hu, Y. Zhou and B. Wang, *ACS Sensors*, 2017, **2**, 569–575.

7 M. Botta, S. Aime, A. Barge, G. Bobba, R. S. Dickins, D. Parker and E. Terreno, *Chem. Eur. J.*, 2003, **9**, 2102–2109.

8 Y. Bretonniere, M. J. Cann, D. Parker and R. Slater, *Org. Biomol. Chem.*, 2004, **2**, 1624–32.

9 D. G. Smith, G. Law, B. S. Murray, R. Pal, D. Parker and K.-L. Wong, *Chem. Commun.*, 2011, **47**, 7347–7349.

10 J. I. Bruce, R. S. Dickins, L. J. Govenlock, T. Gunnlaugsson, S. Lopinski, M. P. Lowe, D. Parker, R. D. Peacock, J. J. B. Perry, S. Aime and M. Botta, *J. Am. Chem. Soc.*, 2000, **122**, 9674–9684.

11 S. V Eliseeva and J.-C. G. Bünzli, *Chem. Soc. Rev.*, 2010, **39**, 189–227.

12 S. H. Hewitt and S. J. Butler, *Chem. Commun.*, 2018, **54**, 6635–6647.

13 R. Carr, N. H. Evans and D. Parker, *Chem. Soc. Rev.*, 2012, **41**, 7673–86.

14 F. Zinna and L. Di Bari, *Chirality*, 2015, **27**, 1–13.

15 O. Laporte and W. F. Meggers, *J. Opt. Soc. Am.*, 1925, **12**, 459–463.

16 O. A. Blackburn, J. D. Routledge, L. B. Jennings, N. H. Rees, A. M. Kenwright, P. D. Beer and S. Faulkner, *Dalton Trans.*, 2016, **45**, 3070–7.

17 J.-C. G. Bünzli and C. Piguet, *Chem. Soc. Rev.*, 2005, **34**, 1048–1077.

18 S. I. Weissman, *J. Chem. Phys.*, 1942, **10**, 214–217.

19 Y. Zheng, C. Tan, G. P. C. Drummen and Q. Wang, *Spectrochim. Acta - Part A Mol. Biomol. Spectrosc.*, 2012, **96**, 387–394.

20 T. M. George, M. S. Krishna and M. L. P. Reddy, *Dalt. Trans.*, 2016, **45**, 18719–18729.

21 S. Dasari, S. Singh, S. Sivakumar and A. K. Patra, *Chem. Eur. J.*, 2016, **22**, 17387–17396.

22 B. Alpha, J. M. Lehn and G. Mathis, *Angew. Chemie Int. Ed. English*, 1987, **26**, 266–267.

23 E. B. van der Tol, H. J. van Ramesdonk, J. W. Verhoeven, F. J. Steemers, E. G. Kerver, W. Verboom and D. N. Reinhoudt, *Chem. Eur. J.*, 1998, **4**, 2315–2323.

24 A. Dadabhoy, S. Faulkner and P. G. Sammes, *J. Chem. Soc. Perkin Trans. 2*, 2000, **2**, 2359–2360.

25 A. Picot, F. Malvolti, B. Le Guennic, P. L. Baldeck, J. A. G. Williams, C. Andraud and O. Maury, *Inorg. Chem.*, 2007, **46**, 2659–2665.

26 N. M. Shavaleev, S. V. Eliseeva, R. Scopelliti and J. C. G. Bünzli, *Inorg. Chem.*, 2014, **53**, 5171–5178.

27 M. Kasha, *Discuss. Faraday Soc.*, 1950, **9**, 14–19.

28 E. R. Neil, PhD Thesis, University of Durham, 2015.

29 M. H. V. Werts, M. A. Duin, J. W. Hofstraat and J. W. Verhoeven, *Chem. Commun.*, 1999, 799–800.

30 A. D'aléo, A. Picot, A. Beeby, J. A. G. Williams, B. Leguennic, C. Andraud and O. Maury, *Inorg. Chem.*, 2008, **47**, 10258–10268.

31 H. K. Yong, S. B. Nam and K. K. Hwan, *ChemPhysChem*, 2006, **7**, 213–221.
32 A. D'Aléo, F. Pointillart, L. Ouahab, C. Andraud and O. Maury, *Coord. Chem. Rev.*, 2012, **256**, 1604–1620.
33 M. Kleinerman, *J. Chem. Phys.*, 1969, **51**, 2370–2381.
34 C. Yang, L. M. Fu, Y. Wang, J. P. Zhang, W. T. Wong, X. C. Ai, Y. F. Qiao, B. S. Zou and L. L. Gui, *Angew. Chemie - Int. Ed.*, 2004, **43**, 5010–5013.
35 M. Latva, H. Takalob, V. M. Mukkala, C. Matachescu, J. C. Rodríguez-Ubis and J. Kankare, *J. Lumin.*, 1997, **75**, 149–169.
36 K. T. Rim, K. H. Koo and J. S. Park, *Saf. Health Work*, 2013, **4**, 12–26.
37 M. Magerstadt, O. A. Gansow, M. W. Brechbiel, D. Colcher, L. Baltzer, R. H. Knop, M. E. Girton and M. Naegele, *Magn. Reson. Med.*, 1986, **3**, 808–812.
38 W. P. Cacheris, S. K. Nickle and A. D. Sherry, *Inorg. Chem.*, 1987, **26**, 958–960.
39 S. N. M. Chilla, C. Henoumont, L. Vander Elst, R. N. Muller and S. Laurent, *Isr. J. Chem.*, 2017, **57**, 800–80.
40 M. C. Heffern, L. M. Matosziuk and T. J. Meade, *Chem. Rev.*, 2014, **114**, 4496–4539.
41 C. Gateau, M. Mazzanti, J. Pécaut, F. a. Dunand and L. Helm, *Dalt. Trans.*, 2003, 2428.
42 J. W. Walton, L. Di Bari, D. Parker, G. Pescitelli, H. Puschmann and D. S. Yufit, *Chem. Commun.*, 2011, **47**, 12289–12291.
43 G. Nocton, A. Nonat, C. Gateau and M. Mazzanti, *Helv. Chim. Acta*, 2009, **92**, 2257–2273.
44 J. W. Walton, R. Carr, N. H. Evans, A. M. Funk, A. M. Kenwright, D. Parker, D. S. Yufit, M. Botta, S. De Pinto and K. L. Wong, *Inorg. Chem.*, 2012, **51**, 8042–8056.
45 L. Seveus, M. Väisälä, S. Syrjänen, M. Sandberg, A. Kuusisto, R. Harju, J. Salo, I. Hemmilä, H. Kojola and E. Soini, *Cytometry*, 1992, **13**, 329–338.
46 M. Räsänen, J. Rosenberg, J. Lukkari, K. Haapakka, J. Kankare and H. Takalo, *J. Lumin.*, 2017, **187**, 471–478.
47 H. Takalo, T. Sutela and M. Latva, *Helv. Him. Acta*, 1996, **79**, 789–802.
48 M. Delbianco, V. Sadovnikova, E. Bourrier, G. Mathis, L. Lamarque, J. M. Zwier and D. Parker, *Angew. Chemie - Int. Ed.*, 2014, **53**, 10718–10722.
49 M. Delbianco, L. Lamarque and D. Parker, *Org. Biomol. Chem.*, 2014, **12**, 8061–8071.
50 B. K. McMahon, R. Pal and D. Parker, *Chem. Commun.*, 2013, **49**, 5363.
51 P. Atkinson, K. S. Findlay, F. Kielar, R. Pal, D. Parker, R. A. Poole, H. Puschmann, S. L. Richardson, P. a Stenson, A. L. Thompson and J. Yu, *Org. Biomol. Chem.*, 2006, **4**, 1707–22.
52 R. Pal, D. Parker and L. C. Costello, *Org. Biomol. Chem.*, 2009, **7**, 1525–8.
53 A. C. Croce and G. Bottiroli, *Eur. J. Histochem.*, DOI:10.4081/ejh.2014.2461.
54 L. C. Costello and R. B. Franklin, *Prostate Cancer Prostatic Dis.*, 2009, **12**, 17–24.
55 A. Thibon and V. C. Pierre, *J. Am. Chem. Soc.*, 2009, **131**, 434–435.
56 R. Carr, L. Di Bari, S. Lo Piano, D. Parker, R. D. Peacock and J. M. Sanderson, *Dalton Trans.*, 2012, **41**, 13154–8.
57 B. N. Samoilov, *J. Exp. Theor. Phys*, 1948, **18**, 1030–1040.
58 C. A. Emeis and L. J. Oosterhoff, *Chem. Phys. Lett. 1*, 1967, **1**, 129–132.
59 G. Muller, in *Luminescence of Lanthanide Ions in Coordination Compounds and Nanomaterials*, ed. A. De Bettencourt-Dias, Wiley, 2014.
60 E. M. Sanchez-Carnerero, A. R. Agarrabeitia, F. Moreno, B. L. Maroto, G. Muller, M. J. Ortiz and S. De La Moya, *Chem. Eur. J.*, 2015, **21**, 13488–13500.
61 R. Carr, R. Puckrin, B. K. McMahon, R. Pal, D. Parker and L. O. Palsson,

Methods Appl. Fluoresc., 2014, **2**, 24007.
62 J. E. Field, G. Muller, J. P. Riehl and D. Venkataraman, *J. Am. Chem. Soc.*, 2003, **125**, 11808–11809.
63 R. S. Walters, C. M. Kraml, N. Byrne, D. M. Ho, Q. Qin, F. J. Coughlin, S. Bernhard and R. A. Pascal, *J. Am. Chem. Soc.*, 2008, **130**, 16435–16441.
64 M. Schadt, *Annu. Rev. Mater. Sci.*, 1997, **27**, 305–79.
65 H. Maeda, Y. Bando, K. Shimomura, I. Yamada, M. Naito, K. Nobusawa, H. Tsumatori and T. Kawai, *J. Am. Chem. Soc.*, 2011, **133**, 9266–9269.
66 E. M. Sanchez-Carnerero, F. Moreno, B. L. Maroto, A. R. Agarrabeitia, M. J. Ortiz, B. G. Vo, G. Muller and S. de la Moya, *J. Am. Chem. Soc.*, 2014, **136**, 3346–3349.
67 H. Maeda, W. Hane, Y. Bando, Y. Terashima, Y. Haketa, H. Shibaguchi, T. Kawai, M. Naito, K. Takaishi, M. Uchiyama and A. Muranaka, *Chem. Eur. J.*, 2013, **19**, 16263–16271.
68 H. Maeda, T. Shirai, Y. Bando, K. Takaishi, M. Uchiyama, A. Muranaka, T. Kawai and M. Naito, *Org. Lett.*, 2013, **15**, 6006–6009.
69 R. Clarke, K. L. Ho, A. A. Alsimaree, O. J. Woodford, P. G. Waddell, J. Bogaerts, W. Herrebout, J. G. Knight, R. Pal, T. J. Penfold and M. J. Hall, *ChemPhotoChem*, 2017, 513–517.
70 C. Ray, E. M. Sánchez-Carnerero, F. Moreno, B. L. Maroto, A. R. Agarrabeitia, M. J. Ortiz, Í. López-Arbeloa, J. Bañuelos, K. D. Cohovi, J. L. Lunkley, G. Muller and S. de la Moya, *Chem. Eur. J.*, 2016, **22**, 8805–8808.
71 N. Saleh, M. Srebro, T. Reynaldo, N. Vanthuyne, L. Toupet, V. Y. Chang, G. Muller, J. A. Williams, C. Roussel, J. Autschbach and J. Crassous, *Chem Commun*, 2015, **51**, 3754–3757.
72 C. Shen, E. Anger, M. Srebro, N. Vanthuyne, K. K. Deol, T. D. Jefferson, G. Muller, J. A. G. Williams, L. Toupet, C. Roussel, J. Autschbach, R. Réau and J. Crassous, *Chem. Sci.*, 2014, **5**, 1915–1927.
73 G. Mazzeo, M. Fusè, G. Longhi, I. Rimoldi, E. Cesarotti, A. Crispini and S. Abbate, *Dalt. Trans.*, 2015, **17**, 8649–8652.
74 N. Saleh, B. Moore, M. Srebro, N. Vanthuyne, L. Toupet, J. A. G. Williams, C. Roussel, K. K. Deol, G. Muller, J. Autschbach and J. Crassous, *Chemistry*, 2015, **21**, 1673–1681.
75 J. Crassous, *Chem. Commun.*, 2012, **48**, 9684–9692.
76 F. S. Richardson, *Inorg. Chem.*, 1980, **19**, 2806–2812.
77 J. P. Leonard, P. Jensen, T. McCabe, J. E. O'Brien, R. D. Peacock, P. E. Kruger and T. Gunnlaugsson, *J. Am. Chem. Soc.*, 2007, **129**, 10986–10987.
78 E. Kreidt, A. Lorenzo, F. Zinna, L. Di Bari and M. Seitz, *Chem. Eur. J.*, 2018, **24**, 13556–13564.
79 J. L. Lunkley, D. Shirotani, K. Yamanari, S. Kaizaki and G. Muller, *Inorg. Chem.*, 2011, **50**, 12724–12732.
80 J. L. Lunkley, D. Shirotani, K. Yamanari, S. Kaizaki and G. Muller, *J. Am. Chem. Soc.*, 2008, **130**, 13814–13815.
81 D. Shirotani, T. Suzuki and S. Kaizaki, *Inorg. Chem.*, 2006, **45**, 6111–6113.
82 F. Zinna, U. Giovanella and L. Di Bari, *Adv. Mater.*, 2015, **27**, 1791–1795.
83 F. Stomeo, C. Lincheneau, J. P. Leonard, J. E. O'Brien, R. D. Peacock, C. P. McCoy and T. Gunnlaugsson, *J. Am. Chem. Soc.*, 2009, **131**, 9636–9637.
84 C. P. Montgomery, E. J. New, D. Parker and R. D. Peacock, *Chem. Commun.*, 2008, 4261–4263.
85 E. R. Neil, M. A. Fox, R. Pal and D. Parker, *Dalt. Trans.*, 2016, **45**, 8355–8366.
86 S. J. Butler, B. K. McMahon, R. Pal, D. Parker and J. W. Walton, *Chem. Eur. J.*, 2013, **19**, 9511–9517.

87 K. T. Hua, J. Xu, E. E. Quiroz, S. Lopez, A. J. Ingram, V. A. Johnson, A. R. Tisch, A. De Bettencourt-Dias, D. A. Straus and G. Muller, *Inorg. Chem.*, 2012, **51**, 647–660.
88 R. S. Dickins, J. A. K. Howard, C. L. Maupin, J. M. Moloney, D. Parker, J. P. Riehl, G. Siligardi and J. A. G. Williams, *Chem. Eur. J.*, 1999, **5**, 1095–1105.
89 J. I. Bruce, D. Parker, S. Lopinski and R. D. Peacock, *Chirality*, 2002, **14**, 562–567.
90 E. R. Neil, M. A. Fox, R. Pal, L. O. Palsson, B. A. O'Sullivan and D. Parker, *Dalt. Trans*, 2015, **44**, 14937–14951.
91 G. Weaving, G. F. Batstone and R. G. Jones, *Ann. Clin. Biochem.*, 2016, **53**, 106–111.
92 T. Hochepied, F. G. Berger, H. Baumann and C. Libert, *Cytokine Growth Factor Rev.*, 2003, **14**, 25–34.
93 A. Agostoni and B. Marasini, *Am. J. Clin. Pathol.*, 1977, **67**, 146–148.
94 P. Blain, J. Mucklow, M. Rawlins, D. Roberts, P. Routledge and D. Shand, *Br. J. Clin. Pharmacol.*, 1985, **20**, 500–502.
95 K. Matsumoto, K. Nishi, M. Kikuchi, D. Kadowaki, Y. Tokutomi, N. Tokutomi, K. Nishi, A. Suenaga and M. Otagiri, *Biol. Pharm. Bull.*, 2007, **30**, 1226–30.
96 K. Schmid, H. Kaufmann, S. Isemura, F. Bauer, J. Emura, T. Motoyama, M. Ishiguro and S. Nanno, *Biochemistry*, 1973, **12**, 2711–2724.
97 F. Albani, R. Riva, M. Contin and A. Baruzzi, *Br. J. Clin. Pharmacol.*, 1984, **18**, 244–246.
98 J.-C. Duché, F. Hervé and J.-P. Tillement, *J. Chromatogr. B Biomed. Sci. Appl.*, 1998, **715**, 103–109.
99 F. Clerc, K. R. Reiding, B. C. Jansen, G. S. M. Kammeijer, A. Bondt and M. Wuhrer, *Glycoconj. J.*, 2016, **33**, 309–343.
100 T. Fournier, N. Medjoubi and D. Porquet, *Biochim.Biophys.Acta*, 2000, **1482**, 157–171.
101 D. Biou, C. Bauvy, H. N'Guyen, P. Codogno, G. Durand and M. Aubery, *Clin. Chim. Acta*, 1991, **204**, 1–12.
102 D. Biou, P. Chanton and G. Durand, *Clin. Chim. Acta*, 1989, **186**, 59–66.
103 V. Chuang and M. Otagiri, *Molecules*, 2013, **18**, 13831–13859.
104 S. Urien, E. Albengres, R. Zini and J.-P. Tillement, *Biochem. Pharmacol.*, 1982, **31**, 3687–3689.
105 J. Kerkay and U. Westphal, *Biochim. Biophys. Acta*, 1968, **170**, 324–333.
106 J. Schley and B. Mueller-Oerlinghausen, *J. Pharm. Pharmacol.*, 1986, **38**, 102–106.
107 J. M. H. Kremer, J. Wilting and L. H. M. Janssen, *Pharmacol. Rev.*, 1988, **40**, 1–47.
108 I. Fitos, J. Visy, M. Simonyi, G. Mády and F. Zsila, *Biochim. Biophys. Acta - Gen. Subj.*, 2010, **1800**, 367–372.
109 I. Fitos, Á. Simon, F. Zsila, G. Mády, Á. Bencsura, Z. Varga, L. Orfi, G. Kéri and J. Visy, *Int. J. Biol. Macromol.*, 2012, **50**, 788–795.
110 J. Ishizaki, A. Fukaishi, C. Fukuwa, S. Yamazaki and M. Tabata, *Biol. Pharm. Bull.*, 2010, **33**, 95–99.
111 L. Jennings, R. S. Waters, R. Pal and D. Parker, *ChemMedChem*, 2017, **12**, 271–277.
112 F. P. Abramson, *Clin. Pharmacol. Ther.*, 1982, **32**, 652–58.
113 J. L. Behan, Y. E. Cruickshank, G. Matthews-Smith, M. Bruce and K. D. Smith, *Biomed Res. Int.*, , DOI:10.1155/2013/108902.
114 E. F. Mccance-Katz, *Addiction*, 2011, **106**, 687–688.
115 C. Lin, T. Somberg, J. Molnar and J. Somberg, *Cardiology*, 2009, **113**, 59–65.

116 T. Ahmad, M. A. Valentovic and G. O. Rankin, *Biochem. Pharmacol.*, 2018, **153**, 196–204.
117 A. Sekiya and E. M. V. Williams, *Brit. J. Pharmacol.*, 1963, **21**, 462–472.
118 C. M. Mokler and C. G. Van Arman, *J. Pharmacol. Exp. Ther.*, 1962, **136**, 114–124.
119 A. Baldzizhar, E. Manuylova, R. Marchenko, Y. Kryvalap and M. G. Carey, *Crit. Care Nurs. Clin. North Am.*, 2016, **28**, 317–329.
120 J.-S. Chu, S. Kishion, A. Nomura and K. Miyazaki, *Acta Pharacologica Simca*, 1997, **18**, 408–410.
121 A. Amini and D. Westerlund, *Anal. Chem.*, 1998, **70**, 1425–1430.
122 J. M. Goldman and J. V Melo, *N. Engl. J. Med.*, 2003, **349**, 1451–1464.
123 P. C. Nowell, *Natl. Acad. Sci.*, 1960, **132**, 1497.
124 G. Q. Daley, R. A. Van Etten and D. Baltimore, *Science*, 1990, **247**, 824–830.
125 C. Gambacorti-Passerini, R. Barni, P. le Coutre, M. Zucchetti, G. Cabrita, L. Cleris, F. Rossi, E. Gianazza, J. Brueggen, R. Cozens, P. Pioltelli, E. Pogliani, G. Corneo, F. Formelli and M. D'Incalci, *J. Natl. Cancer Inst.*, 2000, **92**, 1641–50.
126 I. Fitos, J. Visy, F. Zsila, G. Mády and M. Simonyi, *Biochim. Biophys. Acta*, 2006, **1760**, 1704–12.
127 F. Herve, J. C. Duche, P. D'Athis, C. Marche, J. Barre and J. P. Tillement, *Pharmacogenetics*, 1996, 6, 403–415.
128 J. Franz, US Pat., US3799758 A, 1974.
129 C. M. Benbrook, *Environ. Sci. Eur.*, 2016, **28**, 3.
130 D. M. Shah, S.G. Rogers, R. B. Horsch, R. T. Fraley, US Pat., US4940835, 1990.
131 International Agency for Research on Cancer Monographs - 112 Glyphosate, http://monographs.iarc.fr/ENG/Monographs/vol112/mono112-02.pdf, (accessed 5 February 2016).
132 *European Food Safety Authority, EFSA J.*, 2015, **13**, 11:4302.
133 Glyphosate not classified as a carcinogen by ECHA, https://echa.europa.eu/-/glyphosate-not-classified-as-a-carcinogen-by-echa, (accessed 4 September 2017).
134 The European Commission Extention of Glyphosate, https://eur-lex.europa.eu/legal-content/EN/TXT/?uri=CELEX%3A32016R1056, (accessed 8 September 2017).
135 Safe Drinking Water and Toxic Enforcement Act of 1986, https://oehha.ca.gov/media/downloads/proposition-65//p65single01272017.pdf, (accessed 7 August 2017).
136 S. Levin and P. Greenfield, Monsanto ordered to pay $289m as jury rules weedkiller caused man's cance, https://www.theguardian.com/business/2018/aug/10/monsanto-trial-cancer-dewayne-johnson-ruling, (accessed 15 August 2018).
137 M. R. Boocock and J. R. Coggins, *FEBS Lett.*, 1983, **154**, 127–133.
138 J. M. Becerril, S. O. Duke and J. Lydon, *Phytochemistry*, 1989, **28**, 695–699.
139 E. G. Jaworski, *J. Agric. Food Chem.*, 1972, **20**, 1195–1198.
140 National Primary Drinking Water Regulations, https://www.epa.gov/ground-water-and-drinking-water/national-primary-drinking-water-regulations, (accessed 8 September 2017).
141 S. Brosillon, D. Wolbert, M. Lemasle, P. Roche and A. Mehrsheikh, *Water Res.*, 2006, **40**, 2113–2124.
142 Joint FAO / WHO meeting on pesticide residues, http://www.who.int/foodsafety/call4data_2017JMPR.pdf, (accessed 9 August 2017).
143 EU pesticide database, http://ec.europa.eu/food/plant/pesticides/eu-pesticides-

database/public/?event=activesubstance.selection&language=EN, (accessed 8 September 2017).
144 Agricultural and Veterinary Chemicals Code Instrument No. 4 (MRL Standard) 2012, https://www.legislation.gov.au/Details/F2017C00649, (accessed 28 August 2017).
145 Code of Federal Regulations, https://www.gpo.gov/fdsys/pkg/CFR-2014-title40-vol24/xml/CFR-2014-title40-vol24-part180.xml, (accessed 28 September 2017).
146 A. J. Burns and D. F. Tomkins, *J. Chromatogr. Sci.*, 1979, **17**, 333–335.
147 H. A. Moye and A. J. J. Boning, *Anal. Lett.*, 1979, **12**, 25–35.
148 A. Steinborn, L. Alder, B. Michalski, P. Zomer, P. Bendig, S. A. Martinez, H. G. J. Mol, T. J. Class and N. Costa Pinheiro, *J. Agric. Food Chem.*, 2016, **64**, 1414–1421.
149 R. L. Glass, *J. Agric. Food Chem.*, 1983, **31**, 280–282.
150 F. Fitri, H. Muhamad, D. Omar and N. Asib, *J. Chromatogr. Sep. Tech.*, 2017, **8**, 1–6.
151 M. Meador and M. Jie, *Maximum Residue Limits for Pesticides in Food*, 2014.
152 W. Skeff, C. Recknagel and D. E. Schulz-Bull, *J. Chromatogr. A*, 2016, **1475**, 64–73.
153 R. E. Visco and E. A. Chandross, *J. Am. Chem. Soc.*, 1964, **86**, 5350–5351.
154 N. E. Tokel-Takvoryan, R. E. Hemingway and A. J. Bard, *J. Am. Chem. Soc.*, 1973, **95**, 6582–6589.
155 G. Marzari, M. V. Cappellari, G. M. Morales and F. Fungo, *Anal. Methods*, 2017, **9**, 2452–2457.
156 A. Habekost, *Talanta*, 2017, **162**, 583–588.
157 C. Zhang, Y. She, T. Li, F. Zhao, M. Jin, Y. Guo, L. Zheng, S. Wang, F. Jin, H. Shao, H. Liu and J. Wang, *Anal. Bioanal. Chem.*, 2017, **409**, 7133–7144.
158 Y. C. Chang, Y. S. Lin, G. T. Xiao, T. C. Chiu and C. C. Hu, *Talanta*, 2016, **161**, 94–98.
159 Y. Chang, Z. Zhang, J. Hao, W. Yang and J. Tang, *Sensors Actuators, B Chem.*, 2016, **228**, 410–415.
160 Y. Liu and M. Bonizzoni, *J. Am. Chem. Soc.*, 2014, **136**, 14223–14229.
161 T. Minami, Y. Liu, A. Akdeniz, P. Koutnik, N. A. Esipenko, R. Nishiyabu, Y. Kubo and P. Anzenbacher, *J. Am. Chem. Soc.*, 2014, **136**, 11396–11401.
162 K. A. Rawat, R. P. Majithiya, J. V. Rohit, H. Basu, R. K. Singhal and S. K. Kailasa, *RSC Adv.*, 2016, **6**, 47741–47752.
163 L. K. S. De Almeida, S. Chigome, N. Torto, C. L. Frost and B. I. Pletschke, *Sensors Actuators, B Chem.*, 2015, **206**, 357–363.
164 M. Wang, H. Ye, L. You and X. Chen, *Appl. Mater. Interfaces*, 2016, **8**, 574–581.
165 J. Guo, Y. Zhang, Y. Luo, F. Shen and C. Sun, *Talanta*, 2014, **125**, 385–392.
166 D. Wang, B. Lin, Y. Cao, M. Guo and Y. Yu, *J. Agric. Food Chem.*, 2016, **64**, 6042–6050.
167 J. Pouessel, S. Abada, N. Le Bris, M. Elhabiri, L. J. Charbonnière and R. Tripier, *Dalt. Trans.*, 2013, **42**, 4859.
168 E. Engvall and P. Perlmann, *Immunochemistry*, 1971, **8**, 871–874.
169 B. S. Clegg, G. R. Stephenson and J. C. Hall, *J. Agric. Food Chem.*, 1999, **47**, 5031–5037.
170 S. A. Tittlemier, D. Drul, B. Lake, T. Zirdum, D. Hammond, Emily Sobering, W. J. Lin, M. Tran and M. Roscoe, *Cereal Chem.*, 2017, **94**, 1028–1036.
171 Determination of glyphosate in drinking water by direct-aqueous-injection HPLC, post-column derivatization, and fluorescence detection, https://www.o2si.com/docs/epa-method-547.pdf, (accessed 27 February 2018).

172 Z. Kovacs and A. D. Sherry, *Chem. Commun.*, 1995, 185–186.
173 G.-L. Law, C. Man, D. Parker and J. W. Walton, *Chem. Commun.*, 2010, **46**, 2391–3.
174 A. Beeby, I. M. Clarkson, R. S. Dickins, S. Faulkner, D. Parker, L. Royle, A. S. De Sousa, J. A. G. Williams and M. Woods, *J. Chem. Soc. Perkin Trans. 2*, 1999, **2**, 493–504.
175 F. Kielar, C. P. Montgomery, E. J. New, D. Parker, R. Poole, S. L. Richardson and P. Stenson, *Org. Biomol. Chem.*, 2007, **5**, 2975–82.
176 R. Carr, PhD Thesis, University of Durham, 2014.
177 K. Nishi, T. Ono, T. Nakamura, N. Fukunaga, M. Izumi, H. Watanabe, A. Suenaga, T. Maruyama, Y. Yamagata, S. Curry and M. Otagiri, *J. Biol. Chem.*, 2011, **286**, 14427–14434.
178 C. Bi, R. Matsuda, C. Zhang, Z. Isingizwe, W. Clarke and D. S. Hage, *J. Chromatogr. A*, 2017, **1519**, 64–73.
179 G. F. Somers, *Br. J. Pharmacol. Chemother.*, 1960, **15**, 111–116.
180 S. W. Smith, *Toxicol. Sci.*, 2009, **110**, 4–30.
181 F. Fonseca and M. Torrens, *Mol. Diagnosis Ther.*, 2018, **22**, 57–78.
182 L. Pasteur, *C R Séances Acad Sci*, 1848, **26**, 535–538.
183 A. Larsen, B. Tullar, B. Elpern and J. S. Buck, *J. Am. Chem. Soc.*, 1948, **70**, 4194–4197.
184 D. Parker and R. J. Taylor, *Tetraherdon*, 1987, **43**, 5451–5456.
185 F. Zsila and Y. Iwao, *Biochim. Biophys. Acta*, 2007, **1770**, 797–809.
186 H. Xuan and D. S. Hage, *Anal. Biochem.*, 2005, **346**, 300–310.
187 S. Taheri, L. P. Cogswell, A. Gent and G. R. Strichartz, *J. Pharmacol. Exp. Ther.*, 2003, **304**, 71–80.
188 S. Soman, M. J. Yoo, Y. J. Jang and D. S. Hage, *J. Chromatogr. B Anal. Technol. Biomed. Life Sci.*, 2010, **878**, 705–708.
189 M. J. Yoo and D. S. Hage, *J. Sep. Sci.*, 2011, **34**, 2255–2263.
190 J. X. Mazoit, L. S. Cao and K. Samii, *J. Pharmacol. Exp. Ther.*, 1996, **276**, 109–15.
191 J. P. Guthrie, *J. Am. Chem. Soc.*, 1977, **99**, 3991–4001.
192 M. M. Peixoto, G. F. Bauerfeldt, M. H. Herbst, M. S. Pereira and C. O. Da Silva, *J. Phys. Chem. A*, 2015, **119**, 5241–5249.
193 T. G. Appleton, J. R. Hall and I. J. McMahon, *Inorg. Chem.*, 1986, **25**, 726–734.
194 B. Schneider and M. Kabelá, *J. Am. Chem. Soc.*, 1998, **120**, 161–165.
195 C. S. Uniti, V. Pado, C. Farmaceutica, A. V Amedeo and C. Borsalino, *Inorg. Chem.*, 2003, **42**, 1319–1324.
196 C. A. Carbonari, D. O. Latorre, G. L. G. C. Gomes, E. D. Velini, D. K. Owens, Z. Pan and F. E. Dayan, *Planta*, 2016, **243**, 925–933.
197 R. M. Hafez, T. M. Abdel-Rahman and R. M. Naguib, *J. Adv. Res.*, 2017, **8**, 475–486.
198 D. Müller-Schwarze and P. W. Houlihan, *J. Chem. Ecol.*, 1991, **17**, 715–734.
199 P. Bansal, G. Bhanjana, N. Prabhakar, J. S. Dhau and G. R. Chaudhary, *J. Mol. Liq.*, 2017, **248**, 651–657.
200 M. Masiol, B. Giannì and M. Prete, *Environ. Sci. Pollut. Res.*, 2018, 1–11.
201 J.A. Sabbaton, US Pat., 7534, 1850.
202 B. D. Curwin, M. J. Hein, W. T. Sanderson, C. Striley, D. Heederik, H. Kromhout, S. J. Reynolds and M. C. Alavanja, *Ann. Occup. Hyg.*, 2007, **51**, 53–65.
203 M. Krüger, P. Schledorn, W. Schrödl, H.-W. Hoppe, W. Lutz and A. A. Shehata, *J. Environ. Anal. Toxicol.*, 2014, **4**, 1–5.
204 S. J. Butler and D. Parker, *Chem. Soc. Rev.*, 2013, **42**, 1652–66.

205 S. J. A. Pope and R. H. Laye, *Dalt. Trans.*, 2006, **44**, 3108.
206 S. Shuvaev, M. A. Fox and D. Parker, *Angew. Chemie Int. Ed.*, 2018, 7488–7492.
207 Glyphosate and Drinking Water, http://www.health.state.mn.us/divs/eh/risk/guidance/gw/glyphosateinfo.pdf, (accessed 30 August 2018).
208 NWL, Water Quality Summary Report, https://www.nwl.co.uk/_assets/files/wq/W206.pdf, (accessed 6 September 2018).
209 E. A. Boss, S. H. Moolenaar, L. F. A. G. Massuger, H. Boonstra, U. F. H. Engelke, J. G. N. De Jong and R. A. Wevers, *NMR Biomed.*, 2000, **13**, 289–296.
210 S. Shuvaev, R. Pal and D. Parker, *Chem. Commun.*, 2017, **53**, 6724–6727.
211 R. H. Linnell, *J. Org. Chem.*, 1960, **25**, 290.
212 I. U. Haque, W. Akram, M. Tariq and A. Khan, *Electrochem. Soc.*, 2011, **33**, 41–48.
213 A. D. Becke, *J. Chem. Phys.*, 1993, **98**, 5648–5652.
214 C. Lee, W. Yang and R. G. Parr, *Phys. Rev.*, 1988, **37**, 785–789.
215 J. S. Binkley, J. A. Pople and J. W. Hehre, *J. Am. Chem. Soc.*, 1980, **102**, 939–947.
216 M. S. Gordon, J. S. Binkley, J. A. Pople, W. J. Pietro and W. J. Hehre, *J. Am. Chem. Soc.*, 1982, **104**, 2797–2803.
217 W. J. Pietro, M. M. Francl, W. J. Hehre, D. J. Defrees, J. A. Pople and J. S. Binkley, *J. Am. Chem. Soc.*, 1982, **104**, 5039–5048.
218 K. D. Dobbs and W. J. Hehre, *J. Comp. Chem.*, 1986, **7**, 359–378.
219 K. D. Dobbs and W. J. Hehre, *J. Comp. Chem.*, 1987, **8**, 861–879.
220 K. D. Dobbs and W. J. Hehre, *J. Comp. Chem.*, 1987, **8**, 880–893.
221 G. Gaussian 09, Revision A.02, M. J. Frisch, G. W. Trucks, H. B. Schlegel, G. E. Scuseria, M. A. Robb, J. R. Cheeseman, G. Scalmani, V. Barone, B. Mennucci, G. A. Petersson, H. Nakatsuji, M. Caricato, X. Li, H. P. Hratchian, A. F. Izmaylov, J. Bloino and 2009.
222 M. Soulié, F. Latzko, E. Bourrier, V. Placide, S. J. Butler, R. Pal, J. W. Walton, P. L. Baldeck, B. Le Guennic, C. Andraud, J. M. Zwier, L. Lamarque, D. Parker and O. Maury, *Chemistry*, 2014, **20**, 8636–8646.
223 T. T. da Cunha, J. Jung, M.-E. Boulon, G. Campo, F. Pointillart, C. L. M. Pereira, B. Le Guennic, O. Cador, K. Bernot, F. Pineider, S. Golhen and L. Ouahab, *J. Am. Chem. Soc.*, 2013, **135**, 16332–16335.
224 K. Sénéchal-David, A. Hemeryck, N. Tancrez, L. Toupet, J. A. G. Williams, I. Ledoux, J. Zyss, A. Boucekkine, J.-P. Guégan, H. Le Bozec and O. Maury, *J. Am. Chem. Soc.*, 2006, **128**, 12243–12255.
225 F. Pointillart, B. Le Guennic, O. Maury, S. Golhen, O. Cador and L. Ouahab, *Inorg. Chem.*, 2013, **52**, 1398–1408.
226 J. Tomasi, B. Mennucci and E. Cances, *J. Mol. Struct.*, 1999, **464**, 211–226.
227 C. F. Macrae, I. J. Bruno, J. A. Chisholm, P. R. Edgington, P. McCabe, E. Pidcock, L. Rodriguez-Monge, R. Taylor, J. van de Streek and P. A. Wood, *J. Appl. Cryst*, 2008, **41**, 466–470.
228 Z. Kovacs and A. D. Sherry, *Synthesis (Stuttg).*, 1997, **7**, 759–763.
229 L. Lamarque, C. Montgomery, D. Parker, Br., Pat., GB2467012-A; WO2010084090-A1, 2010.
230 P. Nantka-Namirski and J. Piechaczek, *Pol. J. Pharmacol. Pharm.*, 1974, **26**, 545–548.
231 P. Nantka-Namirski and J. Piechaczek, *Pol. J. Pharmacol. Pharm.*, 1974, **28**, 89–94.
232 P. Liu, Y. Chen, J. Deng and Y. Tu, *Synthesis (Stuttg).*, 2001, **14**, 2078–2080.
233 R. Pal, PhD Thesis, University of Durham, 2007.

234 A. Bourdolle, M. Allali, J. C. Mulatier, B. Le Guennic, J. M. Zwier, P. L. Baldeck, J. C. G. Bünzli, C. Andraud, L. Lamarque and O. Maury, *Inorg. Chem.*, 2011, **50**, 4987–4999.
235 G. Chessa, L. Canovese, F. Visentin, C. Santo and R. Seraglia, *Tetrahedron*, 2005, **61**, 1755–1763.
236 V. S. I. Sprakel, J. A. A. W. Elemans, M. C. Feiters, B. Lucchese, K. D. Karlin and R. J. M. Nolte, *European J. Org. Chem.*, 2006, 2281–2295.